Universidad Autónoma de Madrid

Facultad de Ciencias
Departamento de Física Teórica

Consejo Superior de Investigaciones Científicas

Instituto de Física Teórica
IFT UAM-CSIC

Running of the renormalised strong coupling constant with 4 flavours of staggered quarks

Memoria de Tesis doctoral

Paula Pérez Rubio

presentada ante el Departamento de Física Teórica
de la Universidad Autónoma de Madrid
para la obtención del título de Doctor.

Proyecto dirigido por

Stefan Sint

de School of Mathematics
de Trinity College Dublin

Madrid, junio 2010.

Contents

1 Introduction and motivation **1**

2 The lattice Schrödinger Functional with staggered fermions **9**

2.1 Lattice QCD with staggered fermions 11

2.2 Pure gauge theory 14

2.2.1 Continuum limit and counting of lattice sites. 15

2.2.2 Fields at the boundaries 16

2.2.3 Equations of motion 17

2.2.4 Analytic solution of the equations of motion 18

2.2.5 Cooling program 20

2.3 Including staggered fermions 22

2.3.1 SF fermionic action with staggered fermions 25

2.3.2 Reconstruction of the four-component spinors 26

2.3.3 Free fermionic propagator in terms of four component spinors . 32

2.3.4 Free fermionic propagator in terms of single component spinors 34

2.4 Definition of the renormalised coupling $\bar{g}^2$ and the observable $\bar{v}$ 36

3 Tree level O(a) improvement **39**

3.1 Pure gauge theory 40

3.1.1 Possible counterterms 41

3.1.2 Identification of the O(a) effects in the action 41

3.1.3 Determination of $c_t^{(0)}$ 42

3.2 Fermionic action 42

3.2.1 O(a) improvement contributions from the volume 43

3.2.2 O(a) improvement at the boundaries 46

4 One loop O(a) improvement **51**

4.1 One loop O(a) improvement in a SF framework 54

4.2 Pure gauge contribution 56

4.2.1 Gauge fixing . . . 56
4.2.2 Structure of the operators Δ_0 and Δ_1 . . . 59
4.2.3 Computation of $m_{1,0}(L/a)$ . . . 61
4.2.4 Determination of $c_t^{(1,0)}$ . . . 64
4.3 Fermionic contribution . . . 65
4.3.1 Structure of Δ_2 and computation of $m_{1,1}(L/a)$ . . . 66
4.3.2 Determination of $c_t^{(1,1)}$ . . . 68

5 Details of the numerical simulations. 69
5.1 Algorithms . . . 70
5.1.1 Importance sampling . . . 70
5.1.2 Markov chains . . . 72
5.1.3 The HMC algorithm . . . 76
5.1.4 Final remarks concerning the algorithm . . . 78
5.2 Characteristics of the machines available . . . 79
5.3 Modifications of the MILC code . . . 80
5.3.1 Implementation of the computation of $\bar{v}$ . . . 81
5.3.2 Changes in the pure gauge part . . . 82
5.3.3 Changes in the fermionic part . . . 82
5.4 Tests of the algorithm . . . 84
5.4.1 ΔH as a function of ϵ^2 . . . 84
5.4.2 Reversibility of the algorithm . . . 85
5.4.3 Expectation value of $e^{-\Delta H}$ . . . 85
5.4.4 Performance of the algorithm . . . 88
5.4.5 Seeking the optimal acceptance rate . . . 90
5.5 Simulation results . . . 93
5.5.1 Sampling of the configuration space. . . . 94
5.5.2 Estimation of the observables . . . 94

6 Implementation of finite size techniques and results 97
6.1 Finite size techniques . . . 98
6.1.1 Gell-Mann and Law renormalisation group . . . 98
6.1.2 Step scaling function . . . 101
6.1.3 Scaling of the coupling with energy . . . 101
6.1.4 Physical units . . . 102
6.2 Step scaling technique with a lattice cutoff . . . 103
6.2.1 Continuum limit . . . 103
6.2.2 Computational strategy followed . . . 109

6.3 Analysis of the data . . . 110
6.3.1 χ^2 - fitting . . . 110
6.3.2 Analysis of the lattice artifacts . . . 112
6.3.3 Lattice step scaling function . . . 115
6.3.4 Alternatives to the proposed data handling . . . 116
6.4 Results . . . 118

7 Conclusions and outlook **125**

Resumen en castellano **129**

A Notation **135**
A.1 Dirac matrices . . . 135
A.2 Flavour structure . . . 135
A.3 Momenta on the lattice . . . 136
A.4 Completeness relations . . . 136

B Symmetries of the staggered fermions **138**
B.1 Chiral symmetry, $U(1)_\epsilon$ . . . 138
B.2 Reflections with respect to a hyperplane . . . 139
B.3 Rotations by $\pi/2$ around the centre of an hyperplane . . . 140
B.4 Translations by one lattice unit . . . 141
B.5 $U(1)$ invariance . . . 141
B.6 Interchange symmetry. (Charge conjugation symmetry) . . . 142

C Derivation of the SF action in terms of the reconstructed fermions **143**
C.1 Intermediate fields . . . 143
C.2 Reconstructed fermions . . . 146

D Free staggered propagator **150**
D.1 Plane wave solutions . . . 150
D.2 Solution of the Dirac equation with boundary values . . . 151
D.3 Propagator . . . 152
D.3.1 Infinite lattice propagator . . . 153
D.3.2 Boundary conditions . . . 154
D.3.3 Solution of the homogeneus Dirac equation . . . 154
D.3.4 Expression for the propagator . . . 155

E Possible counterterms of dimension 3, 4, 5 **157**
E.1 Dimension 3 157
E.2 Dimension 4 158
E.3 Dimension 5 159

F Coefficient matrices for the determination of Δ_1 **161**

G Values of $m_{1,0}(L/a), m_{1,1}(L/a)$ **165**

H Simulation results **168**

List of Figures

2.1 Reconstruction on a $T = L + a$ lattice. 27
2.2 Reconstruction on a $T = L - a$ lattice. Left $s = 1^+$, right, $s = 1^-$ . . . 27

5.1 $|\Delta H|$ as a function of ϵ^2 85
5.2 Distribution of the observable $\partial S/\partial \eta$ at the largest couplings for lattices with $L = 4, 6, 8, 12, 16$ and $s = \pm 1$. 95

6.1 Finding fixed points of the bare coupling. 107
6.2 Sketch of step scaling techniques 110
6.3 $\bar{g}^2(\beta)$ as a function of β. The errors are statistical. 111
6.4 Analysis of the lattice artifacts of our system. Diamond (blue) points are the values of $\bar{g}^2(L/a)$. Dashed lines correspond to the fitting of these data and asterisks (green), the continuum extrapolation. Circles, (magenta) are the values for the same data after performing the perturbative subtraction, and the dotted lines their fittngs. Squares (orange) represent their continuum limit (displaced from the origin). The solid horizontal (red) lines are the lines of constant physics, given also by a (red) circle that is slightly displaced from the origin. 122
6.5 Continuum limit extrapolation of the step scaling function. Diamond (blue) points are the values of the "normal" lattice step scaling function and the solid lines represent the fittings. Circles (red) represent the "crossed" lattice step scaling function and the dashed lines their fittings. Asterisks (magenta) are the continuum extrapolations $\sigma(u)$ of the lattice step scaling function. The renormalisation prescriptions, (values of u) are explicitly given in the plots. The graphs on top correspond to the regularisation $s = 1$ and the ones underneath to $s = -1$. 123
6.6 Step scaling function $\sigma(u)$. The dotted-dashed (red), dashed (blue) and solid (magenta) lines represent, correspondingly, the perturbative 1-loop, 2-loop and 3-loop $\sigma(u)$. Diamonds (red) represent the extrapolated $\sigma(u)$ from the $s = 1$ regularisation and circles (green) from the $s = -1$. Their fittings (excluding the largest value) are given by the dotted lines. . . . 124

List of Tables

2.1 $c_t^{(0)}$ coefficients. 20
2.2 Values of f_2 for different lattice sizes. 20
2.3 Values of $1 - S_{latt}(s)/S_{cont}$ for $s = 0, \pm 1$. 21
2.4 Values of the action obtained with the cooling program 22

4.1 Precision obtained for $m_1(L/a)$ values. 63
4.2 $m_{1,0}(L/a)$ asymptotic expansion coefficients, $s = 0$. 64
4.3 $m_{1,0}(L/a)$ asymptotic expansion coefficients, $s = 1$. 64
4.4 $m_{1,0}(L/a)$ asymptotic expansion coefficients, $s = -1$. 64
4.5 The first two 'non-log' terms in the expansion Eq. (4.1.8) of $m_{1,1}$. . . 67

5.1 Reversibility of the algortihm, V = 6x6x6x5, $\beta = 7.0$. 86
5.2 Reversibility of the algorithm, V =8x8x8x7, $\beta = 7.0$. 86
5.3 Reversibility of the algorithm, V =10x10x10x9, $\beta = 7.0$. 87
5.4 Reversibility of the algorithm, V =12x12x12x11, $\beta = 7.0$. 87
5.5 Reversibility of the algorithm, V =16x16x16x15, $\beta = 7.0$. 88
5.6 Reversibility of the algorithm, V =20x20x20x19, $\beta = 7.0$. 88
5.7 Results for $\overline{e^{-\delta H}}, e^{-\overline{\delta H}}$, for a 6x6x6x7 lattice, 2000 measurements , $\tau = \frac{1}{2}$ and $\beta = 7$. 89
5.8 Performance of the algorithm. 89
5.9 Optimal number of processors 89
5.10 Time(s)·#Proc 90
5.11 Run time needed when Vol/Proc$\sim 1000, 5000$ 90
5.12 Test simulations for a 6x6x6x5 lattice with $\beta = 7.0$. 91
5.13 Test simulations for a 8x8x8x7 lattice with $\beta = 7.0$. 91
5.14 Test simulations for a 6x6x6x5 lattice with $\beta = 7.0$. 92
5.15 Test simulations for a 12x12x12x11 lattice with $\beta = 7.0$. 92
5.16 Test simulations for a 16x16x16x15 lattice with $\beta = 7.0$. 92
5.17 Test simulations for 20x20x20x19 & 24x24x24x23 lattices with $\beta = 7.0$. 93

5.18 Optimal values for N_0, estimated statistics and time needed to get $\frac{\Delta\bar{g}^2}{\bar{g}^2} \sim$ 0.5%. In the Time entry, h stands for hours, and d for days. 94

6.1 Values of $c_{1,1}$ 100
6.2 Values of $\bar{g}^(a/L, -1)$ for $s = -1$ corresponding to a fixed $\bar{g}^2(a/L, 1) = u_1$. 113
6.3 Values of $\bar{g}^(a/L, 1)$ for $s = 1$ corresponding to a fixed $\bar{g}^2(a/L, -1) = u_{-1}$. 114
6.4 Continuum limit of $u_s^{(1)}(a/L)$ (1-loop perturbative effects have been subtracted.) 115
6.5 Lattice step scaling function Σ, for $s = 1$. 117
6.6 Lattice step scaling function Σ, for $s = -1$. 117
6.7 Discretisation error of the SSF. 119
6.8 Continuum limit extrapolation of the step scaling function for the two given regularisations 120

E.1 Possible counterterms of dimension 3. 158

F.1 Values of C_a, S_a obtained for $m_1(L/a)$ values 163

G.1 $m_{11}(L/a)$ for $s = 1$ 165
G.2 $m_{11}(L/a)$ for $s = -1$ 166
G.3 The one loop coefficient, $m_{1,0}(L/a)$ for $s = 1, 0, -1$. Last digits may be ruined 167

H.1 Simulation data for a 4x4x4x3 lattice. 169
H.2 Simulation data for a 6x6x6x5 lattice. 170
H.3 Simulation data for a 8x8x8x7 lattice. 171
H.4 Simulation data for a 12x12x12x11 lattice. 172
H.5 Simulation data for a 16x16x16x15 lattice. 173
H.6 Simulation data for a 4x4x4x5 lattice. 174
H.7 Simulation data for a 6x6x6x7 lattice. 175
H.8 Simulation data for a 8x8x8x9 lattice. 176
H.9 Simulation data for a 12x12x12x13 lattice. 177
H.10 Simulation data for a 16x16x16x17 lattice. 178

Chapter 1

Introduction and motivation

Since the beginning of the twentieth century, the vast majority of scientists were convinced that the world needed quantum mechanics (QM) to be explained. In a quantum mechanical system, position and momentum are thought of as operators acting on a Hilbert space of states. Some classical concepts such as the trajectory of a particle are no longer well defined.

On the other hand, some aspects of nature were explained in terms of fields. Maxwell's theory of electromagnetism was developed in the nineteenth century. It was thus desirable to formulate it implementing the newly developed quantum concepts[1] . Fields were then promoted to operators acting on a Hilbert space $\mathcal{H}$. The states were constructed in terms of particle excitations. Therefore, the prior conceptual distinction between fields and particles ceased to exist. Another important aspect that is worth mentioning is that the quantisation of a field theory predicted the existence of antiparticles.

That was the birth of quantum field theory, (QFT). The most relevant QFT's describing interactions with particles are gauge field theories. The aforementioned electromagnetic theory was the first to be quantised, leading to quantum electrodynamics (QED), established in the 1930's. At a classical level, the vector potential was introduced as a convenient auxiliary tool, whereas at a quantum level, A_μ acquires a fundamental significance, since it has the geometrical interpretation as the connection in a fibre bundle. The gauge symmetry in this case is the abelian group U(1).

To study the consequences of QED, perturbation theory (PT) was applied. The results of the lowest order were in good agreement with experiment. However, one could not continue in the approximation. Higher order terms led to divergent integrals. Between 1946 and 1949, Schwinger [1, 2, 3], Tomonaga [4, 5], Feynman [6, 7, 8] and Dyson [9] presented a covariant form of the perturbation expansion together with the idea of renormalisation that allowed the computation of higher order corrections. These corrections could account for the increasingly more precise experimental findings. Faith

[1]Concerning gravitation, Einstein developed at the beginning of last century general relativity (GR). A quantum version of it is not available at present time.

in QED was restored.

However, there were unignorable sources of dissatisfaction. The theory could not be formulated without invoking perturbation expansions. The renormalisation procedure was not fully understood. It was regarded as a "trick" of sweeping the infinities under the rug. In addition, the QFT's developed to explore the weak (Fermi theory [10]) and the strong (Yukawa interaction, [11]) interactions posed fundamental problems. The former seemed to work at lowest order in PT, but was not renormalisable. The latter's perturbation expansions were not useful. These are a few of the issues that made QFT fall into disuse during the decade of the 50's.

This controversy concerning QFT was a motivation to search for a deeper understanding of the underlying principles and for a more concise mathematical formulation. In quantum mechanics, it can be shown (v.Neumann, Rellich, Stone, H. Weyl) that under natural requirements, the canonical commutation relations the operators satisfy fix their representation in the Hilbert space up to unitary equivalence. This statement is referred to as *von Neumann's uniqueness theorem*. The main point is that it no longer applies if the number of degrees of freedom is infinite, as it is the case in QFT's. When perturbation theory is applied, it is done in the Hilbert space of the free theory $\mathcal{F}$ (it is a Fock space, a direct product of Hilbert spaces). The vacuum state of the free theory, Ω_0 is distinct from the vacuum state of the theory with interactions, Ω_g. From Haag's theorem [12] it can be concluded then that the Hilbert space of the interacting theory, $\mathcal{H}$, is not unitarily equivalent to the Fock space of the free theory, $\mathcal{F} \neq \mathcal{H}$. The interacting fields are more singular objects than in the free theory. These issues can be considered as the stems of renormalisation. The need to base the discussion of QFT on clearly stated postulates led Wightman and Gårding to give mathematically precise axioms (*Wightman axioms*, [13]) for quantum field theories in Minkowski space time. Besides, one of the achievements of axiomatic field theory that is actually going to be crucial for the safe implementation of the methods used in this work, was the establishment of a rigorous connection between an Euclidean invariant field theory in an euclidean space-time and a Lorentz-invariant field theory in Minkowski space-time in both directions. This was done by Osterwalder and Schrader in [14, 15], and it allows the use of path integral methods with the consequent interpretation in the framework of measure theory.

The mathematical formulation of QFT's still leaves the problem of understanding strong and weak interactions unsolved. During the decade of the 1950's, Yang Mills (YM) theory was developed [16]. It was natural to inquire whether a non-abelian gauge theory could describe the weak and the strong forces. However, the massless nature of classical Yang-Mills was a serious obstacle to applying it to these forces for they are short ranged and many of the particles are massive. Besides, concerning the strong interactions, there was another big problem: which fields should be used? The decade of the 1960's was a period of experimental supremacy. The proliferation of particles was immense. All the hadrons, strange baryons and mesons appeared to be equally fundamental.

These obstacles were overcome for the weak interactions through the Glashow-Salam-Weinberg electroweak theory [17] with the gauge group SU(2) × U(1). With the inclusion of an additional scalar field, the Higgs boson, H, the massless nature of classical YM theory was avoided. The theory describes the electromagnetic and weak forces in a unified way.

Concerning the strong interactions (which are the ones studied in this work), the solution was given by discovering a property a non abelian YM theory possesses solely at the quantum level: *asymptotic freedom*, discovered by Gross, Wilczeck and Politzer in 1973, [18, 19] (see [20] for a review). Roughly speaking it means that at short distances the field displays quantum behaviour resembling the classical one whereas at long distances, the classical behaviour cannot be used as a guide to describe the quantum fields. This feature together with other experimental (e.g., deep-inelastic scattering at SLAC showed that the proton behaved, when observed over short times as if it was made out of point-like objects of spin 1/2) and theoretical (Björken scaling, Feynman parton model, t'Hooft work on the renormalisability of YM theories, ...), discoveries made in the 1960's and 1970's, led to the description of the nuclear strong force by a non-abelian gauge theory whose gauge group is SU(3). The gauge fields are called "gluons" and the additional 1/2 spin fields are the "quarks". They transform in the fundamental representation of SU(3). The non-abelian gauge theory of the strong interactions is called quantum chromodynamics, (QCD) and its characteristic quantum number, colour.

QCD is believed to be a theory at all scales. And, as it was expected due to asymptotic freedom, the nuclear interaction's behaviour at low energies are very different from the predictions of classical YM theories. For QCD to describe the strong force successfully it must possess the following properties, each of which differs drastically from the classical theory's behaviour,

I. *Mass gap*, $\Delta > 0$ so that any excitation of the vacuum has energy $E \geq \Delta$, since the strong force is short ranged, [21].

II. *Confinement*, all physical particle states are SU(3) invariant (colour singlets). Quarks are never observed isolated,

III. *Chiral symmetry breaking*, the vacuum is potentially invariant only under a certain subgroup of the full symmetry group of the quark fields. This property is required in order to explain the pion's phenomenology.

These properties are, at present time, not fully understood theoretically. Both experiment and computer simulations carried out since the late 1970's have given strong encouragement that QCD does have the properties listed above. What are we referring to when we say computer simulations? At large distances, PT is useless for investigating the strong interactions. A non perturbative approach is thus needed. One year after asymptotic freedom was discovered, Wilson, in [22], suggested approximating continuum euclidean space time by a lattice (cf. chapter 2), on which he defined a

gauge invariant action. The path integral has a finite number of variables of integration and is therefore mathematically well defined. In order to recover QCD, one must then verify[2] the existence of limits of expectation values of observables as the lattice spacing a vanishes and the volume tends to infinity (thermodynamic limit). Moreover, in 1980, Creutz pointed out that the lattice formulation of a QFT could be simulated on a computer, [23, 24]. He performs simulations in SO(2) and SU(2) using Monte Carlo integration techniques (cf. chapter 5). With more computer power, this technique could be easily extended to SU(3). Since then, the lattice approach, together with numerical simulations, has become the most powerful tool for the performance of non perturbative calculations. It is this framework that we are going to use throughout this work. Since the 1980's, lattice QCD or more generally, the lattice formulation of QFT's, has become a branch of theoretical physics itself, with a widespread domain of applicability. Some of the goals of the lattice formulation would be,

- Test whether QCD is the correct theory of strong interactions. The results of simulations back up the theory so far.
- Calculation of matrix elements occuring in weak decays.
- Investigate the topological structure of the QCD vacuum and the mechanisms responsible for confinement and spontanoeusly broken χ- symmetry
- Calculate hadronic properties like wave functions, decay constants, form factors, structure functions...
- Analyse QCD at high temperatures.

Non perturbative renormalisation

As it has been aforementioned, interacting QFT's need to be renormalised before any predictions can be done. The theory is first formulated with an UV cutoff (regularisation). There are many ways of introducing such a cutoff. In the lattice regularisation, the lattice spacing a plays the role of such a cutoff. Since the physical observables are not to be cutoff dependent, it needs to be removed before making predictions. The theory needs to be renormalised. That is done through the so called renormalisation prescriptions, that define the "renormalisation scheme" (not unique, either).

Let us focus on the lattice regularisation. Renormalisation is an ultraviolet phenomenon with relevant momentum scales of order a^{-1}. Renormalising a theory defined with a lattice cutoff is equivalent to taking the continuum limit of the theory. Because of asymptotic freedom, the bare coupling of QCD is expected to be weak as one approaches the continuum limit. Nonetheless, in order to keep the computer simulations tractable, one is obliged to work at lattice spacings that are not small enough in order for perturbation theory to be reliable. Therefore, one is required to find a way of implementing renormalisation in a non-perturbative fashion. It has to be noted that this problem is more manifest when we are performing simulations to investigate the low energy behaviour of QCD, where the renormalised coupling is unnegligibly large.

[2] A rigorous proof of existence is lacking.

The only free parameters of QCD are the bare coupling and the bare masses of the quarks. These parameters can be fixed by fixing as many low energy parameters (e.g., $m_\pi/f_\pi, m_K/f_\pi, \dots$) to their physical values as there are bare parameters in the theory. This procedure is known as hadronic renormalisation scheme. In particular, in QCD with massless quarks (which will be the system under consideration throughout this work), the only free parameter is the fundamental scale of the theory which can be adjusted through the computation of one low energy quantity. The theory is in this way renormalised with no reference to perturbation theory. Now, any other physical quantity should be computable, i.e., should be a prediction of the theory.

Lattice QCD allows us to study the phenomenon of confinement[3], by computing hadronic quantities at low energies. The experiments at the particle colliders, on the other hand, probe the interactions of the quarks and gluons at high energies (where perturbation theory can be applied). Strong interaction physics is believed to be described by the same underlying theory at both regimes. Establishing the connection between the low-energy sector and the perturbative regime of the theory is one of the fundamental problems in QCD. Some reviews about this issue can be found in [25, 26, 27, 28, 29, 30, 31]. **This project is devoted to establishing such a connection for QCD with four flavours of massless quarks**.

We want to match a given hadronic scheme with a perturbative scheme, (e.g., $\overline{\text{MS}}$ of dimensional regularisation). This can be done through the computation of a non-perturbatively defined renormalised running coupling (it should be a prediction of the theory once the hadronic renormalisation scheme has been implemented) over a large range of energies. Eventually, at high energies, one can compare to perturbation theory and estimate the scales. However, a technical problem arises due to the large scale difference. In order to measure hadronic quantities keeping finite volume effects small, we require, $L^{-1} << m_\pi$. On the other hand, one would like to have simulations with a cutoff a^{-1} much larger than the largest energy scale μ_{pert}. This implies,

$$L^{-1} << m_\pi, \Lambda << \mu_{\text{pert}} << a^{-1}. \tag{1.0.1}$$

This corresponds to lattices with $L/a \sim \text{O}(10^3)$, which are inaccessibly large for the current computer power.

Many procedures have been applied to overcome this difficulty: mean field perturbation theory, introduced by Lepage and Mackenzie in [32], intermediate renormalisation, introduced by Martinelli et al. in [33] and recursive finite size technique, introduced by Lüscher et al. in [34]. It is the latter the one that is going to be used for our computations. We will give a brief description of this technique. More details will be given in chapter 6.

[3] As it has been pointed out before, the continuum limit extrapolation lacks of a rigorous mathematic justification.

Finite size techniques

Recursive finite size technique methods were introduced in [34] where they were applied to the O(3) σ-model with satisfactory results. The running coupling constant is defined in a finite volume, so that L, the spatial size plays the role of the natural external scale. A coupling is introduced that runs with L. There are infinitely many ways of introducing such a coupling, and at large L their behaviours can be completely different. The important feature that they all have to fulfill is that at small L, we can use PT to compute them as a power series in a perturbatively defined coupling, (e.g., $\bar{g}_{\overline{\rm MS}}$). Our coupling is going to be defined in the framework of the Schrödinger Functional (cf. chapter 2), since, as it was argued in [35], this set up provides us with a convenient definition of the renormalised coupling for the purposes under consideration. A computation of the evolution of such a coupling was carried out in [36, 37] for SU(2) Yang Mills with satisfactory results.

Once a coupling depending on the external scale has been defined $\bar{g}^2(L)$, the strategy to connect a hadronic with a perturbative scheme consists on,

i) Set the scale of the lattice with largest physical extent, $L = L_{\rm max}$. Run a simulation to establish the physical value of $L_{\rm max}$ (e.g, ~ 0.5fm). Compute $\bar{g}^2(L)$ at this volume.

ii) Evolve the running coupling non perturbatively (cf. chapter 6) towards higher energies, or, correspondingly, smaller values of L, (e.g., $L \sim 0.005$fm).

iii) Assuming the perturbative region has been reached in 2, the coupling evolution can be continued in the framework of PT. The Λ_{SF}[4] parameter in this scheme can be computed and given in physical units.

iv) Establish the connection between $\bar{g}^2(L)$ and a perturbatively defined renormalised running coupling, (e.g., $\bar{g}^2_{\overline{\rm MS}}$).Now, the ratio of Λ- parameters can be established, and hence $\Lambda_{\overline{\rm MS}}$ in physical units.

The aforementioned finite size techniques together with the SF formulation to compute the evolution of the renormalised coupling constant, have been also applied to SU(3) pure Yang Mills theory [38], QCD with two [39] and 2+1 [40] dynamical flavours. Here, we present the evolution for 4 massless dynamical flavours. Finite size techniques have also been used to carry out lattice studies of the conformal behaviour of YM theories, [41]. Recently, the results for QCD with 4 flavours with Wilson fermions were published [42]. Throughout this work, we use a different regularisation for the fermions, the so called staggered fermions. The results we present here agree with the ones in [42] within errors.

[4]SF stands for Schrödinger functional, since it ts the framework used in this work

Overview

This work is organised as follows. In chapter 2, we will give a description of the SF framework on the lattice with four flavours of staggered quarks. As we have stated before, this set up allows us to define a renormalised running coupling constant, $\bar{g}^2(L)$ suitable for our computations.

Lattice spacings a used in simulations are not always desirably small. We want the continuum extrapolation to depend as little as possible on the lattice artifacts. Chapters 3 and 4 are completely devoted to implementing the so called Symanzik O(a) improvement in order to remove the linear lattice artifacts at tree level and one loop in lattice perturbation theory.

Once this improvement was implemented, simulations were run. Tests of the algorithm used are presented in chapter 5. They represent a check on the reliability of the computer simulation. Chapter 6 deals with the application of the finite size techniques to our data. We present the results obtained for the evolution of the coupling with the scale. We will arrive at a value for the dimensionless quantity $\Lambda L_{\max}$. The value of $L_{\max}$ in physical units remains to be determined by large volume simulations. Chapter 7 contains some conclusions, final remarks and an outlook.

Chapter 2

The lattice Schrödinger Functional with staggered fermions

To implement the program outlined in the introduction, that will be more accurately described in chapter 6, we need a definition of the coupling constant $\bar{g}^2(L)$ satisfying the following requisites,

a) It has to be non-perturbatively defined.

b) It has to be accurately measurable on any given lattice in the scaling region.

c) Its lattice artifacts have to be rather small.

d) It should be reasonably easily computable in the perturbative regime up to two loop order.

Members of the Alpha Collaboration found that couplings based on the Schrödinger Functional (SF) would satisfy a) - d) [35, 37, 36]. In our work the SF framework is used to define $\bar{g}^2$ and compute its evolution with the scale. The coupling constant is not the unique observable for which this program can be implemented. Other applications include the quark mass, moments of structure functions, the static axial current and four quark operators. See [43] and references therein.

The Schrödinger Functional is defined to be the propagation kernel for going from a field configuration at time $x_0 = 0$, to another at $x_0 = T$. Prescribing the value of the fields on a boundary involves using the Schrödinger picture of a Quantum Field Theory (QFT). The question now is whether it is mathematically well defined for a renormalisable QFT. This problem was not addressed until 1981, when Symanzik concluded in [44] (see [45], for a review) that it is indeed.

The idea behind it is the following. The quantisation of a classical theory is usually presented by applying the canonical quantisation procedure. Classical fields are promoted to Quantum operators $\pi(x), \phi(x)$ satisfying the canonical commutation relations,

$$\begin{aligned} [\pi(x), \phi(y)]_{x_0=t_0} &= -i\delta(\mathbf{x}-\mathbf{y}), \\ [\pi(x), \pi(y)]_{x_0=y_0} &= [\phi(x), \phi(y)]_{x_0=y_0} = 0. \end{aligned} \tag{2.0.1}$$

Let us focus on a scalar theory with quartic interactions. The Hamilton operator $\mathbb{H}$ is defined and given by,

$$\mathbb{H} = \int d^3x \left\{ \tfrac{1}{2}\pi^2(x) + \tfrac{1}{2}m^2\phi^2(x) + \tfrac{1}{4!}g\phi^4(x) \right\}. \tag{2.0.2}$$

The dynamics is given by the Heisenberg equations of motion,

$$\begin{aligned} \partial_0\phi(x) &= i\left[\mathbb{H}, \phi(x)\right], \\ \partial_0\pi(x) &= i\left[\mathbb{H}, \pi(x)\right]. \end{aligned} \tag{2.0.3}$$

The question now is whether a Schrödinger representation can be obtained. In this representation, the states are time dependent and the operators are not. The Hilbert space $\mathcal{H}$ of states is isomorphic to a linear space of wave functionals $\psi[A]$, where $A(\mathbf{x})$ is a classical field defined at a time, e.g. $x_0 = 0$. In analogy with QM $|\psi[A]|^2$ represents the probability for the quantum field $\phi(x)$ to assume the value $A(\mathbf{x})$ at time $x_0 = 0$. $\phi(0, \mathbf{x})$ is diagonal in the Schrödinger representation:

$$\phi(0, \mathbf{x})\psi[A] = A(\mathbf{x})\psi[A]. \tag{2.0.4}$$

Does Eq. (2.0.4) hold? Quantum fields $\phi(x)$ are not well behaved operators in general, but operator valued distributions [13]. Physically, that means that one cannot measure $\phi(x)$ at a single point, but only averages of $\phi(x)$ over a space time region (see [46]). That is,

$$\phi_f \equiv \int \phi(x) f(x) d^4x, \tag{2.0.5}$$

for any infinitely differentiable complex function $f(x)$ of compact support defined in space time, is an operator. This procedure is known as smearing. Products of distributions do not always make sense. Some care has to be taken to define these products snsibly. This is the subject of renormalisation. Thus, the question is whether the smearing over a hypersurface,

$$\phi'_f = \int \phi(x) f(x) \delta(x_0) d^4x, \tag{2.0.6}$$

defines an operator. That is, is the usual renormalisation program enough to make $\phi(0, \mathbf{x})$ well defined so that Eq. (2.0.4) holds? The answer is no, but there is a substitute which reads,

$$\lim_{x_0 \to 0} a(x_0)\phi(x) = A(\mathbf{x}), \tag{2.0.7}$$

where $a_0(x_0)$ is a renormalisation coefficient. What Symanzik proves is that by adding boundary counterterms to the action (counterterms at a given surface), wave functionals become renormalised at all orders in perturbation theory (PT), and they admit a path integral formulation. That is, it is necessary to "correct" the object in Eq. (2.0.6) with a counterterm in order to make it well defined.

This provides us with strong arguments to believe that the Schrödinger functional aforementioned is renormalisable by adding the appropriate counterterms at the boundaries. The expectation is that these are local polynomials in the fields and derivatives

thereof, integrated over the boundary. They are further restricted since their dimension has to be ≤ 3 (we will assume we are in a 4 dimensional space-time) and they have to respect all symmetries of the theory.

The Schrödinger Functional for SU(N) Yang Mills theories has been extensively discussed in [35]. Lüscher et al. defined the SF for such theories and argued that, there are no candidates for boundary counterterms and showed that there were no extra-divergences arising at one-loop order in PT. The extension of this program to QCD was performed by Sint in [47] where the Schrödinger functional in QCD was defined in the continuum and on the lattice with Wilson quarks. In [48] he shows that its perturbative renormalisability works up to one loop in PT.

In [49, 50], the formulation of the SF on the lattice by means of staggered fermions is addressed. Since we want to compute the evolution of the renormalised coupling constant for QCD with four flavours of quarks, staggered fermions[1] seem to be a suitable choice[2]. In what follows, we will be purely concerned with the establishment of a definition of the SF on the lattice with staggered fermions. It has to be noted that our approach differs slightly from the author's above, since some effort was put to remove $O(a)$ artifacts at tree level (cf. chapter 3) and one loop (cf. chapter 4). The existence of order a effects already at tree level makes us modify the pure gauge action (cf chapter 3).

In this chapter, we first introduce some notation and general aspects of lattice QCD. Then, the pure gauge SF on the lattice is revisited, we discuss the SF action including staggered fermions, and explicitly work out its free propagator. The last part of the section is devoted to define a renormalised coupling in this scheme, suitable for the implementation of the finite size techniques briefly introduced in the previous chapter.

2.1 Lattice QCD with staggered fermions

Lattice field theory, first introduced by Wilson in [22], addressing pure gauge theories, is a regularisation of an euclidean quantum field theory (EQFT) by a space-time lattice.

In [51, 52] Symanzik established the foundations of EQFT, (see [53] for a review). EQFT is obtained from Minkowski field theory [13], by analytical continuations to imaginary time. The Wightman functions (vacuum expectation values of products of fields) are thus analytically continued to euclidean functions, the Schwinger functions. Symanzik recognised that they can be interpreted as the statistical mechanics of a classical, euclidean invariant field theory in d dimensions. Then, a measure $d\mu$ can be defined, and the path integral formulation can be constructed.

Symanzik proposed constructing the Schwinger functions directly. The question is: is there a way to ensure analytic continuation of the Schwinger functions back into the Wightman functions of a Lorentz-covariant field theory? After [14, 15], we know

[1] as

[2] When using staggered fermions, four species of quarks arise naturally

that this is indeed the case. In their work, Osterwalder and Schrader established the necessary and sufficient conditions the Schwinger's functions have to satisfy for them to be analytical continuations of Wightman functions. The most relevant for the lattice formulation would be: Euclidean invariance, reflection positivity and symmetry of their arguments.

Hence, the use of EQFT is justified. However, it has not been proven that gauge theories satisfy the Wightman axioms. Nevertheless, a regularised theory is always well defined. In 1974, K. Wilson quantised gauge field theories in a discrete lattice in Euclidean space-time, [22]. The lattice spacing, a acts as a regulator of the theory rendering it sensible from a mathematical point of view with no further considerations. The path integral formulation is then well posed for a theory with $1/a$ playing the role of a cutoff. The aim is to try to construct the lattice formulation in such a way that we can expect to obtain a EQFT when the continuum limit, $(a \to 0)$ is sensibly taken. This regularisation is useful because it can be simulated in a computer, and has been the source of a huge amount of satisfactory results.

In order to establish the conventions and notation used in this work, we briefly describe the basic features of lattice QCD with staggered fermions. For an extensive and detailed description on the topic, see [54, 55, 56, 57, 58].

The euclidean space time on the lattice is taken to be Γ_E, a set of points given by,

$$\Gamma_E = \left\{ x \middle| x/a \in \mathbb{Z}^4, 0 \leq x_0 < T, 0 \leq x_k < L, k = \{1,2,3\} \right\}. \tag{2.1.1}$$

Gauge fields on the lattice are parallel transporters $U_\mu(x)$ that reside on the straight lined directed links $(x \to x + a\hat{\mu})$ ($\hat{\mu}$ denotes a unit vector in the μ-direction). They are elements of the gauge group, assumed to be SU(3) unless otherwise specified. Their relation to the Yang Mills gauge fields in the continuum, $A_\mu \in \mathrm{su}(3)$, the Lie algebra of the group, is given by [3] $U_\mu(x) = e^{-aA_\mu(x)}$.

Including the fermions on the lattice is somehow more cumbersome. If they are naively discretised, the so called "doubling problem" is encountered (appeareance of several, 16, in 4 dimensions fermion species per fermion field, in the lattice action). This is a manifestation of the No-go Nielsen and Ninomiya theorem, [59]. This theorem prevents us from solving the species "doubling problem" of Dirac fermions on a lattice in a chirally invariant way (if we want to keep our theory local, translationally invariant and we exige its hamiltonian to be hermitian). Several proposals have been made to implement the quarks on the lattice, either breaking chirality or keeping doublers. The fermion lattice regularisation introduced by Susskind [60] is the one we are going to use for our computations, as we have already stated. These fermions are commonly referred to as staggered fermions. Their construction can be outlined here. Take the naïve discretisation of the action, diagonalise the spin structure. Then, the four dirac

[3] Strictly speaking, there should be a path ordered integration along the path connecting the two points $(x \to x + a\hat{\mu})$. We present a formal expression when introducing the fields at the boundary in the SF, Eq. (2.2.4).

components of the fermions are decoupled. Keep only one single component per site. Hence, the fermionic degrees of freedom are one-component Grassmann variables and will be denoted by $\chi(x)$, $\bar{\chi}(x)$. If temporal and spatial periodicity are assumed, the action can be written as $S = S_g + S_f$ with,

$$S_g[U] = \frac{1}{g_0^2}\sum_p \mathrm{tr}\left\{1 - U(p)\right\}, \tag{2.1.2}$$

$$\begin{aligned} S_f[\chi,\bar{\chi},U] &= a^4 \sum_{x\in\Gamma_E}\sum_{\mu=0}^{3}\frac{1}{2a}\eta_\mu(x)\bar{\chi}(x)\times \\ &\quad \left[U_\mu(x)\chi(x+a\hat{\mu}) - U_\mu^\dagger(x-a\hat{\mu})\chi(x-a\hat{\mu})\right]. \end{aligned} \tag{2.1.3}$$

Here, the sum in the gauge fields runs over all oriented plaquettes p (cf. 2.2) and $U(p)$ denotes the parallel transporter around p. The plaquette field is given by,

$$P_{\mu\nu}(x) = U_\mu(x)U_\nu(x+\hat{\mu})U_\mu^\dagger(x+\hat{\nu})U_\nu^\dagger(x). \tag{2.1.4}$$

$\eta_\mu = (-1)^{\sum_{\nu<\mu} x_\nu}$ in Eq. (2.1.2) are the staggered phase factors that encode the reminiscences of the Dirac structure. Note that we have avoided the inclusion of a mass term in the action since the whole program implemented throughout this work can be carried out for a massless theory. Besides, in [61] Sharatchandra, Thun and Weisz showed that in the staggered formulation no mass counterterm is required if one starts with a zero quark mass. In the same work, the transfer matrix $\mathbb{T}$ (that can be thought of as the time step evolution operator) was shown to be hermitian but not positive definite. Its square is positive and that suffices to define the Hamiltonian of the system as $\mathbb{H} = -(2a)^{-1}\ln\mathbb{T}^2$ (this ensures reflection positivity). Then, $\mathbb{T}^2$ is the natural transfer matrix of the system, and it can be interpreted as the transition amplitude from two time slices to two time slices. As a result, we conclude that the number of distinct temporal lattice sites in the staggered formulation has to be even. If we are in Γ_E, T/a is even for periodic boundary conditions and odd for Dirichlet boundary conditions (since the Γ_E will be extended to $x_0 = T$, where the boundary conditions are established). We underline this feature here because it will be relevant when T, L are determined in the Schrödinger Functional framework.

In order to recover the continuum limit, four component spinors have to be reconstructed from the one component Grassmann variables. Two explicit reconstructions in the Schrödinger Functional framework will be described in section 2.3 (in the free case), inspired in the reconstruction proposed in [62]. Even though we will not give explicit expressions here, two aspects of the result are to be noted:

- The reconstructed fermions ψ can be interpreted of four flavours of quark fields defined on hypercubes of size a. Hence, the effective lattice spacing for the reconstructed fermions will be $\bar{a} = 2a$. This tells us that the number of distinct lattice sites in any given direction is has to be even. Then, if the spatial boundary conditions are periodic, L/a will be an even number.

- There exists a remnant chiral symmetry that is flavour non singlet. By using staggered fermions we have reduced the 16-fold degeneracy of fermionic species to 4. So, regarding the No-go theorem stated above, we have partially cured the doubling problem by partially breaking chiral symmetry.

2.2 Pure gauge theory

In [35], the SF for SU(N) Yang Mills theory has been addressed in the continuum and on the lattice. Its renormalisability has been established up to one loop in perturbation theory (PT). In this section, we will restrict ourselves to give a description on the lattice for the regularisation used in this work, which slightly differs from the one presented in the previous reference for reasons that will be shortly explained cf. subsection 2.2.1.

The SF is well defined on the lattice, since it is a regularised theory. The operators in the Schrödinger picture will be L-periodic gauge fields on a spatial lattice $\Gamma \subset \Gamma_E$ at a fixed value of x_0, $\hat{U}_k(\mathbf{x})$. The wave functions form a Hilbert space $\mathcal{H}$ with inner product and measure given by,

$$\langle \varphi_1 | \varphi_2 \rangle = \int \mathcal{D}[U] \varphi_1(U)^* \varphi_2(U), \quad \mathcal{D}[U] = \prod_{\mathbf{x}\in\Gamma} \prod_{k=1}^{3} dU_k(\mathbf{x}). \tag{2.2.1}$$

Here, the measure denotes the normalised invariant measure of SU(3) (Haar measure). The eigenstates of the operators, $|U\rangle$ form a complete set in the Hilbert space. The wave functions will be given by $\varphi(U) = \langle U|\varphi\rangle$. It has to be noted that only gauge invariant wave functions are physical. We can project any wave function into the physical space by applying the projector operator $\mathbb{P}$. Gauge transformations, $\Lambda(\mathbf{x})$, are L periodic SU(3) elements living on the lattice sites. The links are transformed as $U^\Lambda = V(\mathbf{x}) U_\mu(\mathbf{x}) V(\mathbf{x} + a\hat{k})^{-1}$. The projected wave function reads,

$$(\mathbb{P}\varphi)(U) = \int \prod_{\mathbf{x}\in\Gamma} dV(\mathbf{x}) \varphi(U^\Lambda). \tag{2.2.2}$$

Now, the Schrödinger functional can be given through the transfer matrix ($\mathbb{T} = \mathbb{T}_0\mathbb{P}$) construction [63, 64, 65]. The boundary values of the lattice regularised SF are,

$$W_k(\mathbf{x}) = U_k(x)|_{x_0=0}, \qquad W'_k(\mathbf{x}) = U_k(x)|_{x_0=T}. \tag{2.2.3}$$

To make contact with the continuum limit theory, the relation between W, W' and the continuum boundary values, denoted by C, C' (elements of su(N)) must be established. In the previous section we have defined the gauge links to be the parallel transporters for colour vectors. Then, the relation reads,

$$W_k(\mathbf{x}) = \mathcal{P} \exp\left\{ a \int_0^1 dt C_k(\mathbf{x} + a(1-t)\hat{\mathbf{k}}) \right\}, \tag{2.2.4}$$

and anagolously for $W'_k(\mathbf{x})$. $\mathcal{P}$ denotes that the integral must be path ordered. This construction is gauge covariant. Now, we can give the definition of the Schrödinger Functional in terms of the transfer matrix,

$$\mathcal{Z}[C', C] = \langle W'|(\mathbb{T}_0)^{T/a}\mathbb{P}|W\rangle. \tag{2.2.5}$$

The Schrodinger Functional can also be expressed as a functional integral over all gauge fields with fixed boundary conditions Eq. (2.2.3),

$$\mathcal{Z}[C', C] = \int \mathcal{D}[U]e^{-S[U]}, \qquad \mathcal{D}[U] = \prod_{x,\mu} dU_\mu(x). \tag{2.2.6}$$

The SF is regarded as a functional of the continuum boundary gauge fields C, C'. The action $S[U]$ is taken to be,

$$S_g[U] = \frac{1}{g_0^2}\sum_p w(p)\mathrm{tr}\left\{1 - U(p)\right\}, \tag{2.2.7}$$

where the interpretation of $U(p)$ is the same as in Eq. (2.1.2). $w(p)$ are weight factors whose significance will be discussed later on, cf. chapter 3, 4. For further details on the derivation of Eq. (2.2.6) from the Hamiltonian formalism, we refer the reader to reference [35].

We address the question of the possible appearance of boundary countertems. As we have stated at the beginning of the chapter, they are expected to be proportional to local composite fields of dimension three or less integrated over the hypersurfaces at $x_0 = 0, T$. They have to respect the symmetries of the theory. For a Yang Mills theory there are no candidates for such counterterms. If they exist, they should be expressable in a gauge invariant way, without involving the ghosts. The Chern Simons action is a dimension 3 operator. However it violates parity, so it is also excluded. Hence, we expect the Yang Mills SF to be finite after the coupling is renormalised.

2.2.1 Continuum limit and counting of lattice sites.

The fact of using staggered fermions, as we have anticipated, (cf. section 2.1) will put constraints on the values of $L/a, T/a$. The 4 four-component spinors are usually reconstructed from the 2^4 one-component spinors of the corners of a hypercube, and then assumed to live on a lattice with effective lattice spacing $\bar{a} = 2a$. In order to get an integer multiple of 4 four-component spinor fields, it is thus necessary that L/a is even and T/a odd.

The continuum limit for the SF coupling is usually taken setting $T = L$. Obviously this is not possible if L/a is even and T/a is odd. In order to define the continuum limit, it is convenient to set $T' = T + sa$ with $s = \pm 1$. One may thus interpret T' as the physical time extent and take the continuum limit at fixed $T'/L = 1$.

In conclusion, lattices with $T = L \pm a$ are interpreted as having physical time extent T' with $T' = T + sa$ ($s = \pm 1$), and it is then possible to set $T' = L$. In particular,with

this prescription it is then clear how to double the lattice in order to compute the step-scaling function (cf. chapter 5): one first doubles the dual lattice and then uses the relation $T' = T + sa$ for the doubled lattice size. In this way one would pair, for instance, a $4^3 \times 5$ lattice with a $8^3 \times 9$ lattice, or a $4^3 \times 3$ with a $8^3 \times 7$ lattice.

This fact provides the SF with staggered fermions with a different regularisation, also for the pure gauge part of the action. In particular, O(a) effects will be present in the action. It is desirable to cancel them in order for the continuum limit to be extracted in a cleaner way, cf chapters 2, 3.

2.2.2 Fields at the boundaries

There are two aspects to be taken into account when the values of the fields at the boundaries are chosen,

a) They have to ensure the absolute minimum of the action $S[U]$ to be degenerate up to gauge transformations. The minimising configuration $V \in \mathrm{SU}(3)$ should converge to the minimal classical action in the continuum theory. On the lattice, then, the boundary conditions induce a background field, $B \in \mathrm{su}(3)$ [4], that is unique up to gauge transformations, and is a solution of the equations of motion of the lattice action leading to the absolute minimum of the action on the lattice and in the continuum limit.

b) The renormalised coupling constant will be defined by differentiating the effective action with respect to a parameter of the background field, cf. section 2.4. Hence, B has to be carefully chosen in order for the lattice artifacts of the effective action to be reasonably small.

Concerning b), experience with simulations has shown that the lattice artifacts are not too large if the background fields are taken to be abelian and spatially constant. The *"stability theorem"* of section 5.2 in [35] establishes sufficient conditions for a) to hold. In the following we restrict our attention to the abelian boundary fields which have been used in [38, 66].

$$C_k = \frac{i}{L}\begin{pmatrix} \phi_1 & 0 & 0 \\ 0 & \phi_2 & 0 \\ 0 & 0 & \phi_3 \end{pmatrix}, \qquad C'_k = \frac{i}{L}\begin{pmatrix} \phi'_1 & 0 & 0 \\ 0 & \phi'_2 & 0 \\ 0 & 0 & \phi'_3 \end{pmatrix}, \tag{2.2.8}$$

where the angles satisfy $\sum_{i=1}^{3}\phi_i = \sum_{i=1}^{3}\phi'_i = 0$. A possible choice is,

$$\begin{aligned} \phi_1 &= \eta - \tfrac{\pi}{3}, & \phi'_1 &= -\phi_1 - \tfrac{4\pi}{3}, \\ \phi_2 &= \eta\left(\nu - \tfrac{1}{2}\right), & \phi'_2 &= -\phi_3 + \tfrac{2\pi}{3}, \\ \phi_3 &= -\eta\left(\nu + \tfrac{1}{2}\right) + \tfrac{\pi}{3}, & \phi'_3 &= -\phi_2 + \tfrac{2\pi}{3}, \end{aligned} \tag{2.2.9}$$

[4] We will refer to B and V as the background field, related through $V_\mu(x) = e^{aB_\mu(x)}$.

where η, ν are two dimensionless parameter that will become relevant when the precise definition of the renormalised coupling $\bar{g}^2$ is discussed, cf. section 2.4. We have taken η to be 0. Then, the links at the boundary will take the values,

$$W_k(\mathbf{x}) = \mathrm{diag}\left(e^{-\frac{i\pi}{3L}a}, 1, e^{\frac{i\pi}{3L}a}\right), \qquad W'_k(\mathbf{x}) = \mathrm{diag}\left(e^{-\frac{i\pi}{L}a}, e^{\frac{i\pi}{3L}a}, e^{\frac{2i\pi}{3L}a}\right). \tag{2.2.10}$$

2.2.3 Equations of motion

We solve the equations of motion relying on the fact that the minimal action configuration, given by the background field $B_\mu(x) \in \mathrm{su}(3)$ is unique up to gauge transformations. This is guaranteed for the boundary conditions chosen by the *"stability theorem"* aforementioned.

The plaquette field is given by Eq. (2.1.4). Taking into account the weight factors $w[P_{\mu\nu}(x)]$, we define the covariant divergence of the plaquette as,

$$\begin{aligned} d_w^* P(x,\mu) &= \sum_{\nu=0}^{3} \{ w[P_{\mu\nu}(x)] P_{\mu\nu}(x) \\ &- w[P_{\mu\nu}(x-\hat{\nu})] U_\nu^\dagger(x-\hat{\nu}) P_{\mu\nu}(x-\hat{\nu}) U_\nu(x-\hat{\nu}) \big\} . \end{aligned} \tag{2.2.11}$$

The lattice action will be stationary if and only if the traceless antihermitian part of $d_w^* P(x,\mu)$ vanishes,

$$d_w^* P(x,\mu) - d_w^* P^\dagger(x,\mu) - \frac{1}{3}\mathrm{tr}\ \left\{ d_w^* P(x,\mu) - d_w^* P^\dagger(x,\mu) \right\} = 0. \tag{2.2.12}$$

We solve the equations of motion in order to obtain an analytic expression of the classical action as a function of $(L, \phi_i, \phi'_i, s, w)$. Also and albeit not needed, a relaxation program has been written to guarantee the background field being indeed a minimal action configuration. This program has also been run with satisfactory results for lattices of size 4×3 where the stability theorem does not hold.

It has to be noted that a discussion concerning the weight factors has not been carried out yet. This issue will be postponed until we address O(a) Symanzik improvement (cf. chapters 3, 4) [67]. However, we need to specify their values if we want to solve the equations of motion. So, we introduce,

$$w(p) = \begin{cases} \frac{1}{2}c_s(g_0) & p \text{ spatial plaquette at } x_0 = 0, T, \\ c_t(g_0) & p \text{ time - like plaquette attached to a boundary plane,} \\ 1 & \text{in all other cases,} \end{cases} \tag{2.2.13}$$

c_t, c_s can be perturbatively expanded in powers of the bare coupling,

$$c_x(g_0) = c_x^{(0)} + c_x^{(1)} g_0^2 + \cdots \qquad x = s, t. \tag{2.2.14}$$

In the following subsections, only $c_t^{(0)}$ will be involved. It is to be chosen in such a way that the action leads to the continuum limit with no linear lattice artifacts present (cf. chapter 3,4).

2.2.4 Analytic solution of the equations of motion

Assumming:

- the temporal gauge to be chosen, i.e. $U_0(x) = \mathbb{1}_{3\times3}$,
- the links of the solution to be spatially constant, i.e., $U_k(x) = e^{aB_k(x_0)}$,
- the fields $B_k(x_0)$ (traceless) to be diagonal in their colour structure,

we will present two different ways of solving the equations of motion. $F_{\mu\nu} = F^a_{\mu\nu}T^a$ is taken to be the field strength tensor, where T^a represent the Gell-Mann matrices. The background field strength tensor is denoted as $G_{\mu\nu}$. The previous assumptions taken, only the components $G_{0k} = -G_{k0}$ will be non zero,

$$G_{0k}(x_0) = \partial_0 B_k(x_0) = \frac{B_k(x_0+a) - B_k(x_0)}{a} = f(x_0). \tag{2.2.15}$$

Note that $f(x_0)$ is independent of the spatial index, k, as the boundary conditions, Eq(2.2.8) are the same for the three spatial directions. With these assumptions, Eqs(2.2.12) reduce to,

$$\begin{aligned}
0 &= \frac{1}{3}\mathrm{tr}\left\{c_t^{(0)}\sinh\left\{a^2f(0)\right\} - \sinh\left\{a^2f(a)\right\}\right\} \\
&\quad - \left\{c_t^{(0)}\sinh\left\{a^2f(0)\right\} - \sinh\left\{a^2f(a)\right\}\right\}, \\
0 &= \frac{1}{3}\mathrm{tr}\left\{c_t^{(0)}\sinh\left\{a^2f(T-a)\right\} - \sinh\left\{a^2f(T-2a)\right\}\right\} \\
&\quad - \left\{c_t^{(0)}\sinh\left\{a^2f(T-a)\right\} - \sinh\left\{a^2f(T-2a)\right\}\right\}, \\
0 &= \frac{1}{3}\mathrm{tr}\left\{\sinh\left\{a^2f(x_0)\right\} - \sinh\left\{a^2f(x_0-a)\right\}\right\} \\
&\quad - \left\{\sinh\left\{a^2f(x_0)\right\} - \sinh\left\{a^2f(x_0-a)\right\}\right\}, \quad \text{with } x_0 \in [2a, T-2a]^5.
\end{aligned} \tag{2.2.16}$$

Here, $f(x_0)$ is a diagonal traceless matrix,

$$f(x_0) = \mathrm{diag}(f_1(x_0), f_2(x_0), f_3(x_0)). \tag{2.2.17}$$

We now expand $f_\alpha(x_0)$ in powers of a,

$$f_\alpha(x_0) = \sum_{n=0}^{\infty} a^n f_{\alpha,n}(x_0). \tag{2.2.18}$$

Substituting this expression in Eqs(2.2.16) and performing a Taylor expansion, we proved by induction that $f_{\alpha,n}(x_0)$ takes the form,

$$f_{\alpha,n}(x_0) = \begin{cases} h_{\alpha,n} & \text{if } x_0 = 0, T-a, \\ f_{\alpha,n} & \text{if } x_0 \in [a, T-2a], \end{cases} \tag{2.2.19}$$

with x_0 - independent constants $h_{\alpha,n}$ and $f_{\alpha,n}$, related through,

$$h_{\beta,n} = \frac{1}{c_t^{(0)}}\left\{-f_{\beta,n} + \frac{1}{3}\sum_{\alpha=1}^{3}\left[c_t^{(0)}P(\vec{h}_{\alpha,n}) - P(\vec{f}_{\alpha,n})\right]\right\}, \tag{2.2.20}$$

where $\vec{f}_{\alpha,n} = (f_{\alpha,0}, \cdots, f_{\alpha,n-1})$ and P is a polynomial in its arguments. After some algebra, the expression of the fields $B_k(x_0)$ can be written as a linear function of f.

$$B_k(x_0) = \begin{cases} C_k & x_0 = 0 \\ f\left(x_0 - \frac{T}{2}\right) + \frac{C_k + C'_k}{2} & x_0 \in [a, T-a], \\ C'_k & x_0 = T. \end{cases}$$

The equations fulfilled by the f_α's are (as a function of T'),

$$\begin{aligned} 0 &= \tfrac{1}{3}\sum_{\alpha=1}^{3}\left\{c_t^{(0)}\sinh\left\{f_\alpha a\left[a\left(1+\tfrac{s}{2}\right)-\tfrac{T'}{2}\right]+a\tfrac{\phi'_\alpha-\phi_\alpha}{2L}\right\}-\sinh\left\{a^2 f_\alpha\right\}\right\}- \\ &\quad c_t^{(0)}\sinh\left\{f_\beta a\left[a\left(1+\tfrac{s}{2}\right)-\tfrac{T'}{2}\right]+a\tfrac{\phi'_\beta-\phi_\beta}{2L}\right\}-\sinh\left\{a^2 f_\beta\right\}, \end{aligned} \tag{2.2.21}$$

for $\beta = 1, 2, 3$. Since $\phi'_2 - \phi_2 = \phi'_3 - \phi_3$, then, $f_2 = f_3$. Besides, f has to be traceless. Thus, $f_1 = -2f_2 = -2f_3$. Eqs. (2.2.21) are reduced to the following equation for $f_2 = f_3$,

$$\begin{aligned} 0 &= \left\{c_t^{(0)}\sinh\left\{-2a\left(f_2\left[a\left(1+\tfrac{s}{2}\right)-\tfrac{T'}{2}\right]+a\tfrac{\phi'_2-\phi_2}{2L}\right)\right\}-\sinh\left\{-2a^2 f_2\right\}\right\} \\ &- \left\{c_t^{(0)}\sinh\left\{af_2\left[a\left(1+\tfrac{s}{2}\right)-\tfrac{T'}{2}\right]+a\tfrac{\phi'_2-\phi_2}{2L}\right\}-\sinh\left\{a^2 f_2\right\}\right\}. \end{aligned} \tag{2.2.22}$$

To get the solution we have written two programs in Maple. One that solves Eq. (2.2.22) expanding f in powers of a and the second one that solves the equation using Newton's method.

Taylor expansion

In the Maple program, 15 digits of precision have been used. f_2 defined above has been expanded as a Taylor series,

$$f_2 = f_{2,0} + a f_{2,1} + a^2 f_{2,2} + \cdots$$

The analytic expression of the $f_{2,i}$ coefficients as function of $\{\phi'_2, \phi_2, T', s, c_t^{(0)}\}$ are,

$$\begin{aligned} f_{2,0} &= \frac{\phi'_2 - \phi_2}{T'}, \\ f_{2,n} &= f_{2,0}\left(\frac{-2+(2+s)c_t^{(0)}}{c_t^{(0)}T'}\right)^n, \qquad n \in \{1,2,3,4\} \\ f_{2,5} &= f_{2,0}\left(\frac{-2+(2+s)c_t^{(0)}}{c_t^{(0)}T'}\right)^5 - (f_{2,0})^3\,\frac{-1+\left(c_t^{(0)}\right)^2}{T'\left(c_t^{(0)}\right)^3}, \\ f_{2,6} &= f_{2,0}\left(\frac{-2+(2+s)c_t^{(0)}}{c_t^{(0)}T'}\right)^6 - 4\,(f_{2,0})^3\,\frac{\left[-1+\left(c_t^{(0)}\right)^2\right]\left[-2+(2+s)c_t^{(0)}\right]}{(T')^2\left(c_t^{(0)}\right)^3}, \end{aligned} \tag{2.2.23}$$

We have calculated the coefficients until $O(a^{11})$. In order to evaluate them numerically, we need the values of $c_t^{(0)}$. Although this will be justified in chapter 3, we present the values of $c_t^{(0)}$ in Table 2.1.

T	s	$c_t^{(0)}$
L	0	1
$L+a$	-1	2
$L-a$	1	2/3

Table 2.1: $c_t^{(0)}$ coefficients.

Numerical results

The numerical evaluation of the the results obtained coincide with the ones obtained using the Newton's method up to the level of accuracy considered here. We show the results obtained with the Newton's method in Table 2.2. The quantities $\frac{f_2(s=\pm 1)}{f_{2,0}} - 1$ for the colour index 2 (or 3, as they are the same) are shown. The results for the colour index 1 can be obtained from the results of f_2 by just imposing, $f_1 = -2f_2$. From the results obtained for f, the value of the action has been calculated. In Table

L/a	$s=-1;\ f_2/f_{2,0}-1$	$s=1;\ f_2/f_{2,0}-1$
4	0.0004023308492	-0.002019841719
6	$5.289988613e-05$	-0.0002648375787
8	$1.255081346e-05$	$-6.278415351e-05$
10	$4.112451666e-06$	$-2.056667544e-05$
12	$1.652676212e-06$	$-8.264286162e-06$
14	$7.646296408e-07$	$-3.823382995e-06$
16	$3.921842614e-07$	$-1.960993874e-06$
18	$2.176340897e-07$	$-1.088196121e-06$
20	$1.285106520e-07$	$-6.425633709e-07$
22	$7.979496710e-08$	$-3.989791809e-07$
24	$5.164551015e-08$	$-2.582295584e-07$
26	$3.461162270e-08$	$-1.730590993e-07$
28	$2.389452992e-08$	$-1.194731595e-07$
30	$1.692319419e-08$	$-8.461624684e-08$
32	$1.225571616e-08$	$-6.127873605e-08$
34	$9.050946176e-09$	$-4.525482130e-08$
36	$6.801051290e-09$	$-3.400531075e-08$
38	$5.190038275e-09$	$-2.595022489e-08$
40	$4.015952611e-09$	$-2.007978425e-08$

Table 2.2: Values of f_2 for different lattice sizes.

2.3. results of the action $S(s=0)$ and the relative difference for the cases $s=\pm 1$ are shown. Results on Tables 2.2, 2.3 have been checked by comparing them with an independent calculation [68].

2.2.5 Cooling program

We have written a program which performs a cooling to calculate the action. It starts by choosing a gauge configuration randomly and then, the action is minimised. The action has been minimised by minimising the SU(2) subgroups of every contributing

L/a	$s=0$	$s=-1$	$s=1$
4	0.001070360092	0.000870178094	0.002073989603
6	0.0002115179988	0.0001850929179	0.0003437559833
8	$6.693034836e-05$	$6.065678204e-05$	$9.830820437e-05$
10	$2.741520033e-05$	$2.535921940e-05$	$3.769657709e-05$
12	$1.322115672e-05$	$1.239486580e-05$	$1.735291297e-05$
14	$7.136472337e-06$	$6.754169253e-06$	$9.048066017e-06$
16	$4.183275102e-06$	$3.987186489e-06$	$5.163742356e-06$
18	$2.611600059e-06$	$2.502784230e-06$	$3.155687762e-06$
20	$1.713471551e-06$	$1.649216695e-06$	$2.034749201e-06$
22	$1.170324435e-06$	$1.130427151e-06$	$1.369812306e-06$
24	$8.263273023e-07$	$8.005046381e-07$	$9.554412927e-07$
26	$5.999343453e-07$	$5.826285781e-07$	$6.864635100e-07$
28	$4.460309800e-07$	$4.340837377e-07$	$5.057673616e-07$
30	$3.384637438e-07$	$3.300021588e-07$	$3.807717604e-07$
32	$2.614551952e-07$	$2.553273439e-07$	$2.920945034e-07$
34	$2.051547293e-07$	$2.006292601e-07$	$2.277821052e-07$
36	$1.632251991e-07$	$1.598246758e-07$	$1.802278336e-07$
38	$1.314809491e-07$	$1.288859314e-07$	$1.444560487e-07$
40	$1.070920560e-07$	$1.050840806e-07$	$1.171319401e-07$

Table 2.3: Values of $1 - S_{latt}(s)/S_{cont}$ for $s = 0, \pm 1$.

link [69, 70]. Every time the cooling function is called, it runs over the entire lattice. Around 400 steps are needed to find the minimum for $L/a = 4$. The number of steps increases with increasing lattice volume and for $L/a = 8$ around 10^3 are needed. As the action function is a complicated function of the fields, there are relative minima as well. The program does not always get to the absolute minimum. An overrelaxation function has been developed. This function changes the configuration without changing the value of the action. In the program we have included functions that try to minimise the rounding off effects. We have used double precision numbers and the sumations have been performed using Kahan's method. We have refreshed the structure of the gauge configuration in order to restore unitarity. The larger the lattice, the lower the precision. The action value for $L = 4a$ lattices has been also calculated. In Table 2.4, we present the values of the action obtained as well as the precision level (we include results for odd L/a).

To obtain the accuracy shown in Table. 2.4, we have declared the variables as long double. Using this declaration with the compiler used, the numbers are accurate to the twentieth decimal place. The rounding errors get bigger for bigger lattices. For a 4^4 lattice, the links $U_k(x)$ in the temporal gauge obtained by the cooling program, coincide with the analytic solution until the eleventh decimal place while for a 8^4 lattice the accuracy only arises to the eighth decimal place. The value of the action is more precise than the value of the links. This fact can be justified as follows. The temporal plaquettes are the only non zero contributions to the action in the temporal gauge. In the situation considered, as we have shown in previous subsections, they must be independent of the position. They must be all the same. And they turn to be the product of two spatial links evaluated in x_0 and $x_0 - a$. Thus, the value of the action is proportional to tr $\{P_{0k} - \mathbb{1}\}$. If we assume the rounding errors to be randomly

distributed, the relative error of the action will be expected to be smaller than the one of the fields. These results are in agreement with the previous ones in tables 3, 4 within

L/a	S, $s=0$	S, $s=-1$	S , $s=1$
4	19.71808074083723	19.72203217508621	19.698269888348
5	19.730552072921	19.73184914504	19.724056950415
6	19.735033604235	19.73555521442	19.732423331048
7	19.7369550270	19.73719642868	19.735747404993
8	19.7378876500	19.7380114853	19.7372682760

Table 2.4: Values of the action obtained with the cooling program

the quoted accuracy. Note that the value of the continuum action is,

$$S_{cont} = 2\pi^2 = 19.73920880217871724. \tag{2.2.24}$$

The solutions obtained with the cooling program assure that our ansatz to solve the equations of motion leads us to the minimal configuration of the action. We can even use this ansatz for the case $L/a = 4$ where the stability theorem in [35] does not hold.

2.3 Including staggered fermions

In [47, 44], Sint formulated the SF with fermion fields. Since classical fermions are described physically by a first order differential equation, only half the degrees of freedom can be fixed at each boundary, in order not to overconstrain them. They are required to satisfy,

$$\begin{aligned} P_+\psi(x)|_{x_0=0} &= \rho_+(\mathbf{x}), & P_-\psi(x)|_{x_0=T} &= \rho'_-(\mathbf{x}), \\ \bar\psi(x)P_-|_{x_0=0} &= \bar\rho_-(\mathbf{x}), & \bar\psi(x)P_+|_{x_0=T} &= \bar\rho'_+(\mathbf{x}), \end{aligned} \tag{2.3.1}$$

where $P_\pm = \frac{1}{2}(1 \pm \gamma_0)$. The structure and the notation of the euclidean Dirac gamma matrices is given in Appendix A.1. One advantage of these boundary conditions is that the system acquires a mass gap $\propto 1/T$ and there is no infrared divergence. The finite volume plays the role of an infrared cutoff. That happens also when the masses are set to 0. That means that numerical simulations can be performed at the chiral limit. In his work, Sint first established the SF on the lattice with Wilson fermions, through the transfer matrix formalism. He noticed there were two additional terms in the action. They are boundary terms at $x_0 = 0, T$, summed over the corresponding hyperplanes. The question is whether this action leads to a sensible theory in the continuum. The continuum limit of these boundary terms leads to,

$$S_f^{\text{Boun}} = -\int_0^L d^3\mathbf{x}\left[\bar\psi(x)P_-\psi(x)\right]_{x_0=0} - \int_0^L d^3\mathbf{x}\left[\bar\psi(x)P_+\psi(x)\right]_{x_0=T}. \tag{2.3.2}$$

Now, it would be desirable to obtain them in the continuum without any reference to the lattice, so that we discard the possibility of them being just a remnant of the

lattice formulation. That was considered by Sint and he concluded that if we want the fermionic fields to satisfy Eq. (2.3.1), then the boundary terms Eq. (2.3.2) emerge naturally after imposing Hamilton's principle on the classical action. Thus, no reference to the regularisation is needed, once we know the boundary conditions, Eq. (2.3.1).

The SF with staggered fermions has been discussed in [49, 50]. The establishment of the SF through the transfer matrix formalism is carried out in both works, as well as the reconstruction of the staggered fermions and the derivation of the boundary conditions they have to satisfy. The reader might wonder why we are discussing the case with staggered fermions if there are already works on the topic. There are three main reasons,

- As we have stated in the previous section, cf. sucsection 2.2.1, the fact that $T \neq L$ introduces boundary O(a) effects in the pure Yang Mills action already at tree level. In chapters 3, 4 we will show how to cancel them at tree level and one loop in perturbation theory. Besides, there are boundary O(a) effects coming from the fermionic part of the action that need to be cancelled as we will see. This is not considered in the previously mentioned works.

- The reconstruction of the 4-component fermions is revisited in detail. By means of a geometrical interpretation, we reconstruct the fermions in three different ways. Besides, a deeper look into the structure of the boundary conditions is taken.

- Simulations to compute the scaling evolution of the strong coupling in a 1-loop O(a) improved model with four flavours of staggered quarks have been run for the first time.

For chirally twisted fermions [71, 72], the formulation of the SF has been performed in [73, 74]. Since the fermionic fields suffer a chiral rotation, so do the boundary conditions. Let $\psi(x), \bar{\psi}(x)$ be isospin doublets of quark and antiquark fields satisfying the homogeneous version of Eq. (2.3.1). Then, if we perform a chiral rotation,

$$\psi(x) = e^{i\alpha\gamma_5\tau_3/2}\psi'(x), \qquad \bar{\psi}(x) = \bar{\psi}'(x)e^{i\alpha\gamma_5\tau_3/2}, \tag{2.3.3}$$

with τ_3 being a SU(2) flavour matrix (the diagonal Pauli matrix, in this case), then the rotated fields satisfy the chirally rotated boundary conditions, that read,

$$\begin{aligned} P_+(\alpha)\psi'(x)|_{x_0=0} &= 0, & P_-(\alpha)\psi'(x)|_{x_0=T} &= 0, \\ \bar{\psi}'(x)P_+(\alpha)|_{x_0=0} &= 0, & \bar{\psi}'(x)P_-(\alpha)|_{x_0=T} &= 0, \end{aligned} \tag{2.3.4}$$

with the projectors,

$$P_\pm(\alpha) = \tfrac{1}{2}\left(1 \pm i\gamma_0\gamma_5\tau_3\right). \tag{2.3.5}$$

The chiral rotation is going to become relevant in the discussion of the boundary conditions for the reconstructed staggered fermions.

The SF formulation for fermions that satisfies the Ginsparg-Wilson relation [75] has been addressed by Taniguchi for domain-wall [76] and overlap [77] fermions. He defined

the SF through and orbifold projection. The boundary conditions are determined by the $\mathbb{Z}_2$ orbifold system which is the product of a time reflection and a chiral rotation. However, the chiral rotation becomes technically cumbersome on the lattice. In [78], Lüscher proposes a construction of the SF with exact chiral symmetry. He states that the symmetries of the SF in lattice QCD should ideally be the same if the Dirac operator preserves chiral symmetry in infinite volume via the Ginsparg-Wilson relation. In the presence of boundaries, the Dirac operator as well as the Ginsparg-Wilson relation should be modified (locally and in relation with the boundary conditions). Otherwise, the Schrödinger functional would not have the correct continuum limit. The solution is based on universality considerations. The idea is that SF boundary conditions do not require any fine-tuning and will thus be satisfied automatically in the continuum limit, as long as the lattice respects locality and the obvious lattice simmetries. he gives an explicit construction of the Dirac operator.

We can combine Lüscher's idea [78] with the chiral twist proposal [73, 74] and apply them to our setup. After some dissertation about the scalar fields, Lüscher concludes that the boundary conditions Eq. (2.3.1) arise naturally. The boundary conditions at $x_0 = 0$, that arise naturally in the continuum limit are of the form $B\psi(x)|_{x_0=0}$, where B is a constant matrix in Dirac and colour space. At $x_0 = T$, the boundary conditions are linked to those at $x_0 = 0$ by time reflection symmetry. Charge conjugation determines the ones for the antiquarks. The conditions over B are,

1. Boundary conditions have to respect the symmetries of the lattice theory.

2. B cannot have maximal rank, since then the fermionic fields would be overconstrained, leading to a vanishing propagator.

The candidates for that in the Wilson approach are $P_\pm$ given above. In Appendix B, a list of the symmetries of the staggered fermions is provided. They are given in terms of the one component Grassmann fields, standard four component reconstructed fermions and in terms of what we will call SF four component spinors. In the literature, we can find such a list in inifinite volume in [79, 80, 81]. In the SF a list can be seen in [50]. We include the transformations of the chirally rotated fermions here. We will address them in the following paragraph. Let us focus on the standardly reconstructed fermions. If we apply the conditions 1,2 stated above, we arrive at the conclusion that B has to take the form of $Q_\pm = \frac{1}{2}(1 \pm i\gamma_0\gamma_5\tau_{05})$, where τ_{05} is a SU(4) flavour matrix (notation given in Appendix A.2).

Now, these boundary conditions suggest we can perform a chiral twist (which will be analogous to Eq. (2.3.3), but with the sublety that now, our flavour group happens to be SU(4)) to recover the standard SF boundary conditions. That was already proposed in [50, 82] . So, once the fermions are reconstructed, we can chirally rotate them so that they satisfy the standard SF boundary conditions Eq. (2.3.1). As a final remark, note (cf. Appendix B) that the remnant chiral symmetry of the staggered fermions is lost when the chiral rotation is performed. That was to be expected if we wanted to restore standard SF boundary conditions, since they explicitly break chiral symmetry.

In what follows we will justify and write the SF action with staggered fermions in terms of the one component spinors. In order to explicitly derive the boundary conditions this action leads to, we will reconstruct the 4 component fields. The reconstruction is going to be performed in three different fashions and some discussion will be given on the issue. Finally, we will construct the free fermionic propagator.

2.3.1 SF fermionic action with staggered fermions

In [49] it was shown that for staggered fermions all degrees of freedom can be fixed at both boundaries. This has to do with the fact that the continuum limit fermions are reconstructed from 16 one component Grassmann fields living at the edges of an hyperbube of size a. The effective lattice spacing for the reconstructed variables is $\bar{a} = 2a$. It can also be seen from the transfer matrix. As we have stated before, the natural transfer matrix in this formulation is $\mathbb{T}^2$ and it can ve regarded as a transition amplitude from two time-slices to two time-slices. The Schrödinger functional including the fermionic fields can thus be represented as the path integral,

$$\mathcal{Z}[W, \chi^{(0)}, \bar{\chi}^{(0)}; W', \chi^{(T)}, \bar{\chi}^{(T)}] = \int [DU] \int \prod_{x_0=a}^{T-a} \prod_{\mathbf{x}} [d\bar{\chi}(x_0, \mathbf{x}) d\chi(x_0, \mathbf{x})] e^{-S_G - S_f}. \tag{2.3.6}$$

Here, we have taken the SF to explicitly depend on W, W', the boundary values of the link variables. This is exactly equivalent to taking the SF as a function of C, C', the gauge fields at the boundary. S_G is the pure gauge action and $[DU]$ the Haar measure over gauge fields. The fermionic contribution to the action is given by [49, 50],

$$\begin{aligned} S_f &= a^4 \sum_{x_0=a}^{T-a} \sum_{\mathbf{x}} \sum_{\mu} \frac{1}{2a} \eta_\mu(x) \bar{\chi}(x) \left[\lambda_\mu U_\mu(x) \chi(x + a\hat{\mu}) - \lambda_\mu^* U_\mu^\dagger(x - a\hat{\mu}) \chi(x - a\hat{\mu}) \right] \\ &+ S_B^{(0)} + S_B^{(T)}, \end{aligned} \tag{2.3.7}$$

where $\eta_\mu = (-1)^{\sum_{\nu<\mu} x_\nu/a}$, the usual staggered phase factors. We also included a constant phase factor [66],

$$\lambda_\mu = e^{ia\theta_\mu/L}, \qquad \theta_0 = 0, \quad -\pi < \theta_k \leq \pi. \tag{2.3.8}$$

It could be removed by an abelian gauge transformation, $\chi(x) \to e^{-i\theta x/L} \chi(x)$, but as a result, the periodic boundary conditions imposed in the spatial directions,

$$\chi(x + L\hat{k}) = \chi(x), \tag{2.3.9}$$

would change. This formulation, where λ_μ is to appear in the difference operators, is technically simpler. At the boundaries, the fields take on their boundary values,

$$\begin{aligned} \chi(0, \mathbf{x}) &= \chi^{(0)}(\mathbf{x}), \qquad & \bar{\chi}(0, \mathbf{x}) &= \bar{\chi}^{(0)}(\mathbf{x}), \\ \chi(T, \mathbf{x}) &= \chi^{(T)}(\mathbf{x}), \qquad & \bar{\chi}(T, \mathbf{x}) &= \bar{\chi}^{(T)}(\mathbf{x}), \end{aligned} \tag{2.3.10}$$

with $\chi^{(0)}, \bar{\chi}^{(0)}, \chi^{(T)}, \bar{\chi}^{(T)}$ independent complex Grassmann fields. The additional boundary terms of the action are,

$$\begin{aligned} S_B^{(0)} &= a^3 \sum_{\mathbf{x}} \sum_{k=1}^{3} \frac{1}{2} \eta_k(0,\mathbf{x}) \bar{\chi}^{(0)}(\mathbf{x}) \left(\lambda_k W_k(\mathbf{x}) \chi^{(0)}(\mathbf{x} + a\hat{\mathbf{k}}) - \lambda_k^* W_k^\dagger(\mathbf{x} - a\hat{\mathbf{k}}) \chi^{(0)}(\mathbf{x} - a\hat{\mathbf{k}}) \right) \\ &+ a^3 \sum_{\mathbf{x}} \frac{1}{2} \eta_0(0,\mathbf{x}) \bar{\chi}^{(0)}(\mathbf{x}) U_0^\dagger(a,\mathbf{x}) \chi(a,\mathbf{x}), \end{aligned} \tag{2.3.11}$$

$$\begin{aligned} S_B^{(T)} &= a^3 \sum_{\mathbf{x}} \sum_{k=1}^{3} \frac{1}{2} \eta_k(T,\mathbf{x}) \bar{\chi}^{(T)}(\mathbf{x}) \left(\lambda_k W_k'(\mathbf{x}) \chi^{(T)}(\mathbf{x} + a\hat{\mathbf{k}}) - \lambda_k^* W_k'^\dagger(\mathbf{x} - a\hat{\mathbf{k}}) \chi^{(T)}(\mathbf{x} - a\hat{\mathbf{k}}) \right) \\ &+ a^3 \sum_{\mathbf{x}} \frac{1}{2} \eta_0(T,\mathbf{x}) \bar{\chi}^{(T)}(\mathbf{x}) U_0^\dagger(T-a,\mathbf{x}) \chi(T-a,\mathbf{x}). \end{aligned} \tag{2.3.12}$$

We state as a reminder that T has to be odd and L even. As we have included the λ_μ factors in the action, the fermionic fields satisfy periodic boundary conditions in the spatial directions, as stated in Eq. (2.3.9).

2.3.2 Reconstruction of the four-component spinors

We construct four-component spinors from the one- component Grassmann fields $\chi, \bar{\chi}$. Note that the reconstruction is going to be carried out in the free fermionic action. Including the gauge fields would be algebraically more cumbersome and not necessary for our purposes. The standard way of doing this reconstruction [62] has been slightly modified here:

- The euclidean time index has been labelled with 0. The motivation for this notation to be used is that it makes it easier to establish an analogy with the same calculation carried out with Wilson quarks. This notation is also consistent with the previous works [68, 83], that deal with the gauge action.

- The four component spinors reside in a coarse lattice. $\bar{a} = 2a$ denotes the lattice spacing of this coarse lattice. As we have pointed out before, L/a is an even number, so $L/\bar{a} = L/(2a)$ is an integer. The question is what happens to the time extent T/a. We have to distinguish the two cases, $T = L \pm a = L - sa$, $s = \pm 1$. As we already discussed in [83] (cf. section 2.2.1), the continuum limit will be taken setting $L = T' = T + sa$. In the case $s = -1$, we set $x = 2y + \xi$, with $\xi_\mu = \{0, 1\}$, as it has been done in [49, 50]. This variable transformation corresponds to Figure 2.1. The fine lines represent the fine lattice where the single component fermions live, whereas the thick lines represent the coarse lattice where the reconstructed fermionic fields live. The one-component fermionic fields which constitute a reconstructed quark field are the ones contained in the circles. For $s = 1$, we extend the single component fermionic fields to all points with $x_0 = -a$ and $x_0 = T + a$. This case is represented in Figure 2.2, There are various ways available to reconstruct them. The dashed lines correspond to the

artificially included single component fermionic fields. The relationship between the variables x and y corresponding to the reconstruction sketched in Figure 2.2 in the left and the right hand side respectively,

$$\begin{aligned} x_0 &= 2y_0 - a + \xi a, & \mathbf{x} &= 2\mathbf{y} + \boldsymbol{\xi} a, \\ x_0 &= 2y_0 - \xi a, & \mathbf{x} &= 2\mathbf{y} + \boldsymbol{\xi} a. \end{aligned} \tag{2.3.13}$$

The interpretation of Figure 2.2 is the same as Figure 2.1.

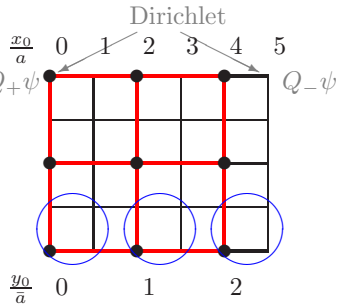

Figure 2.1: Reconstruction on a $T = L + a$ lattice.

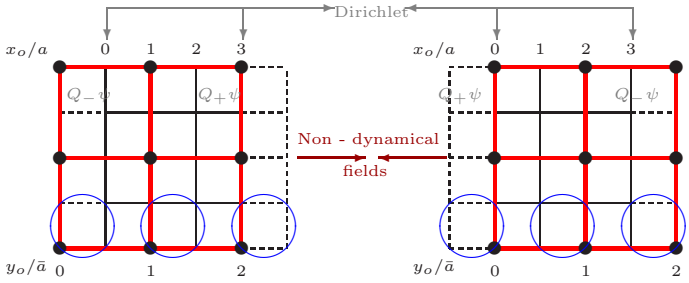

Figure 2.2: Reconstruction on a $T = L - a$ lattice. Left $s = 1^+$, right, $s = 1^-$

We will skip the derivation of the reconstruction here. See appendix C for more details. Concerning the notation,

- S_f^{-1} refers to the case $s = -1$. Boundary terms, $S_{B,-1}^{(0)}, S_{B,-1}^{(T)}$.
- $S_f^{1^+}$ is the action corresponding to the reconstruction sketched in the left hand side of Figure 2.2. Boundary terms, $S_{B,1^+}^{(0)}, S_{B,1^+}^{(T)}$.
- $S_f^{1^-}$ is the action referring to the reconstruction sketched in 2.2. $S_{B,1^-}^{(0)}, S_{B,1^-}^{(T)}$.

Now, introduding the projectors,

$$Q_\pm = \frac{1}{2}(1 \pm i\gamma_0\gamma_5\tau_{05}), \tag{2.3.14}$$

where τ_{05} is a flavour matrix (cf. appendix A.2.). The actions S_f^s in terms of the four component spinors in all cases are now given,

1. Case $s = -1$

$$S_f^{-1} = \bar{a}^4 \sum_{y_0=\bar{a}}^{T'-\bar{a}} \sum_{\mathbf{y}} \sum_{\mu} \bar{\psi}(y) \left[\gamma_\mu D_\mu + i\frac{\bar{a}}{2}\gamma_5\tau_{\mu 5}\Delta_\mu\right] \psi(y) + S_{B,-1}^{(0)} + S_{B,-1}^{(T')}. \quad (2.3.15)$$

The contributions from the boundaries are,

$$\begin{aligned} S_{B,-1}^{(0)} &= \bar{a}^4 \sum_{\mathbf{y}} \sum_{k=1}^{3} \bar{\psi}(0,\mathbf{y}) \left[\gamma_k D_k + i\frac{\bar{a}}{2}\gamma_5\tau_{k5}\Delta_k\right] \psi(0,\mathbf{y}) \\ &\quad + \bar{a}^3 \sum_{\mathbf{y}} \bar{\psi}(0,\mathbf{y}) \left[Q_-\gamma_0\psi(\bar{a},\mathbf{y}) - i\gamma_5\tau_{05}\psi(0,\mathbf{y})\right], \quad (2.3.16) \\ S_{B,-1}^{(T')} &= \bar{a}^4 \sum_{\mathbf{y}} \sum_{k=1}^{3} \bar{\psi}(T',\mathbf{y}) \left[\gamma_k D_k + i\frac{\bar{a}}{2}\gamma_5\tau_{k5}\Delta_k\right] \psi(T',\mathbf{y}) \\ &\quad - \bar{a}^3 \sum_{\mathbf{y}} \bar{\psi}(T',\mathbf{y}) \left[Q_+\gamma_0\psi(T'-\bar{a},\mathbf{y}) + i\gamma_5\tau_{05}\psi(T',\mathbf{y})\right]. \quad (2.3.17) \end{aligned}$$

The projectors $Q_\pm$ project onto the boundary fields,

$$\begin{aligned} Q_+\psi(0,\mathbf{y}) &= \rho(\mathbf{y}), \qquad & Q_-\psi(T',\mathbf{y}) &= \rho'(\mathbf{y}), \\ \bar{\psi}(0,\mathbf{y})Q_+ &= \bar{\rho}(\mathbf{y}), \qquad & \bar{\psi}(T',\mathbf{y})Q_- &= \bar{\rho}'(\mathbf{y}). \end{aligned} \quad (2.3.18)$$

The boundary four component spinors ρ and ρ' are related to the boundary one component spinors $\chi^{(0)}(\mathbf{x}), \chi^{(T)}(\mathbf{x})$ as,

$$\rho^{\alpha a}(\mathbf{y}) = \frac{1}{4}\sum_{\boldsymbol{\xi}} R^{\alpha a}_{(\boldsymbol{\xi},0)}\chi^{(0)}_{\boldsymbol{\xi}}(\mathbf{y}), \quad \rho'^{a\alpha}(\mathbf{y}) = \frac{1}{4}\sum_{\boldsymbol{\xi}} R^{a\alpha}_{(\boldsymbol{\xi},1)}\chi^{(T)}_{\boldsymbol{\xi}}(\mathbf{y}), \quad (2.3.19)$$

and analogously for $\bar{\rho}, \bar{\rho}'$.

2. Case $s = 1^+$

$$S_f^{1^+} = \bar{a}^4 \sum_{y_0=\bar{a}}^{T'-\bar{a}} \sum_{\mathbf{y}} \sum_{\mu} \bar{\psi}(y) \left[\gamma_\mu D_\mu + i\frac{\bar{a}}{2}\gamma_5\tau_{\mu 5}\Delta_\mu\right] \psi(y) + S_B^{(0)} + S_B^{(T')}. \quad (2.3.20)$$

The contributions from the boundaries are,

$$\begin{aligned} S_{B,1^+}^{(0)} &= \bar{a}^4 \sum_{\mathbf{y}} \sum_{k=1}^{3} \bar{\psi}(0,\mathbf{y}) \left[Q_-\gamma_k D_k + i\frac{\bar{a}}{2}Q_-\gamma_5\tau_{k5}\Delta_k\right] \psi(0,\mathbf{y}) \\ &\quad + \bar{a}^3 \sum_{\mathbf{y}} \bar{\psi}(0,\mathbf{y})Q_-\gamma_0\psi(\bar{a},\mathbf{y}), \quad (2.3.21) \\ S_{B,1^+}^{(T')} &= \bar{a}^4 \sum_{\mathbf{y}} \sum_{k=1}^{3} \bar{\psi}(T',\mathbf{y}) \left[Q_+\gamma_k D_k + i\frac{\bar{a}}{2}Q_+\gamma_5\tau_{k5}\Delta_k\right] \psi(T',\mathbf{y}) \\ &\quad - \bar{a}^3 \sum_{\mathbf{y}} \bar{\psi}(T',\mathbf{y})Q_+\gamma_0\psi(T'-\bar{a},\mathbf{y}). \quad (2.3.22) \end{aligned}$$

And the boundary conditions in this case are,

$$\begin{aligned} Q_-\psi(0,\mathbf{y}) &= \rho(\mathbf{y}), \qquad & Q_+\psi(T',\mathbf{y}) &= \rho'(\mathbf{y}), \\ \bar\psi(0,\mathbf{y})Q_- &= \bar\rho(\mathbf{y}), \qquad & \bar\psi(T',\mathbf{y})Q_+ &= \bar\rho'(\mathbf{y}). \end{aligned} \tag{2.3.23}$$

3. Case $s = 1^-$. The action in this last case will read,

$$\begin{aligned} S_f^{1^-} &= \bar a^4 \sum_{y_0=\bar a}^{T'-\bar a} \sum_{\mathbf{y}} \bar\psi(y) \left[\sum_\mu \gamma_\mu D_\mu - i\frac{\bar a}{2}\gamma_5\tau_{05}\Delta_0 + i\frac{\bar a}{2}\sum_k \gamma_5\tau_{k5}\Delta_k \right] \psi(y) \\ &+ S_B^{(0)} + S_B^{(T')}. \end{aligned} \tag{2.3.24}$$

The contributions of the boundaries are,

$$\begin{aligned} S_{B,1^-}^{(0)} &= \bar a^4 \sum_{\mathbf{y}} \sum_{k=1}^{3} \bar\psi(0,\mathbf{y}) \left[Q_+\gamma_k D_k + i\frac{\bar a}{2} Q_+\gamma_5\tau_{k5}\Delta_k \right] \psi(0,\mathbf{y}) \\ &+ \bar a^3 \sum_{\mathbf{y}} \bar\psi(0,\mathbf{y}) Q_+\gamma_0\psi(\bar a,\mathbf{y}), \end{aligned} \tag{2.3.25}$$

$$\begin{aligned} S_{B,1^-}^{(T')} &= \bar a^4 \sum_{\mathbf{y}} \sum_{k=1}^{3} \bar\psi(T,\mathbf{y}) \left[Q_-\gamma_k D_k + i\frac{\bar a}{2} Q_-\gamma_5\tau_{k5}\Delta_k \right] \psi(T'\mathbf{y}) \\ &- \bar a^3 \sum_{\mathbf{y}} \bar\psi(T'-\bar a) Q_-\gamma_0\psi(T',\mathbf{y}). \end{aligned} \tag{2.3.26}$$

And the boundary conditions in this case are,

$$\begin{aligned} Q_+\psi(0,\mathbf{y}) &= \rho(\mathbf{y}), \qquad & Q_-\psi(T',\mathbf{y}) &= \rho'(\mathbf{y}), \\ \bar\psi(0,\mathbf{y})Q_+ &= \bar\rho(\mathbf{y}), \qquad & \bar\psi(T',\mathbf{y})Q_- &= \bar\rho'(\mathbf{y}). \end{aligned} \tag{2.3.27}$$

Staggered action for homogeneus boundary conditions

We will calculate the propagator for homogeneus boundary conditions. Thus, it will be useful to give an expression for the action in this case. We set,

$$\chi^{(0)}(\mathbf{x}) = \bar\chi^{(0)}(\mathbf{x}) = \chi^{(T)}(\mathbf{x}) = \bar\chi^{(T)}(\mathbf{x}) = 0. \tag{2.3.28}$$

Therefore, we also have,

$$\rho(\mathbf{y}) = \bar\rho(\mathbf{y}) = \rho'(\mathbf{y}) = \bar\rho(\mathbf{y}) = 0. \tag{2.3.29}$$

The boundary terms vanish in the case of the single component spinors. Thus, the action will be given by,

$$S_f = a^3 \sum_{x_0=a}^{T-a} \sum_{\mathbf{x}} \sum_\mu \frac{1}{2}\bar\chi(x) \left[\lambda_\mu \chi(x+a\hat\mu) - \lambda_\mu^*\chi(x-a\hat\mu) \right]. \tag{2.3.30}$$

Again, we have to consider the cases $s = \pm 1$ separately. As we have seen so far, we have two reconstructions available for the case $s = 1$. Let us consider, as it has been done above, the three cases separately.

1. Case $s = -1$. Taking into account Eqs. (2.3.18) and the boundary terms, Eqs. (2.3.16,2.3.17), we find that the staggered action can be written as,

$$S_f^{-1} = \bar{a}^4 \sum_{y_0=0}^{T'} \sum_{\mathbf{y}} \sum_{\mu} \bar{\psi}(y) \left[\gamma_\mu D_\mu + i\frac{\bar{a}}{2}\gamma_5\tau_{\mu 5}\Delta_\mu \right] \psi(y). \tag{2.3.31}$$

2. Case $s = 1^+$. Taking into account Eqs. (2.3.23) and the corresponding boundary terms, we will be able to write the action as,

$$S_f^{1^+} = \bar{a}^4 \sum_{y_0=\bar{a}}^{T'-\bar{a}} \sum_{\mathbf{y}} \sum_{\mu} \bar{\psi}(y) \left[\gamma_\mu D_\mu + i\frac{\bar{a}}{2}\gamma_5\tau_{\mu 5}\Delta_\mu \right] \psi(y). \tag{2.3.32}$$

   Note that the summation starts from $y_0 = \bar{a}$ and goes until $y_0 = T - \bar{a}$. As we can extend the fields to all times by "padding" with zeros, we can extend the summation to $y_0 = 0, T'$.

3. Case $s = 1^-$. In this case, taking into account Eqs. (2.3.27) and the corresponding boundary terms, we will be able to write the action as,

$$S_f^{1^-} = \bar{a}^4 \sum_{y_0=\bar{a}}^{T'-\bar{a}} \sum_{\mathbf{y}} \bar{\psi}(y) \left[\sum_{\mu} \gamma_\mu D_\mu - i\frac{\bar{a}}{2}\gamma_5\tau_{05}\Delta_0 + i\frac{\bar{a}}{2}\sum_{k} \gamma_5\tau_{k5}\Delta_k \right] \psi(y). \tag{2.3.33}$$

Relation to the usual Schrödinger functional

In the massless theory, one can perform a chiral rotation to decouple the flavours [50, 82]. After the rotation is done, we get the same boundary terms as the ones encountered for the Wilson action [47, 48]. We define,

$$\psi' = R(\alpha)\psi, \qquad \bar{\psi}' = \bar{\psi}R(\alpha). \tag{2.3.34}$$

$R(\alpha)$ is given by,

$$R(\alpha) = \exp\left(i\frac{\alpha}{2}\gamma_5\tau_{05}\right) = \cos\left(\frac{\alpha}{2}\right) + i\gamma_5\tau_{05}\sin\left(\frac{\alpha}{2}\right). \tag{2.3.35}$$

Setting $\alpha = \pi/2$, we get,

$$R(\pm\pi/2) = \frac{1}{\sqrt{2}}(1 \pm i\gamma_5\tau_{05}), \tag{2.3.36}$$

and,

$$R(\pi/2)Q_\pm R^{-1}(\pi/2) = \frac{1}{2}(1 \pm \gamma_0). \tag{2.3.37}$$

We want to restore the standard Schrödinger Functional for the three cases we have been considering so far. Let us have a look at them separately.

1. Case $s = -1$. If we perform a rotation of $\pi/2$ to the fields,

$$\psi' = R(\pi/2)\psi, \qquad \bar{\psi}' = \bar{\psi}R(\pi/2), \tag{2.3.38}$$

then the boundary conditions read,

$$\begin{aligned} P_+\psi'(0,\mathbf{y}) &= R(\pi/2)\rho(\mathbf{y}), & P_-\psi'(T',\mathbf{y}) &= R(\pi/2)\rho'(\mathbf{y}), \\ \bar{\psi}'(0,\mathbf{y})P_- &= \bar{\rho}(\mathbf{y})R(\pi/2), & \bar{\psi}'(T',\mathbf{y})P_+ &= \bar{\rho}'(\mathbf{y})R(\pi/2). \end{aligned} \tag{2.3.39}$$

If the boundary conditions are taken to be homogeneus, that is, $\rho, \bar{\rho}, \rho', \bar{\rho}'$ are set to 0, the action can be written as,

$$S_f^{-1} = \bar{a}^4 \sum_{y_0=0}^{T'} \sum_{\mathbf{y}} \bar{\psi}'(y) \left[\sum_\mu \gamma_\mu D_\mu + \frac{\bar{a}}{2}\Delta_0 + i\frac{\bar{a}}{2} \sum_k \gamma_5 \tau_{k5} \Delta_k \right] \psi'(y). \tag{2.3.40}$$

2. Case $s = 1^+$. In this case, as the boundary conditions given in Eq. (2.3.23) are the opposite as the ones above, the rotation we have to perform to the fermionic fields to get the standard Schrödinger Functional us the opposite as well. So, if we perform a rotation to the fields,

$$\psi' = R(-\pi/2)\psi, \qquad \bar{\psi}' = \bar{\psi}R(-\pi/2), \tag{2.3.41}$$

then, the boundary conditions read,

$$\begin{aligned} P_+\psi'(0,\mathbf{y}) &= R(-\pi/2)\rho(\mathbf{y}), & P_-\psi'(T',\mathbf{y}) &= R(-\pi/2)\rho'(\mathbf{y}), \\ \bar{\psi}'(0,\mathbf{y})P_- &= \bar{\rho}(\mathbf{y})R(-\pi/2), & \bar{\psi}'(T',\mathbf{y})P_+ &= \bar{\rho}'(\mathbf{y})R(-\pi/2). \end{aligned} \tag{2.3.42}$$

If they are taken homogeneus, then the action would read,

$$S_f^{1^+} = \bar{a}^4 \sum_{y_0=0}^{T'} \sum_{\mathbf{y}} \bar{\psi}'(y) \left[\sum_\mu \gamma_\mu D_\mu - \frac{\bar{a}}{2}\Delta_0 + i\frac{\bar{a}}{2} \sum_k \gamma_5 \tau_{k5} \Delta_k \right] \psi'(y). \tag{2.3.43}$$

3. Case $s = 1^-$. In this reconstruction, the boundary conditions, given in Eq. (2.3.27) are the same as in the case $s = -1$, so the chiral rotation leading to the standard Schrödinger Functional also has to be the same,

$$\psi' = R(\pi/2)\psi, \qquad \bar{\psi}' = \bar{\psi}R(\pi/2), \tag{2.3.44}$$

then the boundary conditions read,

$$\begin{aligned} P_+\psi'(0,\mathbf{y}) &= R(\pi/2)\rho(\mathbf{y}), & P_-\psi'(T',\mathbf{y}) &= R(\pi/2)\rho'(\mathbf{y}), \\ \bar{\psi}'(0,\mathbf{y})P_- &= \bar{\rho}(\mathbf{y})R(\pi/2), & \bar{\psi}'(T',\mathbf{y})P_+ &= \bar{\rho}'(\mathbf{y})R(\pi/2). \end{aligned} \tag{2.3.45}$$

If the boundary conditions are taken to be homogeneus, that is, $\rho, \bar{\rho}, \rho', \bar{\rho}'$ are set to 0, the action can be written as,

$$S_f^{1^-} = \bar{a}^4 \sum_{y_0=0}^{T'} \sum_{\mathbf{y}} \bar{\psi}'(y) \left[\sum_\mu \gamma_\mu D_\mu - \frac{\bar{a}}{2}\Delta_0 + i\frac{\bar{a}}{2} \sum_k \gamma_5 \tau_{k5} \Delta_k \right] \psi'(y). \tag{2.3.46}$$

2.3.3 Free fermionic propagator in terms of four component spinors

We are going to work on the chirally rotated basis. The same steps followed in [84, 85] for Wilson are taken here but with staggered quarks. As it has been worked out in the pevious section, for the case $s = 1$, the action in this basis has the same form. The Dirac staggered operator, D^s has then the following form for the two cases, $s = \pm 1$,

$$D_f^{-1} = \sum_\mu \gamma_\mu D_\mu + \frac{\bar{a}}{2}\Delta_0 + i\frac{\bar{a}}{2}\sum_k \gamma_5\tau_{k5}\Delta_k. \tag{2.3.47}$$

$$D_f^{1} = \sum_\mu \gamma_\mu D_\mu - \frac{\bar{a}}{2}\Delta_0 + i\frac{\bar{a}}{2}\sum_k \gamma_5\tau_{k5}\Delta_k. \tag{2.3.48}$$

Taking into account what has been discussed in the previous section, the defining equations for the propagator $S_s^f(x, y)$, setting the quarks masses to 0 are,

$$D_f^s S_s^f(y, y') = \bar{a}^{-4}\delta_{y,y'} \qquad 0 < y_0 < T', \tag{2.3.49}$$

and

$$P_+ S_s^f(y, y')\big|_{y_0=0} = P_- S_s^f(y, y')\big|_{y_0=T'} = 0. \tag{2.3.50}$$

Our aim is to deduce an explicit expression for $S_s^f(y, y')$ in the time momentum representation. We shall assume that $0 < y_0 < T'$. We will give the final result here. The details on the derivation are given in appendix D.

1. Case $s = -1$

$$y_0 < y_0'$$

$$\begin{aligned} S_{-1}^f(y_0, y_0')_{\mathbf{p}} = \frac{-i}{R_{-1}(\mathbf{p}^+)2\mathring{p}_0^+}\Big\{ & (i\mathring{p}_0^+ - \tilde{A}_{-1})\left(\frac{\bar{a}}{2}\hat{p}_0^{+2} + i\mathring{p}_0^+\right)\gamma_0 e^{-\omega(\mathbf{p}^+)(y_0'-y_0)} \\ & + (\tilde{A}_{-1} + i\mathring{p}_0^+)\left(\frac{\bar{a}}{2}\hat{p}_0^{+2} - i\mathring{p}_0^+\gamma_0\right)\gamma_0 e^{-\omega(\mathbf{p}^+)(y_0+y_0')} \\ & - (\tilde{A}_{-1} + i\mathring{p}_0^+)\left(\frac{\bar{a}}{2}\hat{p}_0^{+2} - i\mathring{p}_0^+\right)\gamma_0 e^{-\omega(\mathbf{p}^+)(2T'-(y_0'-y_0))} \\ & + (\tilde{A}_{-1} - i\mathring{p}_0^+)\left(\frac{\bar{a}}{2}\hat{p}_0^{+2} + i\mathring{p}_0^+\gamma_0\right)\gamma_0 e^{-\omega(\mathbf{p}^+)(2T'-(y_0'+y_0))}\Big\}. \end{aligned} \tag{2.3.51}$$

$$y_0 = y_0'$$

$$\begin{aligned} S_{-1}^f(y_0, y_0')_{\mathbf{p}} = \frac{-i}{R_{-1}(\mathbf{p}^+)2\mathring{p}_0^+}\Big\{ & (i\mathring{p}_0^+\gamma_0 - \tilde{A}_{-1})\left(\frac{\bar{a}}{2}\hat{p}_0^{+2} + i\mathring{p}_0^+\right)\gamma_0 \\ & + (\tilde{A}_{-1} + i\mathring{p}_0^+)\left(\frac{\bar{a}}{2}\hat{p}_0^{+2} - i\mathring{p}_0^+\gamma_0\right)\gamma_0 e^{-\omega(\mathbf{p}^+)(y_0+y_0')} \\ & - (\tilde{A}_{-1} + i\mathring{p}_0^+\gamma_0)\left(\frac{\bar{a}}{2}\hat{p}_0^{+2} - i\mathring{p}_0^+\right)\gamma_0 e^{-\omega(\mathbf{p}^+)(2T')} \\ & + (\tilde{A}_{-1} - i\mathring{p}_0^+)\left(\frac{\bar{a}}{2}\hat{p}_0^{+2} + i\mathring{p}_0^+\gamma_0\right)\gamma_0 e^{-\omega(\mathbf{p}^+)(2T'-(y_0'+y_0))}\Big\}. \end{aligned} \tag{2.3.52}$$

$$y_0 > y_0'$$

$$\begin{aligned} S^f_{-1}(y_0,y_0')_{\mathbf{p}} &= \frac{-i}{R_{-1}(\mathbf{p}^+)2\mathring{p}_0^+}\Big\{\Big(\frac{\bar{a}}{2}\hat{p}_0^{+2}+i\,\mathring{p}_0^+\Big)(-i\,\mathring{p}_0^+-\tilde{A}_{-1})\gamma_0 e^{-\omega(\mathbf{p}^+)(y_0-y_0')} \\ &+ (\tilde{A}_{-1}+i\,\mathring{p}_0^+)\Big(\frac{\bar{a}}{2}\hat{p}_0^{+2}-i\,\mathring{p}_0^+\gamma_0\Big)\gamma_0 e^{-\omega(\mathbf{p}^+)(y_0+y_0')} \\ &- (\tilde{A}_{-1}-i\,\mathring{p}_0^+)\Big(\frac{\bar{a}}{2}\hat{p}_0^{+2}-i\,\mathring{p}_0^+\Big)\gamma_0 e^{-\omega(\mathbf{p}^+)(2T'-(y_0-y_0'))} \\ &+ (\tilde{A}_{-1}-i\,\mathring{p}_0^+)\Big(\frac{\bar{a}}{2}\hat{p}_0^{+2}+i\,\mathring{p}_0^+\gamma_0\Big)\gamma_0 e^{-\omega(\mathbf{p}^+)(2T'-(y_0'+y_0))}\Big\}. \end{aligned} \tag{2.3.53}$$

2. Case $s=1$

$$y_0 < y_0'$$

$$\begin{aligned} S^f_{1}(y_0,y_0')_{\mathbf{p}} &= \frac{-i}{R_{1}(\mathbf{p}^+)2\mathring{p}_0^+}\Big\{(i\,\mathring{p}_0^+-\tilde{A}_{1})\Big(-\frac{\bar{a}}{2}\hat{p}_0^{+2}+i\,\mathring{p}_0^+\Big)\gamma_0 e^{-\omega(\mathbf{p}^+)(y_0'-y_0)} \\ &- (\tilde{A}_{1}+i\,\mathring{p}_0^+)\Big(\frac{\bar{a}}{2}\hat{p}_0^{+2}+i\,\mathring{p}_0^+\gamma_0\Big)\gamma_0 e^{-\omega(\mathbf{p}^+)(y_0+y_0')} \\ &+ (\tilde{A}_{1}+i\,\mathring{p}_0^+)\Big(\frac{\bar{a}}{2}\hat{p}_0^{+2}+i\,\mathring{p}_0^+\Big)\gamma_0 e^{-\omega(\mathbf{p}^+)(2T'-(y_0'-y_0))} \\ &+ (\tilde{A}_{1}-i\,\mathring{p}_0^+)\Big(-\frac{\bar{a}}{2}\hat{p}_0^{+2}+i\,\mathring{p}_0^+\gamma_0\Big)\gamma_0 e^{-\omega(\mathbf{p}^+)(2T'-(y_0'+y_0))}\Big\}. \end{aligned} \tag{2.3.54}$$

$$y_0 = y_0'$$

$$\begin{aligned} S^f_{1}(y_0,y_0')_{\mathbf{p}} &= \frac{-i}{R_{1}(\mathbf{p}^+)2\mathring{p}_0^+}\Big\{(i\,\mathring{p}_0^+\gamma_0+\tilde{A}_{1})\Big(\frac{\bar{a}}{2}\hat{p}_0^{+2}-i\,\mathring{p}_0^+\Big)\gamma_0 \\ &- (\tilde{A}_{1}+i\,\mathring{p}_0^+)\Big(\frac{\bar{a}}{2}\hat{p}_0^{+2}+i\,\mathring{p}_0^+\gamma_0\Big)\gamma_0 e^{-\omega(\mathbf{p}^+)(y_0+y_0')} \\ &+ (\tilde{A}_{1}-i\,\mathring{p}_0^+\gamma_0)\Big(\frac{\bar{a}}{2}\hat{p}_0^{+2}+i\,\mathring{p}_0^+\Big)\gamma_0 e^{-\omega(\mathbf{p}^+)(2T')} \\ &+ (\tilde{A}_{1}-i\,\mathring{p}_0^+)\Big(-\frac{\bar{a}}{2}\hat{p}_0^{+2}+i\,\mathring{p}_0^+\gamma_0\Big)\gamma_0 e^{-\omega(\mathbf{p}^+)(2T'-(y_0'+y_0))}\Big\}. \end{aligned} \tag{2.3.55}$$

$$y_0 > y_0'$$

$$\begin{aligned} S^f_{1}(y_0,y_0')_{\mathbf{p}} &= \frac{-i}{R_{1}(\mathbf{p}^+)2\mathring{p}_0^+}\Big\{\Big(\frac{\bar{a}}{2}\hat{p}_0^{+2}-i\,\mathring{p}_0^+\Big)(i\,\mathring{p}_0^+ +\tilde{A}_{1})\gamma_0 e^{-\omega(\mathbf{p}^+)(y_0-y_0')} \\ &- (\tilde{A}_{1}+i\,\mathring{p}_0^+)\Big(\frac{\bar{a}}{2}\hat{p}_0^{+2}+i\,\mathring{p}_0^+\gamma_0\Big)\gamma_0 e^{-\omega(\mathbf{p}^+)(y_0+y_0')} \\ &+ (\tilde{A}_{1}-i\,\mathring{p}_0^+)\Big(\frac{\bar{a}}{2}\hat{p}_0^{+2}+i\,\mathring{p}_0^+\Big)\gamma_0 e^{-\omega(\mathbf{p}^+)(2T'-(y_0-y_0'))} \\ &+ (\tilde{A}_{1}-i\,\mathring{p}_0^+)\Big(-\frac{\bar{a}}{2}\hat{p}_0^{+2}+i\,\mathring{p}_0^+\gamma_0\Big)\gamma_0 e^{-\omega(\mathbf{p}^+)(2T'-(y_0'+y_0))}\Big\}. \end{aligned} \tag{2.3.56}$$

2.3.4 Free fermionic propagator in terms of single component spinors

Change of basis

We want to relate the propagator in the four component spinor basis with the single component propagator. We are going to work in the time momentum representation. The fourier transform on the intermediate $\chi_\xi(y)$ fields (cf. appendix C.1) is not the usual one,

$$\chi_\xi(y) = L^{-3} \sum_{\mathbf{q}} \sum_{\boldsymbol{\eta}} e^{i(\mathbf{q}+\pi\boldsymbol{\eta}/a)(2\mathbf{y}+\boldsymbol{\xi}a)} f_{\boldsymbol{\eta}}(x_0, \mathbf{q}), \tag{2.3.57}$$

where $\eta_k = \{0, 1\}$ and $\mathbf{q}$ take their values in the fine lattice,

$$q_k = \frac{2\pi n_k}{L}, \qquad n_k = 0, \ldots, \frac{L}{2a} - 1. \tag{2.3.58}$$

Now, we perform the following change of variables, $\mathbf{p} = 2\mathbf{q}$, so that $\mathbf{p}$ takes the values,

$$p_k = \frac{2\pi n_k}{L}, \qquad n_k = 0, \ldots, \frac{L}{\bar{a}} - 1. \tag{2.3.59}$$

We get to the expression,

$$\chi_\xi(y) = L^{-3} \sum_{\mathbf{p}} \sum_{\boldsymbol{\eta}} e^{i\mathbf{p}\mathbf{y}} e^{\left(\frac{\mathbf{p}}{2}+\pi\boldsymbol{\eta}/a\right)\boldsymbol{\xi}a} f_{\boldsymbol{\eta}}(x_0, \mathbf{p}/2). \tag{2.3.60}$$

The Fourier transform of a four component spinor field reads,

$$\psi^{\alpha a}(y_0, \mathbf{y}) = L^{-3} \sum_{\mathbf{p}} e^{i\mathbf{p}\mathbf{y}} \tilde{\psi}^{\alpha a}(y_0, \mathbf{p}). \tag{2.3.61}$$

Then, we can establish what the transformation between the fields $\varphi^{\alpha a}$ and χ_ξ is,

$$\tilde{\psi}^{\alpha a}(y_0, \mathbf{p}) = \frac{1}{4} \sum_{\xi_0=0}^{1} \sum_{\boldsymbol{\eta}} \left(\Lambda_{\boldsymbol{\eta},\mathbf{p}/2}\right)^{\alpha a} f_{\boldsymbol{\eta}}(x_0, \mathbf{p}/2), \tag{2.3.62}$$

with,

$$\Lambda_{\boldsymbol{\eta},\mathbf{p}/2} = \sum_{\boldsymbol{\xi}} e^{i\frac{\mathbf{p}}{2a}\boldsymbol{\xi}} R_\xi e^{i\pi\boldsymbol{\eta}\boldsymbol{\xi}}, \tag{2.3.63}$$

and the corresponding relation when the transformation matrices are $\tilde{R}_\xi$. In the mono-component spinors basis, the propagator can be seen as,

$$\begin{aligned} \langle \chi_\xi(y) \bar{\chi}_{\xi'}(y') \rangle \;\; &= \;\; L^{-6} \sum_{\mathbf{p},\mathbf{p}'} \sum_{\boldsymbol{\eta},\boldsymbol{\eta}'} \langle f_{\boldsymbol{\eta}}(x_0, \mathbf{p}/2) \bar{f}_{\boldsymbol{\eta}'}(x_0', \mathbf{p}'/2) \rangle \\ &\quad e^{i(\mathbf{p}\mathbf{y}+\mathbf{p}'\mathbf{y}')} e^{i\left(\frac{\mathbf{p}}{2}+\pi\frac{\boldsymbol{\eta}}{a}\right)\boldsymbol{\xi}a} e^{i\left(\frac{\mathbf{p}'}{2}+\pi\frac{\boldsymbol{\eta}'}{a}\right)\boldsymbol{\xi}'a} \end{aligned} \tag{2.3.64}$$

Establishing the connection between the two expressions, we arrive at,

$$\left[R(-\alpha)\tilde{S}_s^f(y_0,y_0')_{\mathbf{p}}R(\alpha)\right]_{\alpha\beta}^{ab} = \frac{1}{16}\sum_{\xi_0,\xi_0'}\sum_{\boldsymbol{\eta},\boldsymbol{\eta}'}\left(\Lambda_{\xi_0,\boldsymbol{\eta},\mathbf{p}/2}\right)^{\alpha a}\langle f_{\boldsymbol{\eta}}(x_0,\mathbf{p}/2) \bar{f}_{\boldsymbol{\eta}'}(x_0',-\mathbf{p}/2)\rangle(\Lambda^{\dagger}_{\xi_0,\boldsymbol{\eta}',\mathbf{p}/2})^{b\beta}. \quad (2.3.65)$$

Note that we have to include the chiral rotation as $\tilde{S}_s^f$ in the previous section is given in the chirally rotated basis.

Operator in the single component fermionic action

Now, starting from the free fermionic action for the single component spinors, Eqs. (2.3.7,2.3.11, 2.3.12), we will calculate the inverse of the expression,

$$\langle f_{\boldsymbol{\eta}}(x_0,\mathbf{p}/2)\bar{f}_{\boldsymbol{\eta}'}(x_0,-\mathbf{q}/2)\rangle = \delta_{\mathbf{pq}}M_s^{-1}(x_0,x_0',\boldsymbol{\eta},\boldsymbol{\eta}',\mathbf{p}/2), \quad (2.3.66)$$

M_s is the operator we find in the action in the time momentum representation. After performing the Fourier transform to the action, we get,

$$\begin{aligned} M_s(x_0,x_0',\boldsymbol{\eta},\boldsymbol{\eta}',\mathbf{p}/2) &= \frac{1}{2}\delta_{\boldsymbol{\eta},\boldsymbol{\eta}'}\left[\delta_{x_0,x_0'-a}-\delta_{x_0,x_0+a}\right] \quad (2.3.67)\\ &+ \sum_{k=1}^{3}\bar{\delta}_{\boldsymbol{\eta}+\boldsymbol{\eta}^{(k)},\boldsymbol{\eta}'}\delta_{x_0,x_0'}(-1)^{\eta_k+x_0}i\sin\left(\frac{p_k a}{2}\right), \end{aligned}$$

where $\eta^{(\mu)}$ is,

$$\eta_\nu^{(\mu)} = \begin{cases} 1 & \text{for} \quad \nu<\mu \\ 0 & \text{for} \quad \nu\geq\mu \end{cases}, \quad (2.3.68)$$

and $\bar{\delta}$ means $\delta \mod 2$.

We have written a maple program that calculates this operator and inverts it. Then, we have transformed it to the four component spinors basis using Eq. (2.3.65) and we have shown that the result is consistent with the direct computation of the fermionic propagator.

Now we have the analytical expression for the staggered Dirac operator in the Schrödinger functional. The connection between the four component spinors propagator and the single component spinors propagator has been established. A program has been written in order to check our analytical results.

There are some subleties to be taken into account, the most remarkable one being the fact that the spatial extent is different from the time extent, $T = L \pm a$. As it has been done previously for the gauge part, we have introduced $T' = L = T + sa$, and have computed the quantities depending on this variable, s.

2.4 Definition of the renormalised coupling $\bar{g}^2$ and the observable $\bar{v}$

At the beginning of this chapter, we motivated the Schrödinger Functional formulation because it was going to provide us with a renormalised coupling that fulfilled the requirements needed for its evolution with the scale to be computable on the lattice. That is, we want a coupling that is non perturbatively defined, extractable from numerical simulations with small computational effort, with reasonable small lattice artifacts and that is reasonably easily computed in the perturbative regime up to two loops in PT. However, we have not defined it yet. There are many ways of introducing this coupling. Actually, when the finite size techniques were first introduced, [34], the coupling used was defined related to the force between two infinitely heavy quarks at distance r. The conditions the coupling defined here is going to fulfill are,

i) It depends only on one scale, the size of the box, L.

ii) The coupling $\bar{g}^2$ coincides with g_0^2 to leading order of perturbation theory.

iii) $\bar{g}^2$ is a renormalisation group invariant.

The uniqueness of the induced background field cf. subsection 2.2, allows to unambiguously define the effective action of the Schrödinger functional. Imposing homogeneous boundary conditions for the fermionic fields, we have,

$$\Gamma[B] = -\ln \mathcal{Z}[C', C]. \tag{2.4.1}$$

A detailed analysis shows that the effective action, modulo a divergent additive constant is power renormalisable, with no extra counterterms.

When the boundary fields have been specified, Eqs. (2.2.8, 2.2.9), they have been taken to depend on two dimensionless parameters, namely, η, ν. We can define a renromalised coupling through,

$$\left.\frac{\partial \Gamma}{\partial \eta}\right|_{\eta=\nu=0} = \frac{[\partial \Gamma_0/\partial \eta]_{\eta=0}}{\bar{g}^2(L)}, \tag{2.4.2}$$

where Γ_0 is the classical action of the induced Background field. The derivative with respect to the parameter η eliminates divergent contributions to the effective action that do not depend on the background field. The reasons for setting ν, η to zero is that in numerical simulations of the SF the statistical errors on the coupling are smaller in this case. For a general ν, we have,

$$\left.\frac{\partial \Gamma}{\partial \eta}\right|_{\eta=0} = \left.\frac{\partial \Gamma_0}{\partial \eta}\right|_{\eta=0} \left\{\frac{1}{\bar{g}^2} - \nu \bar{v}\right\}, \tag{2.4.3}$$

where $\bar{v}$ is another renormalised quantity. It is independent of ν. This quantitty can be computed with little extra work and it can be used to test the universality of the SF. Note also that $\bar{v}$ vanishes a tree level since Γ_0 is independent of ν.

This definition of $\bar{g}^2$ does satisfy the conditions a)-d),

Non perturbatively defined, a): From the definition, we see it is non-perturbatively defined.

Easily computed on the lattice, b): Γ' is the observable calculated in the simulations. From its definition,

$$\Gamma' = \left\langle \frac{\partial S}{\partial \eta}\Big|_{\eta=\nu=0} \right\rangle . \tag{2.4.4}$$

The derivative reads,

$$\frac{\partial S}{\partial \eta}\Big|_{\eta=\nu=0} = -\frac{2}{g_0^2 L} a^3 \sum_{\mathbf{x}} \left\{ E_k^8(\mathbf{x}) - (E_k^8)'(\mathbf{x}) \right\}, \tag{2.4.5}$$

where E_k^8 is the eight colour component of the chromoelectric field. Its explicit expression reads,

$$E_k^8(\mathbf{x}) = \frac{1}{a^2} \,\mathrm{Re}\ \mathrm{tr} \left\{ i\lambda^8 U_k(x) U_0(x + a\hat{k}) U_k^\dagger(x + a\hat{0}) U_0^\dagger(x) \right\}_{x_0=0}, \tag{2.4.6}$$

where $\lambda^8 = \mathrm{diag}(1, -1/2, -1/2)$. $(E_k^8)'(\mathbf{x})$ is analogously defined. Thus, $\bar{g}^2$ is given in terms of the expectation value of a local operator. There is no correlation function involved. The evaluation of this quantity on a computer is done with very little computational cost. Besides, it turns out that the level of accuracy that can be achieved with a statistical ensemble of sensible size (slightly large, though) is satisfactory.

Small lattice artifacts, c): In order to monitor the lattice artifacts, we will look into the effective action in the perturbative regime. In the weak bare coupling g_0^2 domain, fields close to B dominate the path integral and the effective action has a regular saddle point expansion in powers of g_0^2,

$$\begin{aligned} \Gamma[B] &= \frac{1}{g_0^2}\Gamma_0[B] + \Gamma_1[B] + g_0^2\Gamma_2[B] + \ldots, \\ \Gamma_0[B] &= g_0^2 S[B]. \end{aligned} \tag{2.4.7}$$

At lowest order in perturbation theory, we have that the effective action coincides with the classical action. As we will in the forthcoming chapters, implementing the Symanzik improvement program [67], the lattice artifacts can be diminished by removing the $\mathrm{O}(a)$ effects order by order in PT. This has been achieved up to one loop order in this wortk. Once they are cancelled, the remaining are expected to be small. This is supposed to be true for the background field chosen (abelian and spatially constant). It allows for reliable extrapolations to the continuum limit.

Computable in PT, d): From the saddle point expansion of the effective action Eq. (2.4.7), a perturbative calculation of $\bar{g}^2$ is possible, [86].

From Eq. (2.4.5), we see that the coupling can be regarded as the response of the system to a constant colour electric field. Besides, we see that *i) - iii)* are fulfilled. This definition of the coupling might seem awkward, since one is used to the strong coupling defined related to the quark gluon vertex (in analogy with QED), or else the one related to the force between two static quarks at a given distance r. These definitions are somehow more intuitive, albeit the definition given here is extremely suitable for the finite size techniques to be carried out.

Chapter 3

Tree level $\mathrm{O}(a)$ improvement

In chapter 2, we have established the SF formulation on the lattice with staggered fermions, specified how the continuum limit is taken and given a definition for the running coupling suitable for the finite scaling techniques to be implemented. In principle, we could start running simulations to compute the coupling and hence its evolution with the scale.

However, numerical simulations of the functional integral are limited to lattice spacings a that are not too small. Their contribution can be larger than desirable. Hence, we would like to keep $\mathrm{O}(a)$ effects as tiny as possible. The continuum extrapolation will be easier to compute and, besides, more reliable.

In order to do that, we are going to apply an $\mathrm{O}(a)$ improvement to our theory. This procedure was first introduced by Symanzik [67] (see [87] for a review). He applied it to the ϕ^4_4 theory [88] and to the O(N) non linear sigma model in perturbation theory [89].

In this chapter, we will restrict ourselves to the classical level. The Symanzik improvement on a quantum level will be discussed in chapter 4. Instead of presenting it in general terms, we are going to discuss the particular problem under consideration.

The observable we are concerned with is the derivative of the effective action Eq. (2.4.1) with respect to the parameter η. At a classical level, it coincides with the derivative of the classical action with respect to this parameter.

Thus, cancelling the $\mathrm{O}(a)$ effects in the observable at a classical level amounts to doing so in the classical action. The general principle of Symanzik improvement (that will also holds in a quantum level, cf. Chapter 4.) is that the a^n effects can be removed by adding counterterms to the action of dimension $d + n$[1]. These counterterms are restricted by their dimensionality and by the symmetries of the lattice. Since they will agree with their continuum counterparts up to lattice effects, we can express them using the continuum notation. This is true for on-shell quantities even at a quantum level, as it was proven in [90]. Besides, as long as only on-shell quantities are involved,

[1] That holds for a theory in d dimensions in infinite volume.

the equations of motion can be used in order to reduce the number of counterterms needed.

The whole procedure at a quantum level can be seen as an extension of the renormalisation procedure to the level of irrelevant operators. In analogy with the discussion carried out in section 2 about the renormalisability of the SF, we expect the need of boundary counterterms to set in for the improvement program to be successfully implemented. At a classical level this is definitely the case.

In this chapter, the O(a) improvement at tree level is carried out for the gauge and the fermionic part of the action. The steps followed are,

i) Identify the O(a) artifacts present in the action
ii) List all the possible counterterms.
iii) Reduce the former to a smaller amount by means of the equations of motion
iv) Adjust the coefficients so that they cancel the O(a) effects in the action.

Summarising, close to the continuum limit, we can expand the lattice action in terms of a local effective theory [2],

$$S_{\text{eff}} = S_0 + aS_1 + a^2 S_2 + \dots \tag{3.0.1}$$

The leading term is the action in the continuum. The correction terms for the SF will come in two forms,

$$S_k = \int d^4x \mathcal{L}_k(x) + \lim_{\epsilon \to 0} \int d^3x \left\{ \mathcal{B}_k(x)|_{x_0=\epsilon} + \mathcal{B}'_k(x)|_{x_0=\epsilon} \right\}, \tag{3.0.2}$$

where the lagrangians $\mathcal{L}_k(x)$ are linear operators of composite fields of dimension $4+k$ and $\mathcal{B}_k(x), \mathcal{B}'_k(x)$ are operators at the boundaries of dimension $3+k$. Moreover, they are related by a time reflection so, only one of them needs to be discussed. The lattice action can be O(a) improved by adding irrelevant operators,

$$S_{\text{imp}}[U, \bar{\psi}, \psi] = S[U, \bar{\psi}, \psi] + \delta S_v[U, \bar{\psi}, \psi] + \delta S_{G,b}[U] + \delta S_{F,b}[U, \bar{\psi}, \psi], \tag{3.0.3}$$

where v indicates the volume and b the boundaries. Since this program will be promoted to the quantum level in the following chapter, the coefficients in front of the irrelevant operators will have a perturbative expansion in terms of the bare coupling. In this chapter, will care about the tree level contribution. We will address the pure gauge theory first, and then the fermionic part of the action.

3.1 Pure gauge theory

The pure gauge part of the SF action is given by Eq. (2.2.7). We look into the possible counterterms that can be added to the action. We will include them in the expression of the action and adjust the coefficients to cancel the O(a) effects.

[2] This is far from trivial at a quantum level, cf. chapter 4. In [91], a proof for a Pauli-Villars regularisation is given

3.1.1 Possible counterterms

At order a the possible counterterms in the volume would have to be operators of dimension 5. There are no such candidates. However, we can find two boundary counterterms of dimension 4. They are obtained by summing any local lattice expression for the fields,

$$a^4\text{tr}\ \{F_{0k}F_{0k}\} \qquad \text{and} \qquad a^4\text{tr}\{F_{kl}F_{kl}\}, \tag{3.1.1}$$

over the $x_0 = 0$ and $x_0 = T$ hyperplanes. $F_{\mu\nu}$ is the field strength tensor,

$$F_{\mu\nu}(x) = \partial_\mu A_\nu(x) - \partial_\nu A_\mu(x) + [A_\mu(x), A_\nu(x)]\,. \tag{3.1.2}$$

The terms in Eq. (3.1.1) are up to $\mathrm{O}(a)$ effects proportional to the contribution of the action coming from the temporal plaquettes attached to a boundary plane and the spatial plaquettes at the boundaries, correspondingly. That is so because the $a^4\,\text{tr}\{F_{\mu\nu}F_{\mu\nu}\} = \text{tr}(P_{\mu\nu} + P^\dagger_{\mu\nu} - 2) + \mathrm{O}(a^5)$. These counterterms can then be absorbed by properly adjusting the weights $w(p)$ in the lattice action of Eq. (2.2.7). That is what we presented in Eq. (2.2.13) with no justification. They have a perturbative expansion, Eq. (2.2.14).

As we are performing a tree level calculation, we are going to determine $c_t^{(0)}$. Nothing can be said about the coefficient $c_s^{(0)}$ because the spatially constant boundary conditions remove the contributions to the action of the spatial plaquettes at $x_0 = 0, T$. If $L = T$, $c_t^{(0)}$ would be equal to 1. But, as we have justified before, we need a lattice in which $T = L \pm a$. This special feature induces a correction in the coefficient c_t even at tree level.

3.1.2 Identification of the $\mathrm{O}(a)$ effects in the action

In section 2.2.4., we have solved the equations of motion analytically. We are certain that the solution leads to a minimal configuration of the action. We can use these results to obain an analytic expression of the $\mathrm{O}(a)$ effects in the action. $c_t^{(0)}$ is to be chosen in such a way that makes $O(a)$ effects vanish. In fact it will be desired that the lattice action coincides with the continuum action up to terms of order a^4. We define the quantity T' in such a way that in the continuum limit $T'/L = 1$. We define then the parameter s as,

$$T' = T + sa, \qquad s = \pm 1, 0. \tag{3.1.3}$$

Let's study in these three cases the lattice effects. In the continuum limit, the action is given by Eq. (3.1.4)

$$S_{cont} = \frac{L}{g_0^2 T}\sum_{k=1}^{3}\sum_{\alpha=1}^{3}(\phi'_{k\alpha} - \phi_{k\alpha})^2 = \frac{3L}{g_0^2 T}\sum_{\alpha=1}^{3}(\phi'_\alpha - \phi_\alpha)^2. \tag{3.1.4}$$

The sumation over the spatial indices has been performed, as we have seen that the boundary conditions chosen are all the same in the three spatial directions. To obtain the values of $c_t^{(0)}$ that make the $\mathrm{O}(a)$ effects vanish, we have calculated the action using

the expression Eq. (2.2.21)) for the gauge fields, with f expanded up to order $\mathrm{O}(a)$. Using this solution, and substituting $T = T' - sa$, the lattice action can be written as,

$$\begin{aligned} S &= \frac{T'-(2+s)a}{g_0^2} 3L^3 \sum_{\alpha=1}^{3} \left\{ \frac{2}{a^2} \sin\left[\frac{a^2}{2L} \frac{\phi'_\alpha - \phi_\alpha}{T' - sa - \frac{2a(c_t^{(0)}-1)}{c_t^{(0)}}} \right] \right\}^2 + \\ & c_t^{(0)} \frac{2a}{g_0^2} 3L^3 \sum_{\alpha=1}^{3} \left\{ \frac{2}{a^2} \sin\left[\frac{a^2}{2Lc_t^{(0)}} \frac{\phi'_\alpha - \phi_\alpha}{T' - sa - \frac{2a(c_t^{(0)}-1)}{c_t^{(0)}}} \right] \right\}^2 . \end{aligned} \tag{3.1.5}$$

We have performed a Taylor expansion of Equation Eq. (3.1.5). We fix $c_t^{(0)}$ as a function of s so that $\mathrm{O}(a)$ effects vanish. In Eq. (3.1.6) we see the $\mathrm{O}(a)$ effects of Eq. (3.1.5),

$$\begin{aligned} S &= \frac{3L}{g_0^2 T'} \sum_{\alpha=1}^{3} (\phi'_\alpha - \phi_\alpha)^2 + \\ & \frac{3L}{g_0^2} \frac{a}{(T')^2} \sum_{\alpha=1}^{3} (\phi'_\alpha - \phi_\alpha)^2 \left\{ -2 + s + \frac{4c_t^{(0)} - 2}{c_t^{(0)}} \right\} + \mathrm{O}(a^2) \\ &= S_{cont} \left\{ 1 + \frac{a}{L} \left[-2 + s + \frac{4c_t^{(0)} - 2}{c_t^{(0)}} \right] + \mathrm{O}(a^2) \right\}, \end{aligned} \tag{3.1.6}$$

3.1.3 Determination of $c_t^{(0)}$.

Eq. (3.1.6) leads to a relation between $c_t^{(0)}$ and s,

$$c_t^{(0)} = \frac{2}{2+s}. \tag{3.1.7}$$

See Table 2.1. for the concrete values of the coefficients (cf. section 2.2.4). It turns out that lattice effects will vanish up to $O(a^4)$ imposing Eq. (3.1.7). That can be seen from the explicit Taylor coefficients of f in Eq. (2.2.23) for all three values of s considered. That had to be the case at least for $s = 0$. We conclude that having $T \neq L$ leads to tree level $\mathrm{O}(a)$ coefficients that are different from the usual ones. However, the proper tuning of these coefficients leads to a cancellation of lattice artifacts up to $\mathrm{O}(a^4)$ at tree level, which coincides with the $T = L$ case.

3.2 Fermionic action

Now, we focus our attention in the fermionic part of the action. The volume action is partially automatically $\mathrm{O}(a)$ improved, so we can proceed the same way as in [74]. We can use the improved staggered fermions to argue that $\mathrm{O}(a)$ effects are absent in the action. Besides, we work out what the boundary terms are and will be able to determine the improvement coefficient d_1 at tree level.

3.2.1 O(a) improvement contributions from the volume

Nature of the O(a) terms in the reconstructed action

The meaning of the statement that there is no term of order a in the staggered fermion action is not clear. It is obvious that there are O(a) effects in the reconstructed action Eqs. (2.3.31, 2.3.32, 2.3.33). That could lead to the conclusion that dimension 5 counterterms are needed in order to improve the action. Nevertheless, in appendix E.3. it is shown that there are no dimension 5 operators available that respect all the symmetries, as it was already pointed out in [92].

The O(a) terms in the action are an artifact of the specific way the reconstruction of the spinors was performed. Starting with the free staggered action in terms of the one component fermionic fields, and following Golterman and Smit [79], it is possible to reconstruct the fermions, so that the resulting action is accurate to O(a^2). However, the reconstructed fermions are non local superpositions of the one component fermions over all lattice sites.

On the other hand, starting with the reconstruction of the previous section, there are various different ways of introducing the so-called improved staggered fields. The transformation into these improved fields is a local change of basis. In this new basis, the action is accurate up to O(a^2) effects. These fields are still local and superior to the nonlocal fields both computationally ant theoretically when gauge couplings are included. Furthermore, if we use the improved fields which remove the order a terms from the action to construct a lattice fermion operator, there will be no O(a) corrections to its free matrix elements.

We also want to keep the fermionic fields as local as possible, so that we can start to perform calculations of correlation functions on small lattices with sensible results. The improved fields proposed in [92], [50] involve the nearest neighbour fields in all directions, that is, an improved fermion is a linear combination of nine fermions. We will shorlty see that we need not improve the fields in the spatial directions. We can restrict ourselves to the computation of operators that are automatically O(a) improved, following the procedure used in [74].

Automatic O(a) improvement

We will restrict ourselves to the reconstruction with $s = -1$. The explicit O(a) terms from our reconstruction reads,

$$i\frac{\bar{a}}{2}\sum_{\mu,y}\bar{\psi}(y)\gamma_5\tau_{\mu 5}\Delta_\mu\psi(y), \tag{3.2.1}$$

They are not invariant under the shift symmetry given in the appendix B. As we have discussed, all dimension 5 counterterms become irrelevant. The counterterms can at

most contribute at $\mathrm{O}(a^2)$. If we split the $\mathrm{O}(a)$ terms of the action,

$$i\frac{\bar{a}}{2}\sum_{k,y}\bar{\psi}(y)\gamma_5\tau_{k5}\Delta_k\psi(y)+i\frac{\bar{a}}{2}\sum_{y}\bar{\psi}(y)\gamma_5\tau_{05}\Delta_0\psi(y), \tag{3.2.2}$$

it can be noted that, for the terms involving the spatial second derivatives, we can apply an analogous argument to the one proposed in [74] for chirally twisted fermions, to prove that there is an automatic $\mathrm{O}(a)$ improvement.

To simplify the discussion, let us assume that the space-time volume is finite, which will always be true in the system we are considering. By doing so, we exclude spontaneous symmetry breaking.

To proceed, we first rotate into the usual SF basis, as it has been done in section 2.3.2. The boundary conditions for the case considered here are given by Eq. (2.3.39). The action for homogeneus boundary conditions is the one in Eq. (2.3.40). We now introduce the τ_5 transformation,

$$\psi\to\tau_5\psi,\qquad \bar{\psi}\to\bar{\psi}\tau_5, \tag{3.2.3}$$

which is a symmetry of four flavour QCD. Introducing the notation,

$$\begin{aligned}
S_0 &= \bar{a}^4\sum_{y_0=0}^{T'}\sum_{\mathbf{y},\mu}\bar{\psi}'(y)\gamma_\mu D_\mu\psi'(y),\\
S_1^t &= \frac{\bar{a}^5}{2}\sum_{y_0=0}^{T'}\sum_{\mathbf{y}}\bar{\psi}'(y)\Delta_0\psi'(y),\\
S_1^s &= i\frac{\bar{a}^5}{2}\sum_{y_0=0}^{T'}\sum_{\mathbf{y},k}\bar{\psi}'(y)\gamma_5\tau_{k5}\Delta_k\psi'(y),
\end{aligned} \tag{3.2.4}$$

we can see that S_0, S_1^t are invariant, but this is not the case for S_1, i.e. one finds,

$$S_0+S_1^t\to S_0+S_1^t,\qquad S_1^s\to -S_1^s. \tag{3.2.5}$$

It is important to note that the τ_5 does not change the projectors of the quark boundary conditions,

$$P_\pm\tau_5=\tau_5 P_\pm. \tag{3.2.6}$$

Using this notation, renormalised connected lattice correlation functions can be analysed in the effective theory,

$$\langle\mathcal{O}\rangle=\langle\mathcal{O}\rangle^{\mathrm{cont}}-\bar{a}\langle S_1^t\mathcal{O}\rangle^{\mathrm{cont}}-\bar{a}\langle S_1^s\mathcal{O}\rangle^{\mathrm{cont}}+\bar{a}\langle\delta\mathcal{O}\rangle^{\mathrm{cont}}+\mathrm{O}(\bar{a}^2), \tag{3.2.7}$$

where the cutoff dependence is explicit. For gauge invariant fields, the transformation of Eq. (3.2.3) squares to the identity, so that one may define an associated parity. For fields O with a definite τ_5 parity, one then finds,

$$\mathcal{O}\to\pm\mathcal{O}\quad\Rightarrow\quad\delta\mathcal{O}\to\mp\delta\mathcal{O}. \tag{3.2.8}$$

By applying the transformation to the integration variables in the functional integral, one may derive the identities between the correlation functions, due to the invariance of the continuum action and functional measure. In particular, if we choose a τ_5-even field $\mathcal{O}$, we find for the correlation functions at $\mathrm{O}(\bar{a})$,

$$\begin{aligned} \langle S_1^s \mathcal{O} \rangle^{\mathrm{cont}} &= -\langle S_1^s \mathcal{O} \rangle^{\mathrm{cont}} = 0, \\ \langle \delta \mathcal{O} \rangle^{\mathrm{cont}} &= -\langle \delta \mathcal{O} \rangle^{\mathrm{cont}} = 0. \end{aligned} \tag{3.2.9}$$

and therefore,

$$\langle \mathcal{O} \rangle = \langle \mathcal{O} \rangle^{\mathrm{cont}} + \bar{a} \langle S_1^t \mathcal{O} \rangle^{\mathrm{cont}} + \mathrm{O}(\bar{a}^2). \tag{3.2.10}$$

For a τ_5-odd operator $\mathcal{O}$, one obtains,

$$\begin{aligned} \langle \mathcal{O} \rangle^{\mathrm{cont}} &= -\langle \mathcal{O} \rangle^{\mathrm{cont}} = 0, \\ \langle S_1^t O \rangle^{\mathrm{cont}} &= -\langle S_1^t \mathcal{O} \rangle^{\mathrm{cont}} = 0, \end{aligned} \tag{3.2.11}$$

which implies,

$$\langle O \rangle = -\bar{a} \langle S_1^s O \rangle^{\mathrm{cont}} + \bar{a} \langle \delta O \rangle^{\mathrm{cont}} + \mathrm{O}(\bar{a}^2). \tag{3.2.12}$$

We may thus conclude that, at least in a small finite volume, the only $\mathrm{O}(a)$ contribution of the correlation functions of τ_5- even fields are coming from the S_1^t term, while those of τ_5-odd fields vanish up to $\mathrm{O}(a)$ terms. Now, we are left with the discussion of the term S_1^t. We will discuss this issue in the following subsection, and introduce improved fermionic fields.

Introduction of improved fermionic fields

Now, we are going to introduce our improved fermionic fields, in order to remove S_1^t from the action. Here, it is going to be specified how to introduce the improvement in the usual staggered basis and in the Schrödinger functional basis for $s = \pm 1$.

Staggered basis

$$\text{Case } s = -1$$

$$\begin{aligned} \psi^I(y) &= \psi(y) + \frac{\bar{a}}{4}(i\gamma_0\gamma_5\tau_{05}) D_0 \psi(y), \\ \bar{\psi}^I(y) &= \bar{\psi}(y) + \frac{\bar{a}}{4}\bar{\psi}(y) \overleftarrow{D}_0 (i\gamma_0\gamma_5\tau_{05}). \end{aligned} \tag{3.2.13}$$

SF basis

$$\begin{aligned} \psi^{I'}(y) &= \psi'(y) + \frac{\bar{a}}{4}\gamma_0 D_0 \psi'(y), \\ \bar{\psi}^{I'}(y) &= \bar{\psi}'(y) - \frac{\bar{a}}{4}\bar{\psi}'(y)\gamma_0 \overleftarrow{D}_0. \end{aligned} \tag{3.2.14}$$

Staggered basis

$$\text{Case } s = 1^+$$

$$\begin{aligned} \psi^I(y) &= \psi(y) + \frac{\bar{a}}{4}(i\gamma_0\gamma_5\tau_{05}) D_0 \psi(y), \\ \bar{\psi}^I(y) &= \bar{\psi}(y) + \frac{\bar{a}}{4}\bar{\psi}(y) \overleftarrow{D}_0 (i\gamma_0\gamma_5\tau_{05}). \end{aligned} \tag{3.2.15}$$

SF basis

$$\begin{aligned}\psi^{I'}(y) &= \psi'(y) - \frac{\bar{a}}{4}\gamma_0 D_0 \psi'(y),\\ \bar{\psi}^{I'}(y) &= \bar{\psi}'(y) + \frac{\bar{a}}{4}\bar{\psi}'(y)\gamma_0 \overleftarrow{D}_0.\end{aligned} \tag{3.2.16}$$

Staggered basis CASE $s = 1^-$

$$\begin{aligned}\psi^{I}(y) &= \psi(y) - \frac{\bar{a}}{4}(i\gamma_0\gamma_5\tau_{05}) D_0 \psi(y),\\ \bar{\psi}^{I}(y) &= \bar{\psi}(y) - \frac{\bar{a}}{4}\bar{\psi}(y)\overleftarrow{D}_0(i\gamma_0\gamma_5\tau_{05}).\end{aligned} \tag{3.2.17}$$

SF basis

$$\begin{aligned}\psi^{I'}(y) &= \psi'(y) - \frac{\bar{a}}{4}\gamma_0 D_0 \psi'(y),\\ \bar{\psi}^{I'}(y) &= \bar{\psi}'(y) + \frac{\bar{a}}{4}\bar{\psi}'(y)\gamma_0 \overleftarrow{D}_0.\end{aligned} \tag{3.2.18}$$

With these improved fields, the action reads, for all cases, in both bases,

$$S_f = \bar{a}^4 \sum_{y_0,\mathbf{y}} \bar{\psi}^I(y) \left[\sum_\mu \gamma_\mu D_\mu + i\frac{\bar{a}}{2} \sum_k \gamma_5 \tau_{k5} \Delta_k \right] \psi^I(y). \tag{3.2.19}$$

At this stage, we can say that the action is O(a) improved, using the arguments given in the previous section for the automatic O(a) improvement and the introduction of the improved fermionic fields. Later on, it will be seen in detail that, if we have an O(a) improved operator at tree level, the O(a) improved action suffices to ensure that the observables are O(a) improved at all orders in perturbation theory. Let us discuss before the improvement at the boundaries.

3.2.2 O(a) improvement at the boundaries

Boundary counterterms involving fermions

The boundary counterterms have to be local composite fields of dimension 4. Before we start discussing them, and for the sake of completeness, we will look into the possible dimension 3 operators that respect all the symmetries and can, therefore be added to the action. They are listed in appendix E.1. It turns out, there is only one candidate,

$$\mathcal{O}_1 = \bar{\psi}\psi. \tag{3.2.20}$$

It is linear in the boundary values $\bar{\rho}, \rho, \bar{\rho}', \rho'$. Since one anyway has to renormalise the boundary values of the quark and antiquark fields [48], the dimension 3 $\mathcal{O}_1$ counterterm need not be included in the action.

In Appendix E.2, we give a list of the possible dimension 4 operators that respect all the symmetries. It has been worked out in the standard Schrödinger functional basis, as we clarify in the appendices. A possible basis of the fields would be,

$$\begin{aligned}
\mathcal{O}_2 &= \bar{\psi}P_+D_0\psi + \bar{\psi}\overleftarrow{D}_0P_-\psi, && (3.2.21)\\
\mathcal{O}_3 &= \bar{\psi}P_-D_0\psi + \bar{\psi}\overleftarrow{D}_0P_+\psi, && (3.2.22)\\
\mathcal{O}_4 &= \bar{\psi}P_+\gamma_kD_k\psi - \bar{\psi}\overleftarrow{D}_k\gamma_kP_-\psi, && (3.2.23)\\
\mathcal{O}_5 &= \bar{\psi}P_-D_k\gamma_k\psi - \bar{\psi}\overleftarrow{D}_k\gamma_kP_+\psi. && (3.2.24)
\end{aligned}$$

So, we are left with the same terms we get in the Wilson case [93]. The formal field equations imply,

$$\begin{aligned}
\mathcal{O}_2 + \mathcal{O}_4 &= 0, && (3.2.25)\\
\mathcal{O}_3 - \mathcal{O}_5 &= 0, && (3.2.26)
\end{aligned}$$

so that two fields can be eliminated. A particularly simple form of the associated boundary counterterms to the lattice action is obtained if we choose,

$$\mathcal{O}_4, \mathcal{O}_5, \tag{3.2.27}$$

in both $y_0 = 0, T$. Note that this choice is different from the usual one made for Wilson fermions. We are thus left with altogether four boundary counterterms, two at $y_0 = 0$ and two at $y_0 = T$. Their coefficients must be such that the time reversal invariance of the theory is preserved. A possible choice of the counterterms then is,

$$\begin{aligned}
\delta S_{F,b}[U,\bar{\psi},\psi] &= \bar{a}^4\sum_{\mathbf{y}}\Big\{(d_{1s}-1)[\hat{\mathcal{O}}_1+\hat{\mathcal{O}}'_1]\\
&+ (d_{2s}-1)[\hat{\mathcal{O}}_2+\hat{\mathcal{O}}'_2]\Big\}, && (3.2.28)
\end{aligned}$$

where,

$$\begin{aligned}
\hat{\mathcal{O}}_1 &= \bar{\psi}(0,\mathbf{y})P_+\gamma_k\mathcal{D}_k\psi(0,\mathbf{y}), && (3.2.29)\\
\hat{\mathcal{O}}'_1 &= \bar{\psi}(T,\mathbf{y})P_-\gamma_k\mathcal{D}_k\psi(T,\mathbf{y}), && (3.2.30)\\
\hat{\mathcal{O}}_2 &= \bar{\rho}(\mathbf{y})\gamma_k\mathcal{D}_k\rho(\mathbf{y}), && (3.2.31)\\
\hat{\mathcal{O}}'_2 &= \bar{\rho}'(\mathbf{y})\gamma_k\mathcal{D}_k\rho'(\mathbf{y}), && (3.2.32)
\end{aligned}$$

with,

$$\mathcal{D}_k\psi(y) = \tilde{\partial}_k\psi(y) + i\frac{\bar{a}}{2}\gamma_k\gamma_5\tau_{k5}\Delta_k\psi(y) \tag{3.2.33}$$

In our system, homogeneous boundary conditions are taken. Hence, there is no need of discussing d_{2s}.

O(a) effects of the propagator

In appendix D, we worked out the explicit form of the free tree level propagator for staggered quaks for the unimproved action. In order to cancel the O(a) effects in the

fermionic action, we are going to identify the O(a) effects in the unimproved propagator. Then, and starting from the improved action, we will build an improved propagator by including the new counterterms as insertions. The coefficients will be tuned in order to cancel the O(a) countertems. We will also explicitly see that the O(a) effects that are also present in the infinite volume case can be removed throught the introduction of imrpoved fields. We work on the SF basis unless otherwise specified. Expanding the propagatior up to O(a^2) we obtain,

$$S^f_{\pm 1}(y_0, y_0')_{\mathbf{p}} = S^{\rm cont}(y_0, y_0')_{\mathbf{p}} + \bar{a}\mathcal{C}_{\pm 1}(y_0, y_0')_{\mathbf{p}} + \bar{a}\mathcal{D}_{\pm 1}(y_0, y_0')_{\mathbf{p}} + {\rm O}(a^2) \tag{3.2.34}$$

where $S^{\rm cont}(y_0, y_0')_{\mathbf{p}}$ is the propagator in the continuum limit,

$$\begin{aligned} \mathcal{C}_{\pm 1}(y_0, y_0')_{\mathbf{p}} &= \frac{\pm 1}{4}\Big\{ S^{\rm cont}(y_0, 0)_{\mathbf{p}} \tilde{A}^{\rm cont}\gamma_0 S^{\rm cont}(0, y_0')_{\mathbf{p}} + \\ &\qquad S^{\rm cont}(y_0, T')_{\mathbf{p}} \tilde{A}^{\rm cont}\gamma_0 S^{\rm cont}(T', y_0')_{\mathbf{p}} \Big\}, \end{aligned} \tag{3.2.35}$$

$$\begin{aligned} \mathcal{D}_{\pm 1}(y_0, y_0')_{\mathbf{p}} &= -\frac{\tilde{B}_{\pm 1}}{2\omega\cosh(\omega T')} \{\gamma_0 \sinh\left(\omega(T' - |y_0' - y_0|)\right) + \\ &\qquad \sinh\left(\omega(T' - y_0 - y_0')\right)\}, \end{aligned} \tag{3.2.36}$$

with,

$$\begin{aligned} \tilde{A}^{\rm cont} &= \sum_k i p_k^+ \gamma_k \gamma_0, \\ \tilde{B}_{\pm 1} &= -\frac{i}{2}\sum_k \gamma_5\gamma_0\tau_{k5}(p_k^+)^2 \mp \frac{1}{2}\gamma_0 (p_0^+)^2 \\ \omega &= \sqrt{\mathbf{p}^{+\mathbf{2}}} \qquad n(T) = \cosh(\omega T). \end{aligned} \tag{3.2.37}$$

The details of this notation are given in appendix D. Now, we are ready to analyse the O(a) effects. The last term in Eq. (3.2.34), $\mathcal{D}_{\pm 1}$ is the one also present in infinite volume. Its spatial components need not be removed since the automatic O(a) improvement sets in for them. Its time component can be removed by introducing improved staggered fermions, cf. section 3.2.1. That is easily verified,

CASE $s = -1$

$$\begin{aligned} \langle \psi'^I(y)\bar{\psi}'^I(y')\rangle &= \langle \psi'(y)\bar{\psi}(y')\rangle - \frac{\bar{a}}{4}\langle \psi'(y)\bar{\psi}(y')\rangle^{\rm cont}\gamma_0 \overleftarrow{D}_0 \\ &\quad + \frac{\bar{a}}{4}\gamma_0 D_0 \langle \psi'(y)\bar{\psi}'(y)\rangle^{\rm cont} + {\rm O}(\bar{a}^2). \end{aligned} \tag{3.2.38}$$

CASE $s = 1$

$$\begin{aligned} \langle \psi'^I(y)\bar{\psi}'^I(y')\rangle &= \langle \psi'(y)\bar{\psi}(y')\rangle + \frac{\bar{a}}{4}\langle \psi'(y)\bar{\psi}(y')\rangle^{\rm cont}\gamma_0 \overleftarrow{D}_0 \\ &\quad - \frac{\bar{a}}{4}\gamma_0 D_0 \langle \psi'(y)\bar{\psi}'(y)\rangle^{\rm cont} + {\rm O}(\bar{a}^2). \end{aligned} \tag{3.2.39}$$

It turns out that,

$$-\frac{1}{4}\frac{\partial}{\partial y_0'}S^{\rm cont}(y_0,y_0')_{\mathbf{p}}\gamma_0+\frac{1}{4}\gamma_0\frac{\partial}{\partial y_0}S^{\rm cont}(y_0,y_0')+\mathrm{O}(a)= \tag{3.2.40}$$
$$=\frac{(p_0^+)^2}{4\cosh(\omega T')}\left\{\sinh(\omega(T-|y_0-y_0'|))+\tilde{A}^{\rm cont}\gamma_0\cosh(\omega(T-y_0-y_0'))\right\}.$$

So, the introduction of the improved fields cancels out the unwanted $\mathrm{O}(a)$ term from the propagator.

Determination of d_1 at tree level

The contribution $\mathcal{C}_{\pm}(y_0,y_0')_{\mathbf{p}}$ can be cancelled by improving the fermionic action, by adjusting the coefficient d_{1s}. The perturbation expansion of the improvement coefficients d_{1s},d_{2s} is of the form,

$$d_s=d_s^{(0)}+d_s^{(1)}g_0^2+d_s^{(2)}g_0^4+\ldots \tag{3.2.41}$$

In order to tune $d_s^{(0)}$, what we do is to calculate the propagator up to $\mathrm{O}(a^2)$ using the improved action given by Eq. (3.0.3). We obtain,

$$S_s^{\rm imp}(y_0,y_0')_{\mathbf{p}} \;=\; S_s^f(y_0,y_0')_{\mathbf{p}}-4\bar{a}(d_{1s}-1)\mathcal{C}_s(y_0,y_0')_{\mathbf{p}}+\mathrm{O}(a^2). \tag{3.2.42}$$

So, in order to cancel the $\mathrm{O}(a)$ effects coming from the boundaries, we choose,

$$d_{1s}^{(0)}=1+\frac{s}{4}. \tag{3.2.43}$$

In the one component spinor action, the improved action is,

$$\begin{aligned}S_f^{\rm imp} \;=\;& a^4\sum_{x_0=a}^{T-a}\sum_{\mathbf{x}}\sum_{\mu}\frac{1}{2a}\eta_\mu(x)\bar{\chi}(x)\left[\lambda_\mu U_\mu(x)\chi(x+a\hat{\mu})-\lambda_\mu^*U_\mu^\dagger(x-a\hat{\mu})\chi(x-a\hat{\mu})\right]\\
&+(d_{1s}-1)\sum_{\mathbf{x},k}\left\{\frac{1}{2a}\eta_k(x)\bar{\chi}(x)\left[\lambda_kU_k(x)\chi(x+a\hat{k})-\lambda_\mu^*U_\mu^\dagger(x-a\hat{k})\chi(x-a\hat{k})\right]\right\}_{x_0=a}\\
&+(d_{1s}-1)\sum_{\mathbf{x},k}\left\{\frac{1}{2a}\eta_k(x)\bar{\chi}(x)\left[\lambda_kU_k(x)\chi(x+a\hat{k})-\lambda_\mu^*U_\mu^\dagger(x-a\hat{k})\chi(x-a\hat{k})\right]\right\}_{x_0=T-a}\\
&+S_B^{(0)}+S_B^{(T)},\end{aligned} \tag{3.2.44}$$

with boundary terms,

$$\begin{aligned}S_B^{(0)} \;=\;& a^4\sum_{\mathbf{x},k}\frac{d_{2s}}{2a}\eta_k(0,\mathbf{x})\bar{\chi}^{(0)}(\mathbf{x})\left(\lambda_kW_k(\mathbf{x})\chi^{(0)}(\mathbf{x}+a\hat{k})-\lambda_k^*W_k^\dagger(\mathbf{x}-a\hat{k})\chi^{(0)}(\mathbf{x}-a\hat{k})\right)\\
&+\;a^4\sum_{\mathbf{x}}\frac{1}{2a}\bar{\chi}^{(0)}(\mathbf{x})U_0^\dagger(a,\mathbf{x})\chi(a,\mathbf{x}),\end{aligned} \tag{3.2.45}$$

$$\begin{aligned}S_B^{(T)} \;=\;& a^4\sum_{\mathbf{x},k}\frac{d_{2s}}{2a}\eta_k(T,\mathbf{x})\bar{\chi}^{(T)}(\mathbf{x})\left(\lambda_kW_k'(\mathbf{x})\chi^{(T)}(\mathbf{x}+a\hat{k})-\lambda_k^*W_k^{'\dagger}(\mathbf{x}-a\hat{k})\chi^{(T)}(\mathbf{x}-a\hat{k})\right)\\
&+\;a^4\sum_{\mathbf{x}}\frac{1}{2a}\bar{\chi}^{(T)}(\mathbf{x})U_0^\dagger(T-a,\mathbf{x})\chi(T-a,\mathbf{x}).\end{aligned} \tag{3.2.46}$$

Chapter 4

One loop $\mathrm{O}(a)$ improvement

In this chapter, we are going to discuss the Symanzik O(a) improvement on a quantum level [67]. We will restrict ourselves to asymptotically free theories ($g_0 \to 0$ in the continuum limit, so that PT can be applied in the small coupling regime). It has to be noted here that we should always refer to it as a conjecture, since a rigorous proof of Symanzik improvement has not been completed. In [88], Symanzik shows the improvement program leads to satisfactory results up to one loop in perturbation theory for ϕ_4^4. He also verifies it for a $O(N)$ non-linear σ model in [89]. He describes the improvement as an extension of renormalisation by oversubtraction and probably considered that the generalisation to all orders in PT was straightforward (using the BPH(Z) renormalisation scheme). Keller, in [94] provides a proof to all orders for ϕ_4^4 and QED. However, ϕ_4^4 is probably trivial.

The idea underneath the improvement at a quantum level is the same we have introduced at a classical level. However, it becomes more cumbersome due to the fact that quantum fields are not smooth fields but distributions. We will introduce the mechanism of improvement through the ϕ_4^4 theory and then give a historical introduction. Concerning correlation functions, the requirement (C stands for continuum and L for lattice),

$$\langle \phi^C(x_1) \dots \phi^C(x_n) \rangle = \langle \phi^L_{x_1/a} \dots \phi^L_{x_n/a} \rangle + \mathrm{O}\left(a^{2n} \ln^k(a)\right), \tag{4.0.1}$$

does not hold due to them being infinite at coincident points and because the fields should be smeared as in Eq. (2.0.5), i.e.,

$$\begin{aligned} \langle \phi^C_{f_1} \dots \phi^C_{f_n} \rangle &= \langle \phi^L_{f_1} \dots \phi^L_{f_n} \rangle + \mathrm{O}\left(a^{2j} \ln^k(a)\right), \\ \phi^L_f &= a^4 \sum_{i \in \Gamma_E} \phi_i f(i). \end{aligned} \tag{4.0.2}$$

That is equivalent to asking the correlation functions in Fourier space of the lattice and of the continuum coincide up to $\mathrm{O}\left(a^{2j} \ln^k(a)\right)$. The objects Symanzik first considered were vertex functions Γ_B (full propagator amputated one particle irreducible parts of

the correlation functions). Their Fourier transforms have in PT the small a expansion,

$$\Gamma_B(p_1 \cdots p_{2n}; a, g_0, \Delta m_0^2) = \sum_{j=0}^{\infty} \sum_{k=0}^{\infty} a^{2j} \ln^k a \bar{f}_{jk}(p_1 \ldots p_{2n}; g_0, \Delta m_0^2), \tag{4.0.3}$$

where $g_0, \Delta m_0^2$ are the bare parameters. The renormalisation procedure absorbs the $j = 0, k \geq 1$ terms. With g, m being the renormalised coupling constant and mass and μ the normalisation (e.g. subtraction) momentum, we can write,

$$\begin{aligned} Z_3(g, a\mu)^n \Gamma_B(p_1, \ldots, p_{2n}; a, g_0(g, a\mu), Z_2^{-1}(g, a\mu) m^2) \; &= \; \Gamma(p_1, \ldots p_{2n}; \mu, g, m^2) \\ &+ \sum_{j=1}^{\infty} \sum_{k=0}^{\infty} a^{2j} \ln^k a \bar{f}_{jk}(p_1, \ldots, p_{2n}; g_0(g, a\mu), Z_2^{-1}(g, a\mu) m^2). \end{aligned} \tag{4.0.4}$$

The aim of action improvement is to remove the $\mathrm{O}(a^2 \ln^k a), \mathrm{O}(a^4 \ln^k a) \ldots$ The conjecture is the following: they can be generated by a local effective lagrangian (LEL). The interpretation rule for it is chosen to be dimensional regularisation. We consider the lattice and continuum theory in $4 + \epsilon$ dimensions. It takes the form,

$$\begin{aligned} \mathcal{L}_{eff} \; &= \; -\tfrac{1}{2} \bar{Z}_3 \sum_{\mu} (\partial_\mu \phi)^2 - \tfrac{1}{2} \bar{Z}_2 \Delta m_0^2 \phi^2 - \tfrac{1}{4!} \bar{Z}_1 g_0 \phi^4 + \\ &\quad a^2 \sum_{i=4}^{10} \bar{Z}_i \mathcal{O}_i + \mathrm{O}(a^4). \end{aligned} \tag{4.0.5}$$

Now, some remarks concerning Eq. (4.0.5),

1. The $\bar{Z}_i$'s are functions of $\{g_0 a^{-\epsilon}, \epsilon\}$ and they have a perturbative expansion.
2. Δm_0^2 appears in the LEL only in positive integer powers.
3. The marginal (dim. 4) and relevant (dim. < 4) alone determine the symmetries of the continuum theory.
4. The operators with a factor a^{2j} in front are fixed by the following requirements. We consider on the continuum the list of all possible operatorsof dimension $4+2j$ which transform as singlets under the symmetry group in the continuum.
5. A LEL exists also if we consider the lattice spacing to be unequal in different directions.
6. As it was already pointed out in the previous chapter, the existence of a LEL to describe large-cutoff behaviour is highly non trivial. In [91] it was proven for Pauli Villars regularisation.

Symanzik results state that the $\mathrm{O}(a^2)$ terms in the action effective lagrangian and consequently the $\mathrm{O}(a^2 \ln^k a)$ terms in the vertex functions can be removed by adding irrelevant counterterms (dim. > 4) to the original action. They consist on lattice version of the continuum $\mathrm{O}(a^2)$ terms.Corresponding statements hold for $\mathrm{O}(a^{2j})$ terms with $j \geq 2$. It has to be noted that,

i) The operators on the lattice have intrinsic cutoff dependence. This fact poses a potential source of difficulty, since they have to be disentangled from the cutoff effects to be cancelled by improving the action. In [90], Lüscher and Weisz refer to this problem and addressing tree level $O(a^2)$ improvement of lattice gauge theories (one loop in [95]), they conclude that it can be avoided if only the improvement of spectral quantities is required. This is the so called on-shell improvement. Besides, the number of irrelevant counterterms can be reduced by using the equations of motion, as we have already done at tree level, cf. chapter 3. The quantities we are interested in $\bar{g}^2, \bar{v}$ are of this kind, so this simplification will always be applied.

ii) The determination of the coefficients of irrelevant terms can be carried out in PT. That is only possible if the theory is asymptotically free, as we have assumed it is.

iii) In Symanzik's approach, the OS positivity conditions, [14] are lost also for the tree level improved action. It is recovered in the continuum. Nevertheless, it is disturbing to lose it in an intermediate stage, since it has important applications in numerical simulations. Parisi, in [87] proposes a strategy to achieve the Symanzik improvement without breaking OS positivity for the on-shell quantities (the spectrum and the S-matrix). It goes through two steps; first the lattice is introduced in the space directions and the usual Symanzik improvement is done. Then, it is introduced in the time direction performing the improvement directly in position space. In [96], Lüscher and Weisz show that the transfer matrix for an improved pure gauge theory can be defined in spite of the transfer matrix positivity being lost. Nevertheless, it presents awkward properties, such as complex eigenvalues.

iv) Wilson, in [97] introduced another strategy to tackle the reduction of lattice artifacts, by introducing block fields. His approach cancels all lattice effects. It is therefore much more ambitious and much more difficult to implement. Symanzik's is systematic and easily carried out. Thus, it has been implemented in a vast number of numerical simulations carried out up to now.

v) The idea Symanzik used is the following. Instead of using the usual minimal subtraction prescription, we extend it to the level of irrelevant operators. That is, from the $\mathscr{L}$ loop graph of a 2n vertex function (VF), which is of order $g_0^{\mathscr{L}+n-1}$, its Taylor expasion in the external momenta at 0 momenta and 0 Δm_0^2 is subtracted. If we want to obtain an $O(a^2)$ action, the subtraction is done up to order $6-2n$.

After Symanzik's work, the program was carried out for lattice gauge theories, [98, 99], up to one loop in PT. This was revisited in [90, 95] underlining the convenience of restricting to an on-shell improvement. Then, in 1985, Sheikholeslami and Wohlert [100] achieved to carry it out for QCD with Wilson quarks. They showed that, in order to reduce the $O(a)$ effects to $O(a^2)$ effects, only an extra dimension 5 operator is needed in the action as long as only on-shell quantities are concerned. The coefficient to be adjusted is commonly denoted as $c_{sw}(g_0)$. It is known to 1-,2-loop order of PT for various gauge actions. However, in the quenched case, [101] the non perturbative result for c_{sw} deviates from the one-loop perturbative one. With 2 flavours of Wilson

quarks, the effect was studied in [102] and a difference with the quenched case was visible. The results for three flavours was investigated in [103]. The inclusion of a third flavour does not affect the coefficient much. The determination for 4 flavours was recently done in [104]. The effect of including a fourth fermion is more dramatic than the inclusion of the third.

Concerning staggered fermions, as it was already stated in section 3.2.1., we have to be careful about the Symanzik improvement program. In section 3.2.1., this issue has already been addressed, concluding that improved local reconstructed staggered fields can be introduced in order to absorbe the illusive O(a) terms present in the reconstructed action. On the other hand, there are no dimension 5 operators that can act as counterterms. The absence of O(a) effects was already discussed in [61, 79] and revisited in [105, 92]. Nevertheless, in chapter 3, we have already discussed how to get an improved fermionic action at tree level. That is all we are going to require for the improvement program under consideration in this work.

Now, we focus our attention in the SF framework. It was already pointed out in chapter 3 that we expect the correction terms to come in two forms, operators from the boundaries and from the volume, Eq. (3.0.2). The boundary O(a) improvement was carried out for SU(2) and SU(3) Yang Mills theories up to one loop [35, 38]. A two loop computation including Wilson fermions can be found in [86]. In [106], the boundary improvement was determined for improved actions. Another way of obtaining an improved action in the SF framework is to perform a chiral twist so that automatic O(a) improvement can set in, as it has been discussed in [107].

That was a rough overview of the status of Symanzik improvement in lattice QCD. Now, we can discuss how it is implemented for our particular set up.

4.1 One loop $\mathrm{O}(a)$ improvement in a SF framework

The effective action Eq. (2.4.1) has a weak coupling saddle point expansion Eq. (2.4.7). In the previous chapter, some effort was put in order to remove the tree level O(a) contributions to this quantity. Now, we focus in the one loop O(a) contributions. That is, we are concerned with the O(a) effects of the quantity $\Gamma_1[B]$. The aim is to compute this quantity using perturbation theory on the lattice and identify the terms linear in the lattice spacing. The irrelevant countertems available should be enough to cancel these effects by tunning their O(g_0^2) coefficients. Here, we briefly discuss the structure of Γ_1 as well as the counterterms whose coefficients will be adjusted to improve the effective action and therefore the renormalised coupling constant $\bar{g}^2$ we are concerned with. It is to be noted that the adjustment of these coefficients will also amount to improve the observable $\bar{v}$ to one loop in PT.

$\Gamma_1[B]$ has the structure,

$$\Gamma_1 = \tfrac{1}{2} \ln\det \Delta_1 - \ln\det \Delta_0 - \ln\det \Delta_2. \tag{4.1.1}$$

The structure of the operators $\Delta_i, i = 0, 1, 2$ is to be discussed explicitly in the subsequent sections, (cf. section 4.2. for Δ_0, Δ_1 and cf. section 4.3. for Δ_2). Some remarks are nevertheless needed,

1. Δ_1, Δ_0 are pure gauge contributions. In order to compute Γ_1, a perturbative expansion if the gauge fields around the background field is needed. That leads us to the necessity of going through the gauge fixing procedure (our fluctuation field variables will not live in the group but in its algebra). Δ_1 is thus purely related to the fluctuation fields whereas Δ_0 is related to the ghost fields, cf. section 4.2. The $\mathrm{O}(a)$ effects will be cancelled by the pure gauge counterterm coming from the boundary, i.e., $c_t \operatorname{tr}\{F_{0k}F_{0k}\}$, since there are no $\mathrm{O}(a)$ counterterms available coming from the volume.
2. Δ_2 is related to the lattice Dirac operator. In chapter 3 we have improved the free version of it at tree level in PT. Therefore, the only $\mathrm{O}(a)$ contributions to Δ_2 are expected to be coming from the presence of gauge fields. Likewise Δ_0, Δ_1 the only pure gauge counterterm available is the boundary counterterm proportional to $c_t \operatorname{tr}\{F_{0k}F_{0k}\}$.

We thus conclude that the $\mathrm{O}(a)$ contributions can be cancelled by adjusting the coefficient c_t, Eq. (2.2.14) at one loop in perturbation theory. The one loop contribution will thus have two parts,

$$c_t^{(1)} = c_t^{(1,0)} + c_t^{(1,1)}(n_f). \tag{4.1.2}$$

Now, we have to relate all this with the observable. Performing an asymptotic expansion of the running coupling,

$$\bar{g}^2 = g_0^2 + m_1(L/a, n_f) g_0^4 + \mathrm{O}(g_0^6), \tag{4.1.3}$$

where m_1 is given by,

$$m_1 = -\frac{1}{k} \left. \frac{\partial \Gamma_1}{\partial \eta} \right|_{\eta=\nu=0} \tag{4.1.4}$$

with $k = \left. \frac{\partial \Gamma_0}{\partial \eta} \right|_{\eta=\nu=0}$. m_1 depends on the number of flavours and L/a. This dependence can be written,

$$m_1(n_f, L/a) = m_{1,0}(L/a) + n_f m_{1,1}(L/a). \tag{4.1.5}$$

Here, the first coefficient carries the pure gauge constributions, and it is linked to $\Delta_{0,1}$ and the second is related to the fermionic contributions and it is thus related to Δ_2. Their explicit relations read,

$$m_{1,0} = \frac{1}{k} \left\{ \frac{\partial}{\partial \eta} \ln \det \Delta_0 - \frac{1}{2} \frac{\partial}{\partial \eta} \ln \det \Delta_1 \right\}_{\eta=\nu=0}, \tag{4.1.6}$$

$$m_{1,1} = \frac{1}{n_f k} \left. \frac{\partial}{\partial \eta} \ln \det \Delta_2 \right|_{\eta=\nu=0}. \tag{4.1.7}$$

We expect $m_{1,0}, m_{1,1}$ to have an asymptotic expansion of the form,

$$m_{1,x}(L/a) \overset{L/a \to \infty}{\sim} \sum_{n=0}^{\infty} (a/L)^n \left(r_{n,x} + s_{r,x} \ln(L/a) \right). \tag{4.1.8}$$

Some details about this expansion will be given in the subsequent sections. From the expression above it is clear that we will be able to identify the $\mathrm{O}(a)$ contributions from the one loop expansion. Hence, we will be capable of adjusting $c_t^{(1)}$ in order to cancel them. The next two sections are entirely devoted to the determination of the quantities $m_{1,0}, m_{1,1}$ for our set up and the extraction of the one loop coefficient achieving the $\mathrm{O}(a)$ improvement.

4.2 Pure gauge contribution

In this section we will be concerned with the determination of $c_t^{(1,0)}$. Since a perturbative computation is required, we need to implement the gauge fixing procedure [108] and discuss how the boundary conditions set in for the fluctuation gauge fields and the ghosts. Then, we will explicitly show the structure of Δ_0, Δ_1 and how to extract $m_{1,0}(L/a)$. We will relate the asymptotic expansion of the latter to the improvement coefficient $c_t^{(1,0)}$ so that the Symanzik's program is implemented up to one-loop in PT for the pure gauge part of the action. Throughout the section, we will restrict ourselves to the pure gauge theory. Fermions will be ignored.

4.2.1 Gauge fixing

The action $S[U]$ and the measure $\mathcal{D}U$ are invariant under arbitrary gauge transformations, $U \to U^{\Omega}$. We are interested in evaluating the group of gauge transformations that leave the SF, $\mathcal{Z}[C, C']$ invariant.

The quantity $\mathcal{Z}[C', C]$ is invariant under all the gauge transformations that leave the boundary fields of Eq.(2.2.3) unchanged. The subgroup of the gauge transformations $\Omega : U \to U^{\Omega}$ compatible with this restriction are going to be denoted by $\hat{\mathcal{G}}$. In [35] its structure is discussed and it turns out that $\Omega(x)$ has to be constant and diagonal at $x_0 = 0, T$. Taking into account that the transformations $\Omega(x)$ such that $\Omega(x) \in C_3$, being C_3 the Cartan subgroup of SU(3) act trivially on the background field, we can conclude that the gauge directions in the space of infinitesimal deformations of the background field are generated by,

$$\mathcal{G} = \hat{\mathcal{G}}/C_3. \tag{4.2.1}$$

This subgroup of transformations is the one that needs to be fixed. The Cartan group survives as a global symmetry of the theory. We can identify $\mathcal{G}$ with the group of all transormations $\Omega \in \hat{\mathcal{G}}$ that are equal to 1 at $x_0 = T$.

Notation and algebra

We use here the same notation used by Lüscher et al. in [35]. $\mathcal{L}$ will be the Lie algebra of $\mathcal{G}$ and is generated by the fields $\omega(x)$ such that the infinitesimal gauge transformation,

$$\Omega(x) = 1 - g_0\omega(x) + \mathrm{O}(g_0^2) \in \mathcal{G}. \tag{4.2.2}$$

The boundary conditions that $\omega(x)$ has to satisfy are,

$$\omega(x)|_{x_0=0} = \kappa, \qquad \omega(x)|_{x_0=T} = 0, \tag{4.2.3}$$

where κ is constant and diagonal. Now a linear space $\mathcal{H}$ of vector fields $q_\mu(x)$ can be introduced in a similar way. If $V_\mu(x)$ is the classical gauge background field, then,

$$U_\mu(x) = \{1 + g_0 a q_\mu(x) + \mathrm{O}(g_0^2)\} V_\mu(x). \tag{4.2.4}$$

We have to guarantee that $U_\mu(x)$ has the same boundary values as $V_\mu(x)$. This feature obliges $q_k(x)$ to vanish at $x_0 = 0, T$. As we are dealing with linear vector spaces, we can define a scalar product. It will be defined as follows,

$$\begin{aligned} (q,r) &= -2a^4 \sum_{x,\mu} \mathrm{tr}\{q_\mu(x) r_\mu(x)\} \qquad \text{if } q, r \in \mathcal{H}, \\ (\omega,\sigma) &= -2a^4 \sum_{x} \mathrm{tr}\{\omega(x)\sigma(x)\} \qquad \text{if } \omega, \sigma \in \mathcal{L}. \end{aligned} \tag{4.2.5}$$

The covariant lattice derivatives are introduced as,

$$D_\mu f(x) = \frac{1}{a}\left[V_\mu(x) f(x + a\hat{\mu}) V_\mu(x)^{-1} - f(x)\right], \tag{4.2.6}$$

$$D_\mu f(x) = \frac{1}{a}\left[f(x) - V_\mu(x - a\hat{\mu}) f(x - a\hat{\mu}) V_\mu(x - a\hat{\mu})^{-1}\right]. \tag{4.2.7}$$

Gauge fixing function

To fix the gauge of the theory, we have to add a gauge fixing term to the Wilson action. This term has to be the square of a gauge fixing function, F. F has to be a mapping from the space of fields integrated over to the Lie algebra $\mathcal{L}$ previously defined. Let us introduce now the operator,

$$d : \mathcal{L} \mapsto \mathcal{H}, \qquad (d\omega)_\mu = D_\mu \omega(x). \tag{4.2.8}$$

It is important to note here that the covariant derivative is well defined for all x, μ, including the boundary values. The gauge fixing function must not vanish on the gauge modes. The function,

$$F(U) = d^* q, \tag{4.2.9}$$

satisfies all the requirements needed, that are specified in [109]. d^* here is the adjoint of d. That is, d^* maps any vector field $q \in \mathcal{H}$ onto an element of $\mathcal{L}$ such that,

$$(d^* q, \omega) = -(q, d\omega) \quad \forall \omega \in \mathcal{L}. \tag{4.2.10}$$

We have to be careful at the boundaries. In these cases, the operator has to be defined as,

$$[d^* q(x)]_{\alpha,\beta} = \begin{cases} (a^2/L^3) \sum_{\mathbf{y}} [q_0(0,\mathbf{y})]_{\alpha,\beta} & \text{if } \alpha = \beta \cap x_0 = 0, \\ 0, & \text{otherwise,} \end{cases} \tag{4.2.11}$$

so that the result belongs to $\mathcal{L}$.

Functional integral after gauge fixing

Now, following the steps described in [109], we can construct the gauge fixed form of the SF. Above, we have described the structure of the gauge fixing function, F. This functions leads to the gauge fixing term,

$$S_{gf}[B,q] = \frac{\lambda_0}{2}(d^*q, d^*q) \tag{4.2.12}$$

The action of the Faddeev-Popov fields is,

$$S_{FP}[B,q,c,\bar{c}] = -(\bar{c}, d^*\delta_c q), \tag{4.2.13}$$

where, $c, \bar{c}$ are the Faddeev-Popov ghost fields and $\delta_c q$ denotes the first order variation of q under the gauge transformation generated by c. To second order in g_0 we have

$$\delta_c q_\mu = D_\mu c + g_0 \mathrm{Ad} q_\mu c + \left[\tfrac{1}{2} g_0 a \mathrm{Ad} q_\mu + \tfrac{1}{12}(g_0 a \mathrm{Ad} q_\mu)^2 + \cdots\right] D_\mu c. \tag{4.2.14}$$

$\delta_c q_\mu$ is a vector field with the correct boundary values. The action given in Eq.(4.2.13) is therefore well defined. Now we can present the gauge fixed form of the Schrödinger functional,

$$\begin{aligned} e^{-\Gamma[B]} &= \int D[U] \int D[c] D[\bar{c}] e^{-S_{total}[B,q,c,\bar{c}]}, & (4.2.15)\\ S_{total}[B,q,c,\bar{c}] &= S[U] + S_{gf}[B,q] S_{FP}[B,q,c,\bar{c}], & (4.2.16) \end{aligned}$$

where U and q are related by,

$$U_\mu(x) = \exp\{g_0 a q_\mu(x)\} V_\mu(x). \tag{4.2.17}$$

Eq(4.2.15) is the starting point from which the expansion of the effective action $\Gamma[B]$ is obtained. If we note that,

$$\begin{aligned} D[U] &= D[q]\left\{1 + \mathrm{O}(g_0^2)\right\}, & (4.2.18)\\ S_{total}[B,q,c,\bar{c}] &= S[V] + \tfrac{1}{2}(q, \Delta_1 q) + (\bar{c}, \Delta_0 c) + \mathrm{O}(g_0). & (4.2.19) \end{aligned}$$

So, the first two contributions to the effective action will be,

$$\begin{aligned} \Gamma_0[B] &= g_0^2 S[V], & (4.2.20)\\ \Gamma_1[B] &= \tfrac{1}{2} \ln\det \Delta_1 - \ln\det \Delta_0. & (4.2.21) \end{aligned}$$

These operators Δ_0 and Δ_1 are the ones to be computed. Before discussing their structure, let us review the boundary conditions of the fluctuation vector fields $q_\mu(x)$ and the ghost fields $\bar{c}, c$.

Boundary conditions for the fluctuation and ghost fields

We have already given the boundary conditions that the lattice fields $q_\mu(x)$ and $\bar{c}, c$ have to satisfy. But these boundary conditions established are not enough to assure the desired behaviour of the fields in the continuum limit. As it has been discussed in [35], we can resolve this difficulty in the following way,

- In the case of the fluctuation vector fields, $q_\mu(x)$, what we do is to extend the time component $q_0(x)$ of the lattice to all points with $x_0 = -a$ and $x_0 = T$. Its values there are chosen such as,

$$D_0^* q_0(x) = d^* q(x) \qquad \text{at } x_0 = 0 \text{ and } x_0 = T. \tag{4.2.22}$$

  Eq.(4.2.22) can be interpreted as a boundary condition on q_0. At $x_0 = T$, it implies that $D_0^* q_0(x) = 0$ and at $x_0 = 0$ we have the fields ahve to satisfy the same relation, i.e., $D_0^* q_0(x) = 0$ (Neumann boundary conditions) with the exception of the spatially constant diagonal modes, that vanish at $x_0 = -a$ and thus have to satisfy Dirichlet boundary conditions.
- In the case of the Faddeev-Popov fields, the spatially constant diagonal modes satisfy Neummann boundary conditions at $x_0 = 0$. In our choice of the boundary values, it turns out that we have Dirichlet boundary conditions for all modes.

Summarising, the boundary conditions for q are a mixture of Dirichlet and Neumann boundary conditions. Now we are ready to determine Δ_0 and Δ_1 for the cases taken into account in this work.

4.2.2 Structure of the operators Δ_0 and Δ_1

Here, we discuss the structure of the operators, Δ_0 and Δ_1. The structure of these operators for lattices satisfying $T = L$ has been described in [35, 110]. As we are considering lattices with $T = L \pm a$ we have to include some modifications. With $L = T' = T + sa$, the expression for the background field is given by Eq. (2.2.21). The values of f have been computed and listed in Table 2.2 for a wide range of L/a. An independent calculation was done in [68] and our results were confirmed. What is important to note here is that the background field is linear in x_0 in the bulk, but, the slope of the function $B(x_0)$ has a discontinuity in $x_0 = 0, T$. That leads to the following expression for $G_{\mu\nu}(x) = \partial_\mu B_\nu(x) - \partial_\nu B_\mu(x)$ (the only non zero contribution is G_{0k}),

$$\begin{aligned} G_{0k} &= f \qquad x_0 \in [a, T-a] \\ G_{0k} &= F \qquad x_0 = 0, T, \end{aligned} \tag{4.2.23}$$

with,

$$F = \left(1 - \frac{T/a}{2}\right) f + \frac{C'_k - C_k}{2}. \tag{4.2.24}$$

Structure of Δ_0

The modification introduced leaves Δ_0 unchanged. Thus, the operator Δ_0 will be given by,

$$\Delta_0 = -d^* d, \tag{4.2.25}$$

being d, d^* the operators defined in the previous subsection. Note that we will have to insert the new background fields in the derivatives.

Structure of Δ_1

Δ_1 will be, as in [35, 110],

$$\Delta_1 = \Delta_1' - \lambda_0 dd^*, \tag{4.2.26}$$

where $-\lambda_0 dd^*$ comes from the gauge fixing term and Δ_1' is obtained by expanding the Wilson action $S[U]$ to second order in q. This part of Δ_1 is the one that suffers a modification. As it has been done in [35], we introduce the $\star$ product notation. Let M, X be two $N \times N$ matrices. Then,

$$M \star X = \tfrac{1}{2}\left(MX + XM^\dagger\right) - \tfrac{1}{2N}\mathrm{tr}\left(MX + XM^\dagger\right). \tag{4.2.27}$$

$M \star X$ is contained in the Lie algebra of $SU(N)$, $\mathcal{L}_{SU(N)}$ $\forall X \in \mathcal{L}_{SU(N)}$ and arbitrary M. The modifications arise when $x_0 = 0$ and $\mu = 0$, $x_0 = a$ and $\mu = 1, 2, 3$ and when $x_0 = T - a$. In the rest of the cases, we have,

$$\begin{aligned} \Delta_1' q_\mu(x) \;=\; & \sum_{\nu \neq \mu} \big\{ \cosh(a^2 G_{\mu\nu}) \star [-D_\nu^* D_\nu q_\mu(x) + D_\nu^* D_\mu q_\nu(x)] \\ & -a^{-2} \sinh(a^2 G_{\mu\nu}) \star \left[2q_\nu(x) + a(D_\nu^* + d_\nu) q_\mu(x) + a^2 D_\nu^* D_\mu q_\nu(x).\right] \big\} \end{aligned} \tag{4.2.28}$$

Defining,

$$C^{F-f} = c_t^{(0)} \cosh(a^2 F) - \cosh(a^2 f), \tag{4.2.29}$$

and,

$$(\Delta_1')(f) q_\mu(x) = \Delta_1' q_\mu(x), \qquad \text{with } G_{\mu\nu} = f, \tag{4.2.30}$$

$$(\Delta_1')(F) q_\mu(x) = \Delta_1' q_\mu(x), \qquad \text{with } G_{\mu\nu} = F, \tag{4.2.31}$$

the operator Δ_1' will be,

$$\begin{aligned} \Delta_1' q_k(a, \mathbf{x}) &= (\Delta_1')(f) q_k(a, \mathbf{x}) + C^{F-f} \star \left(q_k(a, \mathbf{x}) + D_0^* D_k q_0(a, \mathbf{x}) - D_k q_0(a, \mathbf{x})\right), \\ \Delta_1' q_k(T-a, \mathbf{x}) &= (\Delta_1')(f) q_k(T-a, \mathbf{x}) + C^{F-f} \star \left(q_k(T-a, \mathbf{x}) + D_k q_0(T-a, \mathbf{x})\right), \\ \Delta_1' q_0(0, \mathbf{x}) &= c_t^{(0)} (\Delta_1')(F) q_0(0, \mathbf{x}), \\ \Delta_1' q_0(T-a, \mathbf{x}) &= c_t^{(0)} (\Delta_1')(F) q_0(T-a, \mathbf{x}), \\ \Delta_1' q_\mu(x) &= (\Delta_1')(f) q_\mu(x) \qquad \text{otherwise.} \end{aligned} \tag{4.2.32}$$

Note that the latin indices refer to spatial directions, $k = 1, 2, 3$.

4.2.3 Computation of $m_{1,0}(L/a)$

The pure gauge one loop coefficient has two contributions, Eq. (4.1.6). Here, we will use the notation,

$$\begin{aligned} m_{1,0}(L/a) &= h_0 - \tfrac{1}{2}h_1, \\ h_s &= \frac{1}{k}\frac{\partial}{\partial\eta}\ln\det\Delta_s, \qquad s=0,1. \end{aligned} \tag{4.2.33}$$

We will discuss here how to explicitly perform the computation of h_s, $s=0,1$.

Symmetries

As it has been discussed in [111], the operators become diagonalized in colour space decomposing the Hilbert space into,

$$\mathcal{H} = \mathcal{H}_1 \oplus \mathcal{H}_2 \oplus \mathcal{H}_3 \oplus \mathcal{H}_4 \oplus \mathcal{H}_5 \oplus \mathcal{H}_6 \oplus \mathcal{H}_7 \oplus \mathcal{H}_8, \tag{4.2.34}$$

where $\mathcal{H}$ is the space where Δ_1 lives. The same expression holds for $\mathcal{L}$, where Δ_0 lives. Each sector $\mathcal{H}_a$ (or correspondingly, $\mathcal{L}_a$) is proportional to I_a. The explicit form of these I_a's are given in appendix F. The convention used here is the same as the one used by Peter Weisz in [110]. Now, the covariant derivatives and star operation act diagonally and we get,

$$\begin{aligned} \cosh(F)\star I_a = C_a^F I_a \qquad & \cosh(f)\star I_a = C_a^f I_a, \\ \sinh(F)\star I_a = S_a^F I_a \qquad & \sinh(f)\star I_a = S_a^f I_a, \end{aligned} \tag{4.2.35}$$

and,

$$\begin{aligned} (D_k f)(x) &= \sum_a I_a \left[\exp(i\phi_a(x_0)) f^a(x+\hat{k}) - f^a(x)\right], \\ (D_k^* f)(x) &= \sum_a I_a \left[f^a(x) - \exp(-i\phi_a(x_0)) f^a(x-\hat{k})\right], \\ (D_0 f)(x) &= \sum_a I_a \left[f^a(x_0+\hat{0},\mathbf{x}) - f^a(x_0,\mathbf{x})\right], \\ (D_0^* f)(x) &= \sum_a I_a \left[f^a(x_0,\mathbf{x}) - f^a(x_0-\hat{0},\mathbf{x})\right], \end{aligned} \tag{4.2.36}$$

where the coefficients $C_a^f, S_a^f, C_a^F.S_a^F, \phi_a(x_0)$ are given in appendix F. Note that the two previous equations are written in lattice units, and thus, the parameter a has been set to 1. In the following $a=1$. So far we have decomposed the operators Δ_0, Δ_1 in their colour sectors, that is,

$$\begin{aligned} \det\Delta_1 &= \prod_{a=1}^{8} \det\Delta_1|_{\mathcal{H}_a}, \\ \det\Delta_0 &= \prod_{a=1}^{8} \det\Delta_0|_{\mathcal{L}_a}. \end{aligned} \tag{4.2.37}$$

We can obtain a further factorisation of the determinants using the invariance under translations. The eigenfunctions of this symmetry are the plane waves $e^{i\mathbf{px}}$ where,

$$\mathbf{p} = 2\pi\mathbf{n}/L \qquad n_k \in \mathbb{Z}, \qquad -L/2 < n_k \leq L/2. \tag{4.2.38}$$

We introduce the subspaces $\mathcal{H}_a(\mathbf{p})$ and $\mathcal{L}_a(\mathbf{p})$ of all functions proportional to $e^{i\mathbf{px}}$ and have no other dependence on $\mathbf{x}$. The operators Δ_0, Δ_1 do not change the momentum. Thus, it follows that,

$$\begin{aligned} \det \Delta_1 &= \prod_{a=1}^{8} \prod_{\mathbf{p}} \det \Delta_1|_{\mathcal{H}_a(\mathbf{p})}, \\ \det \Delta_0 &= \prod_{a=1}^{8} \prod_{\mathbf{p}} \det \Delta_0|_{\mathcal{L}_a(\mathbf{p})}. \end{aligned} \tag{4.2.39}$$

The problem of computing these operators has been reduced to computing the determinants of a set of finite difference operators in one dimension (x_0).

Computation of h_0

The only colour sectors that contribute to Δ_0 are $a = 1, 2, 4, 5$. And, as it has been discussed in [111], their contributions are equal. So, we are left with,

$$\frac{\partial}{\partial \eta} \ln \det \Delta_0 = 4 \sum_{\mathbf{p}} \frac{\partial}{\partial \eta} \ln \det \Delta_0|_{\mathcal{L}_1(\mathbf{p})}. \tag{4.2.40}$$

Let us focus on the $\mathcal{L}_1(\mathbf{p})$ symmetry sector. The relevant eigenvectors of this sector are,

$$\omega(x) = \psi(x_0) e^{i\mathbf{px}} I_1, \tag{4.2.41}$$

where $\psi(t)$, $0 \leq t \leq T$ is a complex function. As we have discussed before, the ghost fields obey Dirichlet boundary conditions, and, as I_1 is off diagonal, $\kappa = 0$ in Eq.(4.2.3). Thus,

$$\psi(0) = \psi(T) = 0. \tag{4.2.42}$$

On this set of functions, Δ_0 reduces to an ordinary second order difference operator,

$$\Delta_0 \psi(t) = \mathcal{A}(t)\psi(t+1) + \mathcal{B}(t)\psi(t) + \mathcal{C}(t)\psi(t-1). \tag{4.2.43}$$

The coefficients are given by ,

$$\begin{aligned} \mathcal{A}(t) &= \mathcal{C}(t) = -1, \\ \mathcal{B}(t) &= 8 - 2\sum_{k} \cos\left[\phi_1(t) + p_k\right]. \end{aligned} \tag{4.2.44}$$

For small lattices, a program in Maple has been written to calculate the values of Eq.(4.2.40). The determinant of difference operators can be computed by solving a simple recursion relation. The technical issues have been briefly discussed in the Appendices of [35, 66]. We have used this technique to compute Eq.(4.2.40). Using long-double precision, and for lattices with $L < 11$, the maple results coincide with the C results up to the 15^{th} significative digit. The rounding errors will increase with the lattice size, as more operations are needed.

Computation of h_1

As we have discussed before, we extend the fields $q_0(x)$ to $x_0 = -a, T$. The boundary conditions for $q_\mu(x)$ have been already described; they are a mixture of Neumann and Dirichlet boundary conditions. For every $\mathcal{H}_a(\mathbf{p})$ symmetry sector, the wave functions are of the form,

$$\begin{aligned} q_0(x) &= I_a e^{i\mathbf{px}} \psi_0(x_0), \\ q_k(x) &= I_a e^{i\mathbf{px}} e^{i(p_k+\phi_a(x_0))/2} \psi_k(x_0). \end{aligned} \tag{4.2.45}$$

The action of the operator Δ_1 acting on wave functions of Eq. (4.2.45) is of the general form,

$$(\Delta_1\psi)_\mu(t) = \mathcal{A}_{\mu\nu}(t)\psi_\nu(t+1) + \mathcal{B}_{\mu\nu}(t)\psi_\nu(t) + \mathcal{C}_{\mu\nu}(t)\psi_\nu(t-1). \tag{4.2.46}$$

In appendix F, we give the coefficient matrices $\mathcal{A}, \mathcal{B}, \mathcal{C}$ explicitly. The colour indices $a = 1, 2, 4, 5$ give the same contribution to Δ_1 and $a = 6, 7$ contributions are also equal, so we have that,

$$\begin{aligned} \frac{\partial}{\partial\eta} \ln\det\Delta_1 &= \sum_{\mathbf{p}} \frac{\partial}{\partial\eta} \left\{ 4 \ln\det\Delta_1|_{\mathcal{H}_1(\mathbf{p})} + 2\ln\det\Delta_1|_{\mathcal{H}_6(\mathbf{p})} \right. \\ &\quad \left. + \ln\det\Delta_1|_{\mathcal{H}_3(\mathbf{p})} + \ln\det\Delta_1|_{\mathcal{H}_8(\mathbf{p})} \right\}. \end{aligned} \tag{4.2.47}$$

For lattices with $L = 4, 5$ a Maple program has been written to calculate the determinant explicitly. A C program has also been written that obtains the quantity of Eq. (4.2.47) using the techniques described in the appendices of [35, 66]. As in the computation of Δ_0, we have used cuadruple precision for the C program. To estimate the rounding errors, we have compared the results obtained by Maple with the results obtained by C for lattices with $L = 4, 5$. For these lattices, we have 16-17 digits of precision in the C results. We have to take into account that, like it happened with the calculation of Δ_0, the rounding errors increase with the lattice size (as more operations are needed).

Results for $m_{1,0}(L/a)$

In appendix G, Table G.3. we present the results obtained for $m_{1,0}(L/a)$, for lattices with $L \in [4, 54]$ and for $s = 0, \pm 1$.Comparing these results with the ones shown in [68], we can estimate the size of the rounding errors. We compare the data at $L = 4, 32, 54$. In Table 4.1., we present the number of coincident digits.

L/a	$s=1$	$s=0$	$s=-1$
4	15	15	15
32	11	11	12
54	10	12	11

Table 4.1: Precision obtained for $m_1(L/a)$ values.

From Symanzik's analysis of cutoff dependence of Feynman diagrams on the lattice, one expects $m_{1,0}(L/a)$ to have an asymptotic expansion of the form Eq. (4.1.8). r_0 is going to give us information about the ratio of Λ-parameters (when it comes to compare different regularisation). s_0 should be $2b_0$, with $b_0 = 11/(4\pi)^2$ the one loop universal coefficient of the β function. To achieve the $\mathrm{O}(a)$ improvement, r_1 will be needed. If the tree level $\mathrm{O}(a)$ improvement was satisfactorily implemented, $s_0 = 0$. Following the method presented in the appendix of [86], the first coefficients were extracted in [68]. We analise the data for cases $s = 0, 1, -1$ shown in Tables 4.2, 4.3, 4.4. respectively. In these talbes, numbers with no errors have been assumed, entries $\times$ have also been fitted but not listed here and the terms $\sim$ are included one at a time for error analysis as described in [86].

$s_{0,0}$	$r_{0,0}$	$s_{1,0}$	$r_{1,0}$	$s_{2,0}$	$r_{2,0}$	$s_{3,0}$	$r_{3,0}$
0.13931(3)	0.3683(2)	$-0.001(13)$	$-0.17(7)$	$\times$	$\times$	$\sim$	$\sim$
$22/(4\pi)^2$	0.368283(2)	$-0.0003(9)$	$-0.176(6)$	$\times$	$\times$	$\sim$	$\sim$
$22/(4\pi)^2$	0.3682817(7)	0	$-0.1779(3)$	$\times$	$\times$	$\sim$	$\sim$

Table 4.2: $m_{1,0}(L/a)$ asymptotic expansion coefficients, $s = 0$.

$s_{0,0}$	$r_{0,0}$	$s_{1,0}$	$r_{1,0}$	$s_{2,0}$	$r_{2,0}$	$s_{3,0}$	$r_{3,0}$
0.13931(2)	0.3683(1)	0.001(7)	0.12(3)	$\times$	$\times$	$\sim$	$\sim$
$22/(4\pi)^2$	0.368280(1)	0.0007(5)	0.120(3)	$\times$	$\times$	$\sim$	$\sim$
$22/(4\pi)^2$	0.368283(1)	0	0.1232(4)	$\times$	$\times$	$\sim$	$\sim$

Table 4.3: $m_{1,0}(L/a)$ asymptotic expansion coefficients, $s = 1$.

$s_{0,0}$	$r_{0,0}$	$s_{1,0}$	$r_{1,0}$	$s_{2,0}$	$r_{2,0}$	$s_{3,0}$	$r_{3,0}$
0.13931(4)	0.3683(3)	$-0.001(15)$	$-0.23(7)$	$\times$	$\times$	$\sim$	$\sim$
$22/(4\pi)^2$	0.368283(3)	$-0.0004(10)$	$-0.230(6)$	$\times$	$\times$	$\sim$	$\sim$
$22/(4\pi)^2$	0.3682818(7)	0	$-0.2318(3)$	$\times$	$\times$	$\sim$	$\sim$

Table 4.4: $m_{1,0}(L/a)$ asymptotic expansion coefficients, $s = -1$.

4.2.4 Determination of $c_t^{(1,0)}$

To include the $c_t^{(1)}$ coefficient, we expand the action as a Taylor series about $c_t = c_t^{(0)}$,

$$S_{latt} = S_{latt}\big|_{c_t=c_t^{(0)}} + g_0^2 \frac{\partial S_{latt}}{\partial c_t}\Big|_{c_t=c_t^{(0)}} c_t^{(1)}. \tag{4.2.48}$$

Calculating $\partial S_{latt}/\partial c_t$, we get,

$$\frac{\partial S_{latt}}{\partial c_t}\Big|_{c_t=c_t^{(0)}} = 2 \cdot 12 \left(\frac{L}{a}\right)^3 \left(a^2 \frac{\partial F_2}{\partial \eta}\right) \left(\sin\left[2a^2 F_2\right] + \sin\left[a^2 F_2\right]\right). \tag{4.2.49}$$

Now, we can express,

$$\Gamma[B] = g_0^{-2}\Gamma_0|_{c_t=c_t^{(0)}} + c_t^{(1)}\partial_{c_t}\Gamma_0[B]|_{c_t=c_t^{(0)}} + \Gamma_1[B] + g_0^2\Gamma_2[B] + \cdots \tag{4.2.50}$$

To simplify the notation, $\Gamma_{c_t^{(1)}}[B] = \partial_{c_t}\Gamma_0[B]|_{c_t=c_t^{(0)}}$, and $\Gamma_0|_{c_t=c_t^{(0)}} = \Gamma_0[B]$. Now, in the definition of the coupling, we have,

$$\bar{g}^2(L) = \frac{\Gamma_0'[B]}{\Gamma'[B]} = g_0^2 + \left(m_{1,0}(L/a) - c_t^{(1)}\frac{\Gamma_0'[B]}{\Gamma'_{c_t^{(1)}}} \right) g_0^4. \tag{4.2.51}$$

The quantity $\Gamma_0'[B]/\Gamma'_{c_t^{(1)}} \sim \mathrm{O}(a/L)$ and can remove the contribution of r_1. To achieve it, we have to impose,

$$\frac{a}{L}r_1 - c_t^1\frac{\Gamma_0'[B]}{\Gamma'_{c_t^{(1)}}} = 0 \tag{4.2.52}$$

We have calculated the quantity $(L/a)\Gamma_0'[B]/\Gamma'_{c_t^{(1)}}$ in the continuum limit, as a function of s. Recall that $s = 0, \pm 1$. We have arrived at the following expression,

$$\lim_{L/a\to\infty} \frac{\Gamma_0'[B]}{\Gamma'_{c_t^{(1)}}}\frac{L}{a} = 2\left(\frac{2+s}{2}\right)^2 \tag{4.2.53}$$

So, we can write $c_t^{(1,0)}$ as a function of $r_{1,0}$, obtaining,

$$c_t^{(1,0)} = \frac{r_{1,0}}{2}\left(\frac{2}{2+s}\right)^2. \tag{4.2.54}$$

We have written a Maple program to calculate $(L/a)\Gamma_0'[B]/\Gamma'_{c_t^{(1)}}$ for finite lattices, to check the results in Eq.(4.2.53). We could use the results of the analysis of $m_1(L/a)$ presented in [68] to calculate $c_t^{(1,0)}$, then. $c_t^{(1,0)}$ can now be included in a dynamical simulation. The best fit for the extraction of r_1 is the one in the last line of Tables 4.3, 4.4. Using it we arrive at the following values for $c_t^{(1,0)_s}$,

$$c_t^{(1,0)_1} = 0.0274(2) \qquad c_t^{(1,0)_{-1}} = -0.4636(6). \tag{4.2.55}$$

4.3 Fermionic contribution

Now, $c_t^{(1,1)}$ is determined. The strategy followed is similar to the one in the previous section but applied to the fermionic part of the action. We will discuss the structure of the operator Δ_2 and compute $m_{1,1}(a/L)$. From its asymptotic expansion, we will be able to adjust the improvement coefficient $c_t^{(1,1)}$. This coefficient was computed in [66] for Wilson quarks. An attempt for the determination of the same coefficient in the case of staggered quarks is presented in [50]. However, the Dirac operator used in this work did not include the boundary improvement at tree level in PT cf. 3.2.2.

4.3.1 Structure of Δ_2 and computation of $m_{1,1}(L/a)$

The improved fermionic action, fully specified in Eq. (3.2.44) can be written as,

$$S_f^{\rm imp} = \sum_{x,z} \bar{\chi}(x) \left(\Delta_2\right)_{x,z} \chi(z). \tag{4.3.1}$$

The procedure to compute Δ_2 is the exact the same as the one followed to compute the pure gauge operators. In Eq. (2.3.67) the structure of the unimproved Dirac operator is specified in the time momentum representation. Since the eigenfunctions of the lattice operator take the form,

$$\chi(x) = e^{i(\mathbf{q}+\pi\boldsymbol{\eta}/a)\mathbf{x}} u_{n_c} f_{\boldsymbol{\eta}}(x_0), \tag{4.3.2}$$

where,

$$q_k = \frac{2\pi n_k}{L} + \frac{\theta_k}{L}, \qquad n_k = 0, \ldots, \frac{1}{2}L_k - 1, \tag{4.3.3}$$

and $\{u_{n_c}, n_c = 1,2,3\}$ denotes the canonical basis in colour space. Note that the momenta only run until half the Brillouin zone, since we have included the factor $\boldsymbol{\eta}$ that covers the rest of it. This index becomes and "internal" index, loosely corresponding to spin flavour. This decomposition becomes relevant when reconstruction is involved. In section 2.3.4. we have introduced the momenta $\mathbf{p} = 2\mathbf{q}$, Eq. (2.3.59). They are the momenta associated with the Fourier transform of the reconstructed fermions. In this section, we will use the momenta defined above.

So, we can diagonalise in momenta and in colour space, as we have done before. $\det \Delta_2$ can thus be factorised,

$$\det \Delta_2 = \prod_{n_c=1}^{3} \prod_{\mathbf{q}} \det \Delta_2|_{\mathcal{H}_{n_c}(\mathbf{q})}. \tag{4.3.4}$$

We can give an explicit expression for $\Delta_2|_{\mathcal{H}_{n_c}(q)}$,

$$\begin{aligned}
\Delta_2(x_0, x_0', \boldsymbol{\eta}, \boldsymbol{\eta}', \mathbf{q})_{n_c} \;=\; & \frac{1}{2}\left[\delta_{x_0,x_0'-a} - \delta_{x_0,x_0'+a}\right] \\
& + i\sum_{k=1}^{3} \bar{\delta}_{\boldsymbol{\eta}+\boldsymbol{\eta}^{(k)},\boldsymbol{\eta}'} \delta_{x_0,x_0'} (-1)^{\eta_k + x_0} \sin\left(q_k + B_k^{n_c}(x_0)\right) \\
& + i(d_{1s}-1)(\delta_{x_0,a} + \delta_{x_0,T-a}) \sum_{k=1}^{3} \bar{\delta}_{\boldsymbol{\eta}+\boldsymbol{\eta}^{(k)},\boldsymbol{\eta}'} \delta_{x_0,x_0'} (-1)^{\eta_k + x_0} \sin\left(q_k + B_k^{n_c}(x_0)\right),
\end{aligned} \tag{4.3.5}$$

with,

$$\eta_\nu^{(\mu)} = \begin{cases} 1 & \text{for} \quad \nu < \mu \\ 0 & \text{for} \quad \nu \geq \mu \end{cases}, \tag{4.3.6}$$

and $\bar{\delta} = \delta \mod 2$. Some remarks need to be done,

i) Concerning the hermiticity of the staggered fermionic operator, it is a known result that the relation,

$$(-1)^{|x|}(\Delta_2)_{x,z}(-1)^{|z|} = (\Delta_2)^{\dagger}_{z,x}, \tag{4.3.7}$$

with $(-1)^{|x|} = (-1)^{\sum_{\nu=0}^{3} x_\nu/a}$. From this identity, we can conclude that $\mathcal{M}_{x,z} \equiv (-1)^{|x|}(\Delta_2)_{x,z}$ is hermitian and has the same determinant as $(\Delta_2)_{x,z}$.

ii) Concerning the boundary conditions, they amount to,

$$f_{\boldsymbol{\eta}}(0) = 0, \qquad f_{\boldsymbol{\eta}}(T) = 0. \tag{4.3.8}$$

We have thus specified the structure of Δ_2. Now, noticing that,

$$m_{1,0}(L/a)\frac{1}{k}\sum_{n_c=1}^{3}\sum_{\mathbf{q}}\left\{\frac{\partial}{\partial\eta}\ln\det(\Delta_2)|_{\mathcal{H}_{n_c}(\mathbf{q})}\right\}_{\eta=\nu=0}, \tag{4.3.9}$$

where here η is the parameter on which the background field depends. Apologies for the overlapping notation. Now, it can be solved using the same technique used for the pure gauge operators. See [35, 66] for techincal details.

In appendix G, Table G.1, G.2., we present the results obtained for lattices with $L \in [4, 80]$ for different values of the phase factor θ. For our simulations $\theta = \pi/5$ will be used since it was noted in [66] that the condition number (ration between the highest and lowest eigenvalue) of the fermionic operator is minimised for this choice of θ, speeding up the simulations.

The continuum limit is approached when we take L/a to infinity. We expect $m_{1,1}(L/a)$ to have an asymptotic expansion of the form Eq. (4.1.8).The first few coefficients can be extracted. To analyse our data, we are using the MATLAB adaptation of the method in [86] performed by Björn Leder. Details about the program and its implementation to our particular problem are given in [112]. s_0, the coefficient of the logarithmically divergent term in the continuum limit, should be $2b_{0,1} = -1/(12\pi^2)$, the fermionic contribution, per flavour, to the $\beta-$ function [66], and thus be absorbed by renormalisation. $s_{0,1}$ was found to be compatible with zero with four digits of accuracy. To extract $r_{0,1}, r_{1,1}$, we assume the exact value for $s_{0,1}$ and $s_{1,1} = 0$. The results are shown in Table 4.5 for different values of θ.

θ	$r_{0,1}, s=-1$	$r_{1,1}, s=-1$	$r_{0,1}, s=1$	$r_{1,1}, s=1$
0	−0.0044155(2)	−0.0134(2)	−0.0044156(1)	0.0350(1)
$\pi/5$	−0.00579695(4)	−0.01330(4)	−0.005796920(3)	0.035035(2)
1	−0.0068642(1)	−0.0133(1)	−0.0068642(3)	0.0351(3)
2	−0.0087821(3)	−0.0133(3)	−0.0087821(4)	0.0351(4)

Table 4.5: The first two 'non-log' terms in the expansion Eq. (4.1.8) of $m_{1,1}$.

This computation was performed in [66] for Wilson quarks, and later on by Heller in [50] for staggered quarks. However, in his calculation, he took $c_t^{(0)}$ to be 1, he did not

include the boundary counterterms concerning fermions. In his results the coefficient $r_{1,1}$ had a dependence on the phase factor θ for the different values of s. Only when he averaged between the two values of $r_{1,1}$ for the two values of s that he got a θ independent result.

The results shown in Table 4.5 are consistent with our expectations. The values for r_0 coincide with the Heller's results in [50]. Moreover, for a given θ, the values of r_0 are equal within errors for the two cases under consideration, i.e., $s = \pm 1$.

As it will be discussed in the next subsection, $r_{1,1}$ is proportional to $c_t^{(1,1)}$ which is the coefficient for the pure gauge boundary counterterm. Thus, $r_{1,0}$ cannot depend on θ. This fact is also consistent with our results.

4.3.2 Determination of $c_t^{(1,1)}$

Now, We are ready to determine the $c_t^{(1,1)}$ coefficient. Using an analogous argument to the one presented in section 4.2.4., we arrive at,

$$c_t^{(1,1)_s} = \frac{r_{1,1}^s}{2}\left(c_t^{(0)_s}\right)^2. \tag{4.3.10}$$

Thus, we get, for the two values of s,

$$c_t^{(1,1)_1} = 0.0077856(4), \qquad c_t^{(1,1)_{-1}} = -0.0266(8). \tag{4.3.11}$$

Chapter 5

Details of the numerical simulations.

In Chapter 2, we have presented the SF with staggered fermions and given a definition of a renormalised coupling constant. Chapters 3 and 4 have been devoted to achieve an O(a) improvement of our framework. The main motivation was that computer simulations are restricted to lattice spacings that are not desirably small. If we want to obtain renormalised physical quantities, the cutoff dependence has to be removed, i.e., a continuum limit is required. The smaller the measured quantities' cutoff dependence, the more reliable our extrapolation will be.

Now, we are ready to perform simulations on a computer. The fact that the lattice formulation of a QFT could be simulated on a computer was first pointed out by M. Creutz in [23, 24]. He performs his calculations using Monte Carlo integration techniques for SO(2) in 4D, SU(2) in 5D and, in the latter referred paper, SU(2) in 4D. Since then, the lattice approach, together with numerical simulations, has become the most powerful tool for the performance of non perturbative calculations.

As it has been stated in the introduction, the final goal of this project is to obtain the energy dependence of a non perturbative coupling constant from hadronic to perturbative regime for a system with 4 flavours of quarks. The code available on line by the MILC collaboration (version 6.20sep02, http://www.physics.utah.edu/ detar/milc/milcv6.html) with some customisation implements an option for performing simulations on the Schrödinger Functional with staggered fermions. However, it does not include the O(a) improvement discussed in the previous chapters. This code has been used in [41] to perform a lattice study of conformal behaviour in SU(3) Yang-Mills theories, where the simulations were run for the two regularisations available and an average between the two was taken in the end.

For the study under consideration, the original MILC code had to be modified. The changes made are due to the following aspects:

- We want to include the study of the variable $\bar{v}$, so we had to implement its measurement.

- As it has been ulteriorly discussed in chapters 3, 4, since our system has dimensions $T = L - sa$, Heller setup has tree level O(a) effects. We have managed to tune the coefficients c_t and d_s to one loop and tree level in perturbation theory respectively to cancel the O(a) effects. This modifications had to be included in the MILC code as well.

In this chapter, we will give a brief introduction about the algorithm used and describe the characteristics of the machines used to run the simulations. After that, we will discuss the modifications required to implement the Symanzik improvement and we will present the tests that have been performed to the modified code in order to make sure it had been accurately implemented.

5.1 Algorithms

The goal of the numerical simulations in lattice QCD is to obtain estimators of the expectation values of observables of the theory. These expectation values are defined by the Functional Integral. Let $A[U]$ be an observable, that is a function of the field variables U. Then, its expectation value will be given,

$$\langle A \rangle = Z^{-1} \int [dU] e^{-S[U]} A[U], \quad Z = \int [dU] e^{-S[U]}. \tag{5.1.1}$$

Some references that describe the computational strategies in Lattice QCD would be [55, 113, 114, 115, 116]. For a more theoretical approach, see [117]. The QCD simulations we are discussing here are based on:

- Importance sampling,
- Markov chains,
- The HMC algorithm.

Let us discuss these three issues separately.

5.1.1 Importance sampling

In the case of field systems of interest, the number of integration variables is very large. It would be untractable to solve the integral numerically. However, we are interested computing expectation values. Monte Carlo methods can be used to extract these quantities. The Monte Carlo integration is based on identifying probabilities with measures. Let us first restrict to a pure gauge theory on the lattice with link variables $U_\mu(x)$. In that case, the quantity,

$$p[U] = \frac{1}{Z} e^{-S_G[U]}, \qquad Z = \int_\Omega D[U] e^{-S_G[U]}, \tag{5.1.2}$$

is a probability density, and $d\mu_U = p[U]D[U]$ defines a measure. Ω is the domain of integration. If we include the fermions, they have to be integrated out, and it has to

be ensured that the fermionic determinant is positive (which is going to be the case for staggered fermions). Once that is guaranteed, we can proceed just as before and say that a measure can be defined. Now, the expectation value of a quantity, A, can be written as,

$$\langle A \rangle = \int_{\Omega} A[U] d\mu_U. \tag{5.1.3}$$

For the moment being, let us assume that the random variables, namely U_i are independent. The **law of large numbers** together with the **central limit theorem** guarantees that if one produces N outcomes of $U_1, U_2, \ldots, U_N$ with the probability density $d\mu_U$, then

$$\frac{1}{N} \sum_{i=1}^{N} A(U_i) = \langle A \rangle + \mathrm{O}\left(\frac{1}{\sqrt{N}}\right). \tag{5.1.4}$$

Note that U_i stands for a complete gauge configuration throughout the lattice. N has to be sufficiently large for the central limit theorem to apply.

If $p[U]$ was easily sampled, then we would have found a way to compute quantities. The law of large numbers ensures that the estimate is correct and the central limit theorem provides an estimate of the statistical uncertainty in the estimate. This method is known as Monte Carlo integration.

However, we encounter three delicate and cumbersome problems. First, Monte Carlo integration requires random numbers, but computers are deterministic. There has been a huge effort put on this issue in order for the computer to provide pseudo random numbers. The details will not be discussed here.

Secondly, the probability distribution we are facing is sharply peaked. Then, it would be prohibitely expensive to try to generate configurations distributed in the way we want starting with flat distributed numbers. **Importance sampling** can greatly improve the efficiency of the algorithm. Let's assume we know how to produce quantities distributed according to a different probability density, namely, $g[U]D[U]$, such that $h[U] = \frac{p[U]}{g[U]}$ is as close as possible to a flat distribution. Then, starting with U_i's following the distribution given by $g[U]$, it will be computationally feasible to get U_i's distributed according to the desired probability density $p[U]D[U]$.

An additional problem is that it is highly multidimensional integrals we are dealing with. Fortunately, it is possible to deal with them by exploiting **stationary stochastic processes**.

An stochastic process is a collection of random variables in a probability space. A probability space is characterised by the quantities $(\Omega, \mathcal{F}, \mu)$, Ω being a set, $\mathcal{F}$ a sigma algebra in Ω and μ a probability measure [118, 119].

Before we proceed, it is perhaps convenient give a proper definition for a $\sigma-$algebra, $\mathcal{F}$ in a set Ω. The collection of subsets of Ω, $\mathcal{F}$ is a $\sigma-$algebra if,

- $\Omega \in \mathcal{F}$,

- $\forall A \in \mathcal{F}, A^C \in \mathcal{F}$,

- $A_1, A_2, \cdots, A_j, \cdots \in \mathcal{F} \Rightarrow \bigcup_{j=1}^{\infty} A_j \in \mathcal{F}$.

Let the collection of random variables be U_t, $t = 1, 2, \ldots$. We can think of the label variable as a time. Let the system be in the states $U_0, U_1, \ldots, U_{t-1}$ at the corresponding times. Then, the conditional probability of finding the system in state U_t at time t will be given by $p(U_0, \ldots U_{t-1}|U_t)$.

A stochastic process is called **weakly stationary** (most of the times referred to as stationary) if, for all t_1, t_2 and $h > 0$,

$$\langle U_{t_1} \rangle = \langle U_{t_2} \rangle \quad \text{and} \quad \text{cov}(U_{t_1}, U_{t_2}) = \text{cov}(U_{t_1+h}, U_{t_2+h}). \tag{5.1.5}$$

So, stationary processes have a mean value for the variables that is independent of t and a finite variance that does not depend on t, provided it is finite. The problem is now that the U_i's are no longer independent from one another. So, in principle, there is nothing that guarantees that the law of large numbers and the central limit theorem can be used.

However, we can invoke the **law of large numbers for stochastic processes**. If we consider a stationary stochastic process satisfying $\sum_{t=0}^{\infty} |\text{cov}(U_0, U_t)| < \infty$, then the weak law remains true.

Also, we can use the **M-dependent central limit theorem**, that ensures the following. Let's assume $\{U_i\}$, $i = \{1, ...N\}$ to be a stationary M-dependent sequence of random variables (they are independent if the separation between them in "time" is bigger than M) sharing the same been value and with finite variances. Then, the distribution of $(\sum_{i=1}^{N} U_i - N\mu)/(\sigma\sqrt{(N)})$ tends to a normal distribution, with

$$\sigma = \text{cov}(U_1, U_1) + 2\sum_{h=1}^{M} \text{cov}(U_1, U_{1+h}) \tag{5.1.6}$$

Thus, relying on these theorems, we can use stochastic processes in with a non zero variance among the random variables for our purposes. One of the simplest types of stochastic processes are the Markov chains that are going to be discussed in the next subsection.

5.1.2 Markov chains

Let $U = \{U_0, U_1, \ldots\}$ be a stochastic process that take values in S, called the state space. There is, of course, and underlying probability space $(\Omega, \mathcal{F}, \mu_U)$, and each U_t is a $\mathcal{F}-$ measurable function that maps Ω into S.The process U is a **Markov chain** if it satisfies the Markov condition,

$$\mu_U(U_t = s|U_0 = u_0, U_1 = u_1, \ldots, U_{t-1} = u_{t-1}) = \mu_U(U_t = s|U_{t-1} = u_{t-1}), \tag{5.1.7}$$

for all $t \geq 1$ and all $s, u_1, \ldots u_{t-1} \in S$. In words, given the present, the rest of the past is irrelevant for predicting the location of U_{t+1}. The chain U is said to be **homogeneous** if

$$\mu_U(U_{t+1} = j | U_t = i) = \mu_U(U_1 = j | U_0 = i), \tag{5.1.8}$$

for all t, i, j. The **transition matrix** $T(i \to j)$ is the $|S| \times |S|$ matrix of **transition probabilities**,

$$T(i \to j) = \mu_U(U_{t+1} = j | U_t = i). \tag{5.1.9}$$

Here, we restrict our discussion to homogeneus Markov chains. Some of its properties are,

- The transition matrix has only non negative entries.
- $\sum_j T(i \to j) = 1$.
- Every eigenvalue λ of a transition matrix satisfies $|\lambda| \leq 1$.
- Every transition matrix has at least one eigenvalue equal to 1.

Some important concepts to be introduced are,

Multi-step probabilities, T^n: they are determined by taking powers of the transition matrix, T^n. So, the (i, j) element of this matrix will be the probability that a Markov chain, starting at U_i will arrive at U_j in n steps.

First visit probablility $f_{ij}^{(n)}$: probability that a Markov chain, starting at U_i is found for the first time at a state U_j after n steps.

Total visit probability, f_{ij}: probability that, starting from U_i, the chain will ever visit the state U_j, $f_{ij} = \sum_{n=1}^{\infty} f_{ij}^{(n)}$.

Mean first passage time, m_{ij}: expected number of steps to reach U_j from U_i in a Markov chain. $m_{ij} = \sum_n^{\infty} n f_{ij}^{(n)}$.

Mean recurrence time, μ_i: expected number of times to return to state U_i for the first time $\mu_i = \sum_{n=1}^{\infty} n f_{ii}^{(n)}$

The states in a Markov chain fall into **equivalence classes**. A state U_j is accessible from U_i if $T^n(i \to j) > 0$ for some $n < \infty$. It is going to be denoted by $U_i \to U_j$. Two states are said to communicate if $U_i \leftrightarrow U_j$. A class is a set of states that communicate with one another. A Markov chain is **irreducible** if it has only one class. The states can be classified in:

1. Positive recurrent: $f_{ii} = 1 \cap \mu_i < \infty$.
2. Null recurrent:$f_{ii} = 1 \cap \mu_i = \infty$.
3. Transient: $f_{ii} < 1$.

Moreover, the states in a Markov chain can be classified in periodic or aperiodic states. All states in a class of a Markov chain are of the same type and, if they are periodic, they all have the same period.

A probability vector **p** is called **stationary** or **invariant** or a **fixed point** if $p[U'] = \sum_U P[U] T(U \to U')$. If one starts with a Markov chain with an initial probability

vector that is stationary, then the probability vector is always the same (stationary) for the chain. Then, the Markov chain is in **equilibrium**.

Now, we are ready to state the **fundamental limit theorem for irreducible Markov chains.** We are not going to give a demonstration here. For further details, see [114].

> An irreducible, aperiodic, positive recurrent Markov chain with transition matrix $T(i \to j)$ has a stationary ditribution $\mathbf{p}$ satisfying,
>
> - $p[U_j] > 0$,
> - $\sum_j p[U_j] = 1$ and
> - $p[U'] = \sum_s p[U]T(U \to U')$.
>
> Moreover, this stationary distribution is unique and identical to the limiting distribution independent of the initial state. A Markov chain with these properties is **ergodic**.

- Positive recurrent chain $\Rightarrow$ existence of at least one invariant probability vector.

- Irreducibility $\Rightarrow$ uniqueness of the invariant probability vector.
- Aperiodicity $\Rightarrow$ the limit distribution coincides with the invariant distribution.

So, an ergodic Markov chain which starts at any probability vector eventually tends to equilibrium. The process of bringing the chain into equilibrium is know as **thermalisation**. Now, we can adapt the Monte Carlo integration formulas for stationary stochastic processes. With all the properties exposed above, we concluded that the Monte Carlo method of integration using a Markov chain in equilibrium is specified by

$$\int D[U]p[U]A[U] \approx \bar{A} \pm \sqrt{\frac{R_0(A) + 2\sum_{h\geq 1} R_h(A)}{N}}, \tag{5.1.10}$$

$$\bar{A} = \frac{1}{N}\sum_{i=1}^{N} A[U_i], \qquad R_h(A) \equiv \frac{1}{N-h}\sum_{i=1}^{N-h}\left(A[U_i] - \bar{A}\right)\left(A[U_{i+h}] - \bar{A}\right), \tag{5.1.11}$$

where the elements U_i are elements of an ergodic Markov chain and the autocovariance is absolutely summable, as it is needed for the law of large numbers for stochastic processes and the M-dependent limit central theorem to apply.

Summarising, the minimal requirements on $T(U \to U')$ are,

1. $T(U \to U') \geq 0$, $\quad \sum_{U'} T(U \to U') = 1$. T is the transition matrix of a Markov chain.
2. $\sum_s p[U]T(U \to U')$ for $p[U]$ the probability distribution. The Markov chain is in equilibrium.

3. $T(U \to U) > 0$. Aperiodicity and any state can be reached from any other in a finite number of steps (ergodicity).

Since the most popular algorithm used to create the stochastic process fulfills **detailed balance** albeit it is not required for the algorithm to accomplish requirements 1, 2, 3, we are going to describe it here. A Markov chain is **reversible** if the probability of going $U_i \to U_j$ is the same as the probability of going $U_j \to U_i$ once the chain is in equilibrium, i.e., $p[U_i]T(U_{\to}U_j) = p[U_j]T(U_j \to U_i)$. This condition is referred to as detailed balance. It guarantees the fixed point condition, since,

$$\sum_j p[U_j]T(U_j \to U_i) = \sum_j p[U_i]T(U_i \to U_j) = p[U_i]. \tag{5.1.12}$$

It should not be forgotten that the states generated using a Markov chain are not independent. This dependence is known as **autocorrelation**. The autocorrelation is observable dependent. For an observable A, the autocorrelation is defined by,

$$\rho(\tau) = \frac{\overline{A_i A_{i+\tau}} - (\bar{A}_i)^2}{\overline{A_i^2} - (\bar{A}_i)^2}. \tag{5.1.13}$$

Highly correlated points yield an autocorrelation value near unity. Independent points produce a value near zero. Smaller correlations make the Monte Carlo errors decrease. A simple way to reduce autocorrelations is to skip some number of elements in the chain between measurements.

Now, we are going to describe an algorithm that generates an ergodic Markov chain that can be customised to our proble, the so called Metropolis Hastings method.

Valid transition amplitude. The Metropolis-Hasting method

The probability density $p[U]$ we need to sample to evaluate the expectation value of an observable A, $\int A[U]p[U]D[U]$ takes the form of Eq.(5.1.2). There are several ways to construct an ergodic Markov chain whose limiting stationary distribution is $p[U]$. Here, we are going to focus in the Metropolis Hastings method. Let $T_0(U_i \to U_j)$ be the transition matrix of a Markov chain satisfying 1, 2, 3, and whose stationary distribution is easily sampled. Then, the Metropolis Hastings algorithm updates the Markov chain as follows:

1. Use $T_0(U \to U')$ to propose a new value U' from U.
2. Accept the new value with probability,

$$P_{\text{acc}}(U \to U') = \min\left(1, \frac{T_0(U' \to U)p[U']}{T_0(U \to U')p[U]}\right) \tag{5.1.14}$$

3. If rejected, U is kept.

The transition amplitude will thus be,

$$T(U_i \to U_j) = T_0(U_i \to U_j)P_{\text{acc}}(U_i \to U_j) + \delta_{ij}\sum_k T_0(U_i \to U_k)(1 - P_{\text{acc}}(i,k)). \tag{5.1.15}$$

If $T_0(U_i \to U_j) = U_0(U_j \to U_i)$, then, the acceptance probability is simplified and the method is known as the Metropolis method. Both of them satisfy detailed balance.

5.1.3 The HMC algorithm

Simulating QCD is more difficult than Yang-Mills theories because the fermionic fields cannot be simulated directly, since $e^{-S_F} = e^{-\bar{\psi}D\psi}$ is not positive; hence, we get poor importance sampling. Integrating out the fermionic fields is thus needed, getting the fermionic determinant. Including it as part of the observable to be measured is not feasible because it being extensive in the lattice volume leads us to have poor importance sampling. The solution is to represent the fermion determinant as a bosonic Gaussian integral. These new bosonic fields will be called pseudofermions, χ,

$$\det D(U) \propto \int d\bar{\chi} d\chi e^{-\bar{\chi}D^{-1}(U)\chi}, \tag{5.1.16}$$

U being the gauge links. It should be noted that the fermion kernel is no longer local and that it is required that it is positive definite in order for the integral above to converge.

If we introduce an even number of flavours of fermions, which is the case in our setup, then, not only positivity is guaranteed, but it also makes it possible to generate the χ's by applying $D^\dagger$ to a random Gaussian distribution, which can be done.

So, if we want to perform Monte Carlo computations including dynamical fermions, we want an algorithm that,

i) updates the fields globally,

ii) takes large steps through configurations,

iii) does not introduce any systematic errors.

These conditions are fulfilled by the Hybrid Monte Carlo algorithm. The procedure is the following:

a. Introduce "fictitious momenta", canonically conjugate to $U(x,\mu)$, one corresponding to every dynamical degree of freedom, $\pi(s,\mu) = \sum_a \pi^a(x,\mu)T^a$ where T^a are the generators of SU(3). Thus, the momenta are elements of the algebra of the group. Now, we have the "fictitious Hamiltonian" given by,

$$H = \tfrac{1}{2}(\pi,\pi) + S[U], \qquad (\pi,\pi) = \sum_{x,\mu,a} \pi^a(x,\mu)\pi^a(x,\mu), \tag{5.1.17}$$

   and $S(U)$ includes the pseudofermionic action and the pure gauge action. It plays the rôle of the potential in the "fictitious" classical mechanical system.
b. Find a Markov chain with fixed point $p[U,\pi] = \frac{e^{-H(U,\pi)}}{Z'}$. This gives the evolution of the system in a fifth dimension, the "fictitious time", or computer time.
c. This generates the desired distribution $\exp[-S[U]]/Z$, if we ingore the momenta π.

Now, we need a procedure to accomplish b. Now, consider the Hamilton's equations (Molecular Dynamics, MD),

$$\begin{aligned}\dot{\pi}(x,\mu) &= -F(x,\mu), \qquad F^a(x,\mu) = \frac{\partial S[e^{\omega}U]}{\partial \omega^a(x,\mu)}\Big|_{\omega=0}, \\ \dot{U}(x,\mu) &= \pi(x,\mu)U(x,\mu). \end{aligned} \tag{5.1.18}$$

Here, it has to be noted that the force, $F^a(x,\mu)$ will get a contribution coming from the pure gauge action and a contribution from the fermionic part. This second contribution is the most cumbersome to deal with, because it implies the inversion of the fermionic matrix. Some techinical details on the actual structure of this quantity will be given in section 5.3, as in the customisation of the MILC code a modification of the fermioic force was required. The solution π_t, U_t, exists and is uniquely determined by the initial values at "fictitious time", t. The idea of the HMC is to integrate the MD equations, starting from the current fields and to take,

$$\pi'(x,\mu) = \pi_\tau(x,\mu), \qquad U'(x,\mu) = U_\tau(x,\mu), \tag{5.1.19}$$

as the next fields, where $\tau = 1$ for example. The associated transition probability density is,

$$T_{MD}(\pi, U \to \pi', U') = \prod_{x,\mu} \delta(\pi'(x,\mu) - \pi_\tau(x,\mu)) \times \delta(U'(x,\mu), U_\tau(x,\mu)). \tag{5.1.20}$$

If we could integrate the Hamiltonian equations exactly, we could follow a trajectory of ficticious energy that,

- is reversible. Then, the mapping $\pi, U \to \pi', U'$ is an isomorphism,
- preserves the functional integral measure,
- preserves the hamiltonian.

This indicates that T_{MD} satisfies properties 1 and 2 in the previous section. However, T_{MD} is a microcanonical move. It corresponds to a set of equiprobable fictitious phase space configurations. So, it has to be combined with something else to meke it ergodic and to make it fulfill property 3. The proposal is,

$$T_\pi(\pi, U \to \pi' U') = C \times e^{-\frac{1}{2}(\pi',\pi')} \times \prod_{x,\mu} \delta(U'(x,\mu), U(x,\mu)), \tag{5.1.21}$$

which amounts to choosing $\pi'(x,\mu)$ randomly. This is the so called hybrid Monte Carlo. There are more sophisticated ways of providing ergodicity to the algorithm, such as the generalised Monte Carlo Method. We will not discuss them here. For further details, see [113]. Now, the product,

$$T = T_{MD} T_\pi, \tag{5.1.22}$$

then satisfies 1,2 and 3, if the trajectory length τ is chosen randomly in $[0, \tau_{\max}]$. But, the equations can not be integrated exactly. We need to integrate them numerically.

The method has to be reversible and area preserving. One simple choice is the **"leap frog"** integrator. The Taylor expansions,

$$\begin{aligned} \pi_{t+\epsilon} &= \pi_t + \epsilon\dot{\pi}_t + \mathrm{O}(\epsilon^2), \\ U_{t+\epsilon} &= U_t + \epsilon\dot{U}_t + \mathrm{O}(\epsilon^2), \end{aligned} \tag{5.1.23}$$

suggest to define the operations,

$$\begin{aligned} \mathcal{I}_0(\epsilon): &\quad \pi, U \to \pi - \epsilon F, U \\ \mathcal{I}_U(\epsilon): &\quad \pi, U \to \pi, e^{\epsilon\pi}U. \end{aligned} \tag{5.1.24}$$

Them, $\mathcal{I}_0(\frac{\epsilon}{2})\mathcal{I}_U(\epsilon)\mathcal{I}_0(\frac{\epsilon}{2})$ takes π_t, U_t to $\pi_{t+\epsilon}, U_{t+\epsilon}$ up to errors of order ϵ^3. The complete integration from $(\pi_0, U_0) = (\pi, U)$ to $(\pi_\tau, U_\tau = \pi', U')$ amounts to applying,

$$\mathcal{J}_0(\tau, N_0) = \left\{\mathcal{I}_0(\tfrac{\epsilon}{2})\mathcal{I}_U(\epsilon)\mathcal{I}_0(\tfrac{\epsilon}{2})\right\}^{N_0}, \qquad \epsilon = \frac{\tau}{N_0}, \tag{5.1.25}$$

to (π, U). The "leap frog" method preserves the area $D[U]D[\pi]$ and is reversible. The mapping is an isomorphism and has unit Jacobian. However, H is only preserved up to terms of order ϵ^2. That takes the Markov chain out from equilibrium. That is, property 2 is violated. It is accepted with probability,

$$P_{\mathrm{acc}} = \min\left(1, e^{-\delta H}\right), \qquad \delta H = H' - H = \mathrm{O}(\epsilon^2). \tag{5.1.26}$$

Thus, we have found an algorithm that satisfies all the properties needed to generate gauge configurations, with the drawback they are not going to be independent from one another. The steps to be taken are,

i) Choice of normally distributed ficticious momenta π.
ii) Apply the "leap frog" integrator $\mathcal{J}_0$ to (π, U).
iii) Accept U' as the next configuration with probability P_{acc}. If not, keep the pre-existent configuation, U.

5.1.4 Final remarks concerning the algorithm

To finish this section, we give some remarks concerning the algorithm

* The integration requires the force F to be computed N_0+1 points in time. Every time the force is computed, an inversion of the fermionic matrix is needed. The computational effort is going to be proportional to N_0.

* The mean value of the acceptance rate is going to be $\langle P_{\mathrm{acc}}\rangle = 1 - \mathrm{O}(\epsilon^2)$. Optimal values of ϵ are where $\langle P_{\mathrm{acc}}\rangle \sim 0.7 - 0.8$. A compromise has to be encountered for the values of ϵ for each volume in order to make the acceptance rate take a value next to the optimal values.

* Nevertheless, the algorithm is valid for any ϵ. All the requirements are satisfied. The statistics of the observables might be worse when the acceptance rate does not take an optimal value.

* As $\beta = \frac{2N}{g_0^2}$ gets smaller, i.e., as we approach the non perturbative regime, the condition number of the fermionic matrix increases. Therefore a larger computational effort is required to invert the fermionic matrix. As there is a threshold that puts an upper bound in the number of iterations, there is a point in which we have to loosen this condition in order to get results. Hence, simulations at smaller β require more computer time.

* Besides, in the same regime, i.e, for small values of β, when the update of the gauge links and the fictitious momenta is made, we might get unitarity violation problems. That is because $e^{\epsilon\pi}$ in Eq. (5.1.24) is constructed by doing a Taylor expansion of the exponential up to $O(\epsilon^6)$ effects. This approximation is less accurate for small values of beta.

* On the other hand, as we approach the perturbative regime, i.e., large values of β, the action gets bigger,since $S \propto \beta$.That means that our probability distribution function gets more sharply peaked. This fact implies that it becomes more difficult to sample. For fixed values of N_0, ϵ, the acceptance rates drops linearly as we increase β. If we want to keep an "optimal" acceptance rate, we need N_0 to be increased for a fixed trajectory length τ. This effect is not dramatic for the values of β used to compute the step scaling function. But, in the perturbative regime studies on section 8, it could no longer be dismissed.

* The action also increases linearly with the volume. So, in order to keep a sensible value for the acceptance rate, N_0 has to be increased with V. So, as we increase the value, it is not only that the fermionic matrix grows dramatically, but also, more steps are needed.

* When estimating the autocorrelation time, it is always important to make sure the algorithm samples the entire relevant configuration space in an efficient manner. If this is not the case, we might be underestimating the actual autocorrelation times and wrong results can be obtained.

5.2 Characteristics of the machines available

In Tables H1 - H10 in appendix H, we can see a list of all the data obtained from the simulations. Under "machine", we can see the name of the machines used. We will list them here and describe some of its characteristics. For the small volumes, $L/a = 4$, we used scalar machines (Bishma, Madras, Madrid, Vindaloo) to run the simulations. The rest of the simulations were run using two high performance compute clusters available at the TCHPC (Trinity Centre for High Performance Computing), a Trinity College Dublin institution, and two supercomputers from the ICHEC (Irish Centre for High-End Computing). In the tables below, a description of the supercomputers is detailed.

Clusters used from the TCHPC

Machine	Lonsdale	Iitac
Vendor	ClusterVision	IBM
Available to	TCD Researchers	Irish Researchers
Processor Type	Opteron	Opteron
Architecture	64 bits	64 bits
Number of Nodes	154	356
RAM per node	32	4
RAM	3.2 TB	1.4 TB
Clock Speed	2.30 GHz	2.40 GHz
Interconnect	Infiniband DDR	Voltaire Infiniband SDR
Th. Peak Perf.	11.33 TF	3.4 TF
Total No of cores	1232	712
No of cores per node	8	2
Linpack Score	8.9TF	2.724TF

Clusters used from the ICHEC

Machine	Blue Gene/L Lanczos	Stokes
Vendor	IBM Blue Gene/L	SGI Altix ICE 8200EX
Available to	Irish Researchers	Irish Researchers
Processor Type	PowerPC 440	Intel Xeon E5462
Number of Nodes	1024	360
RAM	1024 GB	5120 GB
Clock Speed	700 MHz	2.8 GHz
Interconnect	BG Tree/ Torus	ConnectX Infiniband DDR
Th. Peak Perf.	5.73TF	28.67 TF
Total No of cores	2048	2560
No of cores per Node	2	8
Linpack Score	4.74 TF	25.11 TF

5.3 Modifications of the MILC code

The functions of the MILC code that have been modified are the following,

- `generic_schroed/make_schroed_lattice.c`
- `generic_schroed/coupling.c`
- `generic_ks/d_congrad5.c`
- `generic_ks/generic_ks_includes.h`
- `schroed_pg/control.c`
- `schroed_ks_dyn/control.c`
- `schroed_ks_dyn/schroed_ks_includes.h`
- `schroed_ks_dyn/update_h.c`

5.3.1 Implementation of the computation of $\bar{v}$

$\bar{v}$ can be determined through,

$$\bar{v} = -\frac{1}{k}\frac{\partial}{\partial\nu}\left\{\frac{\partial\Gamma}{\partial\eta}\Big|_{\eta=0}\right\}_{\nu=0}. \tag{5.3.1}$$

The fields at the boundaries are chosen to be abelian and spatially constant. They have been explicitly given in chapter 2. The plaquettes at the boundaries $P_{kl}(x)\big|_{x_0=0,T} = 1$ where the latin indices indicate spatial components. So, we will have, for the derivative with respect to η, including the improvement coefficient c_t,

$$\begin{aligned}\frac{\partial S}{\partial\eta} &= -\frac{c_t}{g_0^2}\sum_{\mathbf{x}}\sum_{k=1}^{3}\left\{\mathrm{tr}\left[\frac{\partial}{\partial\eta}P_{k0}(0,\mathbf{x})\right] + \mathrm{tr}\left[\frac{\partial}{\partial\eta}P_{0k}(0,\mathbf{x})\right]\right.\\ &\quad \left.+\mathrm{tr}\left[\frac{\partial}{\partial\eta}P_{k0}(T-1,\mathbf{x})\right] + \mathrm{tr}\left[\frac{\partial}{\partial\eta}P_{0k}(T-1,\mathbf{x})\right]\right\}.\end{aligned} \tag{5.3.2}$$

A simplification can be done by writing,

$$P_{\mu\nu}(x) = P^{-1}_{\nu\mu}(x) = P^{\dagger}_{\nu\mu}(x). \tag{5.3.3}$$

We get,

$$\frac{\partial S}{\partial\eta} = -\frac{2c_t}{g_0^2}\sum_{\mathbf{x}}\mathrm{Re}\,\mathrm{tr}\left[\frac{\partial}{\partial\eta}e^{\frac{i}{L}\phi}B_0^{\dagger} + \frac{\partial}{\partial\eta}e^{\frac{i}{L}\phi'}B_T^{\dagger}\right]. \tag{5.3.4}$$

Setting,

$$\begin{aligned}\frac{\partial\phi}{\partial\eta} &= \mathrm{diag}\left(1,\nu-\tfrac{1}{2},-\nu-\tfrac{1}{2}\right) \qquad a = \mathrm{Im}\left(e^{\frac{i}{L}\phi}B_0^{\dagger}\right),\\ \frac{\partial\phi'}{\partial\eta} &= \mathrm{diag}\left(-1,\nu+\tfrac{1}{2},-\nu+\tfrac{1}{2}\right) \qquad b = \mathrm{Im}\left(e^{\frac{i}{L}\phi}B_T^{\dagger}\right),\end{aligned} \tag{5.3.5}$$

we finally get,

$$\begin{aligned}\frac{\partial S}{\partial\eta} &= \frac{2c_t}{g_0^2 L}\left\{a_{11} + \left(\nu-\tfrac{1}{2}\right)a_{22} - \left(\nu+\tfrac{1}{2}\right)a_{33}\right.\\ &\quad \left. b_{11} + \left(\nu+\tfrac{1}{2}\right)b_{22} - \left(\nu-\tfrac{1}{2}\right)b_{33}\right\}.\end{aligned} \tag{5.3.6}$$

So, the observables are,

$$\frac{1}{\bar{g}^2} = \frac{2c_t}{kg_0^2 L}\left\{a_{11} - b_{11} - \frac{1}{2}(a_{22}-b_{22}) - \frac{1}{2}(a_{33}-b_{33})\right\}, \tag{5.3.7}$$

$$\bar{v} = \frac{2c_t}{kg_0^2 L}\left\{-a_{22} - b_{22} + a_{33} + b_{33}\right\}. \tag{5.3.8}$$

The computation of $\bar{v}$ was not included in the MILC code. We have implemented it by modifying the files,

i) `generic_schroed/make_schroed_lattice.c`: Originally, since only the coupling was computed, the boundary fields were stored in this function multiplied by the factor $(\frac{1}{L}, -\frac{1}{2L}, -\frac{1}{2L})$ which is useful for the computation of $\bar{g}^2$. We remove the multiplication by this factor in this function

ii) `generic_schroed/coupling.c`: In this function, the computation of the variable $\bar{v}$ is implemented. We include the factors cancelled in the aforementioned file and new factors $(\frac{1}{L}, -\frac{1}{L}, 0)$ that account for $\bar{v}$. In the original code, the information to compute $\partial S/\partial\eta|_{\eta=0}$ is stored in `s->tempmat1`. Here, the variable `s->tempmat2` is used to store the information concerning $\bar{v}$. There is a new argument to be included in the function `coupling`, namely,

```
void coupling(double *ds_deta, double *bd_plaq, double *v)
```

See the code for further details.

5.3.2 Changes in the pure gauge part

As it has been discussed in previous chapters, c_t has to be modified for our setup. This modification is done in the file `generic_schroed/make_schroed_lattice.c`.

OLD CODE	NEW CODE
`c_t=1.-(0.534+c_t11)/beta;`	$s=1$ `c_t=2./3-(-0.1643+c_t11)/beta;` $s=-1$ `c_t=2.-(2.7816+c_t11)/beta;`

5.3.3 Changes in the fermionic part

Inclusion of $c_t^{(1,1)_s}$

Likewise, we have to include the new values of $c_t^{(1,1)}$. The modification is done in the file `schroed_ks_dyn/setup.c`.

OLD CODE
`c_t11=-(float)(nflavors)*0.02841;`
NEW CODE
$s=1$ `c_t11=-(float)(nflavors)*6*0.0077856;` $s=-1$ `c_t11= (float)(nflavors)*6*(0.0267);`

Inclusion of $d_s^{(0)}$

To implement this improvement coefficient, two functions have been modified,

generic_ks/d_congrad.c : It amounts to perform modifications in the function,

`void dslash(field_offset src,field_offset dest,int parity )` [1]

[1] the function `d_slash_special` has been modified in the same fashion.

Including this factor is equivalent to multiplying the gauge links at $n_t = 1, T-1$ by $1+\delta_s^{(0)}$ when computing $\not{D}$, and then dividing by the same factor again once the computation has been performed.

schroed_ks_dyn/update_h.c: It amounts to perform a modification in the function that encodes the implementation of the fermionic force,

```
void fermionic_force(float eps).
```

The modification included in this file is analogous to the one in `dslash`. We give a brief theoretical justification. The variation of the pseudofermionic action is given by,

$$\begin{aligned}\left[\frac{\delta S_{PF}}{\delta U_\mu(x)}\right]_{ab} &= \sum_\beta T^\beta_{ab} \left.\frac{\partial S_{PF}(e^{\omega_\beta T_\beta}U_\mu(x), U')}{\partial \omega_\beta}\right|_{\omega_b=0} = \\ &= \sum_{\beta,c,d} T^\beta_{ab} \left\{ \left.\frac{\partial V_{cd}}{\partial \omega_\beta}\right|_{\omega_\beta=0} \frac{\partial S_{PF}(U)}{\partial V_{cd}} + \left.\frac{\partial V^\dagger_{cd}}{\partial \omega_\beta}\right|_{\omega_\beta=0} \frac{\partial S_{PF}(U)}{\partial V^\dagger_{cd}} \right\} \\ &= \sum_{\beta,c,d} T^\beta_{ab} \left\{ \left[T^\beta U_\mu(x)\right]_{cd} \frac{\partial S_{PF}}{\partial U_\mu(x)_{cd}} - \left[U^\dagger_\mu(x) T_\beta\right]_{cd} \frac{\partial S_{PF}(U)}{\partial U^\dagger_\mu(x)_{cd}} \right\},\end{aligned} \tag{5.3.9}$$

where T^β are the Gell-Mann matrices, assumed to be antihermitian, satisfying, $\mathrm{tr}(\mathrm{T_i T_j}) = -\frac{1}{2}\delta_{\mathrm{ij}}$. Thus, the sum in β goes from $\{1 \ldots 8\}$. $V = e^{\omega_\beta T_\beta} U_\mu(x)$, U' refers to the gauge links different from $U_\mu(x)$, and U denotes all the gauge links. We define the operator T that projects A onto su(3) (Lie algebra of SU(3)), i.e.,

$$\mathrm{T}(A) = \frac{1}{2}(A - A^\dagger) - \frac{1}{2N}\mathrm{tr}(A - A^\dagger) = -2\sum_\beta T^\beta \mathrm{tr}(A T^\beta). \tag{5.3.10}$$

It can be easily proved (we omit the arguments of the functions),

$$\sum_{cd} (T^\beta U)_{cd} \frac{\partial S_{PF}}{\partial U_{cd}} - (U^\dagger T^\beta)_{cd} \frac{\partial S_{PF}}{\partial U^\dagger_{cd}} = \sum_{ce} T^\beta_{ce} \sum_d \left[U_{ed} \frac{\partial S_{PF}}{\partial U_{cd}} - U^\dagger_{dc} \frac{\partial S_{PF}}{\partial U^\dagger_{de}} \right]. \tag{5.3.11}$$

Defining,

$$A_{ec} = \sum_d \left[U_{ed} \frac{\partial S_{PF}}{\partial U_{cd}} - U^\dagger_{dc} \frac{\partial S_{PF}}{\partial U^\dagger_{de}} \right], \tag{5.3.12}$$

we get,

$$\frac{\partial S_{PF}}{\partial U_\mu(x)_{ab}} = \sum_\beta T^\beta_{ab} \left[T^\beta_{ce} A_{ec}(x,\mu)\right] = -\frac{1}{2}\mathrm{T}(A(x,\mu))_{ab}. \tag{5.3.13}$$

Thus, we are left with computing $A(x,\mu)$. To do so, we start with the pseudofermionic action,

$$S_{PF} = \sum_{x,z} \sum_{a',a''} \chi^{\dagger}_{a'}(x)(M^{\dagger}M)^{-1}_{xz,a'a''}\chi_{a''}(z) \tag{5.3.14}$$

Defining,

$$\begin{aligned} \psi_a(y) &= \left[(M^{\dagger}M)^{-1}\chi\right]_a(y), \\ \phi_a(y) &= (M\psi)_a(y), \\ \tilde{U}_{\mu}(x) &= U_{\mu}(x)\eta_{\mu}(x). \end{aligned} \tag{5.3.15}$$

Then, we get,

$$A(x,\mu) = \left[\tilde{U}_{\mu}(x)\psi(x+\hat{\mu})\right] \otimes \phi^{\dagger}(x) + \psi(x) \otimes \left[\tilde{U}_{\mu}(x)\phi(x+\hat{\mu})\right]^{\dagger} - \text{h.c}, \tag{5.3.16}$$

Finally we get

$$\frac{\delta S}{\delta U_{\mu}(x)} = \mathrm{T}\left\{ \left[\tilde{U}_{\mu}(x)\psi(x+\hat{\mu})\right] \otimes \phi^{\dagger}(x) + \psi(x) \otimes \left[\tilde{U}_{\mu}(x)\phi(x+\hat{\mu})\right]^{\dagger} \right\}. \tag{5.3.17}$$

This derivation justifies the modification done in the code.[2]

`schroed_ks_dyn/setup.c`: We include the value of $d_s^{(0)}$ via `delta = s_param/4.;`

To test this modification, we have written a c code that computes the propagator for small lattices in the space-momentum representation numerically, setting the gauge fields to the background fields induced by the boundary conditions. The same quantity has been computed making use the MILC code and it has been checked that the result actually matches.

5.4 Tests of the algorithm

After having modified the code and performed some checks on every single modification, we would like to test that the algorithm is behaving as it should theoretically.

5.4.1 ΔH as a function of ϵ^2

As we have stated before, the Hybrid Molecular Dynamics algorithm, with no Metropolis acceptance step should be exact up to integration errors of order $\mathrm{O}(\epsilon^2)$. We have used trajectories of length $\tau = 1/2$ and we have measured δH for different ϵ's. We have tested that for $\beta = 7$ and different lattice volumes. The test has been done running the programs in single and double precision. In Figure (5.1) we present the results corresponding to a 8x8x8x7 lattice, The results corresponding to the single and double

[2] See the code for further details.

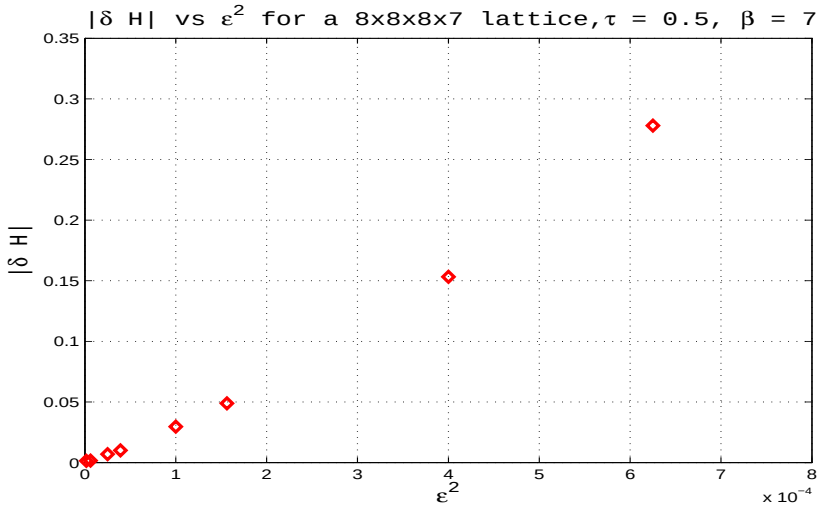

Figure 5.1: $|\Delta H|$ as a function of ϵ^2

precision runs are presented in tables (5.1,5.2,5.3,5.4,5.5,5.6), for the lattice volumes specified. In these tables we also show the corresponding results of next section.

In figure (5.1), we can see that effectively, as expected, $|\delta H|$ scales roughly linearly with ϵ^2 keeping the trajectory length τ fixed.

5.4.2 Reversibility of the algorithm

An important property of the integrator is that it is reversible. So, if we do a trayectory $(\pi, U) \to (\pi', U')$ and flip the momentum $\pi' \to -\pi'$, then, the trajectory with $(-\pi', U')$ as initial values should lead to (π, U). As we have already announced in the previous section, the data obtained for this check for single and double precision are collected in tables (5.1,5.2,5.3,5.4,5.5,5.6), for lattices with $L/a = 6, 8, 10, 12, 16, 20$. We have already included the time needed to perform the calculation. In the tables, we can see that, in the case of single precision the quantity $|\delta H - \delta H'|$ is zero up to round off errors, until δH, itself, reaches this limit. In the case of double precision, we only get 2 more significative digits. That is because the running was performed without changing the tolerance of the conjugate gradient inverter, that was customised for single precision.

5.4.3 Expectation value of $e^{-\Delta H}$

Due to the area preserving property of $(\pi, U) \to (\pi', U')$, we have, for the HMC partition function,

$$Z = \int D[\pi']D[U']e^{-H[\pi',U']} = \int D[\pi]D[U]e^{-H[\pi,U]-\delta H[\pi,U]}. \tag{5.4.1}$$

That implies,

$$1 = \langle e^{-\delta H} \rangle \geq e^{-\langle \delta H \rangle}. \tag{5.4.2}$$

VOLUME: 6x6x6x5, PROC: 4						
	SINGLE PRECISION			DOUBLE PRECISION		
	$H = -9.608045e+03$			$H = -9.763427e+03$		
ϵ	δH	$\lvert\delta H - \delta H'\rvert$	t(s)	δH	$\lvert\delta H - \delta H'\rvert$	t(s)
0.125	2.287217e+01	2.670288e-05	0.16	2.620690e+01	5.008986e-03	0.15
0.1	9.103244e+00	2.708435e-04	0.19	9.416259e+00	2.046754e-03	0.18
0.05	7.725342e-01	2.402306e-03	0.33	8.078637e-01	3.212423e-04	0.31
0.025	1.024959e-01	5.048752e-03	0.58	1.119491e-01	3.384809e-04	0.54
0.02	5.709306e-02	6.270800e-03	0.70	6.444712e-02	4.480560e-04	0.66
0.0125	1.664376e-02	1.178976e-02	1.0	2.214979e-02	3.970174e-04	0.98
0.01	6.447949e-03	1.601868e-02	1.3	1.362687e-02	1.196717e-04	1.2
0.00625	-6.814261e-03	2.253864e-02	1.9	5.236934e-03	2.016031e-05	1.8
0.005	-1.322178e-02	2.314508e-02	2.4	3.615591e-03	2.067136e-05	2.2
0.0025	-2.273659e-02	2.250648e-02	4.3	5.787213e-04	1.293120e-04	4.1
0.00125	-2.339670e-02	2.360782e-02	8.0	1.948542e-04	3.985714e-04	7.5

Table 5.1: Reversibility of the algortihm, V = 6x6x6x5, $\beta = 7.0$.

VOLUME: 8x8x8x7, PROC: 32						
	SINGLE PRECISION			DOUBLE PRECISION		
	$H = -3.449266e+04$			$H = -3.439054e+04$		
ϵ	δH	$\lvert\delta H - \delta H'\rvert$	t(s)	δH	$\lvert\delta H - \delta H'\rvert$	t(s)
0.125	1.599471e+03	7.446289e-03	0.73	2.756502e+02	1.209657e-03	0.68
0.1	3.720949e+01	1.073074e-02	0.81	3.457385e+01	4.536020e-04	0.78
0.05	1.637014e+00	1.951575e-03	1.3	2.506951e+00	4.256741e-04	1.3
0.025	4.843821e-02	8.655205e-03	2.3	2.779349e-01	1.193383e-03	2.2
0.02	6.910437e-03	8.864470e-03	2.8	1.532356e-01	6.380448e-04	2.6
0.0125	-1.351370e-03	1.035901e-02	4.1	4.882755e-02	6.570398e-04	3.8
0.01	2.329141e-03	8.393235e-03	4.9	2.964432e-02	1.492281e-03	4.6
0.00625	6.556197e-03	1.005068e-02	7.4	1.006197e-02	1.374390e-03	6.8
0.005	8.539017e-03	1.096669e-02	8.8	6.972933e-03	1.835611e-03	8.3
0.0025	8.781723e-03	1.139359e-02	16	1.700570e-03	1.543270e-03	15
0.00125	9.781173e-03	8.691952e-03	28	1.451314e-03	1.307594e-03	26

Table 5.2: Reversibility of the algorithm, V =8x8x8x7, $\beta = 7.0$.

The inequality is just the Jensen inequality applied to this case, since the exponential is a convex function. The first equality provides a useful tool for checking the validity of the HMC code being used. Since δH is an observable that thermalises decently fast, we have run 2000 trajectories for a lattice 6x6x6x5, $\beta = 7, \tau = 1/2$, and different values of ϵ, N_0 and computed $\overline{e^{-\delta H}}$ and $e^{-\overline{\delta H}}$. The results are shown in table (5.7).We can see that Jensen inequality, Eq. (5.4.2) is always fulfilled and excepting the cases with $N_0 = 4, 5$, $\overline{e^{-\delta H}} \sim 1$ within errors. When $N_0 = 4, 5$, the results are misleading, because

VOLUME: 10x10x10x9, PROC: 4						
	SINGLE PRECISION			DOUBLE PRECISION		
	$H = -8.991112e+04$			$H = -8.975394e+04$		
ϵ	δH	$\lvert\delta H - \delta H'\rvert$	t(s)	δH	$\lvert\delta H - \delta H'\rvert$	t(s)
0.125	4.800871e+04	1.445312e-01	4.8	1.907153e+04	6.265022e-02	5.9
0.1	3.060769e+03	8.251953e-02	5.0	7.413317e+02	1.782998e-02	6.6
0.05	5.203167e+00	8.060455e-03	8.2	1.739010e+00	3.274931e-03	11
0.025	3.587727e-01	1.950422e-02	14	-5.368170e-01	8.751973e-04	19
0.02	1.500121e-01	2.210666e-02	17	-4.119395e-01	1.538319e-04	23
0.0125	1.495481e-02	2.649698e-02	25	-1.889126e-01	1.357122e-03	34
0.01	-2.829786e-03	2.416544e-02	31	-1.270142e-01	1.836547e-04	41
0.00625	-1.470114e-02	3.433416e-02	46	-5.334019e-02	4.155286e-04	62
0.005	-1.717344e-02	3.426534e-02	55	-3.307007e-02	1.758821e-03	75
0.0025	-3.068045e-02	3.201318e-02	100	-9.402267e-03	5.309236e-03	135
0.00125	-2.801031e-02	3.075338e-02	179	2.073528e-04	6.172532e-04	244

Table 5.3: Reversibility of the algorithm, V =10x10x10x9, $\beta = 7.0$.

VOLUME: 12x12x12x11, PROC: 32						
	SINGLE PRECISION			DOUBLE PRECISION		
	$H = -1.953957e+05$			$H = -1.947237e+05$		
ϵ	δH	$\lvert\delta H - \delta H'\rvert$	t(s)	δH	$\lvert\delta H - \delta H'\rvert$	t(s)
0.125	1.261998e+05	1.406250e-01	1.4	2.796726e+05	9.479585e-02	2.0
0.1	1.620111e+04	6.640625e-02	1.5	2.455383e+04	4.837681e-02	1.8
0.05	9.397316e+00	6.735706e-02	2.3	8.346834e+00	1.364950e-03	2.7
0.025	1.914538e-01	3.798267e-02	3.9	1.886230e-01	2.056979e-03	4.6
0.02	-4.716797e-02	3.171305e-02	4.7	-2.711287e-02	1.041718e-03	5.6
0.0125	-1.021402e-01	1.218232e-02	6.8	-7.506126e-02	5.883279e-03	8.3
0.01	-8.283083e-02	1.235612e-03	8.3	-6.000340e-02	2.729908e-03	10
0.00625	-3.845359e-02	7.114556e-03	12	-2.850454e-02	6.642854e-03	15
0.005	-1.804147e-02	9.852506e-03	15	-1.776802e-02	3.638460e-03	18
0.0025	2.731209e-03	7.998715e-03	26	-3.050983e-03	2.001639e-03	32
0.00125	4.564749e-03	7.599919e-03	46	6.116400e-04	2.201985e-03	56

Table 5.4: Reversibility of the algorithm, V =12x12x12x11, $\beta = 7.0$.

epsilon is effectively too big for the integrator to work. Moreover, we can see that the integrated autocorrelation time for $e^{-\overline{\delta H}}$ for $N_0 = 4$ is ~ 200. Thus, we cannot affirm that thermalisation has been reached and we have enough statistics for the data to be reliable at all.

VOLUME: 16x16x16x15, PROC: 64						
	SINGLE PRECISION			DOUBLE PRECISION		
	$H = -6.424468e+05$			$H = -6.410997e+05$		
ϵ	δH	$\lvert\delta H - \delta H'\rvert$	t(s)	δH	$\lvert\delta H - \delta H'\rvert$	t(s)
0.025	2.333174e+00	1.210955e+00	17	9.672776e+00	1.766676e+00	18
0.02	2.378366e-01	2.181436e+00	20	4.633050e+00	2.116396e+00	21
0.0125	1.118393e+00	3.485899e+00	28	2.646655e+00	2.251183e+00	31
0.01	1.202306e+00	3.944262e+00	34	2.537962e+00	3.461931e+00	38
0.00625	2.148025e+00	5.283862e+00	51	2.411631e+00	4.308307e+00	58
0.005	2.175358e+00	5.212298e+00	64	2.056101e+00	3.920968e+00	68
0.0025	1.311834e+00	3.138322e+00	105	8.910807e-01	1.788337e+00	109
0.00125	6.111011e-01	1.584816e+00	167	2.868643e-01	5.873869e-01	184

Table 5.5: Reversibility of the algorithm, V =16x16x16x15, $\beta = 7.0$.

VOLUME: 20x20x20x19, PROC: 32						
	SINGLE PRECISION			DOUBLE PRECISION		
	$H = -1.617106e+06$			$H = -3.413385e+06$		
ϵ	δH	$\lvert\delta H - \delta H'\rvert$	t(s)	δH	$\lvert\delta H - \delta H'\rvert$	t(s)
0.025	1.580507e+01	5.147676e-01	172	1.668823e+01	2.627687e-01	152
0.02	8.848460e+00	4.318291e+00	197	9.215282e+00	4.392628e+00	175
0.0125	3.581433e+00	7.576009e+00	299	3.841769e+00	7.573270e+00	252
0.01	5.555539e+00	1.063131e+01	342	5.707775e+00	1.047281e+01	296
0.00625	7.856658e+00	1.623155e+01	481	7.775577e+00	1.563021e+01	437
0.005	7.791084e+00	1.608696e+01	597	7.735389e+00	1.564144e+01	536
0.0025	4.670574e+00	9.778172e+00	984	4.047280e+00	8.539503e+00	889
0.00125	2.955937e+00	5.740690e+00	1737	1.701149e+00	3.562616e+00	1551

Table 5.6: Reversibility of the algorithm, V =20x20x20x19, $\beta = 7.0$.

5.4.4 Performance of the algorithm

To analyse the performance of the algorithm, we have fixed the parameters,

- $\beta = 7$,
- $N = 50, \epsilon = 0.01$,
- $\tau = 0.5$,
- $s = 1$.

and one trajectory has been run, for different lattice volumes and different number of processors. In table (5.8), we can see the results.

Some conclusions can be extracted from table (5.8).

N_0	Acc.rate	$\overline{e^{-\delta H}}$	τ_{int}	$e^{-\overline{\delta H}}$	τ_{int}	Time
4	10e-3	2.5(2.5)e16	0.500(22)	2.11(20)e-16	2.06(72)e2	2.08e2
5	3.5e-3	9.7(3.2)e-3	0.500(22)	1.86(20)e-5	0.745(73)	2.38e2
10	0.6075	0.964(27)	0.491(22)	0.594(16)	0.710(62)	3.75e2
20	0.9045	0.9960(47)	0.373(18)	0.9680(46)	0.383(18)	6.04e2
25	0.9330	0.9974(30)	0.365(17)	0.9851(30)	0.364(17)	7.05e2
40	0.9705	0.9988(10)	0.289(14)	0.9970(10)	0.290(15)	9.61e2
50	0.9805	0.99960(67)	0.286(14)	0.99883(67)	0.286(14)	1.13e3
80	0.9910	1.00001(26)	0.275(14)	0.99989(26)	0.275(14)	1.54e3
100	0.9925	0.99990(16)	0.267(13)	0.99985(16)	0.267(13)	1.82e3
200	0.9985	1.000099(46)	0.312(15)	1.000095(46)	0.312(15)	2.76e3
400	0.9980	0.997880(60)	0.494(22)	0.997876(60)	0.494(22)	4.17e3

Table 5.7: Results for $\overline{e^{-\delta H}}, e^{-\overline{\delta H}}$, for a 6x6x6x7 lattice, 2000 measurements , $\tau = \frac{1}{2}$ and $\beta = 7$.

$L \Rightarrow$	6	8	10	12	16	20	24
Proc	$--$	$--$	$--$	$--$	$--$	$--$	$--$
$\Downarrow$	t(s)	t(s)	t(s)	t(s)	t(s)	t(s)	t(s)
1	1.702	8.85	33.8	78.8	309	837	2065
2	0.911	3.94	17.2	42.3	168	456	1127
4	0.498	1.69	9.19	26.2	107	290	719
8	$--$	0.826	$--$	10.9	52.7	149	361
16	$--$	0.492	$--$	3.61	24.6	73.0	182
32	$--$	1.52	$--$	2.35	9.78	34.8	90.2
64	$--$	2.14	$--$	$--$	4.5	$--$	44.9

Table 5.8: Performance of the algorithm.

a) We can decide, for each value of L/a, the optimal number of processors we want to use in the simulation. The results are shown in table (5.9).

L/a	#Proc	L	# Proc
6	4		
8	16	16	64
10	4	20	32
12	32	24	64

Table 5.9: Optimal number of processors

We can see that, excepting the case $L/a = 8$, all of them are faster when a bigger number of processors is used. For $L/a = 8$ if a big number of processors is used, the volume per processor is too small and a big amount of time is lost in the

communication between the nodes.

b) Roughly, with the same exception as in **a)**, we can see that the time needed is reduced by a factor proportional to the number of processors involved. In table (5.10) we specify the value of $t(s) \cdot \#\text{Proc}$.

$L/a \Rightarrow$	6	8	10	12	16	20	24
Proc	$--$	$--$	$--$	$--$	$--$	$--$	$--$
$\Downarrow$	#P·t	#P·t	#P·t	#P·t	#P·t	#P·t	#P·t
1	1.702	8.85	33.8	78.8	309	837	2065
2	1.822	7.88	34.4	84.6	336	912	2254
4	1.992	6.76	36.76	104.8	428	1160	2876
8	$--$	6.61	$--$	87.2	421.6	1192	2888
16	$--$	7.87	$--$	57.76	393.6	1168	2912
32	$--$	$--$	$--$	75.2	313.0	1113.6	2886
64	$--$	$--$	$--$	$--$	288	$--$	2874

Table 5.10: Time(s)·#Proc

c) We can see that, if the volume per processor is similar, then the run time invested does not differ very much. In table(5.11) we show the time needed when the number of points per processor are roughly 1000 and 5000.

1000				5000			
Proc	L/a	V/Proc	t(s)	Proc	L/a	V/Proc	t(s)
1	6	1080	1.70	2	10	4500	17.2
4	8	896	1.69	4	12	4752	26.2
16	12	1188	3.61	32	20	4750	34.8
64	16	960	4.51	64	24	4968	44.9

Table 5.11: Run time needed when Vol/Proc$\sim 1000, 5000$

Nevertheless, we can appreciate that the bigger the lattice, the slower the run for a fixed number of points per node.

5.4.5 Seeking the optimal acceptance rate

As it was stated in subsection 5.1.4, it is desirable for the acceptance rate take its optimal values. We have performed simulations for different volumes and different values of ϵ keeping τ and the total time they have been running fixed for a fixed volume. We have evaluated the acceptance rate in each case. When possible, i.e., when we had enough statistics to perform measurements, we have measured $\bar{g}^2$ and $\bar{v}$, their statistical errors and their integrated autocorrelation time. It has to be taken into account that these observables are cumbersome to evaluate, specially the latter.

Large statistics are required, since fluctuations in these observables are tipically enormous. The results of these tests are shown in tables(5.12,5.13,5.14,5.15,5.16,5.17), for volumes $V = 6^3 \times 5, 8^3 \times 7, 10^3 \times 9, 12^3 \times 11, 16^3 \times 15, 20^3 \cdot 19, 24^3 \cdot 23$ and times **time** = 1,1,3,2,2,4,6 hours respectively. to be taken into account that these observables are cumbersome to evaluate, specially the latter. Large statistics are required, since fluctuations in these observables are tipically enormous. The results of these tests are shown in tables(5.12,5.13,5.14,5.15,5.16,5.17), for volumes $V = 6^3 \times 5, 8^3 \times 7, 10^3 \times 9, 12^3 \times 11, 16^3 \times 15, 20^3 \times 19, 24^3 \times 23$ and times **time** = 1,1,3,2,2,4,6 hours respectively.

VOLUME: 6x6x6x5, PROC: 4 $\beta = 7.0$, **TIME: 1h**						
N_0	$N_{\rm traj}$	$\overline{P_{\rm acc}}$	$\bar{g}^2$	τ_{int}	$\bar{v}$	τ_{int}
10	19231	0.622	1.880(17)	7.70(74)	0.146(11)	23.5(3.6)
20	12103	0.902	1.860(15)	4.23(40)	0.141(12)	17.3(2.8)
25	10320	0.939	1.898(19)	4.80(50)	0.166(12)	14.3(3.3)
40	7524	0.970	1.882(21)	4.61(53)	0.154(13)	13.2(2.3)
50	6442	0.981	1.862(21)	4.31(52)	0.154(17)	16.8(3.5)
80	4680	0.992	1.867(30)	5.85(90)	0.130(16)	12.4(2.6)
100	4018	0.995	1.893(26)	3.52(47)	0.137(15)	10.2(2.1)
200	2608	0.997	1.854(35)	4.52(81)	0.145(25)	13.7(3.7)
400	1772	0.996	1.876(37)	3.22(58)	0.160(32)	14.6(4.6)

Table 5.12: Test simulations for a 6x6x6x5 lattice with $\beta = 7.0$.

VOLUME: 8x8x8x7, PROC: 16 $\beta = 7.0$, **TIME: 1h**						
N_0	$N_{\rm traj}$	$\overline{P_{\rm acc}}$	$\bar{g}^2$	τ_{int}	$\bar{v}$	τ_{int}
10	16991	0.339	1.914(34)	18.5(2.7)	0.146(21)	48(10)
20	10834	0.813	1.920(31)	8.9(1.2)	0.152(15)	19.0(3.3)
25	9487	0.880	1.973(34)	8.4(1.1)	0.116(17)	21.4(4.2)
40	6972	0.952	1.972(40)	8.4(1.3)	0.154(18)	16.6(3.3)
50	6050	0.970	2.011(38)	6.4(1.0)	0.119(19)	15.2(3.1)
80	4510	0.987	2.003(41)	5.58(87)	0.189(21)	13.5(3.0)
100	3951	0.992	1.934(42)	5.8(1.0)	0.139(24)	16.2(4.0)
200	2655	0.998	2.027(53)	5.5(1.0)	0.110(29)	14.8(4.0)
400	1915	0.991	1.957(50)	4.51(90)	0.161(30)	15.7(4.9)

Table 5.13: Test simulations for a 8x8x8x7 lattice with $\beta = 7.0$.

From these data, we can decide the values for N_0, ϵ for each volume. In the cases in which we were capable of computing the observables, we can estimate the amount of

VOLUME: 10x10x10x9, PROC: 4 $\beta = 7.0$, **TIME: 3h**						
N_0	$N_{\rm traj}$	$\overline{P_{\rm acc}}$	$\bar{g}^2$	τ_{int}	$\bar{v}$	τ_{int}
20	1479	0.701	2.18(12)	8.5(2.4)	0.071(55)	24.2(9.5)
25	1295	0.802	1.745(80)	7.4(2.0)	0.114(32)	8.2(2.4)
40	969	0.918	2.30(28)	17.6(7.0)	0.066(44)	10.8(3.8)
50	807	0.949	1.88(13)	7.4(2.5)	0.217(72)	17.5(7.4)
80	569	0.977	2.30(18)	5.3(1.8)	0.226(38)	5.6(1.2)
100	501	0.976	2.31(20)	5.5(2.0)	0.213(40)	6.3(2.3)
200	352	0.989	2.56(30)	6.0(2.4)	0.106(97)	16.1(7.8)
400	251	0.984	1.91(14)	3.7(1.4)	0.310(23)	1.40(41)

Table 5.14: Test simulations for a 6x6x6x5 lattice with $\beta = 7.0$.

VOLUME: 12x12x12x11, PROC: 32 $\beta = 7.0$, **TIME: 2h**						
N_0	$N_{\rm traj}$	$\overline{P_{\rm acc}}$	$\bar{g}^2$	τ_{int}	$\bar{v}$	τ_{int}
20	3189	0.544	2.27(14)	15.6(4.2)	0.210(35)	16.9(4.6)
25	2902	0.688	2.13(14)	14.1(3.7)	0.105(54)	35(13)
40	2200	0.873	2.05(10)	8.3(2.0)	0.119(31)	10.3(2.7)
50	1904	0.824	1.97(14)	14.0(4.7)	0.204(35)	11.0(3.1)
80	1466	0.974	2.04(16)	14.1(4.7)	0.154(88)	18.2(5.6)
100	1315	0.974	2.20(13)	6.9(1.9)	——	——
200	965	0.995	2.00(13)	7.7(2.4)	——	——
400	805	0.972	2.27(20)	7.3(2.5)	——	——

Table 5.15: Test simulations for a 12x12x12x11 lattice with $\beta = 7.0$.

VOLUME: 16x16x16x15, PROC: 64 $\beta = 7.0$, **TIME: 2h**				
N_0	$N_{\rm traj}$	$\overline{P_{\rm acc}}$	$\bar{g}^2$	τ_{int}
50	275	0.735	2.00(30)	7.3(3.4)
80	254	0.917	1.56(20)	6.4(3.0)
100	226	0.932	2.20(50)	7.3(3.5)
200	140	0.921	1.60(10)	1.8(0.8)
400	128	0.937	1.14(10)	2.9(1.3)

Table 5.16: Test simulations for a 16x16x16x15 lattice with $\beta = 7.0$.

V: 20x20x20x19			**V: 24x24x24x23**		
PROC: 32			**PROC: 64**		
$\beta = 7.0$,		**TIME: 4h**	$\beta = 7.0$,		**TIME: 6h**
N_0	N_{traj}	$\overline{P_{\text{acc}}}$	N_0	N_{traj}	$\overline{P_{\text{acc}}}$
50	148	0.137	50	204	0.064
80	112	0.437	80	139	0.204
100	99	0.535	100	118	0.280
200	91	0.778	200	97	0.536
400	68	0.932	400	84	0.833

Table 5.17: Test simulations for 20x20x20x19 & 24x24x24x23 lattices with $\beta = 7.0$.

statistics needed to obtain a measured quantity with a decently small statistical error, given the integrated autocorrelation time is sensible. The integrated autocorrelation time gives us an estimation of the effective statistics of the measurements, i.e., $N_{\text{traj}}^{\text{eff}} \sim \frac{N_{\text{traj}}}{\tau_{\text{int}}}$ As it has been widely discussed in section 2, the statistical fluctuations are of order $\text{O}\left(\frac{1}{\sqrt{N}}\right)$, N being the number of measurements. In table(5.18) we show the decided optimal values for N_0 and a rough estimation of the real statistics and the time needed for the observable $\bar{g}^2$ to have a relative error $\sim 0.5\%$.

Note that these data are far from being accurate. The test simulations, specially for larger volumes, do not gather enough statistics for us to be able to conclude anything. Actually, for the largest volumes, namely $V = 20^3 \times 19, 24^3 \times 19$, there were not enough trajectories available to compute the observables. Moreover, the test simulations give us information about measurements with $\beta = 7.0$, and our goal is to run simulations over a range of β values, as it was stated in the introductory section. As it was pointed out in the final remarks in section 5.2, the acceptance rate depends on the value of β. All these observations need to be taken into account. However, the results shown in table (5.18) can be a good reference point when we start to perform the "real" simulations. Note that we might abandon the idea of obtaining such good statistics for the big lattices, due to time limitations. As a final remark, it is important to mention that the simulations for $V = 24^3 \times 23$ lattices turned out to be untractable for the machine we are using.

5.5 Simulation results

For reasons that will become evident in the following chapter, we have run simulations for the two regularisations discussed, $s = \pm 1$, lattices with $L/a = 4, 6, 8, 12, 16$ and a set of values of β in the range $[5.1, 12.0]$. For all these system, $\bar{g}^2(a/L, \beta), \bar{v}(a/L, \beta)$ have been measured. The results are recorded in appendix H specifying all the details relevant, such as the autocorrelation length, the acceptance rate, the time it took the machines to run the simulations, etc.

L	N_0	$\overline{P_{\rm acc}}$	No.Proc	$N_{\rm traj}$	Time
6	25	0.939	4	50000	5h
8	25	0.880	16	100000	11h
10	50	0.949	4	100000	10d
12	40	0.873	32	200000	8d
16	80	0.917	64	150000	25d
20	200	0.778	32	——	——
24	200	0.536	64	——	——

Table 5.18: Optimal values for N_0, estimated statistics and time needed to get $\frac{\Delta\bar{g}^2}{\bar{g}^2} \sim 0.5\%$. In the Time entry, h stands for hours, and d for days.

Two aspects have to be discussed regarding the simulations and the results of the measurable observables,

a) Is the algorithm sampling the entire relevant configuration efficiently?
b) How have the mean values of the observables and their statistical errors been measured?

5.5.1 Sampling of the configuration space.

If the algorithm is not sampling the entire configuration space, then autocorrelation times may be largely underestimated and systematically wrong might be obtained. A rough check that can be performed to back up the assumption that our simulations do not suffer from this problem is to evaluate the distribution followed by the observable throughout the Monte Carlo history. The same check was done in the computation of the SF coupling in pure SU(3) Yang Mills [38], in QCD with 2 [39] and 3 [40] flavours. In the latter, a Gaussian distribution was encountered in all cases, whereas in the 2 first ones, the distribution of the observable, $\partial S/\partial\eta = k/\bar{g}^2$ showed long tails toward negative values. This behaviour was believed to set in due to the existence of secondary minima of the action.

In figure 5.2, we present histograms of measured $\partial S/\partial\eta$ for the largest couplings examined, for both regularisations and all ranges of L/a. We can appreciate the absence of the aforementioned tails. This outcome encourages us to increase our confidence on the efficient sampling of the configuration space. Contrary to the SU(3) and QCD with two flavours, there is no need of reweighting.

5.5.2 Estimation of the observables

In order to estimate the mean values of the observables, as well as their statistical and systemaic errors and autocorrelation times, we have used the downloadable MATLAB routine `UWerr.m` that implements the method discussed in [120]. The analysis of the

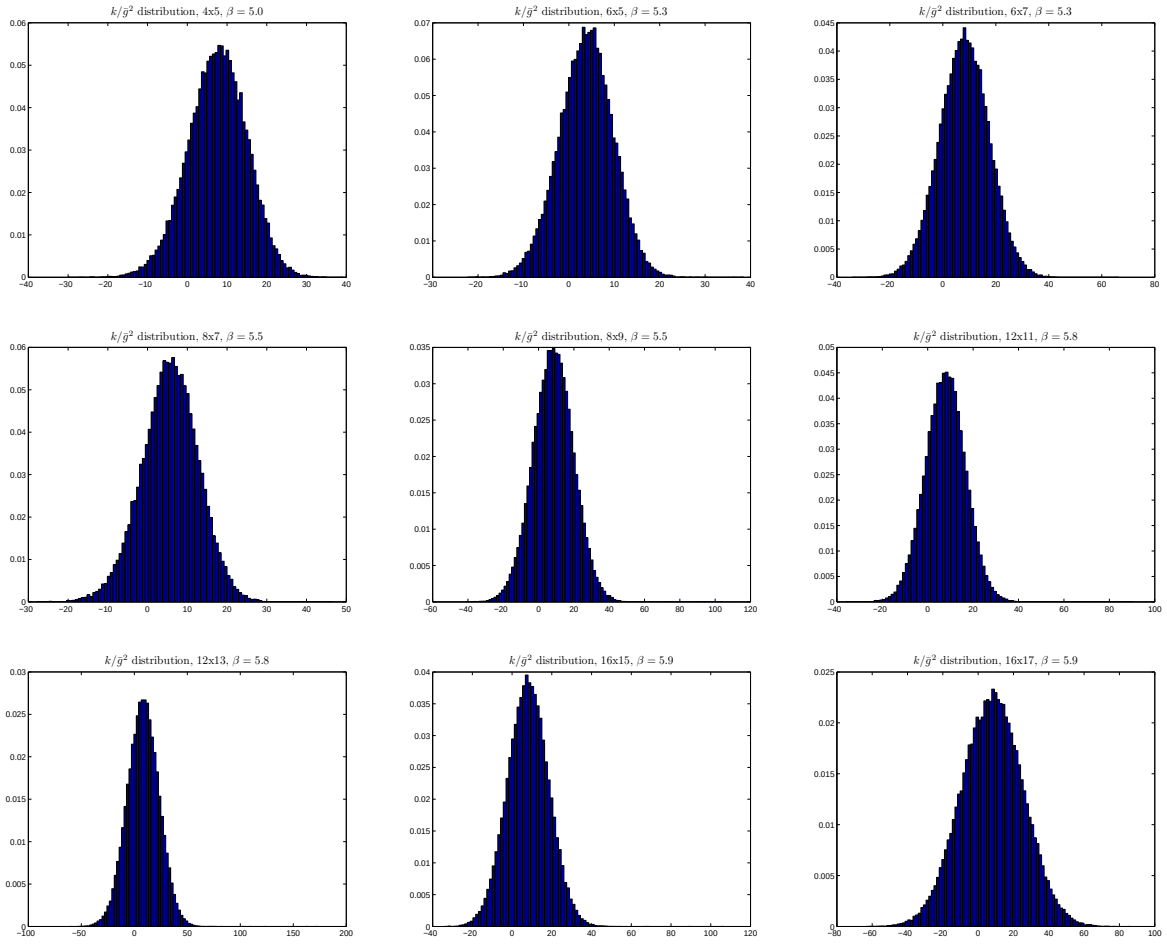

Figure 5.2: Distribution of the observable $\partial S/\partial \eta$ at the largest couplings for lattices with $L = 4, 6, 8, 12, 16$ and $s = \pm 1$.

statistical errors is difficult. The data are correlated and the physical quantities are often extracted after a complicated procedure. Hence, the error propagation is not evident.

The method proposed in [120] estimates and sums the relevant correlation functions. They are argued to produce more reliable error estimates than the usual binning techniques commonly used (jackknife, bootstrap). The method was partially discussed before in [121, 122, 123]. See these works for further details in the estimation of the mean values of the observables, their errors, the errors of the errors, and the integrated correlation time with its error.

Chapter 6

Implementation of finite size techniques and results

The aim of this project is to compute the evolution of the strong running coupling constant from low to high energies. We thus want to relate the high energy regime where perturbation theory can be applied succeSSFully with the observed hadrons and interactions at low energies. As it has been stated in the introduction, the solution to this problem involves rather large scale separations, whose accomodation into computer simulations is currently impossible. Naively, we would like the cutoff to be small enough so that its inverse is well off beyond the settling down of the perturbative regime. Moreover, the system size is demanded to be large enough in order for hadronic quantities to not suffer from large finite volume effects, i.e.,

$$a^{-1} >> \mu_{\rm pert} >> \mu_{\rm had} >> L^{-1}. \tag{6.0.1}$$

That would correspond to unaccesibly large lattices. The finite size technique, introduced in [34] proposes a way to overcome this problem. For these techniques to be applied, we need a non perturbative definition of the running coupling, $\bar{g}^2$. There is an infinite number of renormalised couplings that can be defined as long as they coincide with the bare coupling in PT, they are renormalisation group invariant and they depend on the energy scale. Throughout this work, the volume of the system is going to play the role of the scale of the theory. A coupling fulfilling this conditions has been defined in chapter 2, together with the framework where it is defined, i.e., the Schrödinger Functional, customised for the system addressed here (4 flavours of staggered fermions).

As it has been discussed in chapters 3 and 4, it is desirable to reduce the possible lattice artifacts present in the computation to achieve neater numerical results. The O(a) improvement up to 1 - loop has been implemented reducing the lattice effects. A general description of the numerical simulations needed to compute the renormalised coupling in a non-perturbative way was given in the previous chapter.

In this chapter, we will first present the strategy to be followed from a theoretical point of view. Then, we will explain how this program can be performed through

computer simulations and present the results. The key idea relies on bridging the large scale differences by performing simulations in systems of different volumes and different values of the lattice spacing.

6.1 Finite size techniques

The aim of this work is the computation of the evolution of the renormalised coupling with the energy scale from hadronic energies up to perturbative energies. In this latter regime, the scale evolution is verified to match with perturbation theory and there the Λ parameter can be determined.

6.1.1 Gell-Mann and Law renormalisation group

It is first interesting to give an overview of the so called Gell-Mann and Law renormalisation group [124]. Some emphasis has to be put here in order to make clear that the philosophy behind this renormalisation group method in this section is distinct from the Kadanoff [125] and Wilson [126]. In the framework of finite size techniques we propose to apply, they are disentangled from one another. The latter can be related to the study behaviour of a statistical system when the physical scale is changed, or else with the behaviour of a regularised QFT under a change in the cutoff (a change in the lattice spacing). It is appropriate to study critical phenomena in statistical mechanics and in cutoff regularised QFT's (removal of the cutoff or continuum limit). Gell-Mann and Low apply these methods to study the behaviour of physical quantities under a change in the renormalisation prescription.

There is some arbitrariness in the renormalisation procedure. In the context of perturbative renormalisation, there is some freedom in the choice of the counterterms added to cancel the divergences. They may contain some finite part. The choice of the value of the counterterm is known as the renormalisation prescription. However, a change in the renormalisation prescription cannot affect the theory itself, i.e., the physical quantities. This fact is not easy to see at all orders in perturbation theory. A proof is provided in [46], chapter 7.

A useful type of change of renormalisation prescription is to change the renormalisation scale, μ. Infinitesimal changes are described through differential equations, the Callan - Symanzik [127, 128] renormalisation group equations. These equations follow from the observation that physical quantities like the S-matrix are invariant under a change of the renormalisation prescription (a change in μ, $(\mu, g(\mu), m(\mu)) \rightarrow (\mu', g(\mu')m(\mu'))$),

$$\mu \frac{dS}{d\mu} = 0. \tag{6.1.1}$$

The total derivative with respect to μ can be written as,

$$\mu\frac{d}{d\mu} = \mu\frac{\partial}{\partial\mu} + \beta(\bar{g})\frac{\partial}{\partial\bar{g}} + \tau(\bar{g})\sum_{i=1}^{N_f}\bar{m}_i\frac{\partial}{\partial\bar{m}_i}. \tag{6.1.2}$$

The implied scale dependence of the coupling is given by $\beta(\bar{g})$,

$$\beta(\bar{g}) = \mu\frac{\partial\bar{g}}{\partial\mu}. \tag{6.1.3}$$

This is a renormalisation group coefficient, commonly known as the β-function. Then, any physical observable satisfies,

$$\left\{\mu\frac{\partial}{\partial\mu} + \beta(\bar{g})\frac{\partial}{\partial\bar{g}} + \tau(\bar{g})\sum_{i=1}^{N_f}\bar{m}_i\frac{\partial}{\partial\bar{m}_i}\right\}P = 0. \tag{6.1.4}$$

Once the coupling has been defined non-perturbatively for all scales, then the β-function is defined beyond perturbation theory. In the perturbative regime, the β-function can asymptotically be expanded as,

$$\beta(\bar{g}) = -\bar{g}^3(b_0 + b_1\bar{g}^2 + b_2\bar{g}^4 + \dots), \tag{6.1.5}$$

where the two first coefficients are universal,

$$\begin{aligned} b_0 &= \frac{1}{(4\pi)^2}\left(11 - \frac{2}{3}N_f\right), \\ b_1 &= \frac{1}{(4\pi)^4}\left(102 - \frac{38}{3}N_f\right), \end{aligned} \tag{6.1.6}$$

while the higher order coefficients depend on the choice of $\bar{g}^2$. b_0, b_1 are universal provided the couplings defined in two different mass independent renormalisation schemes (e.g. $\overline{\text{MS}}, \bar{g}_{\overline{\text{MS}}}$ and SF,$\bar{g}_{SF}$) can, in the perturbative regime, be expanded as a Taylor series of each other,

$$\bar{g}^2_{\overline{\text{MS}}} = \bar{g}^2_{SF}\left(1 + C_g^{(1)}\bar{g}^2_{SF} + \dots\right). \tag{6.1.7}$$

In the SF scheme, b_2 is known and presented in [86], using the results of the corresponding 3-loop coefficient in the $\overline{\text{MS}}$ scheme,[129], and its conversion to the minimal subtraction scheme of the lattice regularisation, [130, 131, 132, 133]. Its value takes the form,

$$b_2 = \frac{1}{(4\pi)^3}\left\{0.483(7) - 0.275(5)N_f + 0.0361(5)N_f^2 - 0.00175(1)N_f^3\right\}. \tag{6.1.8}$$

By inspection of the perturbative solution of the β-function, Eq. (6.1.5), it can be inferred that $\bar{g}(\mu) \to 0$ as $\mu \to \infty$. β is negative in the perturbative regime. Our theory is asymptotically free.

Every solution of the renormalisation group equations can be expressed in terms of special solutions. The Λ-parameter (that introduces the scale of QCD) is one of such special solutions. It is important to note that it is a renormalisation group invariant (RGI) albeit scheme dependent. Regardless of the scheme being mass independent, the Λ-parameter does not involve the quark masses, $\Lambda = \mu L(\bar{g})$. Its exact solution can be extracted and reads,

$$\Lambda = \mu(b_0\bar{g}^2(\mu))^{-b_1/(2b_0^2)} e^{1/(2b_0\bar{g}^2(\mu))} \exp\left\{ -\int_0^{\bar{g}(\mu)} dx \left[\frac{1}{\beta(x)} + \frac{1}{b_0 x^3} - \frac{b_1}{b_0^2 x} \right] \right\}. \quad (6.1.9)$$

The relationship between the Λ parameters of the two schemes under consideration is exactly given by,

$$\Lambda_{\overline{\rm MS}} = \Lambda_{SF} e^{C_g^{(1)}/(2b_0)}. \quad (6.1.10)$$

We can split $C_g^{(1)}$ into its pure gauge part and fermionic contribution,

$$C_g^{(1)} = \frac{1}{4\pi}\left(c_{1,0} + N_f c_{1,1}\right), \quad (6.1.11)$$

where $c_{1,0}$ has been computed in reference [38],

$$c_{1,0} = 1.25563(4), \quad (6.1.12)$$

and we should obtain the same result for $c_{1,1}$ as in [66]. This coefficient is given by,

$$c_{1,1} = -4\pi[P_4 + r_{0,1}], \quad (6.1.13)$$

with $P_4 = 0.026247371$ is the finite contribution from staggered fermions to the one loop relation between lattice and $\overline{\rm MS}$ coupling, computed in [61][1]. Using $r_{0,1}$ from Table 4.5, we obtain,

θ	$c_{1,1}$
0	0.022503(3)
$\pi/5$	0.0398632(5)
1	0.053274(1)
2	0.077375(4)

Table 6.1: Values of $c_{1,1}$

These values are in good agreement with the results of Sint and Sommer with Wilson fermions, [66].

[1]The better accuracy quoted here is taken from [50], where Heller obtains it from Eq. (6.12) of [61] using the more accurate values for P_1, P_2 from [85].

6.1.2 Step scaling function

Our framework is the Schrödinger functional. It is a finite toroidal space manifold with temporal Dirichlet boundary conditions. Our system has a natural scale, its spatial length, L. This quantity plays the role of the scale of the theory $L^{-1} \sim \mu$. The non perturbative renormalised coupling defined in section 2.4. depends only on this scale. In what follows we will show that this coupling can be computed numerically from large volumes down to very small scales L with controlled errors, thus providing a bridge to the perturbative regime. The β-function as a function of L reads,

$$\beta(\bar{g}^2) = -L\frac{\partial \bar{g}^2}{\partial L}. \tag{6.1.14}$$

It gives us information about the behaviour of the renormalised running coupling constant as the size of the system is changed infinitesimally. A discretised version of it, the "step scaling function" (SSF), $\sigma(s,u)$ was introduced in [34] and it describes how the coupling changes as L scales by a factor s. In our calculations, $s = 2$. Then,

$$\bar{g}^2(2L) = \sigma(2, \bar{g}^2(L)). \tag{6.1.15}$$

The step scaling function $\sigma(2,u)$ and $\beta(u)$ are related through,

$$\ln 2 = -\int_u^{\sigma(2,u)} \frac{dv}{\beta(v)}. \tag{6.1.16}$$

When $u = \bar{g}^2$ is small, the SSF can be expanded in renormalised perturbation theory,

$$\sigma(u) = u + s_0 u^2 + s_1 u^3 + \ldots, \tag{6.1.17}$$

with the coefficients,

$$\begin{aligned} s_0 &= 2b_0 \ln 2, \\ s_1 &= (2b_0 \ln 2)^2 + 2b_1 \ln 2, \\ s_2 &= (2b_0 \ln 2)^3 + 10 b_0 b_1 (\ln 2)^2 + 2b_2 \ln 2. \end{aligned} \tag{6.1.18}$$

This construction suggests we can compute the step scaling function and thus the scale evolution of the coupling by simulating two lattices with sizes L and $L' = 2L$ at the same value of the bare coupling. In both lattices, we compute $\bar{g}^2$ and this yields a point in a diagram where $u' = \sigma(2,u)$ can be plotted versus u. This procedure can be iterated for different values of g_0 so that the behaviour of $\sigma(2,u)$ vs u can be studied. In practice, this is complicated due to the presence of lattice artifacts.

6.1.3 Scaling of the coupling with energy

Let us assume throughout this subsection that the continuum step scaling function is known for the scale factor 2 and for a range of u that goes from the hadronic to the

perturbative regime. Then, the coupling at low energies can be related to the one in the perturbative regime by constructing the following series of couplings,

$$\begin{aligned} u_0 &= \bar{g}^2(L), \\ u_1 &= \bar{g}^2(2L) = \sigma(2,u), \\ &\dots \\ u_n &= \bar{g}^2(2^n L) = \sigma(2,u_{n-1}). \end{aligned} \tag{6.1.19}$$

The largest box size $L_{\max} = 2^n L$ is expected to be $\sim 1/m_{\rm had}$.

In the perturbative regime, a computation of $\Lambda_{\rm SF}$ is possible and the SF scheme can be converted into the $\overline{\rm MS}$ scheme. The reference to finite volume is no longer present and we have managed to relate the hadronic properties of the theory with the perturbative regime.

In this work, we present the evolution of the running coupling with energy. As it has been pointed out above, the implementation of this tactic on the lattice is somehow complicated since it is not the step scaling function in the continuum $\sigma(2,u)$ we compute, but its lattice version $\Sigma(2,u,a/L)$. An extrapolation to 0 lattice spacing is thus needed. Next section (cf. 6.2) is devoted to discuss this issue. The connection with physical units, that is, the computation of a hadronic quantity in a large volume has not yet been performed, nor the conversion into the $\overline{\rm MS}$ scheme (physical units are required to do that).

6.1.4 Physical units

We sketch how the establishment of physical units can be implemented. This amounts to a renormalisation of the system.

i) In the SU(2) theory [36, 37] , all physical momenta were given in units of the string tension, K, that was already known from studies in large lattices, [134, 135].

ii) In the SU(3) pure Yang Mills [38], and in $N_f = 2$ [39], the connection was established by using r_0 (Sommer scale, [136]), the distance at which $r_0^2 F(r_0) = 1.65$. Here, $F(r)$ is the force between two infinitely heavy quarks at distance r. This change was due to the fact that the use of K turned out to be technically problematic, since in practice it is determined by extrapolating $F(r)$ from distances $r < 1$ fm. The merits of this definition were discussed in [136]. The most remarkable ones being,

   - r_0 is well defined in gauge theories with and without matter fields.
   - r_0 is estimated to be ~ 0.5 fm in nature.
   - r_0 is easy to compute on the lattice and no extrapolation is required.

iii) In [40], where the computation for QCD with three flavours is performed, they employ hadron masses m_π, m_K, m_Ω as input. These are direc hadronic observables, opposed to the previously used quantities, r_0, K.

Let us assume the Sommer scale had been chosen. Then, the procedure is the following. Let us define $L_{\max}$ as the quantity at which $\bar{g}^2(L_{\max})$ assumes a fixed value, $\bar{g}^2_{L_{\max}}$. We want to compute $L_{\max}/r_0$. We thus select g_0 on a large lattice (e.g. $L/a \sim 48$) so that r_0/a can be computed with small finite volume effects. At this same g_0 one computes $\bar{g}^2$ on smaller lattices and obtains $L_{\max}/a$ by interpolation, and hence $(L_{\max}/r_0)(g_0)$. Now, the procedure is repeated at other values so that finally an extrapolation to the continuum limit can be performed.

6.2 Step scaling technique with a lattice cutoff

Our goal is to compute the scale evolution of $\bar{g}^2(L)$. The tool presented above to achieve this, is the step scaling function $\sigma(2,u)$, defined in the continuum limit of the theory. However, all our computations will be performed on the lattice. Then, an extrapolation to the continuum limit is a neccessity. For a given value of the renormalised coupling, u, the bare parameter, $\beta = 2N/g_0^2$ (N is the number of colours), is adjusted so that $\bar{g}^2(L) = u$. u implicity determines the size of the system, L. We simulate a lattice with twice the linear size at the same bare parameters and thus corresponding to a physical extent $2L$. This determines the scale evolution of the renormalised coupling and defines the lattice step scaling function,

$$\Sigma(u, a/L) = \bar{g}^2(2L)\big|_{\bar{g}^2(L)=u}\,. \tag{6.2.1}$$

The step scaling function is finally obtained by repeating these three steps for finer and finer lattice spacings and taking the continuum limit,

$$\sigma(u) = \lim_{a/L\to 0} \Sigma(u, a/L). \tag{6.2.2}$$

Taking the continuum limit is a conceptually non trivial task. Hence, we will discuss it in more detail in the subsequent subsection. Then, the exact strategy to obtain the step scaling will be described.

6.2.1 Continuum limit

One of the most difficult questions in lattice field theories is the consideration of how the continuum limit is taken. Taking the continuum limit of a lattice regularised theory amounts to renormalising the theory (the cutoff is removed since $a \to 0$) .

If a free theory was analysed, since its analytical solution is at our disposal, the results after taking the continuum limit could be compared with the actual solutions of the theory in order to determine whether it had been successfully implemented. However, this is far from being the case in interacting theories. Moreover, taking the continuum limit naively for such theories leads to inconsistencies. Hence, some care has to be taken.

Let us give a qualitative description of how the continuum limit should be taken. Consider an infinite lattice with am_0, g_0 being bare dimensionless parameters of a given field theory. These parameters may not have any physical interpretation (they are bare parameters of the theory). The physical mass, m, might be defined through,

$$am = f_1(am_0, g_0). \tag{6.2.3}$$

The continuum limit is achieved in a region in which the physical quantities are kept finite, while the lattice spacing is pushed to take decreasing values, $a \to 0$. The resolution of the lattice becomes finer and finer so that the physical distance scales are much greater than the lattice spacing. We expect $f_1 \to 0$ in the continuum limit. However, it has to do so along a critical curve in the plane of the bare parameters.

Thus, continuum behaviour sets in when the bare parameters (e.g. (am_0, g_0), the set depends on the particularities of the theory) are near a critical curve. We also want the renormalised coupling to assume a certain value. If our coupling is dimensionless, we will have,

$$g = f_2(am_0, g_0). \tag{6.2.4}$$

As it happened with the physical mass, m, we cannot simply fix g_0 and expect a sensible continuum limit. It also has to be reached by approching a critical curve for fixed physical coupling g. Thus, the procedure is the following. First, the physical parameters are elected. That infers a dependence of the bare couplings on the lattice regulator in a complicated manner.

It seems like we have encountered a way of sensibly taking the continuum limit. However, there are some questions one can pose:

- Are the equations obtained for m, g solvable? If so, are they sufficient for the dependence on the regulator to entirely dissapear? The main problem is that f_1, f_2 are not a priori known. PT can be used to extract them. However, g_0 might be driven to large values near criticality which leads to the impossibility of using PT.
- The dynamics described by a lagrangian is local. Hence, the scales involved are $\sim a$. However, the physical properties near criticality are associated with scales $>> a$. It could happen that small changes in the micriscopic level outreagoulsy change the emergent properties of the system.
- Renormalisable theories are meant to not suffer from the problem just pointed out. In the continuum limit, renormalisable theories lead to a unique, finite dimensional manifold of QFT's. The theories used in elementary particla physics have been shown to be renormalisable in perturbation theory. Nebertheless, it is not clear that non perturbative continuum limit of the corresponding lattice model leads to the renormalised theory we are seeking.

Despite all the problems mentioned above, the results obtained so far from QFT's formulated on a lattice and simulated on a computer lead to sensible results. Hence,

they constitute a strong encouragement to back up the procedure used to renormalise the theory. In what follows, will rely on the assumption that the continuum limit of the theory leads to the renormalised theory.

Connection with statistical mechanics

It has been mentioned that the continuum limit sets in in the vicinity of critical curves. Near the continuum limit, the physical scales are much larger than the lattice regulator. This suggests to establish an analogy between the critical behaviour of QFT's and statistical mechanical systems. In such systems, the critical behaviour is characterised by a blow up of the correlation length; They present emergent macroscopic properties. A rough way of making this analogy evident is the following. When the contlinuum limit of a lattice theory is taken, $ma \to 0$. This quantity gives the correlation length,

$$\xi = (ma)^{-1}. \tag{6.2.5}$$

We are thus inspecting the behaviour of the theory near a point in the space of bare parameters where the correlation length diverges. That is, near a critical point or a second order phase transition.

Nature of the fixed points

Let us restrict to a theory with only one bare parameter, the coupling constant g_0. A physical observable H in the regularised theory will be a function of the bare coupling, the cutoff scale and the scale $L \sim 1/\mu$ at which it is defined. That is,

$$H = H(L, g_0(a), a). \tag{6.2.6}$$

There are many ways of regularising the theory. For example, as it has been discussed in chapters 3 and 4, there is a freedom of adding certain irrelevant operators in order for the continuum limit to set in faster. Thus, the particular dependence of the bare coupling on the regulator will be different for different renormalisation schemes. Let us assume H to be a dimensionless quantity. As the continuum limit is approached, it should lose its dependence in a and keep the one in L. This can only occur at special values of g_0 where critical behaviour involving vastly different scales. If we change change the cutoff by a factor of 2, we obtain,

$$H(L, a/2, g_0(a/2)) = H(L, a, g_0(a)) + \mathrm{O}(a^2) \tag{6.2.7}$$

The size of the cutoff corrections are monitored by the scale $1/L \sim \mu$ and the scale of the physical spectrum of the theory. The continuum limit sets in when the cutoff is considerably smaller than the inverse of these quantites. Now, we can ask ourselves which value g_0 takes when the continuum limit is taken. The procedure to be followed involves playing with the energy scaling properties of the observable and changes in the value of the cutoff. Since H is dimensionless, if we double L, a in Eq. (6.2.7), we obtain,

$$H(2L, a, g_0(a/2)) = H(L, a, g_0(a) + \mathrm{O}(a^2). \tag{6.2.8}$$

This equation relates the bare coupling at two values of the cutoff with the observable measured at two different energy $\sim 1/L$ scales. Supposing,

a) The analytical dependence of H on the scales L, a is known.

b) The continuum limit of H at a given scale L is H_0.

Neglecting lattice artifacts, the following relations hold,

$$H_0 = H(2L, a, g_0(a/2)), \tag{6.2.9}$$

Once $g_0(a/2)$ is known, we can compute,

$$H_1 = H(L, a, g_0(a/2)). \tag{6.2.10}$$

This process can be iterated until we find,

$$\begin{aligned} H_n &= H(L, a, g_0(a/2^n)), \\ H_n &= H(2L, a, g_0(a/2^{n+1})). \end{aligned} \tag{6.2.11}$$

In that way, we can arrived at the fixed point of the bare coupling g_0. This method is sketched in figure 6.1 for three different cases,

a) Asymptotically free theory. The fixed point of the theory occurs at vanishing bare couplings. Thus, $g_0(0) = 0$

b) Theories with a non trivial fixed point. In this case, there is a crossing between $H(2L, a, g_F)$ and $H(L, a, g_F)$. At this fixed point, the theory becomes scale invariant. Morover, the fixed point is atractive. One could also imagine it to be repulsive in which case it is reached only if the bare coupling g_0 we start with has exactly the value it is supposed to assume at the fixed point, g_F

c) Theories with no trivial fixed points. The procedure has no solution. That leads to the conclusion that these theories have no continuum limit unless they are trivial, i.e., free theories. At the present time, it is strongly believed that this is the case of the four dimensional ϕ^4 theory although there is no rigorous proof of this statement.

Wilson approach of the Renormalisation group

The flows of the coupling described are nothing but a simplified version of the renormalisation group transformations applied to system of this type introduced by Kadanoff and Wilson in the early seventies. It has to be remarked that while in particle physics, we are generally interested in the continuum limit, in statistical mechanics the procedure just sketched is discused in the reverse way. We start with system with a small lattice sp[acing and one tries to find an effective theory with larger lattice spacing.

a) Asymptotically free theory **b) Non trivial fixed point**

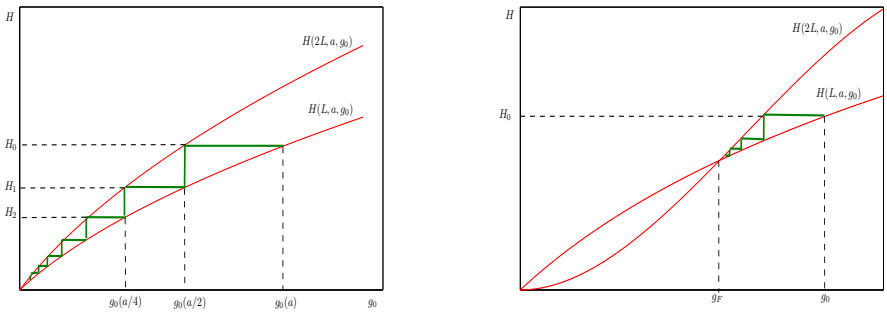

c) A theory without a non-trivial continuum limit

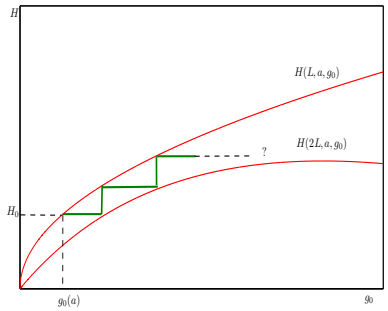

Figure 6.1: Finding fixed points of the bare coupling.

The good news is that the renormalisation group equations introduced in the 50's (cf. 6.1.1.) are applicable on this domain. Let us impose a renormalisation prescription on the quantity H. We set it to be H_0 at the scale L, for all values of a. Then, the condition,

$$a\frac{d}{da}H(L,a,g_0(a)) = 0, \tag{6.2.12}$$

holds. Thus,

$$\left\{a\frac{\partial}{\partial a} - \beta_0(g_0)\frac{\partial}{\partial g_0}\right\}H(L,a,g_0) = 0, \tag{6.2.13}$$

where $\beta_0 = -a\frac{\partial g_0(a)}{\partial a}|_{H_0}$. These are the so called Callan and Symanzik equations. The subscript 0 is to differenciate it from the β function describing the evolution of the renormalised coupling with the scale. Zeros in $\beta_0(g_0)$ correspond to fixed points of the theory. Furthermore, if we want the fixed points to be atractive, then its first derivative has to be negative.

In general, the particular form of β_0 depends on the renormalisation scheme taken. Nevertheless, its zeros have to be universal since they correspond to critical points of the theory. We do not want the continuum limit of a theory to depend on the renormalisation scheme [2]

[2] All fall in the same universality class. Decir algo más aqu'i sobre las universality classes.

Connection between the Callan Symanzik equations for g_0 and $\bar{g}$

Let us focus in asymptotically free theories. In these theories in the weak coupling domain, perturbation theory can be used and β_0 can be computed order by order in powers of g_0. The functional behaviour is the exact the same as the one for β function obtained in subsection 6.1.1. Actually, the first two coefficients are universal and, if $N = 3$ they are b_0, b_1 previously specified Eq. (6.1.6). That is,

$$\beta_0(g_0) = -g_0^3(b_0 + b_1 g_0^2 + \dots). \tag{6.2.14}$$

Let us try to relate the evolution of the bare coupling towards the continuum limit and the evolution of the renormalised coupling with the physical scale. We refresh that for $\bar{g}$ to be a renormalised coupling, it has to,

- remain finite in the continuum limit.
- be normalised so that it coincides with the bare coupling in lowest order when the cutoff is still in place.

In general, $\bar{g}$ depends on the physical scale $\bar{g}(L)$. In the continuum limit, we should be capable of re-expressing the physical quantities in terms of the renormalised parameters. Let H be such an observable defined at the scale r_0. Then, in the continuum limit, and for energy regimes where PT can be applied,

$$H(r_0, L, \bar{g}(L)) = h_0 + h_1 \bar{g}^2(L) + \mathrm{O}(\bar{g}^2). \tag{6.2.15}$$

It is not to be forgotten that in the regularised theory, H is expanded in PT in powers of g_0, in the weak coupling domain,

$$H(r_0, a, g_0(a)) = h_0 + h_1 g_0^2 + \mathrm{O}(\mathrm{g}_0^2). \tag{6.2.16}$$

The coefficients in both expansions are in general distinct. However, they coincide to second order. L has been elected arbitrarily. Hence, the observable should not depend on it, and the Callan and Symanzik equation Eq. (6.1.4) holds with $L = 1/\mu$. Now,

$$\beta(\bar{g}) = -L\frac{\partial \bar{g}}{\partial L}. \tag{6.2.17}$$

When the coupling is still in place, $\bar{g} = \bar{g}(L, a, g_0)$. The coupling has no dimensions, then, $\bar{g}$ depends on a, L through their ratio. This observation leads to,

$$L\frac{\partial}{\partial L}\bar{g} = -a\frac{\partial}{\partial a}\bar{g}. \tag{6.2.18}$$

From here, it can be concluded that the two first coefficients of β and β_0 coincide.

Application to our problem

As we have just seen, in order to take the continuum limit sensibly, it is required we provide sensible renormalisation prescriptions. When that happens, then, the dependence of the bare parameters with the lattice spacing is fixed, and the system is thus expected to flow into a critical point. In our work the continuum limit has to be taken in two domains:

Physical units Although this task has not been accomplished yet, in subsection 6.1.4 it was briefly discussed how to provide our system with physical units. If the Sommer scale was to be chosen, then, if we substitute $H = r^2F(r)$ and $H_0 = 1.65$ and $r_0 = 0.5$ fm, the discussion carried out above justifies this election to be an appropriate way of taking the continuum limit

Step scaling function Concerning the scaling techniques implemented to evolve the coupling with energies, a renormalisation prescription is required per step (energy scale) considered. It is the renormalised coupling $\bar{g}^2$ itself that is assumed to take a particular value, $\bar{g}^2(L_i) = u_i$. This renormalisation prescription is valid and enough for the continuum limit to set in sensibly.

6.2.2 Computational strategy followed

The step scaling procedure is generally [34, 36, 37, 38, 39, 40] implemented in the following fashion,

a) Choose a value for the renormalised coupling, u_0.

b) Tune β so that $\bar{g}^2(L) = u$ within errors in the siumulations. Compute $\Sigma(2, u, a/L) = \bar{g}^2(2L)$ at the tuned value of β.

c) Repeat *b*) for various different values of L/a. Typically, $L/a = 4, 6, 8$.

d) Take the continuum limit and obtain $u' = \sigma(2, u)$.

e) Tune β again so that $\bar{g}^2(L') = u' > u$ and iterate steps $a) - d)$.

In figure 6.2 we present a sketch of steps $a) - d)$. Following this procedure, in n steps the size of the box is incremented by a factor 2^n. Tipically, the iteration is carried out $\sim 7, 8$ times, so we expect a factor of a few hundreds.

Carrying out the above procedure directly can be expensive in computational power since each tuning of β might need several attempts. Moreover, the rate at which computations may be performed is not too high since one must wait for each simulation to finish, and the value of $\sigma(2, u)$ must be extracted for step *e*) to be accomplished.

Instead, we have followed the procedure proposed in [41]. We measure $\bar{g}^2(L)$ for a set of values $\beta, L/a$ and generate an interpolating function. This function is then used to tune β as already described. The extraction of the step scaling function no

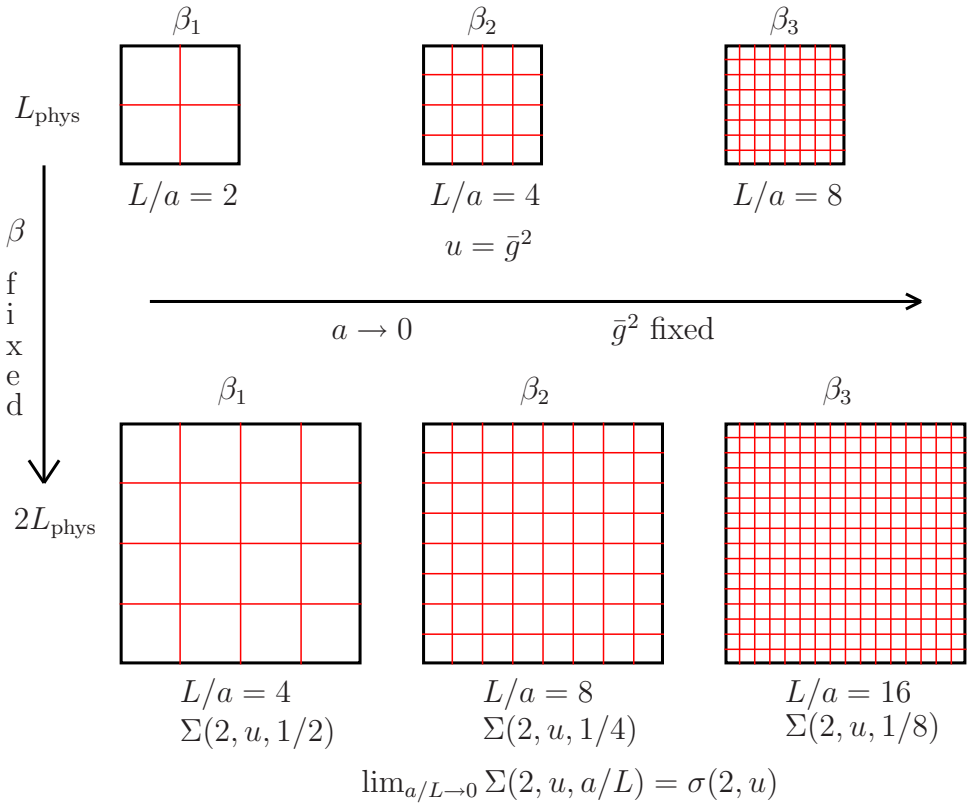

Figure 6.2: Sketch of step scaling techniques

longer depends so severely on the number of steps taken. Now, the set of simulations discussed in the previous chapter, whose results are listed in Appendix H are justified. It is not to be forgotten that since two regularisations are available, $T = L - sa$, with $s = \pm 1$, two sets of simulations have been run.

In the simulations, the measurement of the renormalised quantity $\bar{v}$ has been also carried out. However, an analysis of it is not going to be provided in this work. We will be focused in the renormalised running coupling and its scaling.

6.3 Analysis of the data

Here, we are going to deal with the technicalities involved in the analysis of the data until $\Sigma(2, u, a/L)$ for precise values of u and $a/L = 1/4, 1/6, 1/8$ are obtained. The whole data analysis has been carried out using routines that are MATLAB readable.

6.3.1 χ^2 - fitting

In Figure 6.3, we show the estimate of $\bar{g}^2$ and statistical errors for the two regularisations $s = \pm 1$ and for $L/a = 4, 6, 8, 12, 16$.

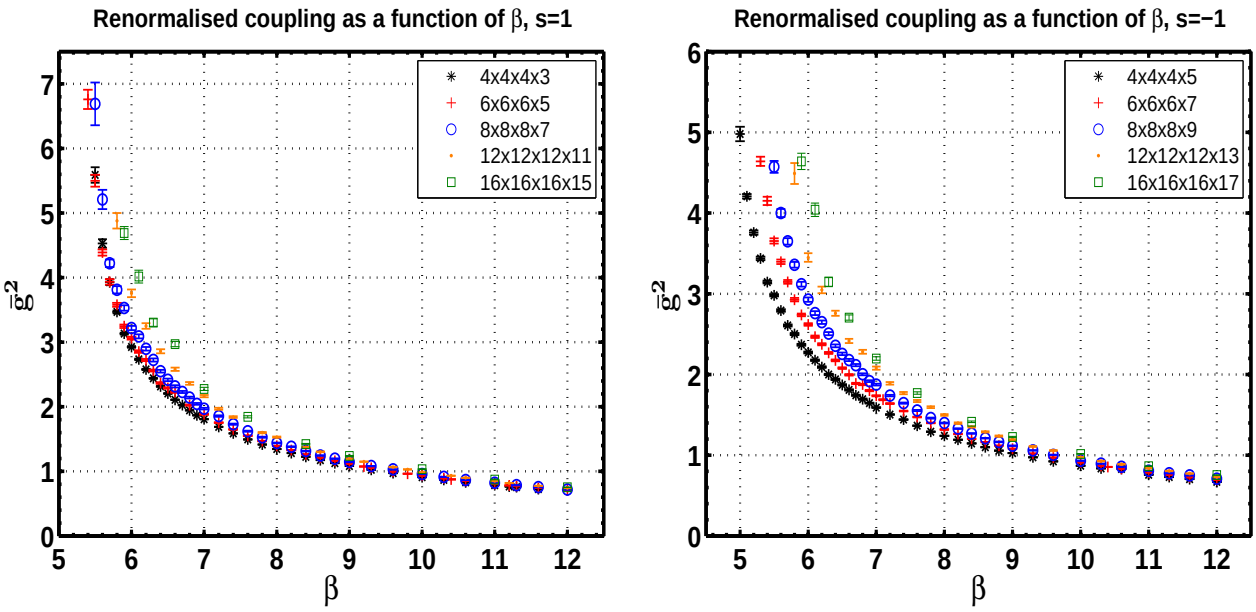

Figure 6.3: $\bar{g}^2(\beta)$ as a function of β. The errors are statistical.

We are dealing with several hundreds of estimators. With so many independent statistical estimators, occasional large statistical fluctuations are expected. So, we model our estimator with a smooth interpolating function based on a truncated Laurent series, as it has been done in [41]. The functional form is,

$$\frac{1}{\bar{g}^2(\beta, L/a)} = \frac{\beta}{2N} + \sum_{i=1}^{r} x_i \left(\frac{2N}{\beta}\right)^{i-1} . \tag{6.3.1}$$

This form is motivated by the following fact. In the weak coupling domain, the Schrödinger functional can be computed by performing a saddle point expansion of the functional integral about the induced background field B. For the effective action, an asymptotic series of the form,

$$\Gamma[B] = g_0^{-2}\Gamma_0[B] + \Gamma_1[B] + g_0^2\Gamma_2[B] + \cdots ,$$

holds. From the definition of the renormalised coupling, we can thus infer the behaviour of Eq. (6.3.1). However, using this function to fit the data is not implying that perturbation theory is applicable to our non perturbative results.

The data have been fitted by making use of the least squares method. This can be done with no further considerations, since the data are believed to be independent identically distributed random variables following a gaussian distribution. The goal is to find the values of the coefficients x_i that best reproduce the behaviour of the function. Three MATLAB routines have been written in order to accomplish this task. Some details about the numerical methods implemented in the mentioned programs can be found in [137, 138].

The data have been fitted using the three routines leading to similar results, in the sense that the interpolated points coincide within errors. The degree of the polynomial

used was chosen for different values of L/a in order to achieve the optimal χ^2 per degree of freedom when fitted to our data. This fitted function is then used for interpolation within the measured range and it is thus the basis for the step scaling procedure.

6.3.2 Analysis of the lattice artifacts

Now, we are going to perform an analysis of the lattice artifacts of our data. The steps followed are,

1. We choose a regularisation ($s = \pm 1$) to define a line of constant physics. The whole procedure will be done for each regularisation.

2. We fit the quantities $u = \frac{1}{\bar{g}^2}$ of every data set for a fixed L/a and fixed s to a polynomial in $t = \frac{2N}{\beta}$, by using the least squares methods described in the previous subsection.

3. Take the data of the regularisation we have chosen to describe the line of constant physics. Focus on the biggest lattice $L/a = 16$. Each data point $\bar{g}^2$ of this set is going to describe a line of constant physics. Find the values of β for $L/a = 4, 6, 8, 12, 16$ that correspond to the fixed values of $\bar{g}^2$ and the corresponding errors by using the linear regression techniques.

4. For the values of beta obtained in step 3., and for the other regularisation, compute the corresponding values of $\bar{g}^2$.

5. The deviation of the data obtained in 4. from the horizontal line defined by the the data in 3. consists just on lattice artifacts. The two quantities should coincide in the continuum limit. The values of the observables in the continuum limit are the ones in 3., by construction.

Error handling

Here, we will discuss how the error analysis has been performed. The error analysis carried out for the implementation of the program above is the exact the same as the one used for the computation of the step scaling function.

When the program above is implemented, the quantities $\bar{g}^2(a/L, s)$ computed in step 4 inherit two sources of errors:

a) Statistical errors coming from the least squares fitting $\Delta(\bar{g}^2)^{\text{stat}}$.

b) Systematic errors coming from the uncertainties in the quantities $u(a/L, s')$ that fix the physics, $\Delta(\bar{g}^2)^{\text{sys}}$.

Thus, the total error reads,

$$\Delta\bar{g}^2(a/L, s) = \sqrt{(\Delta(\bar{g}^2)^{\text{stat}})^2 + (\Delta(\bar{g}^2)^{\text{sys}})^2}. \tag{6.3.2}$$

Since, in the continuum limit, we expect,

$$\lim_{a\to 0} \bar{g}^2(a/L, s) = \lim_{a\to 0} \bar{g}^2(a/L, s') = u_{s'}, \tag{6.3.3}$$

then, it is reasonable to take $\Delta(\bar{g}^2)^{\rm sys}$ to be,

$$\Delta(\bar{g}^2)^{\rm sys}(a/L, s) = \Delta\bar{g}^2(a/L, s'). \tag{6.3.4}$$

Results

We expect the dominant lattice artifacts to be $O(a^2)$. Hence, the continuum extrapolation has taken to be a square polynomial in a/L in all cases. In tables 6.2, 6.3 we present:

COLUMN **1:** Renormalisation prescription $u = \bar{g}^2(a/L, s')$ with $s' = 1, -1$ in tables 6.2, 6.3 correspondingly.

COLUMN **2-5:** Values of the renormalised coupling for $s = -s'$ taken at the β's corresponding to the renormalisation prescription, for lattices with $L/a = 4, 6, 8, 12, 16$.

COLUMN **6:** Continuum extrapolation of these quantities, performing the fitting excluding lattices with $L/a = 4$.

COLUMN **7:** Continuum extrapolation including all data available.

Fixed $\bar{g}^2$	L/a					Extrapolation	
u	16	12	8	6	4	5 points	4 points
4.772(77)	4.73(12)	4.39(11)	3.920(60)	3.486(27)	2.8750(40)	4.712(82)	4.228(43)
3.968(41)	3.843(57)	3.673(53)	3.423(27)	3.127(16)	2.6549(18)	3.874(39)	3.654(22)
3.407(25)	3.265(36)	3.177(29)	3.034(17)	2.827(12)	2.4600(93)	3.309(24)	3.207(14)
2.823(16)	2.693(24)	2.661(16)	2.588(11)	2.4608(77)	2.2067(50)	2.735(15)	2.6991(87)
2.310(11)	2.211(17)	2.207(10)	2.1618(66)	2.0881(45)	1.9290(32)	2.2463(94)	2.2302(53)
1.8283(76)	1.767(11)	1.7734(60)	1.7378(44)	1.6982(30)	1.6123(20)	1.7913(58)	1.7784(34)
1.4410(47)	1.4094(67)	1.4148(36)	1.3867(29)	1.3657(19)	1.3198(13)	1.4238(36)	1.4122(21)
1.2477(33)	1.2284(52)	1.2309(27)	1.2091(21)	1.1950(13)	1.1627(9)	1.2370(27)	1.2275(15)
1.0232(21)	1.0143(34)	1.0125(18)	1.0006(16)	0.9922(10)	0.9715(8)	1.0173(19)	1.0127(11)
0.8694(19)	0.8647(28)	0.8600(14)	0.8555(12)	0.8490(07)	0.8347(6)	0.8644(14)	0.8622(8)
0.7568(20)	0.7537(31)	0.7473(18)	0.7479(12)	0.7414(07)	0.7312(5)	0.7529(17)	0.7511(9)

Table 6.2: Values of $\bar{g}^(a/L, -1)$ for $s = -1$ corresponding to a fixed $\bar{g}^2(a/L, 1) = u_1$.

In figure 6.4, we present a plot of the results. In it, the data after the perturbative effects subtraction have also been included. We will shortly discuss this issue. From the data it cannot be concluded that the dominant lattice artifacts are quadratic in the lattice spacing, since some of the continuum extrapolations are 4-5 sigmas away from the expected values. Actually, some tests were done including a linear term in the fitting as well as a quadratic term leading to satisfactory results. Nevertheless, it

Fixed $\bar{g}^2$	L/a					Extrapolation	
u	16	12	8	6	4	5 points	4 points
4.734(87)	4.77(12)	5.15(14)	6.36(19)	9.77(27)	−32.2(9.6)	3.88(12)	3.91(12)
3.843(38)	3.968(57)	4.159(64)	4.64(52)	5.769(52)	15.8(1.4)	3.607(51)	3.586(51)
3.265(25)	3.407(36)	3.506(33)	3.733(22)	4.257(20)	6.96(15)	3.219(27)	3.148(26)
2.693(19)	2.823(24)	2.859(17)	2.956(13)	3.182(10)	4.092(21)	2.7356(16)	2.636(12)
2.211(13)	2.310(17)	2.314(10)	2.3673(70)	2.4717(54)	2.8311(50)	2.2587(97)	2.2203(59)
1.7668(74)	1.828(11)	1.8211(60)	1.8607(45)	1.9104(32)	2.0529(25)	1.7980(59)	1.7970(35)
1.4094(48)	1.4410(67)	1.4353(35)	1.4659(30)	1.4912(20)	1.5555(15)	1.4238(36)	1.4322(22)
1.2284(40)	1.2477(52)	1.2451(27)	1.2685(21)	1.2852(14)	1.3275(11)	1.2377(27)	1.2454(16)
1.0143(27)	1.0232(34)	1.0251(18)	1.0379(17)	1.0474(10)	1.0725(08)	1.0196(19)	1.0238(12)
0.8647(20)	0.8694(28)	0.8741(14)	0.8790(12)	0.8860(08)	0.9026(06)	0.8694(15)	0.8711(09)
0.7537(24)	0.7568(31)	0.7632(17)	0.7629(12)	0.7696(07)	0.7810(05)	0.7577(16)	0.7592(09)

Table 6.3: Values of $\bar{g}^(a/L,1)$ for $s=1$ corresponding to a fixed $\bar{g}^2(a/L,-1)=u_{-1}$.

has to be noted that if we only include a coefficient monitoring the lattice artifacts, the quadratic term leads to the best continuum limit extrapolations. The fact that the two renormalised couplings coincide in the continuum limit can be regarded as a check of universality, since the two possible values of s define two different regularisations. However, the lattice artifacts are considerably large. Two remarks are to be mentioned,

- The results including the data corresponding to lattices with $L/a=4$ are, specially for large couplings, less reliable. Actually, they will not be considererd when we evaluate the step scaling function. In particular, lattices of volume $4^3\times 3$ are too small for us to rely on the results they might provide.

- The results involving large values of the coupling (non-perturbative regime) show bigger lattice artifacts. In addition, we can see that for the largest coupling when the renormalisation prescription is taken in $s=-1$, the results obtained are completely misleading.

Cancellation of the perturbative effects

Since the O(a) improvement has been implemented in the simulations, we expect that in the weak coupling domain, the relation between the renormalised and the bare coupling reads,

$$\bar{g}_s^2 = g_0^2 + m_1^{s'} g_0^4 + \mathrm{O}(g_0^6), \quad m_1^{s'} = m_1^s - (a/L)(r_{0,1}^s + N_f r_{1,1}^s). \tag{6.3.5}$$

In the perturbative regime, we thus have, if $u_s(a/L)=\bar{g}_s^2(a/L)$,

$$u_s(a/L) = u_{s'}(a/L) + u_{s'}^2(a/L)(m_1^s(L/a) - m_1^{s'}(L/a)) + \mathrm{O}(u^3). \tag{6.3.6}$$

So, the quantity,

$$u_s^{(1)}(a/L) = \frac{u_s}{1+(m_1^s(L/a)-m_1^{s'}(L/a))u_{s'}}, \tag{6.3.7}$$

will have no one loop perturbative lattice artifacts. We have constructed this quantity, so that we can evaluate whether the lattice artifacts are renderred smaller. In table

6.4 we present, for the two renormalisation prescriptions available, the continnum extrapolation of the renormalised couplings with regularised with the opposite value of s, fitting 4 and 5 points respectively. We include the values $u_{s'}$ taken to fix the physics in the system.

u_1	4 points	5 points	u_{-1}	4 points	5 points
4.772(77)	4.743(83)	4.320(46)	4.734(87)	3.92(12)	3.95(12)
3.968(41)	3.890(40)	3.706(23)	3.843(38)	3.620(51)	3.599(50)
3.407(25)	3.319(24)	3.240(14)	3.265(25)	3.223(27)	3.153(26)
2.823(16)	2.740(15)	2.7187(89)	2.693(19)	2.736(16)	2.639(11)
2.310(11)	2.2494(95)	2.2426(54)	2.211(13)	2.2577(96)	2.2180(58)
1.8283(76)	1.7931(59)	1.7853(34)	1.7668(74)	1.7972(59)	1.7934(35)
1.4410(47)	1.4249(37)	1.4161(22)	1.4094(48)	1.4232(36)	1.4295(22)
1.2477(33)	1.2377(27)	1.2306(16)	1.2284(40)	1.2372(27)	1.2431(16)
1.0232(21)	1.0178(19)	1.0146(11)	1.0143(27)	1.0192(19)	1.0222(11)
0.8694(19)	0.8647(15)	0.8636(9)	0.8647(20)	0.8691(15)	0.8699(9)
0.7568(20)	0.7531(17)	0.7522(9)	0.7537(24)	0.7575(16)	0.7581(9)

Table 6.4: Continuum limit of $u_s^{(1)}(a/L)$ (1-loop perturbative effects have been subtracted.)

In order to have a better insight of how the lattice artifacts are reduced after this subtraction has been implemented, in figure 6.4 we present four graphs showing the data before and after the subtraction has been implemented. On top, the physics has been fixed for $s = 1$ and in the ones below, it is for $s = -1$ that the renormalisation prescription was taken. The two couplings with largest values have been excluded from the plots. The fits exclude the $L/a = 4$ data in all cases.

From the results we can see that the lattice artifacts are effectively reduced but not significantly. Moreover, even though after subtracting the one loop effects, in principle we would expect linear lattice artifacts to be present, it seems like $\mathrm{O}(a^2)$ are dominant. If we perform a perturbative analysis, only the boundaries contribute linear lattice artifacts at two loop order.

6.3.3 Lattice step scaling function

Now, let us finally carry out the computation of the step scaling function. As we just checked, we expect to have non-negliglible lattice effects. The program to compute the step scaling function is the following,

i) Pick up a regularisation. The values of $\Sigma(u, 1/8) = \bar{g}^2(16a)$ are going to be given by the simulation data.

ii) Interpolate to compute $u = \bar{g}^2(L)$ at the same β values $\Sigma(u, 1/8)$ is given. Here, we can choose to compute the values of u using same regularisation the lattice step scaling function has been computed at or using the other regularisation. These values of the coupling constant fix the physics of the problem.

iii) We perform interpolations to obtain the values of β that lead to the same values of u for the lattices with $L/a = 4, 6$.

iv) We use these values of β to compute $\Sigma(u, a/L)$ for $L/a = 4, 6$.

We thus see there are two ways of computing the step scaling function per regularisation. We can compute it by fixing the physics with the same regularisation and with the other regularisation, since their continuum limit should be the same.

As it happened in the previous subsection for the observable $\bar{g}^2(L/a, s)$, the sources of errors of the step scaling function are both, statistical and systematic. Hence, analogously to the previous analysis,

$$\Delta\Sigma = \sqrt{(\Delta\Sigma^{\text{stat}})^2 + (\Delta\Sigma^{\text{sys}})^2} \tag{6.3.8}$$

The systematic error has been estimated by propagating the error from ui.e.,

$$\Delta\Sigma^{\text{sys}} = \frac{\partial\Sigma(u, a/L)}{\partial u}\Delta u \tag{6.3.9}$$

In the continuum limit and in the perturbative regime, we know that Eq. (6.1.17) holds. Then, we could assume,

$$\Sigma'(u, a/L) = \frac{\partial\Sigma(u, a/L)}{\partial u} \approx \frac{\partial\sigma(u)}{\partial u} \approx 1 + 2s_0u + 3s_1u^2 + 4s_2u^3. \tag{6.3.10}$$

This approximation is justified for the data under consideration through the following argument. For a given value of a/L, a fitting of $\Sigma(u, a/L)$ vs u was performed and thus, it was possible to compute $\Sigma'(u, a/L)$ and hence the systematic errors of the lattice step scaling function. The outcome obtained justified the use of the above formula. It is preferred to include the systematic errors using the perturbative relation rather than the results from the fittings in order not to increase the correlations between the data.

The step scaling function for the different lattice spacings are listed in tables 6.5, 6.6 for $s = 1$ and $s = -1$ fixing the physics, correspondingly. We will refer to the "NORMAL" data when the regularisation of Σ and u coincide and to the "CROSSED" data when they do not.

In order to obtain the evolution with energy, we will have to perform a continuum limit extrapolation. The results will be shown in the next section. We can see here already that the lattice artifacts are far from negligible. Nevertheless, the lattice effects for the "NORMAL" SSF's are considerably smaller than the ones for the "CROSSED" SSF's. That was to be expected, from the results obtained in the previous subsection.

6.3.4 Alternatives to the proposed data handling

Two different attempts to obtain the continuum limit of the step scaling function were performed. However, they led to less accurate results. Nevertheless, they are mentioned here for the sake of completeness.

	Normal			Crossed		
$u_{s=1}$	$\Sigma_1(u_1,4)$	$\Sigma_1(u_1,6)$	$\Sigma_1(u_1,8)$	$\Sigma_{-1}(u_1,4)$	$\Sigma_{-1}(u_1,6)$	$\Sigma_{-1}(u_1,8)$
3.555(16)	3.970(24)	4.553(59)	4.77(10)	3.425(90)	4.196(76)	4.73(16)
3.053(11)	3.401(14)	3.839(34)	3.968(52)	3.030(35)	3.559(38)	3.843(74)
2.6990(80)	2.999(11)	3.322(21)	3.407(32)	2.727(11)	3.102(22)	3.265(43)
2.3211(52)	2.5673(73)	2.768(11)	2.823(19)	2.3793(56)	2.613(13)	2.693(25)
1.9725(37)	2.1674(47)	2.2721(68)	2.310(13)	2.0382(36)	2.1733(89)	2.211(16)
1.6202(28)	1.7623(34)	1.8022(45)	1.8283(86)	1.6785(29)	1.7496(52)	1.7668(89)
1.3129(17)	1.4102(22)	1.4250(27)	1.4410(52)	1.3585(19)	1.3997(29)	1.4094(54)
1.1506(14)	1.2260(16)	1.2367(19)	1.2477(37)	1.1891(14)	1.2203(23)	1.2284(44)
0.9560(11)	1.0076(12)	1.0173(12)	1.0232(25)	0.9860(12)	1.0067(16)	1.0143(30)
0.8198(7)	0.8570(9)	0.8656(10)	0.8694(21)	0.8438(8)	0.8563(12)	0.8647(22)
0.7195(11)	0.7474(10)	0.7536(12)	0.7568(23)	0.7387(10)	0.7441(16)	0.7537(27)

Table 6.5: Lattice step scaling function Σ, for $s = 1$.

	Normal			Crossed		
$u_{s=-1}$	$\Sigma_{-1}(u_{-1},4)$	$\Sigma_{-1}(u_{-1},6)$	$\Sigma_{-1}(u_{-1},8)$	$\Sigma_1(u_{-1},4)$	$\Sigma_1(u_{-1},6)$	$\Sigma_1(u_{-1},8)$
3.141(11)	4.952(82)	4.74(12)	4.734(89)	6.86(24)	5.152(81)	4.772(86)
2.7686(82)	3.980(27)	3.884(52)	3.843(41)	4.876(60)	4.204(43)	3.968(47)
2.4878(61)	3.368(14)	3.314(26)	3.264(27)	3.885(22)	3.562(24)	3.407(29)
2.1712(41)	2.7726(91)	2.739(14)	2.693(20)	3.058(11)	2.911(12)	2.823(17)
1.8665(31)	2.2706(55)	2.2465(91)	2.211(14)	2.4377(63)	2.3542(67)	2.310(12)
1.5500(24)	1.8042(36)	1.7889(52)	1.7668(80)	1.9025(39)	1.8453(43)	1.8283(82)
1.2692(15)	1.4264(23)	1.4202(29)	1.4094(51)	1.4844(25)	1.4467(27)	1.4410(50)
1.1193(12)	1.2363(17)	1.2341(24)	1.2284(42)	1.2771(18)	1.2510(19)	1.2477(36)
0.9374(10)	1.0156(13)	1.0154(17)	1.0143(29)	1.0392(14)	1.0261(13)	1.0232(24)
0.8083(7)	0.8653(10)	0.8637(12)	0.8647(21)	0.8796(10)	0.8730(10)	0.8694(21)
0.7118(11)	0.7562(10)	0.7518(16)	0.7537(27)	0.7655(10)	0.7613(12)	0.7568(23)

Table 6.6: Lattice step scaling function Σ, for $s = -1$.

Global fit. Version I

A global fit analogous to the one proposed in [39] was performed. However, there are some technical difficulties that are present in our case, due to the fact that our data were not tuned to a constant physical line.

A global fit of this type is of the following form,

$$\Sigma(u, a/L) = \sigma(u)\rho u^n(a/L) \tag{6.3.11}$$

where n will be 2 if we do not subtract the one loop perturbative effects and 3 if we do so. Note that the slope ρ is the same for all data. Thus, we do not want our data for different u's to be correlated to each other. That implies that the interpolation of the data through the fittings provided before is not to be done. We performed local fittings correcting small mismatches by using,

$$\Sigma(u, a/L) = \Sigma(\tilde{u}, a/L) + \Sigma'(u, a/L) \times (u - \tilde{u}), \tag{6.3.12}$$

and taking the derivative to be the expression in Eq. (6.3.10). The results of the

extrapolated SSF, $\sigma(u)$ obtained by doing so were consistent with the ones presented in the following section. However, they were less accurate.

Global fit. Version II

In this global fit we propose to apply, all data are involved, and in principle, the outcome would be the functional relation between $\sigma(u)$ and u, that is, the results presented in figure 6.6.

The observables, $\Sigma(u, a/L)$ are functions of u, a/L. We will assume this functions to present a polynomial behaviour in both variables. In principle, there should be a logarithmic behaviour for the lattice spacing, but we are going to neglect that for the moment being. The expansion that can be performed is,

$$\Sigma(u, a/L) = \sum_{i=0}^{M_1} \sum_{j=0}^{M_2} b_i^j u^i (a/L)^j. \tag{6.3.13}$$

A multiple regression can be done, using all data available. Then, the relation between the continuum SSF, $\sigma(u)$ and the renormalised coupling, u is given through a polynomial with coefficients b_i^0. A global fitting routine has been written and it leads to sensible results. However, the dependence on the precise coefficients chosen to be fitted is high. Thus, the results are not stable enough to be relied on.

6.4 Results

It would be now desirable to extract the values of $\sigma(u)$, i.e., the continuum limit of the data above. To extract the continuum limit, i.e., the step scaling function,

$$\sigma(u) = \lim_{a/L \to 0} \Sigma(u, a/L),$$

there are various different ways we can proceed. Since we have cancelled the order $\mathrm{O}(a)$ effects up to one loop in perturbation theory, we expect the $\mathrm{O}(a)$ effects of the data above to be small. Therefore we can fit this data to,

$$\Sigma(u, a/L) = \sigma(u) + A(a/L)^2,$$

Before going on, let us introduce some notation regarding the two possible ways of computing $\Sigma(u, a/L)$ discussed above. $\Sigma_{s'}(u_s, a/L)$ will denote the step scaling function of the s' regularised data, for values of u obtained from the s regularisation. Correspondingly, we will denote the continuum limit extrapolation $\sigma_{s'}(u_s)$. Since both $\Sigma_{\pm 1}(u_s, a/L)$ are meant to have the same continuum limit, and the data are independent from one another, a combined fit using both data can be done in the following fashion,

$$\Sigma_1(u_s, a/L) = \sigma_{mixed}(u_s) + A_1(a/L)^2,$$
$$\Sigma_{-1}(u_s, a/L) = \sigma_{mixed}(u_s) + A_2(a/L)^2.$$

A χ^2 fit can be done to obtain $\sigma_{mixed}(u_s)$. We will perform the continuum extrapolation through a combined fit. If we do so, we can avoid using the data corresponding to the lattices $L/a = 4$.

We have already noted that the lattice artifacts are pretty large. Proceeding in the exact the same way we did in subsection 6.3.2. for the analysis of the lattice artifacts and cancel the one loop perturbative effects.

Close to the continuum limit, we expect the relative deviation of the lattice step scaling function $\delta(u, a/L)$ to be a pure lattice artifact,

$$\delta(u, a/L) = \frac{\Sigma(u, a/L) - \sigma(u)}{\sigma(u)} = \delta_1(a/L)u + \delta_2(a/L)u^2 + \mathrm{O}(u^3).$$

Since the action is $\mathrm{O}(a)$ improved, we expect,

$$\begin{aligned}
\delta_1(a/L) &\sim \left(d_{0,1} + d_{1,1} \ln \frac{a}{L}\right) \left(\frac{a}{L}\right)^2 + \ldots, \\
\delta_2(a/L) &\sim e_{0,2}\frac{a}{L} + \left(d_{0,2} + d_{1,2} \ln \frac{a}{L} + d_{2,2} \left(\ln \frac{a}{L}\right)^2\right) \left(\frac{a}{L}\right)^2 + \ldots
\end{aligned}$$

Now, expanding σ perturbatively, we obtain,

$$\delta_1^{s,s'}(a/L) = p_1(2L/a, s) - p_1(L/a, s') - s_0.$$

The coefficients $\delta_1(a/L)$ are collected in table 6.7.

L/a	$\delta_1^{1,1}(a/L)$	$\delta_1^{-1,1}(a/L)$	$\delta_1^{1,-1}(a/L)$	$\delta_1^{-1,-1}(a/L)$
4	-0.0139	-0.0215	0.0117	0.0041
6	-0.0079	-0.0114	0.0051	0.0016
8	-0.0050	-0.0070	0.0026	0.0005

Table 6.7: Discretisation error of the SSF.

We cancel the known perturbative cutoff effects by using,

$$\Sigma^{(1)}(u, a/L) = \frac{\Sigma(u, a/L)}{1 + \delta_1(a/L)u},$$

in the analysis of our data. The perturbative estimate of the relative cutoff effects is expected to behave as $(a/L) \times u^2$ close to the continuum limit. Now, we can analyse the data after having performed the subtraction. After having performed some tests, we concluded by inspection that the data were best described through a dependence on $(a/L)^2$. This result is not a wonder since we already encounter such a behaviour when pure lattice artifacts were analysed and we restricted ourselves to only one parameter monitoring the lattice effects. In table 6.8 we present the continuum limit extrapolation of the step scaling function for both regularisations after having performed a combined fitting, quadratic in (a/L) and including solely the points corresponding to the SSF for $L/a = 6, 8$ (i.e. the data with L/a have been neglected). Also, in Figure 6.5 we show the approach of the step scaling function $\Sigma^{(1)}(u, a/L)$ to the continuum limit.

s = 1		s = -1	
u	$\sigma(u)$	u	$\sigma(u)$
3.555(16)	5.19(21)	3.141(11)	4.49(17)
3.053(11)	4.18(11)	2.7686(82)	3.741(83)
2.6990(80)	3.5156(63)	2.4878(61)	3.212(50)
2.3211(52)	2.8672(36)	2.1712(41)	2.682(32)
1.9725(37)	2.3264(24)	1.8665(31)	2.219(22)
1.6202(28)	1.8313(15)	1.5500(24)	1.775(14)
1.3129(17)	1.4452(90)	1.2692(15)	1.4165(85)
1.1506(14)	1.2543(68)	1.1193(12)	1.2352(65)
0.9560(11)	1.0294(46)	0.9374(10)	1.0176(44)
0.8198(7)	0.8759(36)	0.8083(7)	0.8659(35)
0.7195(11)	0.7638(42)	0.7118(11)	0.7536(42)

Table 6.8: Continuum limit extrapolation of the step scaling function for the two given regularisations

We interpolate the data of table 6.8 by a polynomial in u. In figure 6.6 we present such interpolation, plotting $\sigma(u)/u$ vs u, together with the perturbative approximations to 1,2 and 3 loop in perturbation theory. Our fitting was a polynomial of dimension 6 where the first coefficients where set to the perturbative coefficients up to 2 loop in PT. The values corresponding to the largest coupling were not included in the fits. We can appreciate from the plot that, for small couplings, the results are in agreement with the ones obtained in PT. For large couplings we observe a deviation. It appears likely that higher orders would not improve the agreement at the largest order. It seems like we have reached a value of $\bar{g}^2$ where PT breaks down.

In the plot, we show the results obtained from the two different regularisations. They are correlated and thus they cannot be used simultaneously to fit the behaviour to a polynomial. However, the fact that their agreement encourages us to rely on the results obtained. The differences between the two can be regarded as systematic errors.

We use the parametrisation of the step scaling function to compute the Λ- parameter in lattice units. From $u_{\max}$, the recursive step $\sigma(\bar{g}^2(L/2)) = \bar{g}^2(L)$ is numerically solved to get a set of couplings u_i at scales $L_{\max}/2^i$. The insertion of these quantities into the equation for the Λ parameter, Eq. (6.1.9). From these considerations, we could obtain a result for the quantity $L_{\max}\Lambda$ parameter. $L_{\max}$ is going to be the scale at which $u_{\max} = 3.45$, since it is the one chosen in [42] so that we can compare it easily.

It would have been interesting to perform a comparative analysis with the results in [42] in this work. However, the work just cited appeared only shorlty before this dissertation had to be submitted.

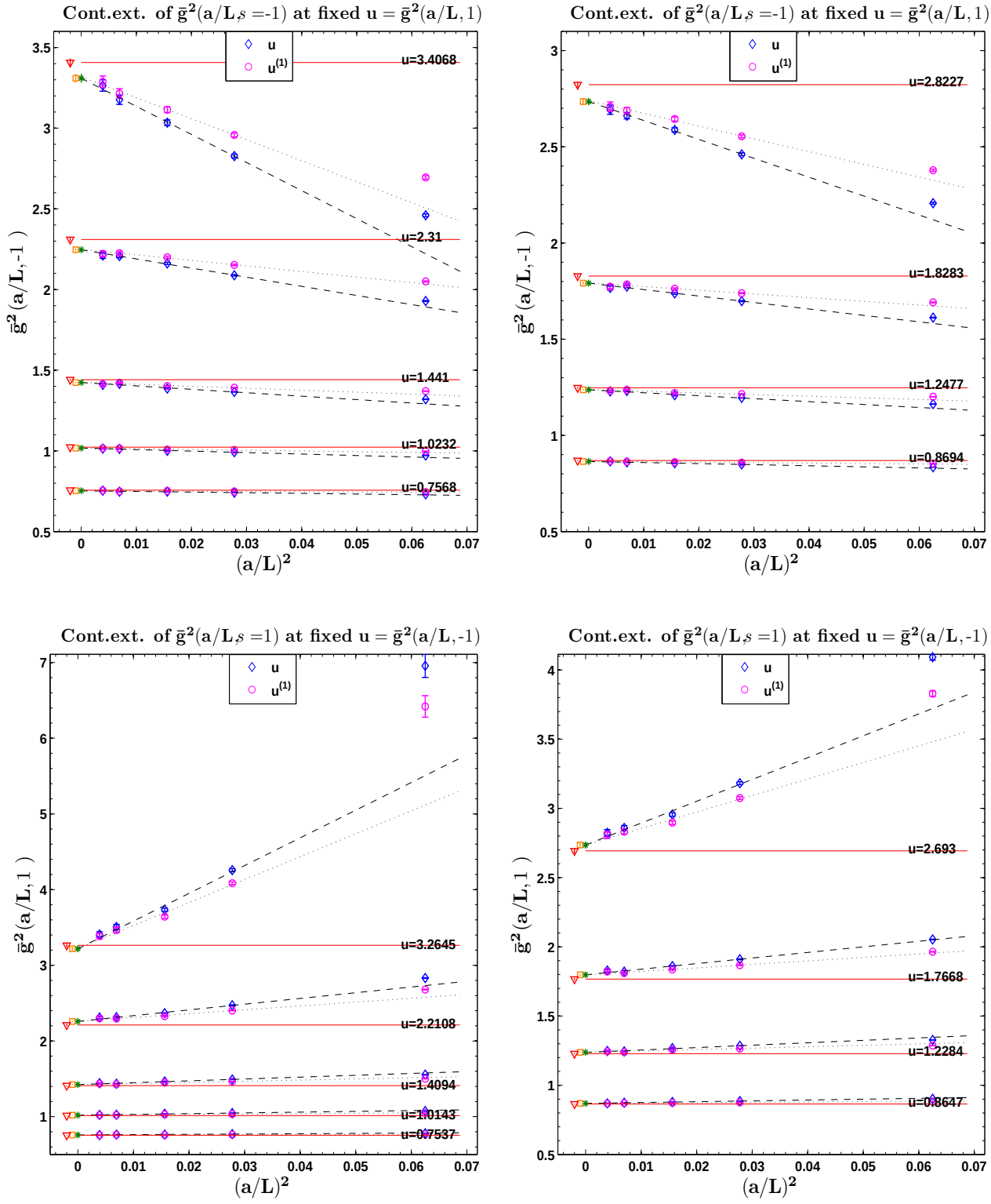

Figure 6.4: Analysis of the lattice artifacts of our system. Diamond (blue) points are the values of $\bar{g}^2(L/a)$. Dashed lines correspond to the fitting of these data and asterisks (green), the continuum extrapolation. Circles, (magenta) are the values for the same data after performing the perturbative subtraction, and the dotted lines their fittngs. Squares (orange) represent their continuum limit (displaced from the origin). The solid horizontal (red) lines are the lines of constant physics, given also by a (red) circle that is slightly displaced from the origin.

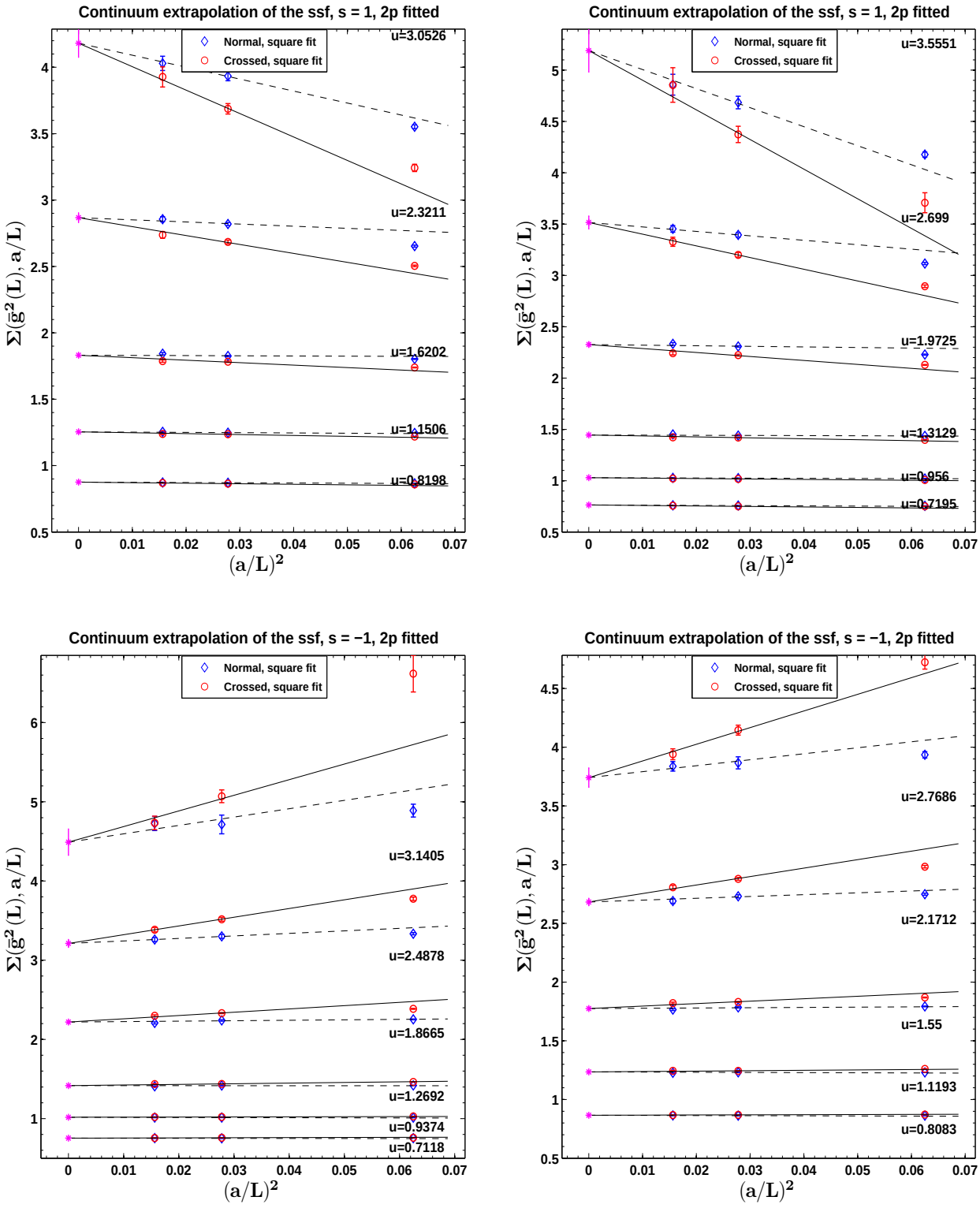

Figure 6.5: Continuum limit extrapolation of the step scaling function. Diamond (blue) points are the values of the "normal" lattice step scaling function and the solid lines represent the fittings. Circles (red) represent the "crossed" lattice step scaling function and the dashed lines their fittings. Asterisks (magenta) are the continuum extrapolations $\sigma(u)$ of the lattice step scaling function. The renormalisation prescriptions, (values of u) are explicitly given in the plots. The graphs on top correspond to the regularisation $s = 1$ and the ones underneath to $s = -1$.

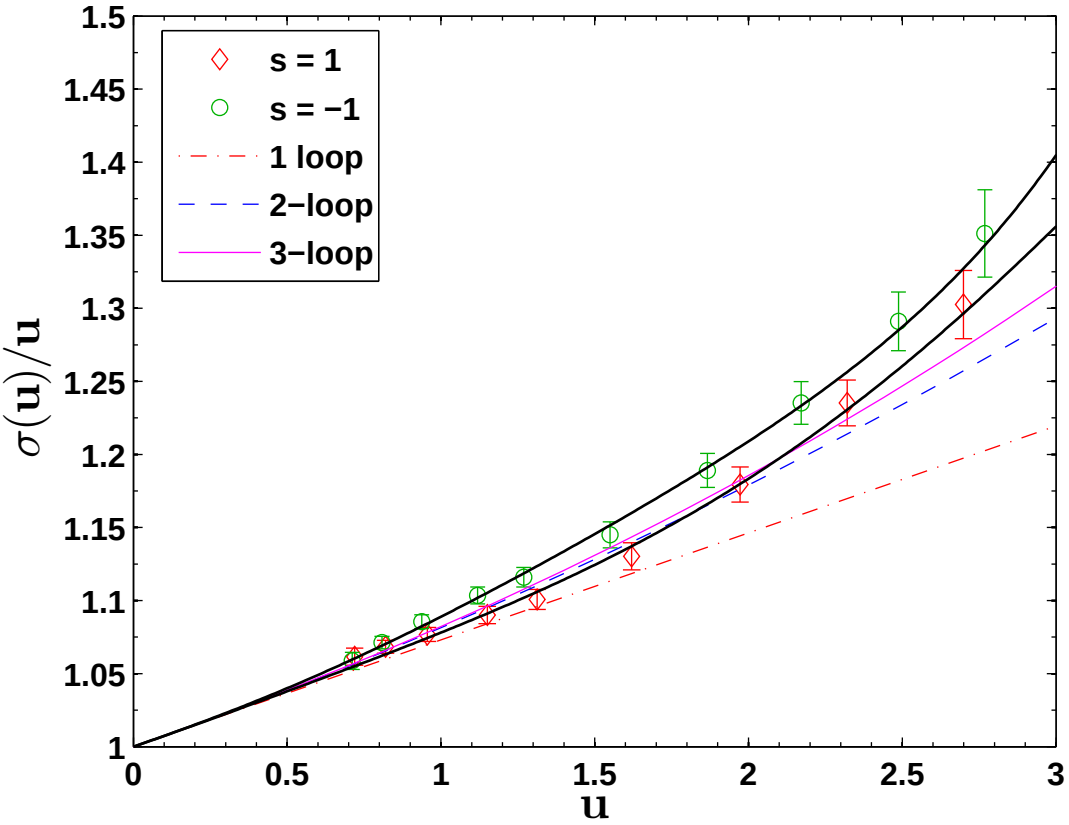

Figure 6.6: Step scaling function $\sigma(u)$. The dotted-dashed (red), dashed (blue) and solid (magenta) lines represent, correspondingly, the perturbative 1-loop, 2-loop and 3-loop $\sigma(u)$. Diamonds (red) represent the extrapolated $\sigma(u)$ from the $s = 1$ regularisation and circles (green) from the $s = -1$. Their fittings (excluding the largest value) are given by the dotted lines.

Chapter 7

Conclusions and outlook

In this work the evolution of the renormalised strong coupling constant with the scale has been performed for QCD with four flavours of quarks. The computations have been carried out in the framework of lattice field theories (the space time is discretised and our system is "put" on a lattice), since a non-perturbative analysis is required and QFT's on the lattice are possibly the best tool available at present time to perform calculations of this kind.

When attempting to evaluate the running of the renormalised coupling with the scale, large scale differences are to be faced. The formulation of the theory on the lattice is usually associated with computer simulations to perform the calculations. It is not surprising that accomodating large scale differences on a computer poses technical problems. A first naive look into the problem leads to the conclusion that it is impossible to address it in one single lattice since it would have to have $O(10^3)$ points, size untractable for the computers available at present time.

In order to overcome this problem, step scaling techniques [34] have been applied throughout this work. The key idea is to put the theory in a finite volume system, and to treat the size of the system as the scale of the theory $L \sim 1/\mu$. In this way, we go around the large scale differences by performing simulations on lattices with different volumes.

It is also required a clever and consistent definition of the renormalised coupling, $\bar{g}$. Such quantity must be a coupling (that is, it must coincide with the bare coupling g_0 to leading order in perturbation theory and has to remain finite when the continuum limit is taken), it should depend on the scale L and it should be easily calculated in computer simulations. To this end, the Schrödinger functional framework [35] was introduced. It can be defined as the propagation kernel of going from a field configuration at time $x_0 = 0$ to a different one at time $x_0 = T$. An convenient renormalised coupling can be defined within this set up, cf. section 2.4.

It is necessary to formulate the Schrödinger functional on the lattice. We refresh it is QCD with 4 flavours of quarks we are to examine. The lattice formulation of

a theory in the continuum is not unique. One has some freedom to play with as long as the continuum limit of the lattice regularisation leads to the desired theory in the continuum. In this work, we have chosen the gauge action to be the Wilson action and the fermions were taken to be staggered fermions[1]. Some discussions on the implementation of staggered fermions in the SF are available in the literature, [49, 50]. The main issue concerning these fermions when put in the SF is that it is impossible to set $L = T$, since $L/a = 0 \mod(2)$ and $T/a = 1 \mod(2)$. Hence, the best we can do is $L = T + sa$ with $s = \pm 1$. This fact introduces extra boundary lattice artifacts in our system, already at tree level in perturbation theory. In [50] this problem is overcome by averaging the two regularisations available, $s = \pm 1$. In our approach, we propose to keep them separated, and revisit the structure of the lattice artifacts present.

Before discussing the lattice artifacts is is worth mentioning that a prescription concerning the reconstruction of the staggered fermions [2] is needed in order to be able to interpret the results conveniently. The reconstruction is not unique. Two possible ways of doing it were explicitly derived throughout this work, cf. section 2.3.

The lattice artifacts of our system are of two types. On the one hand we have the usual artifacts coming from the volume. On the other hand there are extra lattice effects arising from the presence of boundaries in our system. We expect our lattice artifacts to be considerably large, because of two reasons: i) The impossibility of setting $T = L$ as we have already mentioned, introduces extra boundary artifacts already at three level, that were not present in the Wilson case. ii) Staggered fermions present large lattice artifacts in general, albeit not linear but quadratic, $\mathrm{O}(a^2)$. Symanzik developed a program to remove the lattice artifacts order by order in PT by adding appropriate counterterms to the theory. Chapters 3 and 4 are devoted to implement these ideas to our system at three level and one loop in perturbation theory. As a result, we managed to give prescriptions so that the $\mathrm{O}(a)$ lattice artifacts in the running coupling constant are cancelled up to one loop in PT. The outcome can be summarised here.

1. The pure gauge part only needed a counterterm at the boundary, monitored by the coefficient c_t, that allows an expansion in PT, $c_t = c_t^{(0)} + g_0^2 c_t^{(1)} + \mathrm{O}(g_0^4)$. $c_t^{(0)}$ was extracted and so was $c_t^{(1)}$. The latter has a pure gauge as well as a fermionic contribution (if fermions are present in the theory).
2. The statement that staggered fermions have no volume $\mathrm{O}(a)$ counterterms is subtle. The so called improved staggered fermions have to be introduced to that end. These fermions are "big" objects in the sense that they get contributions from different lattice sites, they are not ultralocal. However, using symmetry arguments and ideas from the formulation of fermions with a chiral twist, we

[1] Since it is 4 quarks one is dealing with, no rooting is needed and thus, there is no controversy in this respect.

[2] We refresh the reader that the formulation of a theory with fermions is somehow cumbersome since there is a NO-GO theorem, the Nielsen and Ninomiya theorem [59] that imposes some conditions, cf section 2.1. The staggered formulation involves the decomposition of the fermions in one dimensional Grassmann variables objects. These are the variables on the lattice formulation. However, they have to be reconstructed into standard spinors when the continuum limit is taken.

managed to argue that the improvement was only required in the time direction, cf. section 3.2.

3. The staggered fermions present O(a) boundary effects, that were cancelled by adding a counterterm monitored by the coefficient $d_{1s} = d_{1s}^{(0)} + g_0^2 d_{1s}^{(1)} + \mathrm{O}(g_0^4)$. Only the tree level coefficient is required for the one-loop improvement of $\bar{g}^2$.

Once the coefficients were determined, they could be implemented in the numerical simulations in order for the O(a) improvement to be achieved. To run our simulations, we have used a customised version of the MILC code. The customisation essentially involves the implementation of the Symanzik improvement and the introduction of a function to measure the observable $\bar{v}$, cf section 2.4, which is also easily computable.

Computer simulations have thus been run and the renormalised coupling $\bar{g}$ and the observable $\bar{v}$ were computed for a wide range of $\beta = 2N/g_0^2$ and L/a. With the results available, the so called step scaling function on the lattice, $\Sigma(u, a/L)$ and its continuum extrapolation $\sigma(u)$ could be computed, cf chapter 6. This object can be thought of as a discretised version of the Callan and Symanzik β function and is thus giving us information about the scaling properties of the coupling. Since there were two regularisations available, expected to present the same behaviour in the continuum, a combined fitting could be performed. The evolution of $\sigma(u)$ vs u was analysed and everything is ready for the Λ -parameter in units of $L_{\max}$ to be obtained. Some remarks about the results would be,

i The evolution of the step scaling function with the scale for small couplings was well described by perturbation theory. For large values of the coupling we encounter not such a case. cf. section 6.4.

ii The extrapolation to the continuum limit of the $\sigma(u)$ was performed in two ways, using the two regularisations available. The results cannot be treated as independent, since a combined fit was used for the extrapolation (cf. section 6.3, 6.4 for further details). It is nevertheless encouraging to see they agree within errors

iii Some attempts of performing global fits have been performed cf. section 6.3. The results were in all cases less accurate, but always consistent with the results presented here. Some effort is being put still to control these fittings.

iv From the results, we can conclude that the lattice artifacts due to the presence of staggered fermions are fairly large, as oposed to what happens when Wilson fermions are considered, [39, 42].

As we have stated several times, this work has been already carried out for Pure Yang Mills, [38], for two [39] and three [40] flavours of Wilson quarks. The case of four Wilson quarks is currently being addressed by a collaboration in Berlin and recently published in [42]. Comparing our results with theirs would constitute a check of universality.

As a final remark, let us mention that, concerning the O(a) improvement, a one loop calculation was required, and the coefficients $m_1(L/a)$ (cf. section 4.2, 4.3 and

appendix G for results) were extracted. For the pure gauge contribution, an independent calculation [68] led to the same results we present here. The coefficient $m_1(L/a)$ was also needed to establish the relation between the Λ- parameter in the SF scheme and the $\overline{\text{MS}}$ scheme. This is done through the coefficient $c_{1,1}$ presented in section 6.1.1. The results obtained agree with the ones obtained for Wilson fermions as they should provided universality is true.

Outlook

As it has already been pointed out in chapter 6, a connection with physical units is still lacking. This would be the primary step to be achieved in the near future, together with a better control of the continuum limit of the step scaling function. Although results were presented here, they are nevertheless preliminary and some further checks need to be accomplished together with a deeper inspection regarding the global fits in order to obtain more solid and controlled results. Once this is done, some further simulations need to be performed to provide results in physical units. This is done through a hadronic renormalisation scheme, cf. section 6.1.4.

Then, the results will be ready to be confronted with analogous results involving Wilson fermions, providing thus a check of universality.

The computation of the running of the renormalised coupling is the first necessary step if physical observables such as four quark operators, correlation functions are desired to be computed within this framework. Some effort was put to establish a definition of f_A, f_P, f_1, fermionic correlation functions related to the axial and vector currents and they were computed at tree level in PT in our framework. Computing them in the simulations would be desired.

Resumen en castellano

Introducción y motivación

La cromodinámica cuántica, (QCD), es la parte del Modelo Estándar, (SM) que se ocupa de las interacciones fuertes. Es una teoría de campos renormalizable[3]. A pesar de que no existe una prueba rigurosa de ello, en el presente se cree que esta teoría es capaz de describir las interacciones fuertes a todas las escalas.

Se trata de una teoría gauge no abeliana donde el grupo gauge es SU(3). Los quarks son las partículas fundamentales que sufren las interacciones fuertes, y vienen descritos por campos espinoriales que viven en la representación fundamental del grupo gauge, i.e., SU(3). Es importante mencionar que la estructura de los campos materia del Modelo Estándar se repite tres veces conformando tres familias o tres generaciones de campos. Cada familia incluye dos sabores de quarks. Los campos que median estas interacciones son los gluones, campos vectoriales sin masa que viven en el álgebra de la representación adjunta del SU(3). Hay, por tanto ocho campos gluónicos.

Aceptando que QCD es la teoría que describe las interacciones fuertes a todas las energías, se puede concluir el carácter altamente predictivo de la misma, dado que los únicos parámetros libres de la teoría son las masas de los quarks (6) y la constante de acoplo. Una vez que estos han sido fijados a una energía determinada, la teoría debería predecir todos los fenómenos que involucren exclusivamente las interacciones fuertes.

Las propiedades más destacables de QCD son,

a) *Libertad asintótica*: A altas energías, los quarks interaccionan débilmente. Este hecho permite que se pueda utilizar teoría de perturbaciones en este régimen.
b) *Confinamiento*: Los quarks no se han observado nunca aislados, así como tampoco los gluones. Se conjetura, aunque no hay una prueba rigurosa que avale esta afirmación, que el confinamiento de los quarks es una propiedad de QCD.

A altas energías, los resultados experimentales destinados a calcular la evolución de la constante de acoplo fuerte con la escala de energía[4] avalan los cálculos perturbativos,

[3]Esta afirmación no es cierta estrictamente en el sentido de que no existe una prueba matemática que garantice que QCD cumple los axiomas de Wightman [13].

[4]La constante de acoplo fuerte es una cantidad que evoluciona con al energía.

disponibles hasta cuatro lazos en PT. Estos resultados se muestran en [139].

A bajas energías, encontramos hadrones (partículas compuestas de estados de quarks ligados): mesones (spin 1) y bariones (spin 3/2). En este régimen, un análisis no perturbativo de la teoría es necesario puesto que la teoría de perturbaciones deja de ser aplicable. La formulación de la teoría en el retículo, introducida por K. Wilson en [22] en 1974 aborda el problema de un modo no-perturbativo. Esta teoría de campos en el retículo junto con simulaciones numéricas, [23], consigue predecir las propiedades básicas de partículas como los piones, kaones y nucleones. La idea básica consiste en la discretización del espacio-tiempo con paso reticular a. Los campos de materia "viven" en los puntos del retículo, mientras que los campos gauge, que van a ser elementos del grupo mismo [5], conectan dos puntos de la red. Algunos aspectos importantes de la construcción en el retículo serían,

- La simetría gauge queda preservada.
- Los detalles de la discretización dejan de ser relevantes en el límite al continuo.
- El retículo proporciona una regularización de las divergencias ultravioletas. Está bien definido matemáticamente.
- La construcción de estas teorías parten de teorías de campos en el $\mathbb{R}^4$ no en el espacio de Minkowski. Cuando se realiza la regularización en la red, la simetría O(4) espacio temporal se pierde, siendo reemplazada por una simetría discreta, el grupo cúbico en 4 dimensiones, con 24 elementos. Es de esperar que cuando se restaura el límite al continuo, la simetría del espacio-tiempo haga lo propio.

Así que, por un lado, tenemos la teoría a altas energías, que se puede describir razonablemente bien utilizando teoría de perturbaciones. Por otro lado, encontramos a bajas energías la física hadrónica, que se puede tratar desde un punto de vista teórico en el retículo. A primera vista, parece que estamos hablando de dos teorías distintas con dos dominios de aplicabilidad disjuntos. No obstante, hay argumentos para pensar que QCD es una teoría a todas las escalas. Por lo tanto, sería interesante establecer una conexión entre estos dos regímenes. **Este es el problema fundamental abordado en el presente trabajo**. Veamos qué se ha hecho exactamente y cómo se ha procedido.

El problema de conectar QCD a bajas energías con QCD a altas energías se puede abordar desde el marco de la teoría de campos en el retículo. Los parámetros de la teoría se fijan a bajas energías. Es decir, elegimos tantas cantidades como parámetros tenga nuestra teoría. El resto de propiedades de la teoría deberían entonces ser predicciones. Necesitamos una definición del acoplo renormalizado, $\bar{g}^2$ que sea no perturbativa. Una vez la tengamos, podemos evolucionar este acoplo desde bajas hasta altas energías. Simulaciones numéricas se pueden utilizar llevar a cabo este proyecto. Una vez que el acoplo se ha evolucionado hasta una escala perturbativa, se puede establecer la conexión con cualquier otro esquema de renormalización aplicable en este régimen.

[5] En la teoría en el continuo hemos remarcado que son campos que viven en el álgebra del grupo

Al intentar llevar a cabo el proyecto arriba mencionado, nos encontramos con que tenemos que lidiar con diferencias de energías bastante grandes. Este hecho supone un problema si queremos obtener resultados a partir de simulaciones numéricas. A día de hoy, y a pesar de que la potencia de las computadoras está en constante crecimiento, sería imposible llevar a cabo el cálculo propuesto en un único retículo, dado que el número de puntos del mismo por dimension espacio-temporal ascendería a órdenes de $O(10^3)$.

Concluimos que no se puede llevar a cabo el proyecto en un único retículo. Una solución fue ofrecida en [34], y el proyecto se ha llevado a cabo para Yang Mills SU(2), [36, 37], Yang Mills SU(3), [38], QCD con 2 [39], 3 [40] y 4 [42] sabores de quarks. Aquí presentamos **la evolución de la constante de acoplo con la energía para cuatro sabores de quarks**. A primera vista, parece el mismo proyecto que [42]. Sin embargo, se ha de tener en cuenta que los cálculos se han hecho utilizando regularizaciones diferentes para los fermiones. En [42] han utilizado los llamados "fermiones de Wilson" mientras que nosotros utilzamos los llamados "fermiones staggered". Además, los cálculos se han realizado aproximadamente simultáneamente sin transferencia de información, de manera que nuestros resultados no se han visto influenciados por los de ellos y viceversa.

La idea clave propuesta en [34] consiste en cubrir la diferencia de energías realizando simulaciones en una secuencia de retículos distintos de tamaño finito, caracterizados por la longitud de sus lados, L. La constante de acoplo renormalizada se introduce de manera que dependa del tamaño del retículo, que va a hacer las veces de escala de la teoría, $L \sim 1/\mu$.

Una vez que se define un acoplo renormalizado que depende del tamaño de la red, la estrategia para conectar el esquema hadrónico con el perturbativo consiste en,

i) Fijar la escala del retículo de mayor longitud física, $L = L_{\max}$. Realizar una simulación numérica para establecer el valor de $L_{\max}$ en unidades físicas (por ejemplo, $L \sim 0.5$ fm.) Computar $\bar{g}^2(L)$ a este volumen.

ii) Evolucionar la constante de acoplo no perturbativamente hacia energías más altas, o, correspondientemente, valores menores de L, (por ejemplo $L \sim 0.005$ fm).

iii) Asumiendo que se ha alcanzado el régimen perturbativo en el punto 2, la evolución del acoplo se puede continuar en el marco de teoría de perturbaciones.

iv) Establecer la conexión entre $\bar{g}^2(L)$ y un acoplo renormalizado definido perturbativamente.

Metodología, desarrollo y presentación del trabajo

El primer capítulo del trabajo aquí presentado comprende una introducción al tema, y el séptimo contiene las conclusiones y las expectativas de futuro. Demos pues, una breve descripción del contenido del resto de los capítulos.

Capítulo 2

En la introducción hemos mencionado la necesidad de introducir un acoplo definido no perturbativa, pero no se ha especificado cómo hacerlo. En [35] se concluye que es posible definir un acoplo altamente conveniente para los cálculos propuestos dentro del marco del llamado funcional de Schrödinger. El capítulo 2 empieza haciendo una breve descripción de la formulación de QCD en el retículo, dando detalles sobre cómo regularizar los fermiones tipo "staggered". Después se da una introducción al funcional de Schrödinger, describiendo en detalle cómo formularlo para QCD con cuatro sabores de fermiones staggered. La característica especial más relevante en esta discusión es que debido al hecho de haber elegido fermiones staggered para regularizar la teoría, la la longitud de la dimensión temporal tiene que tener un número par de puntos (lo que nos lleva a elegir T/a impar, puesto que empezamos en 0) y la espacial un número impar, (esto es, L/a par). Esto nos impide fijar $T = L$, como es costumbre en este tipo de sistemas. Terminamos el capítulo dando una definición no perturbativa del acoplo, y justificando por qué es una definición adecuada para el proyecto que se quiere llevar a cabo.

Capítulo 3 y 4

Describimos estos dos capítulos en conjunto, puesto que abordan el mismo problema. Debido a las limitaciones impuestas por la potencia limitada de las supercomputadoras utilizadas hoy en día para llevar a cabo las simulaciones numéricas necesarias para obtener resultados, muchas veces el paso reticular es considerablemente grande. Nuestros resultados finales involucran una extrapolación al límite en que $a \to 0$. Queremos hacer predicciones sobre la naturalezn; por tanto, es lógico que los resultados no dependan de la estructura del retículo. Para poder realizar esta extrapolación de la forma más segura posible, sería conveniente disminuir los efectos introducidos por la presencia de un retículo subyaciente lo más posible. Este es el objetivo de los capítulos 3 y 4, esencialmente.

Se va a implementar la llamada mejora a orden a, O(a) en nuestra teoría. El métdo utilizado se conoce con el nombre de mejora de Symanzik, pues fue introducido por Symanzik en [67]. En esencia, el método consiste en añadir contratérminos no relevantes a la teoría que cancelen los efectos de orden a, a^2, ... Estos contratérminos vienen monitorizados por unos coeficientes tuneables que tienen una expansión en teoría de perturbaciones. En el capítulo 3 se tunean los coeficientes necesarios para cancelar los efectos de O(a) a nivel árbol en teoría de perturbaciones,(PT), y en el capítulo 4 se hace el correspondiente análisis para tunear los coeficientes a un lazo en PT.

Capítulo 5

Una vez que el acoplo renormalizado se ha definido, y que se ha implementado la mejora de Symanzik hasta un lazo en PT, podemos empezar con las simulaciones. La primera parte del capítulo 5 está consagrado a describir el algoritmo utilizado en las mismas, que recibe el nombre de Monte Carlo híbrido (HMC).

El código utilizado para "correr" las simulaciones es una modificación particular de la versión del código público ofrecido por la colaboración MILC. En el capítulo que nos concierne se dan detalles sobre las modificaciones necesarias implementadas en el código para poder llevar a cabo nuestro proyecto, así como las pruebas que se han realizado para asegurarnos de que las modificaciones han sido implementadas de una manera correcta.

En la última parte de,l capítulo se recoge información sobre las simulaciones llevadas a cabo y sobre cómo se ha realizado el análisis.

Capítulo 6

En este capítulo se describen en detalle las técnicas de tamaño finito, y se aplican a nuestro problema. La clave para el cálculo de la evolución del acoplo mediante estas t'ecnicas es la utilización de la llamada "step scaling function" introducida en [34], que se puede pensar como una versión discretizada de la función β de las ecuaciones de Callan y Symanzik.

Al no poder fijar $T = L$, como se ha mencionado anteriormente, lo que se hace es $T = L \pm a$ dando lugar a dos regularizaciones distintas para nuestro sistema. Se espera que las dos regularizaciones compartan los resultados en el límite al continuo. Al disponer de dos regularizaciones, es posible realizar un análisis cuantitativo de los efectos del retículo en el sistema lo que se discute y se hace en este capítulo.

Finalmente se presentan los resultados en una gráfica donde se representa la "step scaling function" frente al acoplo renormalizado, lo cual nos da información sobre la evolución del mismo con la escala. Estos resultados son ya susceptibles de un análisis comparativo con los presentados en [42].

Conclusiones

En este trabajo se ha calculado la evolución de la constante de acoplo fuerte con la escala para QCD con cuatro sabores de quarks (staggered). Los cálculos se han realizado en el marco de la teoría de campos en el retículo. Esta formulación nos permite realizar simulaciones numéricas en un ordenador y obtener resultados de ellas.

Cuando se intenta realizar este cálculo utilizando simulaciones numéricas, aparece irremediablemente el problema técnico de la imposibilidad de abordar un problema que involucra vastas diferencias de energía con la potencia computacional de las máquinas de hoy en día. Como ya se ha dicho, se implementan las técnicas de volumen finito para superar esta dificultad, donde el tamaño del sistema juega el papel de escala del mismo. Para implementar estas técnicas se necesita una definición no perturbativa del acoplo. Esto se hace construyendo el funcional de Schrödinger y formulándolo en el retículo para el sistema bajo consideración. Además, la mejora de Symanzik se ha implementado para efectos de orden $\mathrm{O}(a)$ tuneando los coeficientes hasta un lazo en teoría de perturbaciones. Se han realizado simulaciones en supercomputadoras

para calcular la cosntante de acoplo renormalizada para distintos valores de $L/a = 4, 6, 8, 12, 16$, para las dos regularizaciones y para distintos valores del acoplo desnudo. Algunas conclusiones que se pueden esgrimir a la vista de los resultados son,

- La evolución del acoplo con la energía para acoplos pequeños viene descrita de un modo bastante preciso por teoría de perturbaciones. Para valores mayores del acoplo, esta afirmación deja de ser verdad. De hecho se observan desviaciones significativas con respecto al cálculo a 3 lazos de PT.
- La extrapolación al continuo de la "step scaling function", $\sigma(u)$ se calculó de dos modos distintos, utilizando las dos regularizaciones disponibles en nuestros resultados. Estas dos series de datos no se pueden combinar, puesto que están correlacionados entre sí. Sin embargo, es alentador que los resultados sean compatibles dentro del margen de error.
- El tratamiento de datos del sistema es tedioso y no único. Se han intentado varias alternativas que por ahora no han ofrecido resultados mejores que los presentados aquí y que necesitan ser mejor controladas. De todas formas, se ha de decir que los resultados obtenidos por otros métodos siempre eran compatibles con los ofrecidos aquí.
- Se puede concluir que los artefactos del retículo debidos a la presencia de fermiones staggered son bastante grandes, contrariamente a lo que ocurre cuando se consideran fermiones Wilson, como se puede ver en [42]
- Cuando comparamos la figura 6.6 con la figura 3 de [42] cualitativamente, vemos que parece que ambos resultados parecen compatibles.

Perspectivas de futuro

- Para empezar, nos gustaría tener el límite al contínuo de la "step scaling function" más controlado.
- Además, se importante controlar el valor de la cantidad $-\ln(L_{\max}\Lambda)$ con errores.

- Una vez que tengamos los puntos anteriores controlados, sería preciso correr las simulacioens necesarias para proporcionar unidades físicas a nuestro sistema.
- Además, sería interesante comparar los resultados con los presentados en [42]. Un resultado satisfactorio constituiría un chequeo de universalidad.
- El cómputo de la evolución de la constante de acoplo renormalizada es el primer paso necesario si se quiere llevar a cabo el cálculo de observables físicas, como operadores de cuarto quarks o funciones de correlación.

Appendix A

Notation

In this appendix, we will specify some notation and useful relations used throughout the work presented here. Lorentz indices $\mu, \nu, \ldots$ are taken from the Greek alphabet and run from 0 to 3. Latin indices $k, l, \ldots$ run from 1 to 3 and are used to label the components of the spatial vectors. Scalar products, such as $px = p_\mu x_\mu$ are always taken with euclidean metric.

A.1 Dirac matrices

A chiral representation is chosen for the Dirac matrices,

$$\gamma_\mu = \begin{pmatrix} 0 & e_\mu \\ e_\mu^\dagger & 0 \end{pmatrix}. \tag{A.1.1}$$

the 2×2 matrices e_μ are taken to be,

$$e_0 = -\mathbb{1}_{2\times 2}, \qquad e_k = -i\sigma_k \tag{A.1.2}$$

with σ_k the Pauli matrices. It is then easy to check that,

$$\gamma_\mu^\dagger = \gamma_\mu, \qquad \{\gamma_\mu, \gamma_\nu\} = 2\delta_{\mu\nu}. \tag{A.1.3}$$

If we define $\gamma_5 = \gamma_0\gamma_1\gamma_2\gamma_3$, we have,

$$\gamma_5 = \begin{pmatrix} 1 & 0 \\ 0 & -1 \end{pmatrix}. \tag{A.1.4}$$

A.2 Flavour structure

We clarify the notation of the flavour structure. The sixteen flavour matrices will be given by,

$$\left\{\mathbb{1}, \tau_\mu, \tau_5, \tau_{\mu 5}, \tau_{[\mu,\nu]}\right\}, \tag{A.2.1}$$

with,

$$\tau_\mu = \gamma_\mu^T, \quad \tau_{\mu 5} = i(\gamma_\mu \gamma_5)^T, \quad \tau_{[\mu,\nu]} = \frac{i}{2}\left[\gamma_\mu^T, \gamma_\nu^T\right] \tag{A.2.2}$$

They are all hermitian and satisfy unitarity and completeness relations,

$$\mathrm{tr}(\tau_i \tau_j) = 4\delta_{ij}, \quad \sum_i (\tau_i^\dagger)_{ab}(\tau_i)_{cd} = 4\delta_{ad}\delta_{bc} \tag{A.2.3}$$

A.3 Momenta on the lattice

If p is any lattice momentum, we set

$$\hat{p}_\mu = (2/\bar{a})\sin(\bar{a}p_\mu/2), \tag{A.3.1}$$
$$\mathring{p}_\mu = (1/\bar{a})\sin(\bar{a}p_\mu). \tag{A.3.2}$$

If we add the constant phase factor, then,

$$p_\mu^\pm = p_\mu \pm \frac{\theta_\mu}{L}. \tag{A.3.3}$$

For the spatial components, the notation,

$$\mathbf{p} = (p_1, p_2, p_3), \tag{A.3.4}$$

is employed. Similarly one defines $\hat{\mathbf{p}}$ and $\mathring{\mathbf{p}}$. We also use,

$$\hat{p}^2 = \sum_\mu \hat{p}_\mu \hat{p}_\mu, \qquad \mathring{p}^2 = \sum_\mu \mathring{p}_\mu \mathring{p}_\mu, \tag{A.3.5}$$

$$\hat{\mathbf{p}}^2 = \sum_k \hat{p}_k \hat{p}_k, \qquad \mathring{\mathbf{p}}^2 = \sum_k \mathring{p}_k \mathring{p}_k. \tag{A.3.6}$$

A.4 Completeness relations

Here, we list some of the properties of the spinors $u(\mathbf{q}, s_p, f)$ and $v(\mathbf{q}, s_p, f)$ where the index s_p stands for spin and f for flavour. Let $U(\mathbf{q}, s_p, f)$ and $V(\mathbf{q}, s_p, f)$ be some arbitrary spinors satisfying,

$$(1-\gamma_0)U(\mathbf{q}, s_p, f) = 0, \qquad U^\dagger(\mathbf{q}, s_1, f_1)U(\mathbf{q}, s_2, f_2) = \delta_{s_1 s_2}\delta_{f_1 f_2}, \tag{A.4.1}$$
$$(1+\gamma_0)V(\mathbf{q}, s_p, f) = 0, \qquad V^\dagger(\mathbf{q}, s_1, f_1)V(\mathbf{q}, s_2, f_2) = \delta s_1 s_2 \delta_{f_1 f_2}. \tag{A.4.2}$$

The completeness relations read,

$$\sum_{s_p, f} U(\mathbf{q}, s_p, f) \otimes U^\dagger(\mathbf{q}, s_p, f) + V(\mathbf{q}, s_p, f) \otimes V^\dagger(\mathbf{q}, s_p, f) = \mathbb{1}. \tag{A.4.3}$$

That leads to,

$$\sum_{s_p,f} U(\mathbf{q},s_p,f)\otimes U^{+}(\mathbf{q},s_p,f) = P_{+}, \tag{A.4.4}$$

$$\sum_{s_p,f} V(\mathbf{q},s_p,f)\otimes V^{+}(\mathbf{q},s_p,f) = P_{-}. \tag{A.4.5}$$

Now, as we have dealt with two propagators, for the cases $s=\pm 1$, we define, two operators that depend on s,

$$\tilde{A}_s = \sum_k i\gamma_k\gamma_0 \overset{\circ}{q}_k - i\frac{\bar{a}}{2}\gamma_5\gamma_0\tau_{k5}\hat{q}_k^2 - s\frac{\bar{a}}{2}\gamma_0\hat{q}_0^2 \tag{A.4.6}$$

$$\tilde{B}_s = \sum_k i\gamma_k\gamma_0 \overset{\circ}{q}_k + i\frac{\bar{a}}{2}\gamma_5\gamma_0\tau_{k5}\hat{q}_k^2 + s\frac{\bar{a}}{2}\gamma_0\hat{q}_0^2. \tag{A.4.7}$$

We now define,

$$u_s(\mathbf{q},s_p,f) = (i\overset{\circ}{q}_0 + \tilde{A}_s)\gamma_0 U(\mathbf{q},s_p,f) \tag{A.4.8}$$

$$v_s(\mathbf{q},s_p,f) = (i\overset{\circ}{q}_0 + \tilde{B}_s)\gamma_0 V(\mathbf{q},s_p,f). \tag{A.4.9}$$

From this equations, we can see that,

$$D_s^{SQ}u_s = 0 \qquad D_s^{SQ}v_s = 0 \tag{A.4.10}$$

The normalization is,

$$\bar{u}_s(\mathbf{q},s_1,f_1)u_s(\mathbf{q},s_2,f_2) = 2s\frac{\bar{a}}{2}\hat{q}_0^2\left(i\overset{\circ}{q}_0 + \frac{\bar{a}}{2}\hat{q}_0^2\right)\delta_{s_1s_2}\delta_{f_1f_2} \tag{A.4.11}$$

$$\bar{v}_s(\mathbf{q},s_1,f_1)v_s(\mathbf{q},s_2,f_2) = -2s\frac{\bar{a}}{2}\hat{q}_0^2\left(i\overset{\circ}{q}_0 + \frac{\bar{a}}{2}\hat{q}_0^2\right)\delta_{s_1s_2}\delta_{f_1f_2}, \tag{A.4.12}$$

with $\bar{\omega}=\omega^{\dagger}\gamma_0$. The completeness relations are,

$$\sum_{s_p,f} u_s(\mathbf{p}^{+},s_p,f)\otimes\bar{u}_s(\mathbf{p}^{+},s_p,f) = \left(i\overset{\circ}{p}_0^{+} + \frac{\bar{a}}{2}\hat{p}_0^{+2}\right)(i\overset{\circ}{p}_0^{+} + \tilde{A}_s)\gamma_0,$$

$$\sum_{s_p,f} v_s(\mathbf{p}^{+},s_p,f)\otimes\bar{v}_s(\mathbf{p}^{+},s_p,f) = \left(i\overset{\circ}{p}_0^{+} + i\frac{\bar{a}}{2}\hat{p}_0^{+2}\right)(i\overset{\circ}{p}_0^{+} + \tilde{B}_s)\gamma_0. \tag{A.4.13}$$

Appendix B

Symmetries of the staggered fermions

In this appendix, we review the symmetries of staggered fermions. We are going to write explicitly how the one component spinors, the four component spinors and the standard Schrödinger functional four component spinors transform under these symmetries. The Schrödinger functional four component spinors are related to the standard staggered four component spinors by $R(\alpha) = e^{i\frac{\alpha}{2}\gamma_5\tau_{05}}$,

$$\begin{aligned} \psi'(y) &= R(\pi/2)\psi(y) = \frac{1}{\sqrt{2}}(1 + i\gamma_5\tau_{05})\psi(y) \\ \bar{\psi}'(y) &= \bar{\psi}(y)R(\pi/2) = \bar{\psi}(y)\frac{1}{\sqrt{2}}(1 + i\gamma_5\tau_{05}), \end{aligned} \tag{B.0.1}$$

in the cases $s = -1, 1^-$. The transformation for the case $s = 1^+$ is $R(-\pi/2)$. In these notes, we will restrict ourselves to the case given above.

B.1 Chiral symmetry, $U(1)_\epsilon$

One component spinors

$$\chi(x) \to e^{i\beta\epsilon(x)}\chi(x), \qquad \bar{\chi}(x) \to \bar{\chi}(x)e^{i\beta\epsilon(x)}, \tag{B.1.1}$$

where $\epsilon(x) = (-1)^{x_0+x_1+x_2+x_3} = (-1)^{|x|}$.

Four component spinors

$$\psi(y) \to e^{i\beta\gamma_5\tau_5}\psi(y), \qquad \bar{\psi}(y) \to \bar{\psi}(y)e^{i\beta\gamma_5\tau_5}. \tag{B.1.2}$$

This chiral symmetry protects the zero-mass limit for staggered fermions, since the usual mass term is not invariant.

SF four component spinors

$$\begin{aligned}\psi'(y) &\rightarrow R(\pi/2)e^{i\beta\gamma_5\tau_5}R(-\pi/2)\psi'(y) = e^{i\beta\tau_0}\psi'(y),\\ \bar{\psi}'(y) &\rightarrow \bar{\psi}'(y)R(-\pi/2)e^{i\beta\gamma_5\tau_5}R(\pi/2) = \bar{\psi}'(y)e^{-i\beta\tau_0}.\end{aligned} \tag{B.1.3}$$

As we can see, the chiral symmetry has turned into a discrete flavour symmetry.

B.2 Reflections with respect to a hyperplane

Here, we consider reflections on hyperplanes through the centre of a hypercube.

One component spinors

$$\begin{aligned}\chi(x) &\rightarrow \eta_{I_H}((I_H^\rho)^{-1}x)\chi((I_H^\rho)^{-1}x),\\ \chi(x) &\rightarrow \bar{\chi}((I_H^\rho)^{-1}x)\eta_{I_H}((I_H^\rho)^{-1}x),\end{aligned} \tag{B.2.1}$$

with,

$$I_H^\rho : \begin{array}{l} x_\rho \rightarrow -x_\rho + a,\\ x_\mu \rightarrow x_\mu \quad \text{for } \mu \neq \rho.\end{array} \tag{B.2.2}$$

and $\eta_{I_H} = (-1)^{x_\rho + \cdots + x_3}$.

Four component spinors

$$I_H^\rho : \begin{array}{l} y_\rho \rightarrow -y_\rho,\\ y_\mu \rightarrow y_\mu \quad \text{for } \mu \neq \rho,\end{array} \tag{B.2.3}$$

and the fields $\psi, \bar{\psi}$ transform as,

$$\begin{aligned}\psi(y) &\rightarrow \gamma_\rho\gamma_5\tau_5\psi((I_H^\rho)^{-1}y),\\ \bar{\psi}(y) &\rightarrow \bar{\psi}((I_H^\rho)^{-1}y)\gamma_5\gamma_\rho\tau_5.\end{aligned} \tag{B.2.4}$$

Combining 3 reflexions, one orthogonal to each spatial direction, gives the parity transformation,

$$P : \begin{array}{l} \mathbf{y} \rightarrow -\mathbf{y},\\ y_0 \rightarrow y_0,\end{array} \tag{B.2.5}$$

with,

$$\begin{aligned}\psi(y) &\rightarrow \gamma_0\tau_5\psi(Py),\\ \bar{\psi}(y) &\rightarrow \bar{\psi}(Py)\gamma_0\tau_5.\end{aligned} \tag{B.2.6}$$

SF four component spinors In this case, the transformation remains the same,

$$\begin{aligned}\psi'(y) &\rightarrow \gamma_\rho\gamma_5\tau_5\psi'((I_H^\rho)^{-1}y),\\ \bar{\psi}'(y) &\rightarrow \bar{\psi}'((I_H^\rho)^{-1}y)\gamma_5\gamma_\rho\tau_5,\end{aligned} \tag{B.2.7}$$

and the transformation I_H^ρ acting on the space-time variables is also the same. The parity transformation is given by the same expression as well, that is,

$$\begin{aligned}\psi'(y) &\rightarrow \gamma_0\tau_5\psi'(Py),\\ \bar{\psi}'(y) &\rightarrow \bar{\psi}'(Py)\gamma_0\tau_5,\end{aligned} \tag{B.2.8}$$

with P being the transformation given in Eq. (B.2.5).

B.3 Rotations by $\pi/2$ around the centre of an hyperplane

Here, we consider rotations around the centre of a hypercube ($\rho < \sigma$)

One component spinors

$$\begin{aligned} \chi(x) &\rightarrow \eta_{R_H}((R_H^{(\rho\sigma)})^{-1}x)\chi((R_H^{(\rho\sigma)})^{-1}x), \\ \bar{\chi}(x) &\rightarrow \bar{\chi}((R_H^{(\rho\sigma)})^{-1}x)\eta_{R_H}((R_H^{(\sigma\rho)})^{-1}x), \end{aligned} \tag{B.3.1}$$

with,

$$R_H^{(\rho\sigma)} : \begin{array}{l} x_\rho \rightarrow x_\sigma, \\ x_\sigma \rightarrow -x_\rho + a, \\ x_\mu \rightarrow x_\mu \quad \text{for } \mu \neq \rho, \sigma. \end{array} , \tag{B.3.2}$$

and,

$$\eta_{R_H}(x) = \frac{1}{2}\left(1 + \eta_\rho(x)\eta_\sigma(x) - \zeta_\rho(x)\zeta_\sigma(x) + \eta_\rho(x)\eta_\sigma(x)\zeta_\rho(x)\zeta_\sigma(x)\right), \tag{B.3.3}$$

with $\zeta_\mu(x) = (-1)^{x_{\mu+1}+\cdots+x_3}$.

Four component spinors

$$R_H^{(\rho\sigma)} : \begin{array}{l} y_\rho \rightarrow y_\sigma, \\ y_\sigma \rightarrow -y_\rho, \\ y_\mu \rightarrow y_\mu \quad \text{for } \mu \neq \rho, \sigma. \end{array} , \tag{B.3.4}$$

and the fields $\psi, \bar{\psi}$ transform as,

$$\begin{aligned} \psi(y) &\rightarrow \frac{1}{2}(1 + \gamma_\rho\gamma_\sigma)(\tau_\sigma - \tau_\rho)\psi((R_H^{(\rho\sigma)})^{-1}y), \\ \bar{\psi}(y) &\rightarrow \bar{\psi}((R_H^{(\rho\sigma)})^{-1}y)\frac{1}{2}(1 - \gamma_\rho\gamma_\sigma)(\tau_\sigma - \tau_\rho). \end{aligned} \tag{B.3.5}$$

SF four component spinors In the Schrödinger functional, we have no rotation symmetry involving the temporal axes, we can restrict ourselves to the case in which k, l are both spatial indices. Being that the case, the transformation in the SF four component spinors is the same as in the previous case, that is,

$$\begin{aligned} \psi'(y) &\rightarrow \frac{1}{2}(1 + \gamma_k\gamma_l)(\tau_k - \tau_l)\psi'((R_H^{(kl)})^{-1}y), \\ \bar{\psi}'(y) &\rightarrow \bar{\psi}'((R_H^{(kl)})^{-1}y)\frac{1}{2}(1 - \gamma_k\gamma_l)(\tau_k - \tau_l), \end{aligned} \tag{B.3.6}$$

with $R_H^{(kl)}$ the one defined in Eq. (B.3.2)

B.4 Translations by one lattice unit

One component spinors

$$\begin{aligned}\chi(x) &\rightarrow \eta_{T_\rho}((T_\rho^{-1}x)\chi(T_\rho^{-1}x),\\ \bar{\chi}(x) &\rightarrow \bar{\chi}(T_\rho^{-1}x)\eta_{T_\rho}(T_\rho^{-1}x),\end{aligned} \tag{B.4.1}$$

with,

$$T_\rho : \begin{array}{l} x_\rho \rightarrow x_\rho + a,\\ x_\mu \rightarrow x_\mu \quad \text{for } \mu \neq \rho,\end{array}$$

and $\eta_{T_\rho}(x) = \zeta_\rho(x)$.

Four component spinors

$$\begin{aligned}\psi(y) &\rightarrow \tau_\rho\psi(y) + \bar{a}\tau_\rho Q_+^{(\rho)}\partial_\rho\psi(y),\\ \bar{\psi}(y) &\rightarrow \bar{\psi}(y)\tau_\rho + \bar{a}\bar{\psi}(y)\overleftarrow{\partial}_\rho Q_+^{(\rho)}\tau_\rho,\end{aligned} \tag{B.4.2}$$

with,

$$Q_\pm^{(\rho)} = \frac{1}{2}(1 \pm i\gamma_\rho\gamma_5\tau_{\rho 5}), \tag{B.4.3}$$

and,

$$\begin{aligned}\partial_\mu f(y) &= \frac{1}{\bar{a}}\left[f(y+\bar{a}\hat{\mu}) - f(y)\right],\\ \partial_\mu f(y) &= \frac{1}{\bar{a}}\left[f(y) - f(y-\bar{a}\hat{\mu})\right].\end{aligned} \tag{B.4.4}$$

SF four component spinors As it happened with the rotations, there is no shift symmetry in the time axis in the Schrödinger functional framework. Therefore, we assume the translations to be in the spatial directions (labelled by k) and we can see that the transformation remains the same,

$$\begin{aligned}\psi'(y) &\rightarrow \tau_k\psi'(y) + \bar{a}\tau_k Q_+^{(k)}\partial_k\psi'(y),\\ \bar{\psi}'(y) &\rightarrow \bar{\psi}'(y)\tau_k + \bar{a}\bar{\psi}'(y)\overleftarrow{\partial}_k Q_+^{(k)}\tau_k,\end{aligned} \tag{B.4.5}$$

with $Q_\pm^{(k)}$ as the ones defined in Eq. (B.4.3).

B.5 $U(1)$ invariance

One component spinors

$$\chi(x) \rightarrow e^{i\alpha}\chi(x), \qquad \bar{\chi}(x) \rightarrow e^{-i\alpha}\bar{\chi}(x). \tag{B.5.1}$$

Four component spinors

$$\psi(y) \rightarrow e^{i\alpha}\psi(y), \qquad \bar{\psi}(y) \rightarrow \bar{\psi}(y)e^{-i\alpha}. \tag{B.5.2}$$

SF four component spinors

$$\psi'(y) \rightarrow e^{i\alpha}\psi'(y), \qquad \bar{\psi}'(y) \rightarrow \bar{\psi}'(y)e^{-i\alpha}. \tag{B.5.3}$$

B.6 Interchange symmetry. (Charge conjugation symmetry)

One component spinors

$$\chi(x) \to \epsilon(x)\bar{\chi}^T(x), \qquad \bar{\chi}(x) \to -\chi^T(x)\epsilon(x), \tag{B.6.1}$$

where T stands for transpose (as a colour vector) and $\epsilon(x)$ was given before in this appendix.

Four component spinors

$$\psi(y) \to \mathcal{C}\bar{\psi}^T(y), \quad \bar{\psi}(y) \to -\psi^T(y)\mathcal{C}. \tag{B.6.2}$$

Here $\mathcal{C} = C_s(C_f^{-1})^T$, where s, f stand for spin and flavour spaces respectively and C is the usual Euclidean charge conjugating symmetry matrix satisfying,

$$\begin{aligned} C\gamma_\mu C^{-1} &= -\gamma_\mu^T, \\ C\gamma_5 C^{-1} &= \gamma_5^T, \\ C\gamma_5\gamma_\mu C^{-1} &= (\gamma_5\gamma_\mu)^T, \\ C = C^T &= C^{-1} = C^\dagger. \end{aligned} \tag{B.6.3}$$

The interchange symmetry for the one component fields becomes a charge conjugation symmetry in the reconstructed fermions.

SF four component spinors The charge conjugation symmetry remains exactly the same.

Appendix C

Derivation of the SF action in terms of the reconstructed fermions

We derive the expression of the SF action in terms of the reconstructed fermions starting from the one as a function of the one component Grassmann variables, (2.3.7, 2.3.11). Three different reconstructions are going to be explicitly specified corresponding to the three sketches in subsection 2.3.2.

The reconstruction is going to be carried out in two steps. Firstly, he action will be expressed in terms of the intermediate fields, $\chi_\xi(y)$ and $\bar{\chi}_\xi(y)$, which have sixteen components,

$$\begin{aligned} \chi_\xi(y) &= \chi(x), \\ \bar{\chi}_\xi(y) &= \bar{\chi}(x), \end{aligned} \tag{C.0.1}$$

and then we will relate them to the reconstructed fermions, $\psi, \bar{\psi}$. The notation for the discrete first and second derivatives are,

$$\begin{aligned} D_\mu f(y) &= \frac{1}{2\bar{a}} \left[(\lambda_\mu)^2 f(y + \bar{a}\hat{\mu}) - (\lambda_\mu^*)^2 f(y - \bar{a}\hat{\mu}) \right], \\ \Delta_\mu f(y) &= \frac{1}{\bar{a}^2} \left[(\lambda_\mu)^2 f(y + \bar{a}\hat{\mu}) + (\lambda_\mu^*)^2 f(y - \bar{a}\hat{\mu}) - 2f(y) \right], \end{aligned} \tag{C.0.2}$$

where $\bar{a} = 2a$, and y is related to x through Eq. (2.3.13).

C.1 Intermediate fields

In Eqs. (C.1.1,C.1.2,C.1.3), we write the action in terms of the intermediate fields. Eq. (C.1.1) refers to the case $s = -1$. Eq. (C.1.2) is the action corresponding to the reconstruction sketched in the left hand side of Figure 2.2. We will keep this notation throughout this appendix, to be consistent with section 2.3.2. We have denoted this action as $S_f^{(s=1^+)}$. The minus sign present in Eq. (C.1.2) is due to the relation between the variables y_0 and x_0 which, in this case is, $x_0 = 2y_0 - a + \xi$. Finally, Eq. (C.1.3)

refers to the reconstruction sketched in the right hand side of Figure 2.2. It has been denoted by $S_f^{(s=1^-)}$. First, we are going to introduce some notation,

The action in terms of $\chi_\xi(y), \bar{\chi}_\xi(y)$ for the three case takes the form,

$$\begin{aligned} S_f^{-1} &= \frac{\bar{a}^4}{16}\sum_{y_0=\bar{a}}^{T'-\bar{a}}\sum_{\mathbf{y}}\sum_{\xi,\xi'}\sum_{\mu}\bar{\chi}_\xi(y)\left\{(\Lambda_\mu)_{\xi\xi'}D_\mu\chi_{\xi'}(y)+\frac{\bar{a}}{2}(\Lambda_\mu^5)_{\xi\xi'}\Delta_\mu\right\}\chi_{\xi'}(y) \\ &\quad +S_{B,s=-1}^{(0)}+S_{B,s=-1}^{(T')}, \end{aligned} \tag{C.1.1}$$

$$\begin{aligned} S_f^{1^+} &= \frac{\bar{a}^4}{16}\sum_{y_0=\bar{a}}^{T'-\bar{a}}\sum_{\mathbf{y}}\sum_{\xi,\xi'}\bar{\chi}_\xi(y)\left\{(\Lambda_0)_{\xi\xi'}D_0\chi_{\xi'}(y)+\frac{\bar{a}}{2}(\Lambda_0^5)_{\xi\xi'}\Delta_0\right\}\chi_{\xi'}(y) \\ &\quad -\frac{\bar{a}^4}{16}\sum_{y_0=\bar{a}}^{T'-\bar{a}}\sum_{\mathbf{y}}\sum_{\xi,\xi'}\sum_{k}\bar{\chi}_\xi(y)\left\{(\Lambda_k)_{\xi\xi'}D_k\chi_{\xi'}(y)+\frac{\bar{a}}{2}(\Lambda_k^5)_{\xi\xi'}\Delta_k\right\}\chi_{\xi'}(y) \\ &\quad +S_{B,s=1^+}^{(0)}+S_{B,s=1^+}^{(T')}, \end{aligned} \tag{C.1.2}$$

$$\begin{aligned} S_f^{1^-} &= \frac{\bar{a}^4}{16}\sum_{y_0=\bar{a}}^{T'-\bar{a}}\sum_{\mathbf{y}}\sum_{\xi,\xi'}\bar{\chi}_\xi(y)\left\{(\Lambda_0)_{\xi\xi'}D_0\chi_{\xi'}(y)-\frac{\bar{a}}{2}(\Lambda_0^5)_{\xi\xi'}\Delta_0\right\}\chi_{\xi'}(y) \\ &\quad +\frac{\bar{a}^4}{16}\sum_{y_0=\bar{a}}^{T'-\bar{a}}\sum_{\mathbf{y}}\sum_{\xi,\xi'}\sum_{k}\bar{\chi}_\xi(y)\left\{(\Lambda_k)_{\xi\xi'}D_k\chi_{\xi'}(y)+\frac{\bar{a}}{2}(\Lambda_k^5)_{\xi\xi'}\Delta_k\right\}\chi_{\xi'}(y) \\ &\quad +S_{B,s=1^-}^{(0)}+S_{B,s=1^-}^{(T')}, \end{aligned} \tag{C.1.3}$$

where $S_{B,s}^{(0)}, S_{B,s}^{(T')}$ are the contributions from the boundaries. The matrices $\Lambda_\mu, \Lambda_\mu^5$ are,

$$\begin{aligned} (\Lambda_\mu)_{\xi\xi'} &= \eta_\mu(\xi)\bar{\delta}_{\xi+\hat{\mu},\xi'}, \\ (\Lambda_\mu^5)_{\xi\xi'} &= \eta_\mu(\xi)(-1)^{\xi'_\mu}\bar{\delta}_{\xi+\hat{\mu},\xi'}, \end{aligned} \tag{C.1.4}$$

where $\bar{\delta} = \delta \bmod 2$. It is also useful to introduce the operators $\tilde{Q}_\pm$, which will lead later to the projectors in the basis of the reconstructed fermionic fields,

$$\begin{aligned} \left(\tilde{Q}_+\right)_{\xi\xi'} &= \delta_{\xi\xi'}\delta_{\xi_0 0}, \\ \left(\tilde{Q}_-\right)_{\xi\xi'} &= \delta_{\xi\xi'}\delta_{\xi_0 1}. \end{aligned} \tag{C.1.5}$$

These matrices can be expressed in terms of the $\Lambda_\mu, \Lambda_\mu^5$ introduced in Eq. (C.1.4),

$$\tilde{Q}_\pm = \frac{1}{2}\Lambda_0\left(\Lambda_0 \pm \Lambda_0^5\right). \tag{C.1.6}$$

We are ready now to write the contributions of the action coming from the boundaries, in the three cases considered here,

1. Case $s=-1$

$$\begin{aligned} S^{(0)}_{B,-1} &= \frac{\bar a^4}{16}\sum_{\mathbf y}\sum_{\xi\xi'}\sum_k \bar\chi_\xi(0,\mathbf y)\left\{(\Lambda_k)_{\xi\xi'}D_k+\frac{\bar a}{2}(\Lambda^5_k)_{\xi\xi'}\Delta_k\right\}\chi_{\xi'}(0,\mathbf y)\\ &+ \frac{\bar a^3}{16}\sum_{\mathbf y}\sum_{\xi\xi'}\bar\chi_\xi(0,\mathbf y)(\tilde Q_-\Lambda_0)_{\xi\xi'}\chi_{\xi'}(\bar a,\mathbf y) \qquad \text{(C.1.7)}\\ &- \frac{\bar a^3}{16}\sum_{\mathbf y}\sum_{\xi\xi'}\bar\chi_\xi(0,\mathbf y)\left(\Lambda^5_0\right)_{\xi\xi'}\chi_{\xi'}(0,\mathbf y).\end{aligned}$$

$$\begin{aligned} S^{(T')}_{B,-1} &= \frac{\bar a^4}{16}\sum_{\mathbf y}\sum_{\xi\xi'}\sum_k \bar\chi_\xi(T',\mathbf y)\left\{(\Lambda_k)_{\xi\xi'}D_k+\frac{\bar a}{2}(\Lambda^5_k)_{\xi\xi'}\Delta_k\right\}\chi_{\xi'}(T',\mathbf y)\\ &- \frac{\bar a^3}{16}\sum_{\mathbf y}\sum_{\xi\xi'}\bar\chi_\xi(T',\mathbf y)(\tilde Q_+\Lambda_0)_{\xi\xi'}\chi_{\xi'}(T'-\bar a,\mathbf y) \qquad \text{(C.1.8)}\\ &- \frac{\bar a^3}{16}\sum_{\mathbf y}\sum_{\xi\xi'}\bar\chi_\xi(T',\mathbf y)\left(\Lambda^5_0\right)_{\xi\xi'}\chi_{\xi'}(T',\mathbf y).\end{aligned}$$

The fields at the boundaries being,

$$\begin{aligned} &\tilde Q_+\chi_\xi(0,\mathbf y)=\chi^{(0)}(\mathbf x), \qquad &&\tilde Q_-\chi_\xi(T',\mathbf y)=\chi^{(T)}(\mathbf x),\\ &\bar\chi_\xi(0,\mathbf y)\tilde Q_+=\bar\chi^{(0)}(\mathbf x), \qquad &&\bar\chi_\xi(T',\mathbf y)\tilde Q_-=\bar\chi^{(T)}(\mathbf x). \qquad \text{(C.1.9)}\end{aligned}$$

2. Case $s=1^+$

$$\begin{aligned} S^{(0)}_{B,1^+} &= -\frac{\bar a^4}{16}\sum_{\mathbf y}\sum_{\xi,\xi'}\sum_k \bar\chi_\xi(0,\mathbf y)\left\{(\tilde Q_-\Lambda_k)_{\xi\xi'}D_k+\frac{\bar a}{2}(\tilde Q_-\Lambda^5_k)_{\xi\xi'}\Delta_k\right\}\chi_{\xi'}(0,\mathbf y)\\ &+ \frac{\bar a^3}{16}\sum_{\mathbf y}\sum_{\xi\xi'}\bar\chi_\xi(0,\bar y)(\tilde Q_-\Lambda_0)_{\xi,\xi'}\chi_{\xi'}(\bar a,\mathbf y). \qquad \text{(C.1.10)}\\ S^{(T')}_{B,1^+} &= -\frac{\bar a^4}{16}\sum_{\mathbf y}\sum_{\xi\xi'}\sum_k \bar\chi_\xi(T',\mathbf y)\left\{(\tilde Q_+\Lambda_k)_{\xi\xi'}D_k+\frac{\bar a}{2}(\tilde Q_+\Lambda^5_k)_{\xi\xi'}\Delta_k\right\}\chi_{\xi'}(T',\mathbf y)\\ &- \frac{\bar a}{16}\sum_{\mathbf y}\sum_{\xi\xi'}\bar\chi_\xi(T',y)(\tilde Q_+\Lambda_0)_{\xi\xi'}\chi_{\xi'}(T'-\bar a,\mathbf y). \qquad \text{(C.1.11)}\end{aligned}$$

The fields at the boundaries are,

$$\begin{aligned} &\tilde Q_-\chi_\xi(0,\mathbf y)=\chi^{(0)}(\mathbf x), \qquad &&\tilde Q_+\chi_\xi(T',\mathbf y)=\chi^{(T)}(\mathbf x),\\ &\bar\chi_\xi(0,\mathbf y)\tilde Q_-=\bar\chi^{(0)}(\mathbf x), \qquad &&\bar\chi_\xi(T',\mathbf y)\tilde Q_+=\bar\chi^{(T)}(\mathbf x). \qquad \text{(C.1.12)}\end{aligned}$$

3. Case $s = 1^-$

$$S^{(0)}_{B,1^-} = \frac{\bar{a}^4}{16}\sum_{\mathbf{y}}\sum_{\xi,\xi'}\sum_{k}\bar{\chi}_\xi(0,\mathbf{y})\left\{(\tilde{Q}_+\Lambda_k)_{\xi\xi'}D_k + \frac{\bar{a}}{2}(\tilde{Q}_+\Lambda^5_k)_{\xi\xi'}\Delta_k\right\}\chi_{\xi'}(0,\mathbf{y}) + \frac{\bar{a}^3}{16}\sum_{\mathbf{y}}\sum_{\xi\xi'}\bar{\chi}_\xi(0,\bar{y})(\tilde{Q}_+\Lambda_0)_{\xi,\xi'}\chi_{\xi'}(\bar{a},\mathbf{y}). \quad \text{(C.1.13)}$$

$$S^{(T')}_{B,1^-} = \frac{\bar{a}^4}{16}\sum_{\mathbf{y}}\sum_{\xi\xi'}\sum_{k}\bar{\chi}_\xi(T',\mathbf{y})\left\{(\tilde{Q}_-\Lambda_k)_{\xi\xi'}D_k + \frac{\bar{a}}{2}(\tilde{Q}_-\Lambda^5_k)_{\xi\xi'}\Delta_k\right\}\chi_{\xi'}(T',\mathbf{y}) - \frac{\bar{a}^3}{16}\sum_{\mathbf{y}}\sum_{\xi\xi'}\bar{\chi}_\xi(T',y)(\tilde{Q}_-\Lambda_0)_{\xi\xi'}\chi_{\xi'}(T'-\bar{a},\mathbf{y}). \quad \text{(C.1.14)}$$

And the fields at the boundaries,

$$\begin{aligned}\tilde{Q}_+\chi_\xi(0,\mathbf{y}) &= \chi^{(0)}(\mathbf{x}), \qquad & \tilde{Q}_-\chi_\xi(T',\mathbf{y}) &= \chi^{(T)}(\mathbf{x}),\\ \bar{\chi}_\xi(0,\mathbf{y})\tilde{Q}_+ &= \bar{\chi}^{(0)}(\mathbf{x}), \qquad & \bar{\chi}_\xi(T',\mathbf{y})\tilde{Q}_- &= \bar{\chi}^{(T)}(\mathbf{x}).\end{aligned} \quad \text{(C.1.15)}$$

We can notice that in the first and the third cases, the boundary conditions are the same, whereas the projectors are exchanged in the second case.

C.2 Reconstructed fermions

Now, the transformation that links the variables $\bar{\chi}_\xi, \chi_\xi$ and the four component spinors, $\bar{\psi}, \psi$ has to be provided. In the cases given by, Eqs. (C.1.1,C.1.3), that is, $S_f^{(s=-1)}$ and $S_f^{(s=1^-)}$, the reconstruction takes the same form as the standard staggered reconstruction. So, using euclidean Dirac matrices, as specified in Appendix A.1 and defining the following matrices,

$$\Gamma_\xi = \frac{1}{2}\gamma_0^{\xi_0}\gamma_1^{\xi_1}\gamma_2^{\xi_2}\gamma_3^{\xi_3}, \quad \text{(C.2.1)}$$

that satisfy unitarity and completeness relations,

$$\begin{aligned}\sum_{\alpha a}(\Gamma^\dagger_\xi)_{a\alpha}(\Gamma_{\xi'})_{\alpha a} &= \mathrm{Tr}\left\{\Gamma^\dagger_\xi\Gamma_{\xi'}\right\} = \delta_{\xi\xi'},\\ \sum_{\xi}(\Gamma^\dagger_\xi)_{\alpha a}(\Gamma_\xi)_{b\beta} &= \delta_{ab}\delta_{\alpha\beta},\end{aligned} \quad \text{(C.2.2)}$$

we will be able to express $\Lambda_\mu, \Lambda^5_\mu$ as a trace of products of gamma matrices. Note here that the reason for introducing latin and greek indices is that, later on, in the four component spinors, the greek indices will be related to the spin indices and the latin ones to the flavour indices. Once Γ_ξ matrices have been introduced, we can express $\Lambda_\mu, \Lambda^5_\mu$ as,

$$\begin{aligned}(\Lambda_\mu)_{\xi\xi'} &= \mathrm{Tr}\left\{\Gamma^\dagger_\xi\gamma_\mu\Gamma_{\xi'}\right\},\\ (\Lambda^5_\mu)_{\xi\xi'} &= \mathrm{Tr}\left\{\Gamma^\dagger_\xi\gamma_5\Gamma_{\xi'}\gamma_5\gamma_\mu\right\}.\end{aligned} \quad \text{(C.2.3)}$$

If we note that,

$$\begin{aligned}\sum_{\xi,\xi'}(\Gamma_\xi)_{\alpha a}(\Lambda_\mu)_{\xi\xi'}(\Gamma^\dagger_{\xi'})_{b\beta} &= (\gamma_\mu)_{\alpha\beta}\otimes(\mathbb{1})^T_{ab} = (\gamma_\mu)_{\alpha\beta}\delta_{ab},\\ \sum_{\xi,\xi'}(\Gamma_\xi)_{\alpha a}(\Lambda^5_\mu)_{\xi\xi'}(\Gamma^\dagger_{\xi'})_{b\beta} &= (\gamma_5)_{\alpha\beta}\otimes(\gamma_5\gamma_\mu)^T_{ab} = i(\gamma_5)_{\alpha\beta}(\tau_{\mu 5})_{ab}.\end{aligned} \tag{C.2.4}$$

Latin indices denote flavour and greek indices denote spin. The notation of flavour matrices, denoted by τ_i is presented in Appendix A.2. These relationships suggest that the transformation that leads to four component spinors is,

$$\psi_{\alpha a}(y) = \frac{1}{4}\sum_\xi(\Gamma_\xi)_{\alpha a}\chi_\xi(y), \qquad \bar\psi_{a\alpha}(y) = \frac{1}{4}\sum_\xi\bar\chi_\xi(y)(\Gamma^\dagger_\xi)_{a\alpha}. \tag{C.2.5}$$

These relations can be inverted, leading to,

$$\chi_\xi(y) = 4\sum_{a\alpha}(\Gamma^\dagger_\xi)_{a\alpha}\psi_{\alpha a}(y), \qquad \bar\chi_\xi(y) = 4\sum_{a\alpha}\bar\psi_{a\alpha}(y)(\Gamma_\xi)_{a\alpha}. \tag{C.2.6}$$

Now, we are ready to express the actions of Eqs. (C.1.1, C.1.3), $S_f^{(s=-1)}$, $S_f^{(s=1^-)}$ in terms of the four component staggered fermions.

But, before we go on, let us give the transformation needed for the reconstruction of the four component spinors in the case of Eq. (C.1.2), i.e., $S_f^{1^+}$. If we have a look at this action, we can see that there is a relative minus sign between the temporal and the spatial terms that will later lead to the kinetic term. We have to reconstruct the four component fermions in such a way that the kinetic term has the usual form. We can note that if we choose,

$$\tilde\Gamma_\xi = \frac{1}{2}(-1)^{\xi_0}\gamma_0^{\xi_0}\gamma_1^{\xi_1}\gamma_2^{\xi_2}\gamma_3^{\xi_3}. \tag{C.2.7}$$

This matrices also satisfy unitarity and completeness relations,

$$\begin{aligned}\sum_{\alpha a}(\tilde\Gamma^\dagger_\xi)_{a\alpha}(\tilde\Gamma_{\xi'})_{\alpha a} &= \mathrm{Tr}\left\{\tilde\Gamma^\dagger_\xi\tilde\Gamma_{\xi'}\right\} = \delta_{\xi\xi'},\\ \sum_\xi(\tilde\Gamma^\dagger_\xi)_{a\alpha}(\tilde\Gamma_\xi)_{b\beta} &= \delta_{ab}\delta_{\alpha\beta}.\end{aligned} \tag{C.2.8}$$

If we note that,

$$\begin{aligned}\sum_{\xi,\xi'}(\tilde\Gamma_\xi)_{\alpha a}(\Lambda_0)_{\xi\xi'}(\tilde\Gamma^\dagger_{\xi'})_{b\beta} &= -(\gamma_0)_{\alpha\beta}\otimes(\mathbb{1})^T_{ab} = -(\gamma_0)_{\alpha\beta}\delta_{ab},\\ \sum_{\xi,\xi'}(\tilde\Gamma_\xi)_{\alpha a}(\Lambda_k)_{\xi\xi'}(\tilde\Gamma^\dagger_{\xi'})_{b\beta} &= (\gamma_k)_{\alpha\beta}\otimes(\mathbb{1})^T_{ab} = (\gamma_k)_{\alpha\beta}\delta_{ab},\\ \sum_{\xi,\xi'}(\Gamma_\xi)_{\alpha a}(\Lambda^5_0)_{\xi\xi'}(\Gamma^\dagger_{\xi'})_{b\beta} &= -(\gamma_5)_{\alpha\beta}\otimes(\gamma_5\gamma_0)^T_{ab} = -i(\gamma_5)_{\alpha\beta}(\tau_{05})_{ab},\\ \sum_{\xi,\xi'}(\Gamma_\xi)_{\alpha a}(\Lambda^5_k)_{\xi\xi'}(\Gamma^\dagger_{\xi'})_{b\beta} &= (\gamma_5)_{\alpha\beta}\otimes(\gamma_5\gamma_k)^T_{ab} = i(\gamma_5)_{\alpha\beta}(\tau_{k5})_{ab}.\end{aligned} \tag{C.2.9}$$

As in the former case, these relationships suggest that the transformation that leads to four component spinors is,

$$\psi_{\alpha a}(y) = \frac{1}{4}\sum_{\xi}(\tilde{\Gamma}_{\xi})_{\alpha a}\chi_{\xi}(y), \qquad \bar{\psi}_{a\alpha}(y) = -\frac{1}{4}\sum_{\xi}\bar{\chi}_{\xi}(y)(\tilde{\Gamma}^{\dagger}_{\xi})_{a\alpha}. \tag{C.2.10}$$

These relations can be inverted, leading to,

$$\chi_{\xi}(y) = 4\sum_{a\alpha}(\tilde{\Gamma}^{\dagger}_{\xi})_{a\alpha}\psi_{\alpha a}(y), \qquad \bar{\chi}_{\xi}(y) = -4\sum_{a\alpha}\bar{\psi}_{a\alpha}(y)(\tilde{\Gamma}_{\xi})_{a\alpha}. \tag{C.2.11}$$

The projectors will have the following form in all cases,

$$Q_{\pm} = \frac{1}{2}(1 \pm i\gamma_0\gamma_5\tau_{05}). \tag{C.2.12}$$

Having all the transformations under control, we can now express the actions S_f^s in terms of the four component spinors in all cases.

1. Case $s = -1$

$$S_f^{-1} = \bar{a}^4\sum_{y_0=\bar{a}}^{T'-\bar{a}}\sum_{\mathbf{y}}\sum_{\mu}\bar{\psi}(y)\left[\gamma_\mu D_\mu + i\frac{\bar{a}}{2}\gamma_5\tau_{\mu 5}\Delta_\mu\right]\psi(y) + S^{(0)}_{B,-1} + S^{(T')}_{B,-1}. \tag{C.2.13}$$

The contributions from the boundaries are,

$$\begin{aligned} S^{(0)}_{B,-1} &= \bar{a}^4\sum_{\mathbf{y}}\sum_{k=1}^{3}\bar{\psi}(0,\mathbf{y})\left[\gamma_k D_k + i\frac{\bar{a}}{2}\gamma_5\tau_{k5}\Delta_k\right]\psi(0,\mathbf{y}) \\ &\quad + \bar{a}^3\sum_{\mathbf{y}}\bar{\psi}(0,\mathbf{y})\left[Q_-\gamma_0\psi(\bar{a},\mathbf{y}) - i\gamma_5\tau_{05}\psi(0,\mathbf{y})\right], \qquad \text{(C.2.14)} \\ S^{(T')}_{B,-1} &= \bar{a}^4\sum_{\mathbf{y}}\sum_{k=1}^{3}\bar{\psi}(T',\mathbf{y})\left[\gamma_k D_k + i\frac{\bar{a}}{2}\gamma_5\tau_{k5}\Delta_k\right]\psi(T',\mathbf{y}) \\ &\quad - \bar{a}^3\sum_{\mathbf{y}}\bar{\psi}(T',\mathbf{y})\left[Q_+\gamma_0\psi(T'-\bar{a},\mathbf{y}) + i\gamma_5\tau_{05}\psi(T',\mathbf{y})\right]. \qquad \text{(C.2.15)} \end{aligned}$$

The projectors $Q_\pm$ project onto the boundary fields,

$$\begin{aligned} Q_+\psi(0,\mathbf{y}) &= \rho(\mathbf{y}), & Q_-\psi(T',\mathbf{y}) &= \rho'(\mathbf{y}), \\ \bar{\psi}(0,\mathbf{y})Q_+ &= \bar{\rho}(\mathbf{y}), & \bar{\psi}(T',\mathbf{y})Q_- &= \bar{\rho}'(\mathbf{y}). \end{aligned} \tag{C.2.16}$$

The boundary four component spinors ρ and ρ' are related to the boundary one component spinors $\chi^{(0)}(\mathbf{x}), \chi^{(T)}(\mathbf{x})$ as,

$$\rho^{\alpha a}(\mathbf{y}) = \frac{1}{4}\sum_{\boldsymbol{\xi}}R^{\alpha a}_{(\boldsymbol{\xi},0)}\chi^{(0)}_{\boldsymbol{\xi}}(\mathbf{y}), \quad \rho'^{a\alpha}(\mathbf{y}) = \frac{1}{4}\sum_{\boldsymbol{\xi}}R^{a\alpha}_{(\boldsymbol{\xi},1)}\chi^{(T)}_{\boldsymbol{\xi}}(\mathbf{y}), \tag{C.2.17}$$

and analogously for $\bar{\rho}, \bar{\rho}'$.

2. Case $s = 1^+$

$$S_f^{1^+} = \bar{a}^4 \sum_{y_0=\bar{a}}^{T'-\bar{a}} \sum_{\mathbf{y}} \sum_{\mu} \bar{\psi}(y) \left[\gamma_\mu D_\mu + i\frac{\bar{a}}{2} \gamma_5 \tau_{\mu 5} \Delta_\mu \right] \psi(y) + S_B^{(0)} + S_B^{(T')}. \quad \text{(C.2.18)}$$

The contributions from the boundaries are,

$$\begin{aligned} S_{B,1^+}^{(0)} &= \bar{a}^4 \sum_{\mathbf{y}} \sum_{k=1}^{3} \bar{\psi}(0,\mathbf{y}) \left[Q_- \gamma_k D_k + i\frac{\bar{a}}{2} Q_- \gamma_5 \tau_{k5} \Delta_k \right] \psi(0,\mathbf{y}) \\ &+ \bar{a}^3 \sum_{\mathbf{y}} \bar{\psi}(0,\mathbf{y}) Q_- \gamma_0 \psi(\bar{a},\mathbf{y}), \quad \text{(C.2.19)} \\ S_{B,1^+}^{(T')} &= \bar{a}^4 \sum_{\mathbf{y}} \sum_{k=1}^{3} \bar{\psi}(T',\mathbf{y}) \left[Q_+ \gamma_k D_k + i\frac{\bar{a}}{2} Q_+ \gamma_5 \tau_{k5} \Delta_k \right] \psi(T',\mathbf{y}) \\ &- \bar{a}^3 \sum_{\mathbf{y}} \bar{\psi}(T',\mathbf{y}) Q_+ \gamma_0 \psi(T'-\bar{a},\mathbf{y}). \quad \text{(C.2.20)} \end{aligned}$$

And the boundary conditions in this case are,

$$\begin{aligned} Q_-\psi(0,\mathbf{y}) &= \rho(\mathbf{y}), \qquad & Q_+\psi(T',\mathbf{y}) &= \rho'(\mathbf{y}), \\ \bar{\psi}(0,\mathbf{y})Q_- &= \bar{\rho}(\mathbf{y}), \qquad & \bar{\psi}(T',\mathbf{y})Q_+ &= \bar{\rho}'(\mathbf{y}). \end{aligned} \quad \text{(C.2.21)}$$

3. Case $s = 1^-$. The action in this last case will read,

$$\begin{aligned} S_f^{1^-} &= \bar{a}^4 \sum_{y_0=\bar{a}}^{T'-\bar{a}} \sum_{\mathbf{y}} \bar{\psi}(y) \left[\sum_{\mu} \gamma_\mu D_\mu - i\frac{\bar{a}}{2} \gamma_5 \tau_{05} \Delta_0 + i\frac{\bar{a}}{2} \sum_{k} \gamma_5 \tau_{k5} \Delta_k \right] \psi(y) \\ &+ S_B^{(0)} + S_B^{(T')}. \quad \text{(C.2.22)} \end{aligned}$$

The contributions of the boundaries are,

$$\begin{aligned} S_{B,1^-}^{(0)} &= \bar{a}^4 \sum_{\mathbf{y}} \sum_{k=1}^{3} \bar{\psi}(0,\mathbf{y}) \left[Q_+ \gamma_k D_k + i\frac{\bar{a}}{2} Q_+ \gamma_5 \tau_{k5} \Delta_k \right] \psi(0,\mathbf{y}) \\ &+ \bar{a}^3 \sum_{\mathbf{y}} \bar{\psi}(0,\mathbf{y}) Q_+ \gamma_0 \psi(\bar{a},\mathbf{y}), \quad \text{(C.2.23)} \\ S_{B,1^-}^{(T')} &= \bar{a}^4 \sum_{\mathbf{y}} \sum_{k=1}^{3} \bar{\psi}(T,\mathbf{y}) \left[Q_- \gamma_k D_k + i\frac{\bar{a}}{2} Q_- \gamma_5 \tau_{k5} \Delta_k \right] \psi(T'\mathbf{y}) \\ &- \bar{a}^3 \sum_{\mathbf{y}} \bar{\psi}(T'-\bar{a}) Q_- \gamma_0 \psi(T',\mathbf{y}). \quad \text{(C.2.24)} \end{aligned}$$

And the boundary conditions in this case are,

$$\begin{aligned} Q_+\psi(0,\mathbf{y}) &= \rho(\mathbf{y}), \qquad & Q_-\psi(T',\mathbf{y}) &= \rho'(\mathbf{y}), \\ \bar{\psi}(0,\mathbf{y})Q_+ &= \bar{\rho}(\mathbf{y}), \qquad & \bar{\psi}(T',\mathbf{y})Q_- &= \bar{\rho}'(\mathbf{y}). \end{aligned} \quad \text{(C.2.25)}$$

Appendix D

Free staggered propagator

The idea is to first deduce an expression for the propagator S_∞^f on the lattice with infinite time-like extent and then to add a suitable solution of the homogeneus equation to fullfill the boundary conditions of Eq. (2.3.50). We are first interested to find the general solution of

$$D_s^f \psi_s(y) = \eta_s(y). \tag{D.0.1}$$

for given source fields $\eta_s(y)$ and Schrödinger functional boundary conditions on the time direction.

D.1 Plane wave solutions

In this section, we discuss plane wave solutions of Dirac's equation Eq. (D.0.1) with source $\eta_s(y) = 0$. We do not yet impose any boundary conditions in the time direction, i.e. the equation is solved for all times y_0.

There are two types of plane waves, those with positive and those with negative energy. We first consider the positive energy solutions

$$\psi(y) = u e^{ipy}, \qquad \mathrm{Im}\, p_0 > 0. \tag{D.1.1}$$

The spatial components of the momentum $\mathbf{p}$ are integer multiples of $2\pi/L$ in the range,

$$-\pi/\bar{a} < p_k \leq \pi/\bar{a} \tag{D.1.2}$$

The constant spinor u and the energy p_0 are constrained by the Dirac's equation, which reduces to the following equations, for the cases $s = \pm 1$ respectively.

1. Case $s = -1$

$$\left\{ i \sum_i \gamma_\mu \mathring{p}_\mu^+ - i \sum_k \frac{\bar{a}}{2} \gamma_5 \tau_{k5} \hat{p}_k^{+2} - \frac{\bar{a}}{2} \hat{p}_0^{+2} \right\} u = 0. \tag{D.1.3}$$

2. Case $s = 1$

$$\left\{ i \sum_i \gamma_\mu \mathring{p}_\mu^+ - i \sum_k \frac{\bar{a}}{2} \gamma_5 \tau_{k5} \hat{p}_k^{+2} + \frac{\bar{a}}{2} \hat{p}_0^{+2} \right\} u = 0. \tag{D.1.4}$$

The notation used here is clarified in Appendix A.3. We now multiply the equation from the left with the hermitic Dirac operator $(D_f^s)^\dagger$, and deduce that,

$$\sum_\mu \hat{p}_\mu^{+2} u = 0. \tag{D.1.5}$$

Solving for the energy p_0 one obtains

$$p_0 = p_0^+ = i\omega(\mathbf{p}^+) \text{mod } 2\pi/\bar{a}, \tag{D.1.6}$$

where $\omega(\mathbf{q})$ is given by

$$\sinh\left[\frac{\omega(\mathbf{q})\bar{a}}{2}\right] = \frac{\bar{a}}{2}\sqrt{\hat{\mathbf{p}}^{+2}}. \tag{D.1.7}$$

$\omega(\mathbf{p}^+)$ is well defined and positive in the specified ranges of momenta $\mathbf{p}$. There are no other postive energy solutions of the Eq. (D.1.5). We still have to determine the spinor u. In Appendix A.4, we give a list of explicit expressions and properties.

Now, we turn to the plane wave solutions with negative energy,

$$\psi(y) = v e^{-ipy}, \qquad \text{Im } p_0 > 0. \tag{D.1.8}$$

We arrive to the following equation,

$$\sum_\mu (\hat{p}_\mu^-)^2 v = 0. \tag{D.1.9}$$

Solving for the energy p_0, one obtains,

$$p_0 = p_0^- = i\omega(\mathbf{p}^-) \text{mod } 2\pi/\bar{a}, \tag{D.1.10}$$

and $\omega(\mathbf{q})$ is given by,

$$\sinh\left[\frac{\omega(\mathbf{q})\bar{a}}{2}\right] = -\frac{\bar{a}}{2}\sqrt{\hat{\mathbf{p}}^{+2}}. \tag{D.1.11}$$

As in the positive energy case, we determine the spinor v in Appendix A.4.

D.2 Solution of the Dirac equation with boundary values

We are interested in finding the solution of homogeneus Dirac's equation

$$D_s^f \psi^s(y) = 0, \qquad 0 < y_0 < T', \tag{D.2.1}$$

with the boundary values,

$$P_+\psi^s(y)\big|_{y_0=0} = \rho_s(\mathbf{y}), \qquad P_-\psi^s(y)\big|_{y_0=T'} = \rho'_s(\mathbf{y}). \tag{D.2.2}$$

As it has been pointed out by Lüscher in [84], $\psi^s(y)$ is a superposition of plane waves. An explicit expression for $\psi^s(y)$ can be written as,

$$\psi^s(y) = \left(D_s^f\right)^\dagger \phi_s(y), \tag{D.2.3}$$

where,

$$\begin{aligned}\phi_s(y) &= L^{-3}\sum_p e^{i\mathbf{py}}\frac{1}{R_s(\mathbf{p}^+)}\left\{\tilde\rho(\mathbf{p})\left[e^{-\omega(\mathbf{p}^+)y_0} - e^{-\omega(\mathbf{p}^+)(2T'-y_0)}\right]\right.\\ &\left. + \tilde\rho'(\mathbf{p})\left[e^{-\omega(\mathbf{p}^+)(T'-y_0)} - e^{\omega(\mathbf{p}^+)(T'+y_0)}\right]\right\},\end{aligned} \tag{D.2.4}$$

where,

$$\tilde\rho(\mathbf{p}) = L^{-3}\sum_{\mathbf{y}} e^{-i\mathbf{py}}\rho(\mathbf{y}), \tag{D.2.5}$$

and the $R_s(\mathbf{p}^+)$ factor is given by,

$$R_{-1}(\mathbf{p}^+) = \left\{-\frac{\bar a}{2}\hat p_0^{+2} - i\,\mathring{p}_0^+\right\} - e^{-2\omega(\mathbf{p}^+)T'}\left\{-\frac{\bar a}{2}\hat p_0^{+2} + i\,\mathring{p}_0^+\right\}, \tag{D.2.6}$$

$$R_1(\mathbf{p}^+) = \left\{\frac{\bar a}{2}\hat p_0^{+2} - i\,\mathring{p}_0^+\right\} - e^{-2\omega(\mathbf{p}^+)T'}\left\{\frac{\bar a}{2}\hat p_0^{+2} + i\,\mathring{p}_0^+\right\}. \tag{D.2.7}$$

D.3 Propagator

As we have pointed out above, the equations for the propagator are given by Eqs. (2.3.49,2.3.50). The propagator $S_s^f(y,y')$ may be computed by making the ansatz,

$$S^f(y,y')_s = S_\infty^{f,s}(y,y') - \psi_s^f(y,y'), \tag{D.3.1}$$

where $\psi_s^f(y,y')$ is a solution of the homogeneus Dirac equation, Eq. (D.2.1). The solution must be such that the boundary conditions of Eq. (2.3.50) are satisfied. So, if we define the boundary fields,

$$\rho(\mathbf{y},y') = P_+S_\infty^{f,s}(y,y')\big|_{y_0=0}, \qquad \rho'(\mathbf{y},y') = P_-S_\infty^{f,s}(y,y')\big|_{y_0=T'}, \tag{D.3.2}$$

the requirement is that,

$$P_+\psi_s^f(y,y')\big|_{y_0=0} = \rho(\mathbf{y},y') \qquad P_-\psi_s^f(y,y')\big|_{y_0=T'} = \rho'(\mathbf{y},y'). \tag{D.3.3}$$

Let us start with the infinite propagator.

D.3.1 Infinite lattice propagator

On the infinite lattice, the propagator is given by,

$$S^{f,s}_{\infty}(y,y') = \left(D^f_s\right)^{\dagger} G^{SF}_{\infty}(y,y'), \tag{D.3.4}$$

where,

$$G_{\infty}(y) = L^{-3}\sum_{\mathbf{p}} e^{i\mathbf{p}\mathbf{y}} \int_{-\pi/\bar{a}}^{\pi/\bar{a}} \frac{dp_0}{2\pi} e^{ip_0 y_0} \left(\hat{p}^{+}\right)^{-2}. \tag{D.3.5}$$

After calculating the integral using the residue theorem, we arrive at,

$$G_{\infty}(y) = L^{-3}\sum_{\mathbf{p}} \frac{i}{2\,\mathring{p}^{+}_0} e^{i\mathbf{p}\mathbf{y}} e^{-|y_0|\omega(\mathbf{p}^{+})}. \tag{D.3.6}$$

The explicit expression for the infinite lattice propagator will then be,

$$S^{f,s}_{\infty}(y,y') = L^{-3}\sum_{\mathbf{p}} e^{i\mathbf{p}(\mathbf{y}-\mathbf{y}')} \tilde{S}^{f,s}_{\infty}(y_0,y'_0). \tag{D.3.7}$$

Now, differentiating between the two cases,

1. Case $s=-1$

$$\tilde{S}^{f,-1}_{\infty}(y_0,y'_0)_{\mathbf{p}} = \begin{cases} (i\,\mathring{p}^{+}_0 - \tilde{A}_{s=-1})\gamma_0 \frac{i}{2\,\mathring{p}^{+}_0} e^{-\omega(\mathbf{p}^{+})|y_0-y'_0|} & y_0 < y'_0 \\ \frac{i}{2\,\mathring{p}^{+}_0}(i\,\mathring{p}^{+}_0\gamma_0 - \tilde{A}_{-1})\gamma_0 & y_0 = y'_0 \\ (-i\,\mathring{p}^{+}_0 - \tilde{A}_{-1})\gamma_0 \frac{i}{2\,\mathring{p}^{+}_0} e^{-\omega(\mathbf{p}^{+})|y_0-y'_0|} & y_0 > y'_0 \end{cases}, \tag{D.3.8}$$

$$\begin{aligned} \tilde{A}_{-1} &= \sum_k \left[i\gamma_k\gamma_0\,\mathring{p}^{+}_k - i\frac{\bar{a}}{2}\gamma_5\gamma_0\tau_{k5}\hat{p}^{+2}_k \right] + \frac{\bar{a}}{2}\gamma_0\hat{p}^{+2}_0, \\ \tilde{A}^2_{-1} &= \mathring{\omega}^2(\mathbf{p}^{+}). \end{aligned} \tag{D.3.9}$$

2. Case $s=1$

$$\tilde{S}^{f,1}_{\infty}(y_0,y'_0)_{\mathbf{p}} = \begin{cases} (i\,\mathring{p}^{+}_0 - \tilde{A}_{s=1})\gamma_0 \frac{i}{2\,\mathring{p}^{+}_0} e^{-\omega(\mathbf{p}^{+})|y_0-y'_0|} & y_0 < y'_0 \\ \frac{i}{2\,\mathring{p}^{+}_0}(-i\,\mathring{p}^{+}_0\gamma_0 - \tilde{A}_{1})\gamma_0 & y_0 = y'_0 \\ (-i\,\mathring{p}^{+}_0 - \tilde{A}_{1})\gamma_0 \frac{i}{2\,\mathring{p}^{+}_0} e^{-\omega(\mathbf{p}^{+})|y_0-y'_0|} & y_0 > y'_0 \end{cases}, \tag{D.3.10}$$

$$\begin{aligned} \tilde{A}_{1} &= \sum_k \left[i\gamma_k\gamma_0\,\mathring{p}^{+}_k - i\frac{\bar{a}}{2}\gamma_5\gamma_0\tau_{k5}\hat{p}^{+2}_k \right] - \frac{\bar{a}}{2}\gamma_0\hat{p}^{+2}_0, \\ \tilde{A}^2_{1} &= \mathring{\omega}^2(\mathbf{p}^{+}). \end{aligned} \tag{D.3.11}$$

D.3.2 Boundary conditions

With this result for the infinite propagator, we arrive at the following expressions for the boundary fields in Eq. (D.3.2),

$$\begin{aligned}\tilde{\rho}_s(\mathbf{p},y_0') &= P_+\tilde{S}_\infty^{f,s}(0,y_0') = iP_+(i\,\mathring{p}_0^+ - \tilde{A}_s)\gamma_0\frac{e^{-\omega(\mathbf{p}^+)y_0'}}{2\,\mathring{p}_0^+},\\ \tilde{\rho}_s(\mathbf{p},y_0') &= P_-\tilde{S}_\infty^{f,s}(T',y_0') = iP_-(-i\,\mathring{p}_0^+ - \tilde{A}_s)\gamma_0\frac{e^{-\omega(\mathbf{p}^+)(T'-y_0')}}{2\,\mathring{p}_0^+}.\end{aligned} \tag{D.3.12}$$

D.3.3 Solution of the homogeneus Dirac equation

Now, the solution for the homogeneus Dirac equation can be obtained as,

$$\psi_s^f(y,y') = L^{-3}\sum_{\mathbf{p}} e^{i\mathbf{p}(\mathbf{y}-\mathbf{y}')}\tilde{\psi}_s^f(y_0,y_0')_{\mathbf{p}}, \tag{D.3.13}$$

with $\tilde{\psi}_s^f(y_0,y_0') = (D_s^{SF})^\dagger\phi_s(y_0,y_0')_{\mathbf{p}}$. $\phi_s(y_0,y_0')_{\mathbf{p}}$ will be given as,

$$\begin{aligned}\phi_s(y_0,y_0')_{\mathbf{p}} = \frac{1}{R_s(\mathbf{p}^+)}\Bigg\{ & P_+(i\,\mathring{p}_0^+ - \tilde{A}_s)\gamma_0\frac{ie^{-\omega(\mathbf{p}^+)y_0'}}{2\,\mathring{p}_0^+}\left[e^{-\omega(\mathbf{p}^+)y_0} - e^{-\omega(\mathbf{p}^+)(2T'-y_0)}\right]\\ - \; & P_-(i\,\mathring{p}_0^+ + \tilde{A}_s)\gamma_0\frac{ie^{-\omega(\mathbf{p}^+)(T'-y_0')}}{2\,\mathring{p}_0^+}\left[e^{-\omega(\mathbf{p}^+)(T'-y_0)} - e^{-\omega(\mathbf{p}^+)(T'+y_0)}\right]\Bigg\}.\end{aligned} \tag{D.3.14}$$

Thus, we get,

$$\begin{aligned}\psi_s^f(y_0,y_0')_{\mathbf{p}} = \; & \frac{i}{2\,\mathring{p}_0^+R_s(\mathbf{p}^+)}\Big\{(-i\,\mathring{p}_0^+ - \tilde{A}_s)P_+(i\,\mathring{p}_0^+ - \tilde{A}_s)\gamma_0e^{-\omega(y_0'+y_0)}\\ & - \; (i\,\mathring{p}_0^+ - \tilde{A}_s)P_+(i\,\mathring{p}_0^+ - \tilde{A}_s)\gamma_0e^{-\omega(2T'+y_0'-y_0)}\\ & + \; (i\,\mathring{p}_0^+ - \tilde{A}_s)P_-(i\,\mathring{p}_0^+ + \tilde{A}_s)\gamma_0e^{-\omega(2T'-y_0'-y_0)}\\ & + \; (i\,\mathring{p}_0^+ + \tilde{A}_s)P_-(i\,\mathring{p}_0^+ + \tilde{A}_s)\gamma_0e^{-\omega(2T-y_0'+y_0)}\Big\}.\end{aligned} \tag{D.3.15}$$

Reorganising the terms and doing some algebra, we can write the propagator as,

1. Case $s=-1$:

$$\begin{aligned}\psi_{-1}^f(y_0,y_0')_{\mathbf{p}} = \; & \frac{i}{2\,\mathring{p}_0^+R_{-1}(\mathbf{p}^+)}\Big\{(\tilde{A}_{-1} - i\,\mathring{p}_0^+)\left(-\frac{\bar{a}}{2}\hat{p}_0^{+2} + i\,\mathring{p}_0^+\right)\gamma_0e^{-\omega(\mathbf{p}^+)(2T'+y_0'-y_0)}\\ & + \; (\tilde{A}_{-1} + i\,\mathring{p}_0^+)\left(\frac{\bar{a}}{2}\hat{p}_0^{+2} - i\,\mathring{p}_0^+\gamma_0\right)\gamma_0e^{-\omega(\mathbf{p}^+)(y_0'+y_0)}\\ & - \; (\tilde{A}_{-1} + i\,\mathring{p}_0^+)\left(\frac{\bar{a}}{2}\hat{p}_0^{+2} - i\,\mathring{p}_0^+\right)\gamma_0e^{-\omega(\mathbf{p}^+)(2T'-y_0'+y_0)}\\ & + \; (\tilde{A}_{-1} - i\,\mathring{p}_0^+)\left(\frac{\bar{a}}{2}\hat{p}_0^{+2} + i\,\mathring{p}_0^+\gamma_0\right)\gamma_0e^{-\omega(\mathbf{p}^+)(2T'-y_0'-y_0)}\Big\}.\end{aligned} \tag{D.3.16}$$

2. Case $s = 1$:

$$\begin{aligned}\psi_1^f(y_0, y_0')_{\mathbf{p}} &= \frac{i}{2\,\mathring{p}_0^+ R_1(\mathbf{p}^+)}\Big\{(\tilde{A}_1 - i\,\mathring{p}_0^+)\left(\frac{\bar{a}}{2}\hat{p}_0^{+2} + i\,\mathring{p}_0^+\right)\gamma_0 e^{-\omega(\mathbf{p}^+)(2T'+y_0'-y_0)} \\ &- (\tilde{A}_1 + i\,\mathring{p}_0^+)\left(\frac{\bar{a}}{2}\hat{p}_0^{+2} + i\,\mathring{p}_0^+\gamma_0\right)\gamma_0 e^{-\omega(\mathbf{p}^+)(y_0'+y_0)} \\ &+ (\tilde{A}_1 + i\,\mathring{p}_0^+)\left(\frac{\bar{a}}{2}\hat{p}_0^{+2} + i\,\mathring{p}_0^+\right)\gamma_0 e^{-\omega(\mathbf{p}^+)(2T'-y_0'+y_0)} \\ &+ (\tilde{A}_1 - i\,\mathring{p}_0^+)\left(-\frac{\bar{a}}{2}\hat{p}_0^{+2} + i\,\mathring{p}_0^+\gamma_0\right)\gamma_0 e^{-\omega(\mathbf{p}^+)(2T'-y_0'-y_0)}\Big\}.\end{aligned} \tag{D.3.17}$$

D.3.4 Expression for the propagator

Now, we can get an expression for the propagator, using Eq. (D.3.1), and arriving at the following expressions corresponding to $s = \pm 1$,

1. Case $s = -1$

$$y_0 < y_0'$$

$$\begin{aligned}S_{-1}^f(y_0, y_0')_{\mathbf{p}} &= \frac{-i}{R_{-1}(\mathbf{p}^+)2\,\mathring{p}_0^+}\Big\{(i\,\mathring{p}_0^+ - \tilde{A}_{-1})\left(\frac{\bar{a}}{2}\hat{p}_0^{+2} + i\,\mathring{p}_0^+\right)\gamma_0 e^{-\omega(\mathbf{p}^+)(y_0'-y_0)} \\ &+ (\tilde{A}_{-1} + i\,\mathring{p}_0^+)\left(\frac{\bar{a}}{2}\hat{p}_0^{+2} - i\,\mathring{p}_0^+\gamma_0\right)\gamma_0 e^{-\omega(\mathbf{p}^+)(y_0+y_0')} \\ &- (\tilde{A}_{-1} + i\,\mathring{p}_0^+)\left(\frac{\bar{a}}{2}\hat{p}_0^{+2} - i\,\mathring{p}_0^+\right)\gamma_0 e^{-\omega(\mathbf{p}^+)(2T'-(y_0'-y_0))} \\ &+ (\tilde{A}_{-1} - i\,\mathring{p}_0^+)\left(\frac{\bar{a}}{2}\hat{p}_0^{+2} + i\,\mathring{p}_0^+\gamma_0\right)\gamma_0 e^{-\omega(\mathbf{p}^+)(2T'-(y_0'+y_0))}\Big\}.\end{aligned} \tag{D.3.18}$$

$$y_0 = y_0'$$

$$\begin{aligned}S_{-1}^f(y_0, y_0')_{\mathbf{p}} &= \frac{-i}{R_{-1}(\mathbf{p}^+)2\,\mathring{p}_0^+}\Big\{(i\,\mathring{p}_0^+\gamma_0 - \tilde{A}_{-1})\left(\frac{\bar{a}}{2}\hat{p}_0^{+2} + i\,\mathring{p}_0^+\right)\gamma_0 \\ &+ (\tilde{A}_{-1} + i\,\mathring{p}_0^+)\left(\frac{\bar{a}}{2}\hat{p}_0^{+2} - i\,\mathring{p}_0^+\gamma_0\right)\gamma_0 e^{-\omega(\mathbf{p}^+)(y_0+y_0')} \\ &- (\tilde{A}_{-1} + i\,\mathring{p}_0^+\gamma_0)\left(\frac{\bar{a}}{2}\hat{p}_0^{+2} - i\,\mathring{p}_0^+\right)\gamma_0 e^{-\omega(\mathbf{p}^+)(2T')} \\ &+ (\tilde{A}_{-1} - i\,\mathring{p}_0^+)\left(\frac{\bar{a}}{2}\hat{p}_0^{+2} + i\,\mathring{p}_0^+\gamma_0\right)\gamma_0 e^{-\omega(\mathbf{p}^+)(2T'-(y_0'+y_0))}\Big\}.\end{aligned} \tag{D.3.19}$$

$$y_0 > y_0'$$

$$
\begin{aligned}
S^f_{-1}(y_0,y_0')_{\mathbf{p}} &= \frac{-i}{R_{-1}(\mathbf{p}^+)2\mathring{p}_0^+}\Big\{\Big(\frac{\bar{a}}{2}\hat{p}_0^{+2}+i\,\mathring{p}_0^+\Big)(-i\,\mathring{p}_0^+-\tilde{A}_{-1})\gamma_0 e^{-\omega(\mathbf{p}^+)(y_0-y_0')} \\
&+ (\tilde{A}_{-1}+i\,\mathring{p}_0^+)\Big(\frac{\bar{a}}{2}\hat{p}_0^{+2}-i\,\mathring{p}_0^+\gamma_0\Big)\gamma_0 e^{-\omega(\mathbf{p}^+)(y_0+y_0')} \qquad \text{(D.3.20)} \\
&- (\tilde{A}_{-1}-i\,\mathring{p}_0^+)\Big(\frac{\bar{a}}{2}\hat{p}_0^{+2}-i\,\mathring{p}_0^+\Big)\gamma_0 e^{-\omega(\mathbf{p}^+)(2T'-(y_0-y_0'))} \\
&+ (\tilde{A}_{-1}-i\,\mathring{p}_0^+)\Big(\frac{\bar{a}}{2}\hat{p}_0^{+2}+i\,\mathring{p}_0^+\gamma_0\Big)\gamma_0 e^{-\omega(\mathbf{p}^+)(2T'-(y_0'+y_0))}\Big\}.
\end{aligned}
$$

2. Case $s=1$

$$y_0 < y_0'$$

$$
\begin{aligned}
S^f_{1}(y_0,y_0')_{\mathbf{p}} &= \frac{-i}{R_{1}(\mathbf{p}^+)2\mathring{p}_0^+}\Big\{(i\,\mathring{p}_0^+-\tilde{A}_{1})\Big(-\frac{\bar{a}}{2}\hat{p}_0^{+2}+i\,\mathring{p}_0^+\Big)\gamma_0 e^{-\omega(\mathbf{p}^+)(y_0'-y_0)} \\
&- (\tilde{A}_{1}+i\,\mathring{p}_0^+)\Big(\frac{\bar{a}}{2}\hat{p}_0^{+2}+i\,\mathring{p}_0^+\gamma_0\Big)\gamma_0 e^{-\omega(\mathbf{p}^+)(y_0+y_0')} \qquad \text{(D.3.21)} \\
&+ (\tilde{A}_{1}+i\,\mathring{p}_0^+)\Big(\frac{\bar{a}}{2}\hat{p}_0^{+2}+i\,\mathring{p}_0^+\Big)\gamma_0 e^{-\omega(\mathbf{p}^+)(2T'-(y_0'-y_0))} \\
&+ (\tilde{A}_{1}-i\,\mathring{p}_0^+)\Big(-\frac{\bar{a}}{2}\hat{p}_0^{+2}+i\,\mathring{p}_0^+\gamma_0\Big)\gamma_0 e^{-\omega(\mathbf{p}^+)(2T'-(y_0'+y_0))}\Big\}.
\end{aligned}
$$

$$y_0 = y_0'$$

$$
\begin{aligned}
S^f_{1}(y_0,y_0')_{\mathbf{p}} &= \frac{-i}{R_{1}(\mathbf{p}^+)2\mathring{p}_0^+}\Big\{(i\,\mathring{p}_0^+\gamma_0+\tilde{A}_{1})\Big(\frac{\bar{a}}{2}\hat{p}_0^{+2}-i\,\mathring{p}_0^+\Big)\gamma_0 \\
&- (\tilde{A}_{1}+i\,\mathring{p}_0^+)\Big(\frac{\bar{a}}{2}\hat{p}_0^{+2}+i\,\mathring{p}_0^+\gamma_0\Big)\gamma_0 e^{-\omega(\mathbf{p}^+)(y_0+y_0')} \qquad \text{(D.3.22)} \\
&+ (\tilde{A}_{1}-i\,\mathring{p}_0^+\gamma_0)\Big(\frac{\bar{a}}{2}\hat{p}_0^{+2}+i\,\mathring{p}_0^+\Big)\gamma_0 e^{-\omega(\mathbf{p}^+)(2T')} \\
&+ (\tilde{A}_{1}-i\,\mathring{p}_0^+)\Big(-\frac{\bar{a}}{2}\hat{p}_0^{+2}+i\,\mathring{p}_0^+\gamma_0\Big)\gamma_0 e^{-\omega(\mathbf{p}^+)(2T'-(y_0'+y_0))}\Big\}.
\end{aligned}
$$

$$y_0 > y_0'$$

$$
\begin{aligned}
S^f_{1}(y_0,y_0')_{\mathbf{p}} &= \frac{-i}{R_{1}(\mathbf{p}^+)2\mathring{p}_0^+}\Big\{\Big(\frac{\bar{a}}{2}\hat{p}_0^{+2}-i\,\mathring{p}_0^+\Big)(i\,\mathring{p}_0^+ +\tilde{A}_{1})\gamma_0 e^{-\omega(\mathbf{p}^+)(y_0-y_0')} \\
&- (\tilde{A}_{1}+i\,\mathring{p}_0^+)\Big(\frac{\bar{a}}{2}\hat{p}_0^{+2}+i\,\mathring{p}_0^+\gamma_0\Big)\gamma_0 e^{-\omega(\mathbf{p}^+)(y_0+y_0')} \qquad \text{(D.3.23)} \\
&+ (\tilde{A}_{1}-i\,\mathring{p}_0^+)\Big(\frac{\bar{a}}{2}\hat{p}_0^{+2}+i\,\mathring{p}_0^+\Big)\gamma_0 e^{-\omega(\mathbf{p}^+)(2T'-(y_0-y_0'))} \\
&+ (\tilde{A}_{1}-i\,\mathring{p}_0^+)\Big(-\frac{\bar{a}}{2}\hat{p}_0^{+2}+i\,\mathring{p}_0^+\gamma_0\Big)\gamma_0 e^{-\omega(\mathbf{p}^+)(2T'-(y_0'+y_0))}\Big\}.
\end{aligned}
$$

Appendix E

Possible counterterms of dimension 3, 4, 5

Using the transformation properties of the staggered fermion action, we try to construct all symmetrical operators of dimension $3, 4, 5$. We have to be aware that the discussion is being done in the Schrödinger functional standard basis.

E.1 Dimension 3

The general form of a dimension 3 operator has the form,

$$\bar{\psi}(y)\gamma_S\tau_F\psi(y), \tag{E.1.1}$$

where γ_S is a spin matrix and τ_F is a flavour matrix. Defining,

$$\bar{\tau} = \sum_{k=1}^{3} \tau_k, \tag{E.1.2}$$

the only terms allowed by reflections and rotations are,

$$\begin{aligned} (\mathbb{1}, \gamma_0) \quad &\otimes \quad (\mathbb{1}, \tau_5, \tau_0\bar{\tau}, \tau_{05}\bar{\tau}) \\ (\gamma_5, \gamma_{05}) \quad &\otimes \quad (\tau_0, \bar{\tau}, \tau_5\bar{\tau}, \tau_{05}) \end{aligned} \tag{E.1.3}$$

In the Table. E.1, we list the terms above and all the symmetries left but the charge conjugation.

Now, we consider the charge conjugation symmetry, and see that,

$$\begin{aligned} \bar{\psi}\psi \quad &\rightarrow \quad -\psi^T\mathcal{C}\mathcal{C}\bar{\psi}^T = \bar{\psi}\psi \\ \bar{\psi}\gamma_0\psi \quad &\rightarrow \quad -\psi^T\mathcal{C}\gamma_0\mathcal{C}\bar{\psi}^T = -\bar{\psi}\gamma_0\psi \end{aligned} \tag{E.1.4}$$

From the results shown in Table E.1, and Eq. (E.1.4), we conclude that the only dimension three term respecting all the symmetries is,

$$\mathcal{O}_1 = \sum_{\mathbf{y}} \bar{\psi}(0, \mathbf{y})\psi(0, \mathbf{y}). \tag{E.1.5}$$

Term	$U(1)_\epsilon$	Shift	$U(1)$	Term	$U(1)_\epsilon$	Shift	$U(1)$
$\bar{\psi}\psi$	$\surd$	$\surd$	$\surd$	$\bar{\psi}\gamma_0\psi$	$\surd$	$\surd$	$\surd$
$\bar{\psi}\tau_5\psi$	$\times$	$\times$	$\surd$	$\bar{\psi}\gamma_0\tau_5\psi$	$\times$	$\times$	$\surd$
$\bar{\psi}\tau_0\bar{\tau}\psi$	$\times$	$\times$	$\surd$	$\bar{\psi}\gamma_0\tau_0\bar{\tau}\psi$	$\times$	$\times$	$\surd$
$\bar{\psi}\tau_{05}\bar{\tau}\psi$	$\surd$	$\times$	$\surd$	$\bar{\psi}\gamma_0\tau_{05}\bar{\tau}\psi$	$\surd$	$\times$	$\surd$
$\bar{\psi}\gamma_5\tau_0\psi$	$\surd$	$\times$	$\surd$	$\bar{\psi}\gamma_{05}\tau_0\psi$	$\surd$	$\times$	$\surd$
$\bar{\psi}\gamma_5\bar{\tau}\psi$	$\times$	$\times$	$\surd$	$\bar{\psi}\gamma_{05}\bar{\tau}\psi$	$\times$	$\times$	$\surd$
$\bar{\psi}\gamma_5\tau_5\bar{\tau}\psi$	$\surd$	$\times$	$\surd$	$\bar{\psi}\gamma_{05}\tau_5\bar{\tau}\psi$	$\surd$	$\times$	$\surd$
$\bar{\psi}\gamma_5\tau_{05}\psi$	$\times$	$\surd$	$\surd$	$\bar{\psi}\gamma_{05}\tau_{05}\psi$	$\times$	$\surd$	$\surd$

Table E.1: Possible counterterms of dimension 3.

E.2 Dimension 4

The counterterms of dimension 4 can be inserted to remove the possible O(a) effects at the boundaries. The discussion here is analogous as the previous case. The general form of the operators is $\bar{\psi}\gamma_S\tau_F f(D,\bar{D})\psi$, where f is a homogeneous real polynomial of degree 1. We look for the terms allowed by the reflections and rotations arriving at,

$$\begin{aligned}
\sum_{k=1}^{3}(\gamma_k,\gamma_k\gamma_0)D_k &\otimes (\mathbb{1},\tau_5,\tau_0\bar{\tau},\tau_{05}\bar{\tau}),\\
\sum_{k=1}^{3}(\gamma_k\gamma_5,\gamma_k\gamma_{05})D_k &\otimes (\tau_0,\bar{\tau},\tau_5\bar{\tau},\tau_{05}),\\
(\mathbb{1},\gamma_0)D_0 &\otimes (\mathbb{1},\tau_5,\tau_0\bar{\tau},\tau_{05}\bar{\tau}),\\
(\gamma_0\gamma_5,\gamma_5)D_0 &\otimes (\tau_0,\bar{\tau},\tau_5\bar{\tau},\tau_{05}).
\end{aligned} \tag{E.2.1}$$

From the terms listed in Eq. (E.2.1), the ones respecting the symmetry U(1)$_\epsilon$ are,

$$\begin{aligned}
\sum_{k=1}^{3}(\gamma_k,\gamma_k\gamma_0)D_k &\otimes (\mathbb{1},\tau_{05}\bar{\tau}),\\
\sum_{k=1}^{3}(\gamma_k\gamma_5,\gamma_k\gamma_{05})D_k &\otimes (\tau_0,\tau_5\bar{\tau}),\\
(\mathbb{1},\gamma_0)D_0 &\otimes (\mathbb{1},\tau_{05}\bar{\tau}),\\
(\gamma_0\gamma_5,\gamma_5)D_0 &\otimes (\tau_0,\bar{\tau},\tau_5\bar{\tau}).
\end{aligned} \tag{E.2.2}$$

Imposing the shift symmetry, we are left with the terms,

$$\begin{aligned}
&\sum_{k=1}^{3}(\gamma_k,\gamma_k\gamma_0)D_k,\\
&(\mathbb{1},\gamma_0)D_0.
\end{aligned} \tag{E.2.3}$$

Now, we have to deal with the charge conjugation symmetry. The four terms left transform,

$$\begin{aligned}
\sum_k \bar\psi\gamma_k D_k\psi &\rightarrow -\psi^T\mathcal{C}\gamma_k\mathcal{C}D_k\bar\psi^T = \sum_k \bar\psi\gamma_k D_k\psi,\\
\sum_k \bar\psi\gamma_k\gamma_0 D_k\psi &\rightarrow -\sum_k \psi^T\mathcal{C}\gamma_k D_k\gamma_0\mathcal{C}\bar\psi^T = \sum_k \bar\psi\gamma_k\gamma_0 D_k\psi(y),\\
\bar\psi D_0\psi &\rightarrow \psi^T\mathcal{C}D_0\mathcal{C}\bar\psi^T = \bar\psi\overleftarrow{D}_0\psi,\\
\bar\psi\gamma_0 D_0\psi &\rightarrow \psi^T\mathcal{C}D_0\gamma_0\mathcal{C}\bar\psi^T = -\bar\psi\overleftarrow{D}_0\gamma_0\psi.
\end{aligned} \tag{E.2.4}$$

A sum over the space is understood in Eq. (E.2.4). We can see that the two first terms respect the charge conjugation symmetry whereas the two last do not. We can symmetrise these two last terms so that they do not change under charge conjugation. We obtain then the possible terms,

$$\begin{aligned}
&\bar\psi(0,\mathbf{y})\gamma_k D_k\psi(0,\mathbf{y}),\\
&\bar\psi(0,\mathbf{y})\gamma_k\gamma_0 D_k\psi(0,\mathbf{y}),\\
&\bar\psi(0,\mathbf{y})D_0\psi(0,\mathbf{y}) + \bar\psi(0,\mathbf{y})\overleftarrow{D}_0\psi(0,\mathbf{y}),\\
&\bar\psi(0,\mathbf{y})\gamma_0 D_0\psi(0,\mathbf{y}) - \bar\psi(0,\mathbf{y})\overleftarrow{D}_0\gamma_0\psi(0,\mathbf{y}).
\end{aligned} \tag{E.2.5}$$

The terms in $y_0 = T'$ are obtained from these imposing reflection symmetry in the time direction.

E.3 Dimension 5

The dimension 5 operators have the general form $\bar\psi\gamma_S\tau_F g(D,\bar D)\psi$ where g is a homogeneous real polynomial of degree 2.

Invariance under $U(1)_\epsilon$ restricts us to the terms,

$$(\mathbb{1},\gamma_\mu,\gamma_5,\gamma_{5\mu},\gamma_{\mu\nu},\gamma_5\gamma_{\mu\nu})\otimes(\mathbb{1},\tau_0,\tau_k\tau_5,\tau_{05}\tau_k,\tau_{kl},\tau_0\tau_{kl}) \tag{E.3.1}$$

From now on, we are going to use the results obtained by Luo in [92]. From the terms listed above, axis reversal invariance allows only the following terms,

$$\gamma_5\tau_0 D_0^2 - i\tau_{05}\tau_k D_k^2, \tag{E.3.2}$$

$$D_0^2 + i\gamma_5\tau_{0k}D_k^2, \tag{E.3.3}$$

$$i\gamma_5[\gamma_k,\gamma_l](\tau_{k5}+\tau_{l5})[D_k,D_l] + 2(1+i\gamma_5\tau_{k5})[\gamma_k,\gamma_0][D_k,D_0] \tag{E.3.4}$$

$$i\gamma_5[\gamma_k,\gamma_l](\tau_{k5}-\tau_{l5})\{D_k,D_l\} + 2(1-i\gamma_5\tau_{k5})[\gamma_k,\gamma_0]\{D_k,D_0\} \tag{E.3.5}$$

The three latter terms are invariant under rotations. Finally, let us discuss invariances under translation by one lattice unit. It turns out that none of the terms

listed above are invariant under lattice translation. So, we conclude that there is no dimension 5 fermion operator which is invariant under the lattice symmetry group, and therefore, no dimension 5 operator can be added to the staggered fermion action.

Appendix F

Coefficient matrices for the determination of Δ_1

The basis I_a of $\mathcal{L}_{SU(3)}$ which diagonalize the operators Δ_0, Δ_1 in the colour space is the following. We choose,

$$T_a = \frac{1}{2i}\tilde{\lambda}_a, \tag{F.0.1}$$

with,

$$\begin{aligned}
\tilde{\lambda}_1 &= \begin{pmatrix} 0 & 1 & 0 \\ 1 & 0 & 0 \\ 0 & 0 & 0 \end{pmatrix} \qquad \tilde{\lambda}_2 = \begin{pmatrix} 0 & -i & 0 \\ i & 0 & 0 \\ 0 & 0 & 0 \end{pmatrix} \\
\tilde{\lambda}_4 &= \begin{pmatrix} 0 & 0 & 1 \\ 0 & 0 & 0 \\ 1 & 0 & 0 \end{pmatrix} \qquad \tilde{\lambda}_5 = \begin{pmatrix} 0 & 0 & -i \\ 0 & 0 & 0 \\ i & 0 & 0 \end{pmatrix} \\
\tilde{\lambda}_6 &= \begin{pmatrix} 0 & 0 & 0 \\ 0 & 0 & 1 \\ 0 & 1 & 0 \end{pmatrix} \qquad \tilde{\lambda}_7 = \begin{pmatrix} 0 & 0 & 0 \\ 0 & 0 & -i \\ 0 & i & 0 \end{pmatrix} \\
\tilde{\lambda}_3 &= \begin{pmatrix} 0 & 0 & 0 \\ 0 & 1 & 0 \\ 0 & 0 & -1 \end{pmatrix} \qquad \tilde{\lambda}_8 = \frac{1}{\sqrt{3}} \begin{pmatrix} 2 & 0 & 0 \\ 0 & -1 & 0 \\ 0 & 0 & -1 \end{pmatrix}.
\end{aligned} \tag{F.0.2}$$

We define,

$$\begin{aligned}
I_1 &= \tfrac{1}{\sqrt{2}}(T_1 + iT_2) \qquad & I_1 &= \tfrac{1}{\sqrt{2}}(T_1 - iT_2) \\
I_4 &= \tfrac{1}{\sqrt{2}}(T_4 + iT_5) \qquad & I_5 &= \tfrac{1}{\sqrt{2}}(T_4 - iT_5) \\
I_6 &= \tfrac{1}{\sqrt{2}}(T_6 + iT_7) \qquad & I_7 &= \tfrac{1}{\sqrt{2}}(T_6 - iT_7) \\
I_3 &= T_3 & I_8 &= T_8.
\end{aligned} \tag{F.0.3}$$

Now, we have to specify the explicit form of the background field, in order to write down the coefficients in Eq.(4.2.35) and Eq.(4.2.36).

$$\begin{aligned} B_k(x_0) &= f\left(x_0 - \frac{T}{2}\right) + \frac{C_k + C'_k}{2} \qquad x_0 \in [a, T-a] \\ B_k(0) &= C_k \\ B_k(T) &= C'_k, \end{aligned} \tag{F.0.4}$$

The fields at the boundaries, C_k, C'_k are given by,

$$C_k = \frac{i}{L}\mathrm{diag}(\varphi_1, \varphi_1, \varphi_3) \qquad C'_k = \frac{i}{L}\mathrm{diag}(\varphi'_1, \varphi'_2, \varphi'_3). \tag{F.0.5}$$

Now, we give the explicit expression for the φ's,

$$\begin{aligned} &\varphi_1 = \eta - \pi/3 && \varphi'_1 = -\eta - \pi \\ &\varphi_2 = -1/2\eta && \varphi'_2 = 1/2\eta + \pi/3 \\ &\varphi_3 = -1/2\eta + \pi/3 && \varphi'_3 = 1/2\eta + 2\pi/3 \end{aligned} \tag{F.0.6}$$

f in Eq.(F.0.4) is a 3×3 diagonal matrix, $f = \mathrm{diag}(f_1, f_2, f_3)$. In chapter 2, a relationship between the three values is established. $f_2 = f_3 = -1/2 f_1$. As f_i are pure imaginary numbers, we define f_2^I as,

$$f_2 = i f_2^I \tag{F.0.7}$$

We are ready now to give the coefficients in Eq.(4.2.35) and Eq.(4.2.36)

- $\phi_a(x_0)$ coefficients

$$\phi_1(x_0) = \begin{cases} \frac{3\eta}{2L} - \frac{\pi}{3L} & x_0 = 0 \\ -3f_2^I\left(x_0 - \frac{T'-s}{2}\right) - \frac{5\pi}{6L} & x_0 \in [a, T-a] \\ -\frac{3\eta}{2L} - \frac{4\pi}{3L} & x_0 = T \end{cases} \tag{F.0.8}$$

$$\phi_4(x_0) = \begin{cases} \frac{3\eta}{2L} - \frac{2\pi}{3L} & x_0 = 0 \\ -3f_2^I\left(x_0 - \frac{T'-s}{2}\right) - \frac{7\pi}{6L} & x_0 \in [a, T-a] \\ -\frac{3\eta}{2L} - \frac{4\pi}{3L} & x_0 = T \end{cases} \tag{F.0.9}$$

$$\phi_6(x_0) = -\frac{\pi}{3L} \qquad \phi_3(x_0) = 0 \qquad \phi_8(x_0) = 0 \tag{F.0.10}$$

$$\phi_2(x_0) = -\phi_1(x_0) \quad \phi_5(x_0) = -\phi_4(x_0) \quad \phi_7(x_0) = -\phi_6(x_0) \tag{F.0.11}$$

- C_a^f, C_a^F coefficients

  Substituting x with f, F, we get C_a^f, C_a^F, respectively.

a	C_a^x	S_a^x
1	$1/2(\cos x + \cos 2x)$	$-i/2(\sin x + \sin 2x)$
4	$1/2(\cos x + \cos 2x)$	$i/2(\sin x + \sin 2x)$
6	$\cos x$	0
3	$\cos x$	0
8	$1/3(\cos x + 2\cos 2x)$	0

Table F.1: Values of C_a, S_a obtained for $m_1(L/a)$ values

We now give the explicit form of matrices $\mathcal{A}_{\mu\nu}, \mathcal{B}_{\mu\nu}$ and $\mathcal{C}_{\mu\nu}$ introduced in section 4.3. Δ_1 being an self-adjoint operator, the matrices satisfy,

$$\mathcal{B}^a_{\mu\nu}(\mathbf{p}, x_0) = (\mathcal{B}^a_{\nu\mu})^*(\mathbf{p}, x_0) \qquad \mathcal{C}^a_{\mu\nu}(\mathbf{p}, x_0) = (A^a_{\nu\mu})^*(\mathbf{p}, x_0 - 1). \tag{F.0.12}$$

We introduce the following notation,

$$\begin{aligned} s^a_k(\mathbf{p}, x_0) &= 2\sin\left[\tfrac{1}{2}(p_k + \phi_a(x_0))\right] \\ c^a_k(\mathbf{p}, x_0) &= 2\cos\left[\tfrac{1}{2}(p_k + \phi_a(x_0))\right]. \end{aligned} \tag{F.0.13}$$

$$\boxed{x_0 \in [2a, T - 2a]}$$

$$\begin{aligned} \mathcal{A}^a_{00}(\mathbf{p}, x_0) &= -\lambda_0 \\ \mathcal{A}^a_{0k}(\mathbf{p}, x_0) &= i(C^f_a - S^f_a)e^{i\partial_0\phi_a(x_0)/2}s^a_k(\mathbf{p}, x_0) - i\lambda_0 s^a_k(\mathbf{p}, x_0 + a) \\ \mathcal{A}^a_{k0}(\mathbf{p}, x_0) &= 0 \\ \mathcal{A}^a_{kl}(\mathbf{p}, x_0) &= -\delta_{kl}(C^f_a - S^f_a)e^{i\partial_0\phi_a(x_0)/2}. \end{aligned} \tag{F.0.14}$$

$$\begin{aligned} \mathcal{B}^a_{00}(\mathbf{p}, x_0) &= \textstyle\sum_k\{C^f_a s^a_k(\mathbf{p}, x_0) - iS^f_a c^a_k(\mathbf{p}, \mathbf{x_0})\}s^a_k(\mathbf{p}, x_0) + 2\lambda_0 \\ \mathcal{B}^a_{0k}(\mathbf{p}, x_0) &= -i\{C^f_a s^a_k(\mathbf{p}, x_0) - iS^f_a c^a_k(\mathbf{p}, x_0)\} - i\lambda_0 s^a_k(\mathbf{p}, x_0) \\ \mathcal{B}^a_{kl}(\mathbf{p}, x_0) &= \delta_{kl}\{2C^f_a + [\mathbf{s}^a(\mathbf{p}, x_0)]^2\} - s^a_l(\mathbf{p}, x_0)s^a_k(\mathbf{p}, x_0)(1 - \lambda_0). \end{aligned} \tag{F.0.15}$$

$$\boxed{x_0 = 0}$$

We have no $\mathcal{C}_{\mu\nu}$ when $x_0 = 0$. The only coefficients that exist are,

$$\begin{aligned} \mathcal{A}^a_{00}(\mathbf{p}, x_0) &= -\lambda_0 \\ \mathcal{A}^a_{0k}(\mathbf{p}, x_0) &= ic^{(0)}_t(C^F_a - S^F_a)e^{i\partial_0\phi_a(x_0)/2}s^a_k(\mathbf{p}, 0) - i\lambda_0 s^a_k(\mathbf{p}, x_0 + a) \end{aligned} \tag{F.0.16}$$

$$\begin{aligned} \mathcal{B}^a_{00}(\mathbf{p}, x_0) &= c^{(0)}_t\textstyle\sum_k\{C^F_a s^a_k(\mathbf{p}, x_0) - iS^F_a c^a_k(\mathbf{p}, \mathbf{x_0})\}s^a_k(\mathbf{p}, x_0) \\ &\quad +\chi_a(\mathbf{p})\lambda_0 \end{aligned} \tag{F.0.17}$$

where,

$$\chi_a(\mathbf{p}) = \begin{cases} 2 & \text{if } (a = 3 \cup a = 8) \cap |\mathbf{p}| = 0 \\ 1 & \text{otherwise} \end{cases} \tag{F.0.18}$$

$$\boxed{x_0 = a}$$

$$\begin{aligned}
\mathcal{A}^a_{00}(\mathbf{p}, x_0) &= -\lambda_0 \\
\mathcal{A}^a_{0k}(\mathbf{p}, x_0) &= i(C^f_a - S^f_a)e^{i\partial_0\phi_a(a)/2}s^a_k(\mathbf{p}, x_0) - i\lambda_0 s^a_k(\mathbf{p}, x_0 + a) \\
\mathcal{A}^a_{k0}(\mathbf{p}, x_0) &= 0 \\
\mathcal{A}^a_{kl}(\mathbf{p}, x_0) &= -\delta_{kl}(C^f_a - S^f_a)e^{i\partial_0\phi_a(x_0)/2}
\end{aligned} \tag{F.0.19}$$

$$\begin{aligned}
\mathcal{B}^a_{00}(\mathbf{p}, x_0) &= \textstyle\sum_k \{C^f_a s^a_k(\mathbf{p}, x_0) - iS^f_a c^a_k(\mathbf{p}, \mathbf{x_0})\}s^a_k(\mathbf{p}, x_0) + 2\lambda_0 \\
\mathcal{B}^a_{0k}(\mathbf{p}, x_0) &= -i\{C^f_a s^a_k(\mathbf{p}, x_0) - iS^f_a c^a_k(\mathbf{p}, x_0)\} - i\lambda_0 s^a_k(\mathbf{p}, x_0) \\
\mathcal{B}^a_{kl}(\mathbf{p}, x_0) &= \delta_{kl}\{2C_a + [\mathbf{s}^a(\mathbf{p}, x_0)]^2 + C^{f-F}_a\} - s^a_l(\mathbf{p}, x_0)s^a_k(\mathbf{p}, x_0)(1 - \lambda_0).
\end{aligned} \tag{F.0.20}$$

$$\boxed{x_0 = T - a}$$

There is no $A_{\mu\nu}$. We have then, for $\mathcal{B}_{\mu\nu}$

$$\begin{aligned}
\mathcal{B}^a_{00}(\mathbf{p}, x_0) &= c^{(0)}_t i\textstyle\sum_k \left\{C^F_a s^a_k(\mathbf{p}, x_0) - iS^F_a c^a_k(\mathbf{pi}, x_0)\right\} s^a_k(\mathbf{p}, x_0) + 2\lambda_0 \\
\mathcal{B}^a_{0k}(\mathbf{p}, x_0) &= -i\left\{C^F_a s^a_k(\mathbf{p}, x_0) - iS^F_a c^a_k(\mathbf{p}, x_0)\right\} - i\lambda_0 s^a_k(\mathbf{p}, x_0) \\
\mathcal{B}^a_{kl}(\mathbf{p}, x_0) &= \delta_{kl}\{2C_a + [\mathbf{s}^a(\mathbf{p}, x_0)]^2 + C^{F-f}_a\} - s^a_l(\mathbf{p}, x_0)s^a_k(\mathbf{p}, x_0)(1 - \lambda_0)
\end{aligned} \tag{F.0.21}$$

Appendix G

Values of $m_{1,0}(L/a), m_{1,1}(L/a)$

L	$\theta = 0$	$\theta = \pi/5$	$\theta = 1$	$\theta = 2$
4	−0.00527681341276	−0.00514806304492	−0.00585172595535	−0.01055537266957
6	−0.01278363172133	−0.01296068816844	−0.01343638879754	−0.01525199926404
8	−0.01715036430333	−0.01761954605007	−0.01817913397253	−0.01962400391953
10	−0.02005180206945	−0.02081712103709	−0.02152895214213	−0.02302086803393
12	−0.02224485328805	−0.02320591819746	−0.02402324301439	−0.02559326394542
14	−0.02401249994143	−0.02509285179174	−0.02597575020807	−0.02760685439074
16	−0.02548967278359	−0.02664495301648	−0.02756993178031	−0.02924689668538
18	−0.02675532473849	−0.02796035668299	−0.02891395089776	−0.03062637953312
20	−0.02786069467882	−0.02910049841968	−0.03007458008173	−0.03181521068896
22	−0.02884088893866	−0.03010601381187	−0.03109535971362	−0.03285886034258
24	−0.02972087360857	−0.03100504251226	−0.03200611262334	−0.03378842394808
26	−0.03051895294474	−0.03181782012621	−0.03282811331315	−0.03462607237977
28	−0.03124890383986	−0.03255935897422	−0.03357704982027	−0.03538815243339
30	−0.03192133446228	−0.03324109010303	−0.03426481125688	−0.03608705005279
32	−0.03254457623501	−0.03387191139949	−0.03490061642640	−0.03673236526293
34	−0.03312528614513	−0.03445888064810	−0.03549175406874	−0.03733168316559
36	−0.03366886401752	−0.03500768794606	−0.03604408427657	−0.03789109679083
38	−0.03417974837624	−0.03552298632566	−0.03656238763899	−0.03841557161835
40	−0.03466163063637	−0.03600862854729	−0.03705061424362	−0.03890920581807
42	−0.03511761309709	−0.03646784018181	−0.03751206502445	−0.03937541992501
44	−0.03555032745603	−0.03690334843431	−0.03794952631124	−0.03981709762840
46	−0.03596202506638	−0.03731747958968	−0.03836537132160	−0.04023669198662
48	−0.03635464662198	−0.03771223380218	−0.03876163786134	−0.04063630673546
50	−0.03672987663229	−0.03808934325468	−0.03914008861119	−0.04101775935486
52	−0.03708918649236	−0.03845031792752	−0.03950225847268	−0.04138263057467
54	−0.03743386888981	−0.03879648200947	−0.03984949216355	−0.04173230366115
56	−0.03776506555395	−0.03912900315314	−0.04018297437306	−0.04206799590616
58	−0.03808378983159	−0.03944891619608	−0.04050375417447	−0.04239078409924
60	−0.03839094520307	−0.03975714255667	−0.04081276495724	−0.04270162530709
62	−0.03868734058247	−0.04005450621686	−0.04111084082966	−0.04300137395817
64	−0.03897370304850	−0.04034174698719	−0.04139873021552	−0.04329079599158
66	−0.03925068850610	−0.04061953159023	−0.04167710720147	−0.04357058065394
68	−0.03951889066919	−0.04088846297861	−0.04194658106667	−0.04384135039740
70	−0.03977884867150	−0.04114908821471	−0.04220770433339	−0.04410366923327
72	−0.04003105354924	−0.04140190517013	−0.04246097960538	−0.04435804982120
74	−0.04027595379026	−0.04164736825099	−0.04270686540664	−0.04460495951633
76	−0.04051396010621	−0.04188589331392	−0.04294578119083	−0.04484482555284
78	−0.04074544955467	−0.04211786190636	−0.04317811165879	−0.04507803950741
80	−0.04097076911452	−0.04234362493960	−0.04340421049570	−0.04530496115928

Table G.1: $m_{11}(L/a)$ for $s = 1$

L	$\theta = 0$	$\theta = \pi/5$	$\theta = 1$	$\theta = 2$
4	−0.02530487470840	−0.02594836643205	−0.02458035859759	−0.01277822078023
6	−0.02511783542320	−0.02487900490088	−0.02413644432010	−0.02028574367418
8	−0.02539775718447	−0.02580720748863	−0.02593758266267	−0.02503059173606
10	−0.02618327594328	−0.02703305305312	−0.02759456265080	−0.02794475826547
12	−0.02713072167434	−0.02819839858635	−0.02896237579383	−0.02990378290677
14	−0.02807868505709	−0.02925489198441	−0.03012105695187	−0.03137339247829
16	−0.02897331750031	−0.03020879120608	−0.03113218794652	−0.03256608081819
18	−0.02980268155839	−0.03107399805811	−0.03203266532807	−0.03358189374225
20	−0.03056878603346	−0.03186366644596	−0.03284575292157	−0.03447306407099
22	−0.03127754716850	−0.03258890344322	−0.03358742478507	−0.03527019074532
24	−0.03193543494407	−0.03325884154718	−0.03426938485194	−0.03599301569882
26	−0.03254843459899	−0.03388095858471	−0.03490058269072	−0.03665522348488
28	−0.03312179201600	−0.03446139966766	−0.03548806131012	−0.03726680439711
30	−0.03366001788103	−0.03500524844454	−0.03603748038794	−0.03783533535407
32	−0.03416696920953	−0.03551674334384	−0.03655346302200	−0.03836673236848
34	−0.03464594533032	−0.03599944665191	−0.03703983694692	−0.03886572166910
36	−0.03509977735406	−0.03645637606881	−0.03749980813831	−0.03933614979087
38	−0.03553090530374	−0.03689010726425	−0.03793608896653	−0.03978119596144
40	−0.03594144250873	−0.03730285424665	−0.03835099472384	−0.04020352235277
42	−0.03633322864851	−0.03769653277931	−0.03874651755845	−0.04060538326786
44	−0.03670787324672	−0.03807281080001	−0.03912438392491	−0.04098870630417
46	−0.03706679133343	−0.03843314882077	−0.03948609979391	−0.04135515386782
48	−0.03741123275660	−0.03877883254929	−0.03983298663309	−0.04170617058596
50	−0.03774230636418	−0.03911099942790	−0.04016621033528	−0.04204302039192
52	−0.03806100004396	−0.03943066037963	−0.04048680469234	−0.04236681591243
54	−0.03836819741072	−0.03973871774971	−0.04079569060472	−0.04267854202615
56	−0.03866469177054	−0.04003598020446	−0.04109369192384	−0.04297907494688
58	−0.03895119786449	−0.04032317518028	−0.04138154861154	−0.04326919782736
60	−0.03922836179282	−0.04060095934605	−0.04165992774390	−0.04354961362710
62	−0.03949676944140	−0.04086992744468	−0.04192943276953	−0.04382095580692
64	−0.03975695366919	−0.04113061980383	−0.04219061134419	−0.04408379728072
66	−0.04000940046593	−0.04138352874756	−0.04244396199657	−0.04433865795777
68	−0.04025455424986	−0.04162910409534	−0.04268993982814	−0.04458601113616
70	−0.04049282244414	−0.04186775789909	−0.04292896141045	−0.04482628895295
72	−0.04072457944541	−0.04209986854096	−0.04316140901136	−0.04505988705442
74	−0.04095017007794	−0.04232578429210	−0.04338763425788	−0.04528716861777
76	−0.04116991261085	−0.04254582641513	−0.04360796132307	−0.04550846783007
78	−0.04138410140237	−0.04276029187828	−0.04382268970946	−0.04572409291063
80	−0.04159300922494	−0.04296945573809	−0.04403209668867	−0.04593432874724

Table G.2: $m_{11}(L/a)$ for $s = -1$

L/a	$s=1$	$s=0$	$s=-1$
4	0.59867564635006385	0.52976131887602069	0.51922066331094546
5	0.62117136258700821	0.56468083125839683	0.55461713132090261
6	0.64113765437070799	0.59321232599981455	0.58442701843014381
7	0.65893111142441375	0.61737811787009622	0.60974739393470162
8	0.67488327354469054	0.63824441829314597	0.63153838271523941
9	0.68928647150162301	0.65654153428089878	0.65057003087364097
10	0.70238903864308802	0.67280038634701944	0.66742121983892173
11	0.71439398959413626	0.68741301652316919	0.68252028857956904
12	0.72546473348301643	0.70067317431899355	0.69618664881505825
13	0.73573276395961912	0.71280479111934452	0.70866242179288317
14	0.74530462655573632	0.72398165609402260	0.72013453722120221
15	0.75426748654695955	0.73434096296455847	0.73074988732724165
16	0.76269338777455524	0.74399271936483262	0.74062578372376441
17	0.77064247215528033	0.75302638176979129	0.74985728431314708
18	0.77816541775427566	0.76151561542170611	0.75852242009405113
19	0.78530529883645214	0.76952176876897567	0.76668599155622038
20	0.79209901867921951	0.77709645174594405	0.77440237357962767
21	0.79857842470262715	0.78428347860819714	0.78171762080518526
22	0.80477118528362614	0.79112035275707051	0.78867107103739184
23	0.81070148601313597	0.79763941632436668	0.79529658268786343
24	0.81639058776392414	0.80386875084304289	0.80162350146808351
25	0.82185727793917046	0.80983289063631291	0.80767742403345886
26	0.82711823835863092	0.81555339356121976	0.81348080743360567
27	0.83218834749448024	0.82104930186717609	0.81905346010774183
28	0.83708093056087357	0.82633751751530950	0.82441294090339149
29	0.84180796784671203	0.83143311025949667	0.82957488596710694
30	0.84638026935694360	0.83634957239642928	0.83455327855159342
31	0.85080762207365805	0.84109903085829275	0.83936067325760364
32	0.85509891481710033	0.84569242491756803	0.84400838361422786
33	0.85926224466335029	0.85013965596714345	0.84850663994188621
34	0.86330500808698590	0.85444971446735487	0.85286472295855835
35	0.86723397937992463	0.85863078810432712	0.85709107745685024
36	0.87105537841668160	0.86269035439316518	0.86119340950763814
37	0.87477492945292666	0.86663526032990589	0.86517876996699599
38	0.87839791234295844	0.87047179120264344	0.86905362653451155
39	0.88192920731676446	0.87420573028207099	0.87282392619177697
40	0.88537333426399287	0.87784241080234770	0.87649514951940602
41	0.88873448731299464	0.88138676139487858	0.88007235812526203
42	0.89201656536325291	0.88484334593899240	0.88356023620527862
43	0.89522319912792745	0.88821639863152864	0.88696312708410143
44	0.89835777515201167	0.89150985494698484	0.89028506544613721
45	0.90142345720374637	0.89472737905126752	0.89352980585123832
46	0.90442320537524014	0.89787238814607281	0.89670084803647420
47	0.90735979318226442	0.90094807414573837	0.89980145942895982
48	0.91023582290682148	0.90395742302994047	0.90283469523001835
49	0.91305373939615786	0.90690323216425240	0.90580341637673730
50	0.91581584250088787	0.90978812583979161	0.90871030564770146
51	0.91852429830862484	0.91261456924592534	0.91155788213294810
52	0.92118114931205926	0.91538488106299742	0.91434851426796011
53	0.92378832362922261	0.91810124483365024	0.91708443159609367
54	0.92634764338015540	0.92076571925410400	0.91976773540748381

Table G.3: The one loop coefficient, $m_{1,0}(L/a)$ for $s = 1, 0, -1$. Last digits may be ruined

Appendix H

Simulation results

Our measurements of the running coupling $\bar{g}^2(L/a)$ and the variable $\bar{v}(L/a)$ are presented in the table below. The data shown contain the following information,

- **Time:** Time it took for the simulation to run
- $\boldsymbol{\beta}$**:** Value of the bare coupling, β.
- **Prcs:** Number of processors used in the simulation.
- **Machine:** Name of the machine used in the simulation.
- **Stats:** Number of measurements performed.
- **Term:** Number of measurements needed for the system to thermalise.
- $\mathbf{P^1_{Ac}}$**:** Probability of acceptance, computed as $\langle \min\{1, e^{-\Delta H}\}\rangle$.
- $\mathbf{P^2_{Ac}}$**:** Probability of acceptance, computed by counting the number of times the Metropolis step accepted the change.
- $\bar{\mathbf{g}}^{\mathbf{2}}$**:** Best estimate for the observable $\bar{g}^2(L/a)$ and its error.
- $\mathbf{dd}\bar{\mathbf{g}}^{\mathbf{2}}$**:** Statistical error of the error in $\bar{g}^2(L/a)$.
- $\boldsymbol{\tau}_{\mathbf{int}}$**:** Integrated autocorrelation time in the computation of $\bar{g}^2(L/a)$.
- $\bar{\mathbf{v}}$**:** Best estimate for the observable $\bar{v}^2(L/a)$ and its error.
- $\mathbf{dd}\bar{\mathbf{v}}$**:** Statistical error of the error in $\bar{v}(L/a)$
- $\boldsymbol{\tau}_{\mathbf{int}}$**:** Integrated autocorrelation time in the computation of $\bar{v}(L/a)$.

4x4x4x3, $N = 20, \epsilon = 0.025$

Time	β	Prcs	Machine	Stats	Term	P^1_{Ac}	P^2_{Ac}	$\bar{g}^2$	$dd\bar{g}^2$	τ_{int}	$\bar{v}$	$dd\bar{v}$	τ_{int}
—	5.1	1	Bishma	17914	50/100	0.9204(3)	0.9173	-611(2029)	120	9.9(1.1)	0.0358(30)	1.3E-04	5.04(42)
—	5.2	1	Bishma	1937	50/100	0.9469(3)	0.9428	27(11)	1.9	12.4(3.6)	0.0643(94)	1.1E-04	5.2(1.1)
3.01h	5.3	1	Vindaloo	60000	50/100	0.9584(4)	0.9598	14.19(81)	4.3E-02	25.0(2.4)	0.0580(19)	5.2E-05	5.97(31)
2.79h	5.4	1	Vindaloo	60000	50/100	0.9637(2)	0.9628	8.09(29)	1.6E-02	27.8(2.0)	0.0726(21)	6.4E-05	7.11(40)
3.52h	5.5	1	Vindaloo	60000	50/100	0.9652(2)	0.9655	5.59(12)	5.7E-03	21.5(1.5)	0.0857(21)	6.5E-05	7.08(40)
2.55h	5.6	1	Vindaloo	60000	50/100	0.9660(2)	0.9658	4.529(66)	3.0E-03	17.5(1.0)	0.0919(24)	7.7E-05	8.24(50)
2.45h	5.7	1	Vindaloo	60000	50/100	0.9668(2)	0.9679	3.929(43)	1.8E-03	13.9(34)	0.1042(25)	8.5E-05	8.90(56)
2.38h	5.8	1	Vindaloo	60000	50/100	0.9670(2)	0.9674	3.470(21)	6.1E-04	6.29(23)	0.1056(27)	9.1E-05	9.18(58)
2.32h	5.9	1	Vindaloo	60000	50/100	0.9673(2)	0.9670	3.133(15)	3.8E-04	4.80(23)	0.1117(26)	8.9E-05	9.02(57)
4.55h	6.0	1	Vindaloo	60000	50/100	0.9670(2)	0.9672	2.927(13)	3.2E-04	4.50(21)	0.1188(28)	1.0E-04	9.91(65)
2.96h	6.1	1	Vindaloo	60000	50/100	0.9670(2)	0.9677	2.735(11)	2.5E-04	4.05(18)	0.1226(27)	9.2E-05	8.86(55)
2.18h	6.2	1	Vindaloo	60000	50/100	0.9665(2)	0.9664	2.5793(94)	2.2E-04	4.08(18)	0.1211(28)	9.1E-05	8.58(53)
2.14h	6.3	1	Vindaloo	60000	50/100	0.9666(2)	0.9668	2.4410(79)	1.8E-05	3.62(15)	0.1270(30)	1.0E-04	9.69(63)
3.25h	6.4	1	Vindaloo	60000	50/100	0.9662(2)	0.9663	2.3162(69)	1.5E-04	3.36(14)	0.1308(30)	1.0E-04	9.42(61)
2.11h	6.5	1	Vindaloo	60000	50/100	0.9655(2)	0.9658	2.2061(61)	1.3E-04	3.15(13)	0.1367(30)	1.0E-04	8.93(56)
3.81h	6.6	1	Bishma	60000	50/100	0.9653(2)	0.9660	2.1083(56)	1.2E-04	3.16(13)	0.1408(33)	1.2E-04	10.35(69)
4.28h	6.7	1	Bishma	60000	50/100	0.9651(2)	0.9650	2.0268(51)	1.1E-04	3.08(12)	0.1423(33)	1.2E-04	10.30(68)
3.17h	6.8	1	Bishma	60000	50/100	0.9650(2)	0.9641	1.9446(46)	9.5E-05	2.98(12)	0.1389(34)	1.2E-04	10.22(68)
2.07h	6.9	1	Bishma	60000	50/100	0.9642(2)	0.9631	1.8682(41)	8.3E-05	2.77(11)	0.1383(31)	1.0E-04	8.55(53)
2.05h	7.0	1	Bishma	60000	50/100	0.9641(2)	0.9647	1.8078(38)	7.8E-05	2.75(10)	0.1461(33)	1.1E-04	9.22(59)
2.01h	7.2	1	Bishma	60000	50/100	0.9632(2)	0.9630	1.6891(33)	6.3E-05	2.533(93)	0.1514(33)	1.1E-04	9.12(58)
1.98h	7.4	1	Bishma	60000	50/100	0.9627(2)	0.9631	1.5881(29)	5.6E-05	2.528(92)	0.1512(34)	1.2E-04	9.32(60)
1.98h	7.6	1	Bishma	60000	50/100	0.9619(2)	0.9614	1.4941(25)	4.6E-05	2.328(81)	0.1516(35)	1.1E-04	9.02(57)
1.96h	7.8	1	Bishma	60000	50/100	0.9613(2)	0.9620	1.4165(21)	3.7E-05	2.082(69)	0.1534(34)	1.1E-04	8.18(49)
1.84h	8.0	1	Vindaloo	60000	50/100	0.9605(2)	0.9600	1.3463(20)	3.8E-05	2.265(79)	0.1615(39)	1.4E-04	9.93(65)
1.82h	8.2	1	Vindaloo	60000	50/100	0.9599(2)	0.9595	1.2832(17)	3.1E-05	2.025(67)	0.1620(37)	1.2E-04	8.67(54)
1.81h	8.4	1	Vindaloo	60000	50/100	0.9592(2)	0.9597	1.2254(15)	2.6E-05	1.910(62)	0.1687(39)	1.3E-04	9.21(58)
1.79h	8.6	1	Vindaloo	60000	50/100	0.9585(2)	0.9579	1.1739(14)	2.4E-05	1.887(61)	0.1632(38)	1.2E-04	8.57(53)
1.78h	8.8	1	Vindaloo	60000	50/100	0.9583(2)	0.9577	1.1270(13)	2.2E-05	1.857(58)	0.1615(36)	1.1E-04	7.71(83)
1.77h	9.0	1	Vindaloo	60000	50/100	0.9579(2)	0.9575	1.0837(12)	1.9E-05	1.723(52)	0.1588(35)	1.1E-04	7.04(40)
1.75h	9.3	1	Vindaloo	60000	50/100	0.9572(2)	0.9567	1.0247(10)	1.7E-05	1.624(50)	0.1693(38)	1.2E-04	7.90(47)
3.90h	9.6	1	Vindaloo	60000	50/100	0.9564(2)	0.9565	0.97205(91)	1.4E-05	1.519(45)	0.1702(37)	1.1E-04	7.02(40)
4.21h	10.0	1	Vindaloo	64818	50/100	0.9559(2)	0.9566	0.90930(74)	1.0E-05	1.368(36)	0.1690(34)	9.4E-05	6.12(32)
3.74h	10.3	1	Bishma	60000	50/100	0.9553(2)	0.9559	0.86924(71)	7.2E-06	1.395(40)	0.1614(33)	8.9E-05	5.24(26)
3.72h	10.6	1	Bishma	60000	50/100	0.9549(2)	0.9557	0.83111(64)	9.2E-06	1.303(36)	0.1690(34)	9.4E-05	6.12(32)
2.94h	11.0	1	Bishma	60000	50/100	0.9541(2)	0.9542	0.78711(56)	7.7E-06	1.182(31)	0.1775(34)	9.3E-05	5.18(26)
1.75h	11.3	1	Bishma	60000	50/100	0.9534(2)	0.9526	0.75566(51)	7.0E-06	1.162(31)	0.1759(35)	9.4E-05	5.25(26)
1.74h	11.6	1	Bishma	60000	50/100	0.9533(2)	0.9540	0.72669(47)	6.3E-06	1.145(29)	0.1751(36)	9.4E-05	5.14(25)
1.75h	11.2	1	Bishma	60000	50/100	0.9538(2)	0.9534	0.76490(53)	7.4E-06	1.218(32)	0.1763(35)	9.4E-05	5.18(26)

Table H.1: Simulation data for a 4x4x4x3 lattice.

6x6x6x5, $N = 25, \epsilon = 0.02$

Time	β	Prcs	Machine	Stats	Term	P^1_{Ac}	P^2_{Ac}	$\bar{g}^2$	$dd\bar{g}^2$	τ_{int}	$\bar{v}$	$dd\bar{v}$	τ_{int}
38h	5.3	4	Lond/Iit	72769	50/100	0.8717(12)	0.875	9.87(45)	2.4E-02	31.0(3.0)	0.0578(29)	9.9E-05	11.25(72)
34.87h	5.4	4	Lonsdale	149299	50/100	0.9085(3)	0.909	6.76(15)	6.0E-03	32.5(2.4)	0.0733(22)	5.9E-05	12.89(64)
32.10h	5.5	4	Lonsdale	160000	50/50	0.9222(3)	0.922	5.500(92)	3.4E-03	29.3(2.0)	0.0832(23)	6.2E-05	13.87(69)
9.92h	5.6	4	Lonsdale	60000	200/100	0.9288(4)	0.931	4.389(48)	1.6E-03	8.40(51)	0.0968(34)	1.3E-04	11.35(79)
9.14h	5.7	4	Lonsdale	60000	50/50	0.9328(4)	0.933	3.935(43)	1.5E-03	9.48(61)	0.0991(39)	1.6E-04	13.5(1.0)
8.56h	5.8	4	Lonsdale	60000	50/50	0.9351(3)	0.936	3.579(31)	9.8E-04	7.66(45)	0.1063(39)	1.5E-04	12.86(94)
8.07h	5.9	4	Lonsdale	60000	50/50	0.9373(3)	0.938	3.247(27)	8.5E-04	7.87(47)	0.1074(41)	1.7E-04	13.9(1.0)
7.72h	6.0	4	Lonsdale	60000	50/50	0.9379(3)	0.939	3.063(22)	6.6E-04	6.79(38)	0.1207(44)	1.9E-04	15.2(1.2)
7.34h	6.1	4	Lonsdale	60000	50/50	0.9386(3)	0.939	2.855(19)	5.5E-04	6.48(35)	0.1239(46)	2.0E-04	16.2(1.3)
7.03h	6.2	4	Lonsdale	60000	50/50	0.9320(3)	0.941	2.725(18)	5.1E-04	6.56(36)	0.1325(45)	1.9E-04	14.8(1.1)
6.86h	6.3	4	Lonsdale	60000	50/50	0.9397(3)	0.941	2.561(15)	4.3E-04	6.12(33)	0.1289(47)	2.0E-04	15.3(1.2)
6.54h	6.4	4	Lonsdale	60000	50/50	0.9397(3)	0.940	2.368(12)	3.3E-04	5.40(27)	0.1441(50)	2.2E-04	16.4(1.3)
6.50h	6.5	4	Lonsdale	60000	50/50	0.9393(3)	0.941	2.291(11)	3.1E-04	5.33(27)	0.1331(50)	2.2E-04	16.1(1.3)
6.31h	6.6	4	Lonsdale	60000	50/50	0.9388(3)	0.940	2.226(11)	3.1E-04	5.69(29)	0.1377(51)	2.2E-04	16.3(1.3)
6.03h	6.8	4	Lonsdale	60000	50/50	0.9384(3)	0.932	2.0262(88)	2.3E-04	4.98(24)	0.1433(51)	2.2E-04	15.4(1.2)
5.79h	7.0	4	Lonsdale	60000	50/50	0.9380(3)	0.940	1.8857(77)	2.0E-04	4.84(23)	0.1529(57)	2.6E-04	18.3(1.6)
5.67h	7.2	4	Lonsdale	60000	50/50	0.9367(3)	0.938	1.7547(67)	1.7E-04	4.79(23)	0.1443(53)	2.3E-04	15.3(1.2)
5.47h	7.4	4	Lonsdale	60000	50/50	0.9354(3)	0.937	1.6505(59)	1.5E-04	4.58(21)	0.1526(58)	2.6E-04	17.2(1.8)
5.35h	7.6	4	Lonsdale	60000	50/50	0.9347(3)	0.936	1.5518(51)	1.2E-04	4.29(20)	0.1536(54)	2.2E-04	14.4(1.1)
5.23h	7.8	4	Lonsdale	60000	50/50	0.9344(3)	0.937	1.4691(46)	1.1E-04	4.17(19)	0.1541(53)	2.2E-04	13.8(1.0)
5.12h	8.0	4	Lonsdale	60000	50/50	0.9334(3)	0.935	1.3942(40)	9.3E-05	3.84(17)	0.1601(61)	2.7E-04	16.7(1.4)
5.05h	8.2	4	Lonsdale	60000	50/50	0.9323(3)	0.934	1.3286(36)	8.3E-05	3.69(16)	0.1513(59)	2.5E-04	14.9(1.2)
4.95h	8.4	4	Lonsdale	60000	50/50	0.9314(3)	0.9327	1.2621(32)	7.3E-05	3.57(15)	0.1625(63)	2.7E-04	16.1(1.3)
4.90h	8.6	4	Lonsdale	60000	50/50	0.9306(3)	0.9321	1.2114(30)	6.6E-05	3.50(15)	0.1656(59)	2.5E-04	14.7(1.1)
4.83h	8.8	4	Lonsdale	60000	50/50	0.9296(3)	0.9307	1.1624(27)	5.9E-05	3.32(14)	0.1574(58)	2.4E-04	13.7(1.0)
4.77h	9.0	4	Lonsdale	60000	50/50	0.9294(3)	0.9310	1.1161(25)	5.3E-05	3.17(13)	0.1680(58)	2.3E-04	12.85(94)
4.90h	9.2	4	Iitac	60000	50/50	0.9283(3)	0.9290	1.0759(23)	5.0E-05	3.18(13)	0.1632(60)	2.4E-04	13.5(1.0)
4.67h	9.3	4	Lonsdale	60000	50/50	0.9279(3)	0.9302	1.0544(23)	4.9E-05	3.25(13)	0.1638(60)	2.4E-04	12.96(96)
4.61h	9.6	4	Lonsdale	60000	50/50	0.9275(4)	0.9292	0.9964(19)	3.9E-05	2.86(11)	0.1753(66)	2.8E-04	14.8(1.2)
4.69h	9.8	4	Lonsdale	60000	50/50	0.9273(4)	0.9283	0.9638(18)	3.8E-05	2.90(11)	0.1545(58)	2.2E-04	11.36(79)
4.51h	10.0	4	Lonsdale	60000	50/50	0.9265(4)	0.9278	0.9335(17)	3.4E-05	2.72(10)	0.1709(57)	2.1E-04	11.21(77)
4.48h	10.3	4	Lonsdale	60000	50/50	0.9260(4)	0.9286	0.8914(16)	3.2E-05	2.82(11)	0.1656(59)	2.2E-04	11.21(77)
5.00h	10.4	4	Iitac	60000	50/50	0.9255(4)	0.9270	0.8756(16)	3.2E-05	2.72(10)	0.1647(59)	2.1E-04	10.23(70)
4.43h	10.6	4	Lonsdale	60000	50/50	0.9250(4)	0.9269	0.8499(14)	2.8E-05	2.60(95)	0.1620(57)	2.0E-04	10.00(66)
4.38h	11.0	4	Lonsdale	60000	50/50	0.9241(4)	0.9261	0.8027(13)	2.5E-05	2.545(93)	0.1674(59)	2.1E-04	10.08(67)
5.00h	11.2	4	Iitac	60000	50/50	0.9244(4)	0.9260	0.7820(12)	2.3E-05	2.427(87)	0.1739(59)	2.1E-04	9.60(63)
4.33h	11.3	4	Lonsdale	60000	50/50	0.9237(4)	0.9253	0.7714(11)	2.1E-05	2.322(81)	0.1701(60)	2.1E-04	10.08(67)
4.28h	11.6	4	Lonsdale	60000	50/50	0.9226(4)	0.9233	0.7434(11)	2.0E-05	2.300(80)	0.1711(60)	2.1E-04	9.79(64)
4.25h	12.0	4	Lonsdale	60000	50/50	0.9215(4)	0.9230	0.70731(97)	1.8E-05	2.268(79)	0.1747(58)	2.0E-04	9.03(57)

Table H.2: Simulation data for a 6x6x6x5 lattice.

8x8x8x7, $N = 40, \epsilon = 0.0125$

Time	β	Prcs	Machine	Stats	Term	P^1_{Ac}	P^2_{Ac}	$\bar{g}^2$	$dd\bar{g}^2$	τ_{int}	$\bar{v}$	$dd\bar{v}$	τ_{int}
17.00h	5.5	16	Lonsdale	50579	100/100	0.9239(5)	0.9267	6.69(33)	2.2E-02	37.9(4.7)	0.0741(50)	2.3E-041	4.8(1.2)
16.99h	5.6	16	Lonsdale	60000	100/100	0.9374(3)	0.9372	5.21(15)	7.9E-03	25.9(2.6)	0.0900(52)	2.4E-041	8.3(1.6)
15.10h	5.7	16	Lonsdale	60000	100/100	0.9442(3)	0.944	4.222(59)	2.1E-03	10.05(66)	0.0953(48)	2.1E-041	5.3(1.2)
14.05h	5.8	16	Lonsdale	60000	100/100	0.9477(3)	0.947	3.811(56)	2.2E-03	12.85(94)	0.0938(59)	2.9E-042	0.9(1.9)
13.01h	5.9	16	Lonsdale	60000	100/100	0.9500(3)	0.949	3.699(75)	3.8E-03	23.3(2.2)	0.1034(56)	2.6E-041	8.9(1.6)
16.65h	5.9b	16	Lonsdale	60000	100/100	0.9495(3)	0.951	3.530(42)	1.5E-03	9.79(64)	0.1177(56)	2.6E-04	18.5(1.6)
12.19h	6.0	16	Lonsdale	60000	100/100	0.9516(3)	0.952	3.220(33)	1.1E-03	8.77(54)	0.1033(56)	2.6E-041	8.5(1.6)
11.52h	6.1	16	Lonsdale	60000	100/100	0.9524(2)	0.952	3.090(32)	1.1E-03	9.48(61)	0.1203(63)	3.1E-042	1.8(2.0)
11.04h	6.2	16	Lonsdale	60000	100/100	0.9529(2)	0.953	2.898(27)	8.7E-04	8.25(50)	0.1257(60)	2.9E-042	0.3(1.8)
10.57h	6.3	16	Lonsdale	60000	100/100	0.9533(2)	0.953	2.725(24)	7.9E-04	8.46(52)	0.1173(63)	3.1E-042	1.1(1.9)
10.09h	6.4	16	Lonsdale	60000	100/100	0.9534(2)	0.953	2.551(22)	7.5E-04	9.01(57)	0.1303(64)	3.1E-042	0.7(1.9)
9.90h	6.5	16	Lonsdale	60000	100/100	0.9534(2)	0.9525	2.417(19)	6.4E-04	8.58(53)	0.1233(63)	3.0E-041	9.5(1.7)
9.67h	6.6	16	Lonsdale	60000	100/100	0.9535(2)	0.9534	2.316(17)	5.6E-04	7.94(47)	0.1269(63)	3.0E-041	9.0(1.6)
9.36h	6.7	16	Lonsdale	60000	100/100	0.9538(2)	0.9533	2.230(16)	5.1E-04	7.74(46)	0.1221(67)	3.3E-042	0.7(1.9)
9.06h	6.8	16	Lonsdale	60000	100/100	0.9533(2)	0.9532	2.143(15)	4.6E-04	7.51(44)	0.1397(64)	3.0E-041	9.0(1.6)
8.89h	6.9	16	Lonsdale	60000	100/100	0.9535(2)	0.9533	2.045(13)	4.0E-04	7.05(40)	0.1395(70)	3.4E-042	1.1(1.9)
8.78h	7.0	16	Lonsdale	60000	100/100	0.9527(2)	0.9533	1.917(13)	4.2E-04	8.05(48)	0.1436(76)	4.0E-042	4.2(2.3)
8.34h	7.2	16	Lonsdale	60000	100/100	0.9524(2)	0.9526	1.857(12)	3.6E-04	7.60(44)	0.1504(74)	3.7E-042	2.3(2.1)
8.10h	7.4	16	Lonsdale	60000	100/100	0.9517(2)	0.9511	1.7300(93)	2.7E-04	6.41(35)	0.1435(71)	3.4E-042	0.0(1.8)
7.92h	7.6	16	Lonsdale	60000	100/100	0.9509(2)	0.9515	1.6214(80)	2.3E-04	6.00(32)	0.1539(75)	3.7E-042	0.0(1.9)
7.65h	7.8	16	Lonsdale	60000	100/100	0.9507(2)	0.9505	1.5288(71)	2.0E-04	5.75(30)	0.1416(76)	3.6E-042	0.5(1.8)
7.50h	8.0	16	Lonsdale	60000	100/100	0.9501(2)	0.9507	1.4401(63)	1.7E-04	5.50(28)	0.1590(70)	3.1E-041	7.2(1.4)
4.45h	8.2	16	Lonsdale	60000	100/100	0.9493(2)	0.9493	1.3812(61)	1.7E-04	5.93(31)	0.1375(73)	3.3E-041	7.7(1.5)
7.24h	8.4	16	Lonsdale	60000	100/100	0.9486(2)	0.9486	1.315(54)	1.5E-04	5.47(28)	0.1528(85)	4.3E-042	2.6(2.1)
7.06h	8.6	16	Lonsdale	60000	100/100	0.9483(3)	0.9475	1.2447(46)	1.2E-04	4.95(24)	0.1552(81)	3.8E-041	9.4(1.7)
7.01h	8.8	16	Lonsdale	60000	100/100	0.9479(3)	0.9494	1.1963(44)	1.1E-04	4.97(24)	0.1627(73)	3.2E-041	5.9(1.3)
6.92h	9.0	16	Lonsdale	60000	100/100	0.9474(3)	0.9468	1.1476(39)	1.0E-04	4.69(22)	0.1525(78)	3.5E-041	7.4(1.5)
6.79h	9.3	16	Lonsdale	60000	100/100	0.9470(3)	0.9457	1.0823(37)	9.6E-05	5.01(24)	0.1553(79)	3.6E-041	7.2(1.4)
6.69h	9.6	16	Lonsdale	60000	100/100	0.9463(3)	0.9461	1.0302(33)	8.4E-05	4.69(22)	0.1525(75)	3.2E-041	5.3(1.2)
6.50h	10.0	16	Lonsdale	60000	100/100	0.9454(3)	0.9442	0.9584(28)	6.9E-05	4.32(20)	0.1625(79)	3.4E-041	5.5(1.2)
6.49h	10.3	16	Lonsdale	60000	100/100	0.9452(3)	0.9446	0.9145(26)	6.2E-05	4.23(19)	0.1586(77)	3.2E-041	4.1(1.1)
6.40h	10.6	16	Lonsdale	60000	100/100	0.9451(3)	0.9439	0.8665(22)	5.2E-05	3.89(17)	0.1785(81)	3.4E-041	5.0(1.2)
6.29h	11.0	16	Lonsdale	60000	100/100	0.9445(3)	0.9447	0.8233(20)	4.6E-05	3.71(16)	0.1706(83)	3.5E-041	4.7(1.1)
6.26h	11.3	16	Lonsdale	60000	100/100	0.9436(3)	0.9442	0.7857(19)	4.3E-05	3.74(16)	0.1606(80)	3.2E-041	3.21(98)
6.14h	11.6	16	Lonsdale	60000	100/100	0.9431(3)	0.9428	0.7553(17)	3.7E-05	3.40(14)	0.1683(78)	3.1E-041	2.76(93)
6.14h	12.0	16	Lonsdale	60000	100/100	0.9423(3)	0.9412	0.7186(15)	3.3E-05	3.27(13)	0.1527(77)	3.0E-041	2.11(87)

Table H.3: Simulation data for a 8x8x8x7 lattice.

12x12x12x11 $N = 50, \epsilon = 0.01$

Time	$\boldsymbol{\beta}$	**Prcs**	**Machine**	**Stats**	**Term**	$\mathbf{P^1_{Ac}}$	$\mathbf{P^2_{Ac}}$	$\bar{\mathbf{g}}^2$	$\mathbf{dd\bar{g}^2}$	τ_{int}	$\bar{\mathbf{v}}$	$\mathbf{dd\bar{v}}$	$\boldsymbol{\tau}_{\mathbf{int}}$
234.4h	5.8	32	Lonsdale	120000	100/300	0.8723(3)	0.8722	4.88(12)	4.9E-03	28.8(2.1)	0.0925(51)	1.8E-04	22.1(1.5)
185.2h	6.0	32	Lonsdale	120000	100/300	0.9100(3)	0.9102	3.757(59)	2.0E-03	18.1(1.1)	0.0908(50)	1.7E-04	19.6(1.3)
60.00h	6.2	32	Stokes	117106	100/300	0.9214(3)	0.9217	3.251(43)	1.4E-03	15.89(95)	0.0975(60)	2.3E-04	24.9(1.8)
55.89h	6.4	32	Stokes	120000	100/300	0.9257(3)	0.9259	2.860(31)	9.4E-04	13.91(78)	0.1133(63)	2.5E-04	26.8(2.5)
53.74h	6.6	32	Stokes	120000	200/300	0.9262(3)	0.9257	2.581(26)	7.8E-04	13.91(78)	0.1325(60)	2.2E-04	23.2(1.6)
49.48h	6.8	32	Stokes	120000	100/300	0.9271(3)	0.9270	2.361(21)	5.8E-04	12.05(64)	0.1235(62)	2.3E-04	22.9(1.6)
119.51h	7.0	32	Lonsdale	120000	100/300	0.9266(3)	0.9258	2.165(17)	4.9E-04	11.93(93)	0.1308(73)	3.0E-04	29.5(2.3)
40.00h	7.2	32	Stokes	105870	200/300	0.9262(3)	0.9256	1.970(15)	4.5E-04	11.51(63)	0.1494(76)	3.3E-04	27.8(2.2)
40.00h	7.4	32	Stokes	110582	200/300	0.9258(3)	0.9259	1.841(13)	3.7E-04	10.96(57)	0.1478(77)	3.3E-04	28.4(2.2)
40.00h	7.8	32	Stokes	117211	100/200	0.9240(3)	0.9240	1.6004(93)	2.4E-04	9.71(47)	0.1512(77)	3.1E-04	27.2(2.1)
99.58h	8.0	32	Lonsdale	120000	100/300	0.9230(3)	0.9222	1.5304(85)	2.1E-04	9.36(44)	0.1470(80)	3.4E-04	29.5(2.3)
37.85h	8.4	32	Stokes	120000	100/300	0.9215(3)	0.9207	1.3749(67)	1.6E-04	8.63(39)	0.1608(77)	3.0E-04	25.6(1.9)
37.17h	8.6	32	Stokes	120000	100/300	0.9211(3)	0.9220	1.3028(64)	1.6E-04	8.95(42)	0.1489(87)	3.7E-04	31.1(2.5)
88.06h	9.0	32	Lonsdale	120000	100/300	0.9200(3)	0.9203	1.1968(51)	1.2E-04	7.93(35)	0.1582(81)	3.2E-04	25.2(1.8)
35.40h	9.2	32	Stokes	120000	100/200	0.9191(3)	0.9191	1.1493(48)	1.1E-04	8.05(36)	0.1529(80)	3.1E-04	24.2(1.7)
34.59h	9.6	32	Stokes	120000	100/200	0.9182(3)	0.9189	1.0671(41)	9.9E-05	7.91(35)	0.1654(82)	3.1E-04	23.6(1.7)
34.20h	9.8	32	Stokes	120000	100/200	0.9182(3)	0.9170	1.0298(40)	9.3E-05	7.89(35)	0.1545(91)	3.7E-04	27.4(2.1)
33.68h	10.0	32	Stokes	120000	100/200	0.9179(3)	0.9179	0.9866(37)	8.6E-05	7.78(34)	0.1540(80)	2.9E-04	21.7(1.5)
33.11h	10.4	32	Stokes	120000	100/200	0.9171(3)	0.9171	0.9329(34)	7.8E-05	7.69(33)	0.1598(98)	3.6E-04	26.3(1.9)
38.51h	10.6	32	Stokes	120000	100/300	0.9168(3)	0.9159	0.9003(27)	5.3E-05	6.48(24)	0.1565(78)	2.7E-04	21.8(1.4)
78.00h	11.0	32	Lonsdale	120000	100/300	0.9154(3)	0.9152	0.8510(27)	5.7E-05	6.57(27)	0.1340(85)	3.1E-04	21.4(1.4)
35.38h	11.2	32	Stokes	140000	100/300	0.9151(3)	0.9141	0.8200(24)	5.1E-05	7.21(28)	0.1697(84)	3.0E-04	23.8(1.6)
36.58h	11.6	32	Stokes	140000	100/300	0.9143(3)	0.9138	0.7747(21)	4.1E-05	6.26(23)	0.1544(82)	2.8E-04	21.3(1.3)
75.00h	12.0	32	Lonsdale	120000	100/300	0.9127(3)	0.9128	0.7429(20)	4.0E-05	5.64(21)	0.1650(90)	3.3E-04	21.4(1.4)

Table H.4: Simulation data for a 12x12x12x11 lattice.

16x16x16x15 $N = 50\epsilon = 0.01$

Time	$\boldsymbol{\beta}$	**Prcs**	**Machine**	**Stats**	**Term**	$\mathbf{P^1_{Ac}}$	$\mathbf{P^2_{Ac}}$	$\bar{\mathbf{g}}^2$	$\mathbf{dd\bar{g}^2}$	τ_{int}	$\bar{\mathbf{v}}$	$\mathbf{dd\bar{v}}$	$\boldsymbol{\tau}_{\mathbf{int}}$
131.59h	5.9	2048	BG	160000	200/400	0.8097(3)	0.8104	4.69(10)	3.5E-03	24.0(1.5)	0.0921(64)	2.4E-04	31.3(2.2)
87.5h	6.1	2048	BG 36h	160000	400/500	0.7278(3)	0.7259	4.016(99)	4.0E-03	25.2(1.9)	0.1023(75)	3.2E-04	28.2(2.2)
71.5h	6.3	2048	BG 36h	145567	400/400	0.8013(3)	0.8022	3.303(58)	2.0E-03	23.7(1.5)	0.1153(77)	3.3E-04	36.8(2.9)
63.8h	6.6	2048	BG 36h	160000	200/300	0.8268(4)	0.8281	2.971(41)	1.3E-03	20.1(1.2)	0.1022(69)	2.6E-04	32.0(2.3)
48.0h	7.0	256	Stokes	144505	300/300	0.8582(4)	0.8598	2.277(25)	7.8E-04	17.7(1.0)	0.1324(84)	3.5E-04	35.4(2.7)
72.7h	7.6	1024	BG 24h	160000	200/300	0.8606(4)	0.8630	1.844(16)	4.6E-04	16.64(89)	0.1427(82)	3.2E-04	33.5(2.4)
46.5h	8.4	2048	BG	165000	300/300	0.8564(4)	0.8555	1.4230(89)	2.2E-04	12.91(61)	0.1441(90)	3.6E-04	36.2(2.7)
63.2h	9.0	1024	BG	160000	200/200	0.8530(3)	0.8539	1.2377(72)	1.8E-04	12.82(61)	0.1417(95)	3.8E-04	34.9(2.6)
138.8h	10.0	2048	BG 36h	160000	200/300	0.8086(4)	0.8097	1.0344(57)	1.8E-04	12.45(63)	0.164(12)	3.2E-04	28.2(2.2)
489.33h	11.0	2048	BG mix	160000	200/300	0.8453(4)	0.8459	0.8729(35)	7.8E-05	9.86(42)	0.182(11)	4.2E-04	34.8(2.5)
53.2h	12.0	1024	BG 1h	162000	200/300	0.8396(5)	0.8365	0.7547(26)	5.8E-05	9.06(37)	0.1591(97)	3.4E-04	25.6(1.6)

Table H.5: Simulation data for a 16x16x16x15 lattice.

4x4x4x5, $N = 20, \epsilon = 0.025$

Time	β	Prcs	Machine	Stats	Term	P^1_{Ac}	P^2_{Ac}	$\bar{g}^2$	$dd\bar{g}^2$	τ_{int}	$\bar{v}$	$dd\bar{v}$	τ_{int}
8.33h	5.0	1	Madras	60000	50/100	0.9303(5)	0.9306	4.979(89)	3.1E-03	9.94(65)	0.1173(31)	8.6E-05	5.99(32)
7.46h	5.1	1	Madras	60000	50/100	0.9399(3)	0.9406	4.207(46)	1.2E-03	5.58(28)	0.1263(30)	8.1E-05	5.51(28)
6.84h	5.2	1	Madras	60000	50/100	0.9443(3)	0.9438	3.758(37)	9.8E-04	5.21(26)	0.1354(32)	9.2E-05	6.15(33)
6.53h	5.3	1	Madras	60000	50/100	0.9460(3)	0.9458	3.438(28)	7.1E-04	4.53(21)	0.1386(32)	8.7E-05	5.62(29)
6.24h	5.4	1	Madras	60000	50/100	0.9472(3)	0.9475	3.145(23)	5.3E-04	3.97(18)	0.1539(31)	8.5E-05	5.40(27)
10.03h	5.5	1	Madras	60000	50/100	0.9479(3)	0.9478	2.981(19)	4.0E-04	3.33(14)	0.1491(30)	7.6E-05	4.72(23)
10.28h	5.6	1	Vindaloo	60000	50/100	0.9478(3)	0.9482	2.793(17)	3.9E-04	3.56(15)	0.1559(33)	8.8E-05	5.39(27)
9.97h	5.7	1	Vindaloo	60000	50/100	0.9475(3)	0.9478	2.607(15)	3.1E-04	3.20(13)	0.1636(33)	8.8E-05	5.30(26)
10.26h	5.8	1	Bishma	60000	50/100	0.9476(3)	0.9474	2.501(13)	2.7E-04	3.02(12)	0.1669(34)	9.0E-05	5.20(26)
9.95h	5.9	1	Bishma	60000	50/100	0.9470(3)	0.9479	2.368(12)	2.6E-04	3.12(12)	0.1696(34)	9.0E-05	5.20(26)
7.83h	6.0	1	Vindaloo	50000	50/100	0.9472(3)	0.9477	2.273(12)	2.6E-04	2.86(12)	0.1646(38)	1.1E-04	5.39(30)
8.27h	6.1	1	Vindaloo	60000	50/100	0.9466(3)	0.9476	2.1769(98)	1.9E-04	2.72(10)	0.1763(36)	9.8E-05	5.44(27)
4.45h	6.2	1	Vindaloo	60000	50/100	0.9461(3)	0.9468	2.0918(90)	1.8E-04	2.616(98)	0.1795(37)	1.0E-05	5.58(28)
4.38h	6.3	1	Vindaloo	60000	50/100	0.9451(3)	0.9450	2.0004(81)	1.5E-04	2.456(88)	0.1789(39)	1.1E-05	5.96(31)
4.32h	6.4	1	Vindaloo	60000	50/100	0.9451(3)	0.9440	1.9396(79)	1.5E-04	2.545(93)	0.1827(39)	1.1E-05	5.58(28)
4.28h	6.5	1	Vindaloo	60000	50/100	0.9446(3)	0.9454	1.8717(72)	1.4E-04	2.469(88)	0.1831(40)	1.1E-05	5.70(29)
5.29h	6.6	1	Vindaloo	60000	50/100	0.9447(3)	0.9449	1.8090(67)	1.3E-04	2.361(84)	0.1890(40)	1.0E-05	5.38(27)
8.41h	6.7	1	Vindaloo	60000	50/100	0.9433(3)	0.9448	1.7424(62)	1.2E-04	2.320(81)	0.1921(34)	1.1E-05	5.37(27)
8.34h	6.8	1	Vindaloo	60000	50/100	0.9430(3)	0.9426	1.6945(59)	1.1E-04	2.254(79)	0.1879(38)	9.0E-04	5.02(24)
7.84h	6.9	1	Vindaloo	60000	50/50	0.9426(3)	0.9436	1.6462(57)	1.1E-04	2.277(79)	0.1945(39)	1.0E-04	5.02(24)
8.91h	7.0	1	Madrid	60000	50/100	0.9421(3)	0.9419	1.5903(51)	9.2E-05	2.110(72)	0.1861(40)	1.1E-04	5.14(25)
8.68h	7.2	1	Madrid	60000	50/100	0.9412(3)	0.9411	1.5045(48)	8.6E-05	2.164(74)	0.1970(42)	1.1E-04	5.16(25)
8.45h	7.4	1	Madrid	60000	50/100	0.9404(3)	0.9403	1.4413(42)	7.2E-05	1.960(63)	0.1906(43)	1.1E-04	5.26(26)
8.64h	7.6	1	Madrid	60000	50/100	0.9402(3)	0.9407	1.3654(38)	6.4E-05	1.870(60)	0.2068(42)	1.1E-04	4.88(23)
8.30h	7.8	1	Madrid	60000	50/50	0.9389(3)	0.9397	1.2906(34)	5.7E-05	1.836(57)	0.2090(43)	1.1E-04	4.82(23)
8.18h	8.0	1	Madrid	60000	50/50	0.9380(3)	0.9393	1.2404(31)	4.9E-05	1.713(52)	0.2033(43)	1.1E-04	4.60(22)
8.06h	8.2	1	Madrid	60000	50/50	0.9379(3)	0.9385	1.1920(29)	4.9E-05	1.746(55)	0.2047(45)	1.2E-04	4.77(23)
8.37h	8.4	1	Madrid	60000	50/50	0.9371(3)	0.9373	1.1464(27)	4.3E-05	1.668(51)	0.2177(44)	1.1E-04	4.50(21)
8.48h	8.6	1	Madrid	60000	50/50	0.9370(3)	0.9381	1.0997(25)	4.1E-05	1.645(50)	0.2033(45)	1.1E-04	4.52(21)
7.70h	8.8	1	Madrid	60000	50/50	0.9361(3)	0.9369	1.0570(22)	3.4E-05	1.483(42)	0.2080(45)	1.1E-04	4.42(20)
3.82h	9.0	1	Bishma	60000	50/50	0.9353(3)	0.9366	1.0266(22)	3.4E-05	1.551(46)	0.2071(45)	1.1E-04	4.24(19)
3.78h	9.3	1	Bishma	60000	50/50	0.9339(3)	0.9344	0.9749(20)	3.0E-05	1.466(42)	0.2041(44)	1.0E-04	3.89(17)
3.76h	9.6	1	Bishma	60000	50/50	0.9337(3)	0.9347	0.9243(17)	2.5E-05	1.352(37)	0.2089(46)	1.1E-04	3.98(18)
3.70h	10.0	1	Bishma	60000	50/50	0.9317(3)	0.9325	0.8701(15)	2.1E-05	1.255(33)	0.2080(45)	1.0E-04	3.68(16)
3.68h	10.3	1	Bishma	60000	50/50	0.9291(3)	0.9284	0.8368(14)	2.0E-05	1.239(32)	0.2172(46)	1.0E-04	3.68(16)
3.66h	10.6	1	Bishma	60000	50/50	0.9278(4)	0.9281	0.8034(13)	1.7E-05	1.144(29)	0.2114(43)	9.0E-05	3.12(12)
7.32h	11.0	1	Bishma	60000	50/50	0.9252(4)	0.9258	0.7582(12)	1.5E-05	1.133(28)	0.2166(47)	1.0E-05	3.45(14)
6.78h	11.3	1	Bishma	60000	50/50	0.9223(4)	0.9223	0.7292(11)	1.4E-05	1.095(27)	0.2134(43)	8.9E-05	2.88(11)
7.24h	11.6	1	Bishma	60000	50/50	0.9191(4)	0.9206	0.7047(10)	1.3E-05	1.044(25)	0.2124(45)	9.5E-05	3.04(12)
7.53h	12.0	1	Bishma	60000	50/50	0.9155(4)	0.9169	0.66952(92)	1.2E-05	1.023(24)	0.2109(44)	8.8E-05	2.76(11)

Table H.6: Simulation data for a 4x4x4x5 lattice.

6x6x6x7 $N = 25, \epsilon = 0.02$

Time	β	Prcs	Machine	Stats	Term	P^1_{Ac}	P^2_{Ac}	$\bar{g}^2$	$dd\bar{g}^2$	τ_{int}	$\bar{v}$	$dd\bar{v}$	τ_{int}
37.44h	5.3	4	Iitac	120000	100/100	0.8979(3)	0.8979	4.640(57)	1.2E-03	6.79(28)	0.0988(38)	7.1E-05	7.24(31)
32.68h	5.4	4	Iitac	120000	100/100	0.9091(3)	0.9091	4.151(51)	1.2E-03	8.17(36)	0.1130(32)	7.0E-05	6.95(29)
29.96h	5.5	4	Iitac	120000	100/100	0.9148(3)	0.9142	3.654(33)	6.6E-04	5.62(21)	0.1192(34)	7.8E-05	7.63(32)
27.89h	5.6	4	Iitac	120000	50/100	0.9178(3)	0.9174	3.396(28)	5.5E-04	5.30(19)	0.1181(33)	7.5E-05	7.22(30)
26.03h	5.7	4	Iitac	120000	50/100	0.9196(3)	0.9190	3.147(23)	4.4E-04	4.85(17)	0.1228(34)	7.8E-05	7.32(31)
25.01h	5.8	4	Iitac	120000	50/100	0.9209(3)	0.9214	2.927(21)	4.0E-04	4.95(18)	0.1316(34)	7.7E-05	7.23(30)
23.86h	5.9	4	Iitac	120000	100/100	0.9221(3)	0.9221	2.738(17)	3.1E-04	4.36(15)	0.1396(36)	8.1E-05	7.46(33)
23.27h	6.0	4	Iitac	120000	50/100	0.9221(3)	0.9228	2.619(16)	2.9E-04	4.37(15)	0.1352(37)	8.6E-05	7.72(34)
22.59h	6.1	4	Iitac	120000	100/100	0.9214(3)	0.9210	2.468(15)	2.7E-04	4.48(15)	0.1365(38)	8.9E-05	7.92(35)
21.80h	6.2	4	Iitac	120000	100/100	0.9221(3)	0.9219	2.374(13)	2.3E-04	4.16(13)	0.1386(36)	8.0E-05	6.93(29)
21.13h	6.3	4	Iitac	120000	100/100	0.9212(3)	0.9207	2.268(12)	2.1E-04	4.02(13)	0.1521(39)	8.9E-05	7.61(33)
20.57h	6.4	4	Iitac	120000	50/100	0.9207(3)	0.9211	2.175(11)	1.9E-04	3.98(13)	0.1533(39)	8.9E-05	7.49(32)
20.22h	6.5	4	Iitac	120000	50/100	0.9208(3)	0.9203	2.079(10)	1.7E-04	3.92(13)	0.1540(38)	8.4E-05	6.97(29)
19.99h	6.6	4	Iitac	120000	100/100	0.9203(3)	0.9194	1.9958(94)	1.6E-04	3.75(12)	0.1541(40)	9.0E-05	7.36(31)
19.47h	6.7	4	Iitac	120000	50/100	0.9195(3)	0.9185	1.8887(81)	1.3E-04	3.44(10)	0.1598(40)	8.9E-05	7.11(30)
19.29h	6.8	4	Iitac	120000	50/50	0.9191(3)	0.9192	1.8761(79)	1.3E-04	3.34(10)	0.1620(40)	8.9E-05	7.13(30)
18.91h	6.9	4	Iitac	120000	50/100	0.9185(3)	0.9178	1.8011(75)	1.2E-04	3.36(10)	0.1573(44)	1.0E-04	8.31(37)
18.63h	7.0	4	Iitac	120000	50/100	0.9181(3)	0.9184	1.7366(67)	1.0E-04	3.094(90)	0.1594(41)	9.1E-05	7.10(30)
18.37h	7.1	4	Iitac	120000	50/100	0.9171(3)	0.9164	1.6879(65)	1.0E-04	3.230(96)	0.1615(41)	9.1E-05	6.97(29)
18.18h	7.2	4	Iitac	120000	50/100	0.9176(3)	0.9181	1.6400(61)	9.4E-05	3.114(91)	0.1662(42)	9.2E-05	6.93(29)
17.74h	7.4	4	Iitac	120000	50/100	0.9162(3)	0.9162	1.5475(55)	8.5E-05	3.062(89)	0.1659(45)	1.0E-04	7.64(33)
17.44h	7.6	4	Iitac	120000	50/100	0.9150(3)	0.9153	1.4732(50)	7.4E-05	2.910(82)	0.1664(45)	1.0E-04	7.19(30)
17.10h	7.8	4	Iitac	120000	50/100	0.9141(3)	0.9135	1.4001(44)	6.4E-05	2.711(47)	0.1731(44)	9.5E-05	6.67(27)
17.00h	8.0	4	Iitac	120000	100/200	0.9135(3)	0.9129	1.3184(40)	5.8E-05	2.714(75)	0.1801(45)	1.0E-04	6.88(28)
16.71h	8.2	4	Iitac	120000	50/100	0.9121(3)	0.9123	1.2636(38)	5.5E-05	2.753(76)	0.1738(46)	1.0E-04	6.95(29)
16.47h	8.4	4	Iitac	120000	50/100	0.9112(3)	0.9113	1.2036(34)	4.7E-05	2.549(57)	0.1768(45)	9.6E-05	6.34(25)
16.21h	8.6	4	Iitac	120000	50/100	0.9103(3)	0.9102	1.1616(30)	4.2E-05	2.369(61)	0.1768(45)	9.4E-05	6.12(24)
16.17h	8.8	4	Iitac	120000	50/100	0.9094(3)	0.9086	1.1185(28)	3.8E-05	2.287(58)	0.1674(44)	8.8E-05	5.59(21)
16.01h	9.0	4	Iitac	120000	50/100	0.9094(3)	0.9091	1.0805(27)	3.8E-05	2.263(57)	0.1766(47)	9.7E-05	6.08(24)
15.54h	9.3	4	Iitac	120000	50/100	0.9075(3)	0.9079	1.0200(23)	3.1E-05	2.117(52)	0.1875(46)	9.2E-05	5.66(21)
15.40h	9.6	4	Iitac	120000	50/100	0.9061(3)	0.9063	0.9705(21)	2.7E-05	2.054(20)	0.1817(47)	9.4E-05	5.59(21)
15.25h	10.0	4	Iitac	120000	50/100	0.9040(3)	0.9036	0.9106(19)	2.4E-05	1.966(46)	0.1780(40)	9.0E-05	5.23(19)
14.93h	10.3	4	Iitac	120000	50/100	0.9027(3)	0.9032	0.8675(17)	2.1E-05	1.896(54)	0.1755(47)	9.0E-05	5.09(18)
15.05h	10.4	4	Iitac	120000	50/50	0.9013(3)	0.9015	0.8550(17)	2.1E-04	1.971(45)	0.1857(48)	9.3E-05	5.02(24)
14.80h	10.6	4	Iitac	120000	50/100	0.9002(3)	0.8998	0.8305(16)	2.0E-05	1.878(44)	0.1832(47)	8.8E-05	5.21(19)
14.74h	11.0	4	Iitac	120000	100/100	0.8971(3)	0.8966	0.7867(14)	1.7E-05	1.780(41)	0.1813(48)	9.1E-05	4.89(17)
14.70h	11.3	4	Iitac	120000	50/100	0.8940(3)	0.8925	0.7550(13)	1.5E-05	1.671(37)	0.1754(47)	8.7E-05	4.55(16)
14.52h	11.6	4	Iitac	120000	50/100	0.8906(4)	0.8908	0.7259(12)	1.3E-05	1.583(34)	0.1838(49)	9.1E-05	4.73(17)
14.37h	12.0	4	Iitac	120000	50/100	0.8861(4)	0.8862	0.6949(11)	1.2E-05	1.533(33)	0.1815(49)	9.0E-05	4.57(16)

Table H.7: Simulation data for a 6x6x6x7 lattice.

8x8x8x9, $N = 40, \epsilon = 0.0125$

Time	β	Prcs	Machine	Stats	Term	$\mathbf{P^1_{Ac}}$	$\mathbf{P^2_{Ac}}$	$\bar{\mathbf{g}}^2$	$\mathbf{dd\bar{g}^2}$	τ_{int}	$\bar{\mathbf{v}}$	$\mathbf{dd\bar{v}}$	$\boldsymbol{\tau}_{\mathbf{int}}$
50.00h	5.5	16	Iitac	117794	100/100	0.9294(3)	0.9285	4.572(74)	1.8E-03	8.30(38)	0.0917(41)	9.7E-05	8.06(36)
45.16h	5.6	16	Iitac	120000	100/100	0.9364(2)	0.9365	4.000(50)	1.0E-03	6.11(24)	0.1058(41)	9.8E-05	8.17(36)
41.86h	5.7	16	Iitac	120000	100/100	0.9399(2)	0.9399	3.649(40)	8.2E-04	5.75(22)	0.1071(44)	1.1E-04	8.84(41)
38.67h	5.8	16	Iitac	120000	100/100	0.9425(2)	0.9423	3.359(35)	7.1E-04	5.91(23)	0.1116(43)	1.0E-04	8.29(37)
36.63h	5.9	16	Iitac	120000	100/100	0.9434(2)	0.9435	3.118(30)	6.0E-04	5.66(21)	0.1224(45)	1.1E-04	8.71(40)
36.46h	6.0	16	Iitac	120000	100/100	0.9442(2)	0.9441	2.928(27)	5.3E-04	5.49(21)	0.1148(44)	1.0E-04	8.06(40)
33.96h	6.1	16	Iitac	120000	100/100	0.9445(2)	0.9452	2.761(24)	4.9E-04	5.59(21)	0.1161(47)	1.1E-04	8.68(40)
32.0h	6.2	16	Iitac	119355	100/100	0.9447(2)	0.9451	2.648(21)	4.1E-04	5.04(18)	0.1353(45)	1.1E-04	8.07(36)
31.16h	6.3	16	Iitac	120000	100/100	0.9446(2)	0.9449	2.506(19)	3.7E-04	5.03(18)	0.1276(46)	1.1E-04	8.00(35)
30.59h	6.4	16	Iitac	120000	100/100	0.9449(2)	0.9446	2.355(17)	3.1E-04	4.68(16)	0.1398(45)	1.0E-04	7.65(33)
29.31h	6.5	16	Iitac	120000	100/100	0.9448(2)	0.9445	2.256(15)	2.8E-04	4.47(15)	0.1331(46)	1.1E-04	7.81(34)
28.77h	6.6	16	Iitac	120000	100/100	0.9443(2)	0.9445	2.179(14)	2.6E-04	4.48(15)	0.1438(47)	1.1E-04	7.61(33)
28.32h	6.7	16	Iitac	120000	100/100	0.9443(2)	0.9443	2.116(14)	2.6E-04	4.64(16)	0.1413(47)	1.1E-04	7.67(33)
27.83h	6.8	16	Iitac	120000	100/100	0.9440(2)	0.9440	2.003(12)	2.3E-04	4.50(16)	0.1429(51)	1.2E-04	8.46(38)
27.10h	6.9	16	Iitac	120000	100/100	0.9437(2)	0.9436	1.918(11)	2.0E-04	4.25(14)	0.1471(50)	1.2E-04	7.88(35)
26.72h	7.0	16	Iitac	120000	100/100	0.9429(2)	0.9428	1.875(11)	2.0E-04	4.32(15)	0.1455(49)	1.1E-04	7.65(33)
25.93h	7.2	16	Iitac	120000	100/100	0.9424(2)	0.9427	1.7381(94)	1.7E-04	4.17(14)	0.1509(52)	1.2E-04	8.08(36)
25.02h	7.4	16	Iitac	120000	100/100	0.9417(2)	0.9417	1.6456(82)	1.4E-04	3.82(12)	0.1581(50)	1.1E-04	7.35(31)
24.59h	7.6	16	Iitac	120000	100/100	0.9415(2)	0.9408	1.5542(71)	1.2E-04	3.46(11)	0.1505(54)	1.3E-04	7.94(35)
24.41h	7.8	16	Iitac	120000	100/100	0.9407(2)	0.9408	1.4601(65)	1.1E-04	3.58(11)	0.1536(54)	1.3E-04	7.79(34)
23.66h	8.0	16	Iitac	120000	100/100	0.9399(2)	0.9400	1.3990(58)	9.3E-05	3.31(10)	0.1529(53)	1.2E-04	7.05(30)
23.26h	8.2	16	Iitac	120000	100/100	0.9393(2)	0.9392	1.3294(53)	8.1E-05	3.146(92)	0.1681(55)	1.2E-04	7.27(31)
23.38h	8.4	16	Iitac	120000	100/100	0.9389(2)	0.9384	1.2697(48)	7.4E-05	3.104(90)	0.1700(56)	1.3E-04	7.33(31)
22.45h	8.6	16	Iitac	120000	100/100	0.9384(2)	0.9385	1.2110(43)	6.4E-05	2.903(82)	0.1635(57)	1.3E-04	7.23(31)
22.28h	8.8	16	Iitac	120000	100/100	0.9378(2)	0.9370	1.1652(42)	6.5E-05	3.103(90)	0.1598(57)	1.3E-04	7.22(30)
21.83h	9.0	16	Iitac	120000	100/100	0.9368(2)	0.9369	1.1171(38)	5.6E-05	2.819(79)	0.1641(57)	1.2E-04	6.73(27)
21.61h	9.3	16	Iitac	120000	100/100	0.9365(2)	0.9356	1.0598(34)	4.9E-05	2.686(74)	0.1750(56)	1.2E-04	6.41(26)
21.34h	9.6	16	Iitac	120000	100/100	0.9358(2)	0.9355	1.0044(30)	4.2E-05	2.488(66)	0.1768(59)	1.3E-04	6.80(28)
20.73h	10.0	16	Iitac	120000	100/100	0.9347(2)	0.9341	0.9321(26)	3.5E-05	2.398(62)	0.1774(54)	1.1E-04	5.42(20)
20.71h	10.3	16	Iitac	120000	100/100	0.9335(2)	0.9335	0.8952(24)	3.2E-05	2.290(58)	0.1597(58)	1.2E-04	5.80(22)
20.63h	10.6	16	Iitac	120000	100/100	0.9323(2)	0.9323	0.8572(22)	2.9E-05	2.217(56)	0.1672(58)	1.2E-04	5.64(21)
20.18h	11.0	16	Iitac	120000	100/100	0.9306(2)	0.9305	0.8084(20)	2.6E-05	2.144(53)	0.1736(57)	1.1E-04	5.35(20)
20.03h	11.3	16	Iitac	120000	100/100	0.9289(2)	0.9287	0.7763(19)	2.5E-05	2.236(57)	0.1700(58)	1.1E-04	5.16(19)
19.89h	11.6	16	Iitac	120000	100/100	0.9266(3)	0.9257	0.7510(17)	2.1E-05	2.064(50)	0.1646(59)	1.1E-04	5.14(19)
19.68h	12.0	16	Iitac	120000	100/100	0.9238(3)	0.9235	0.7089(15)	1.9E-05	1.898(45)	0.1785(62)	1.2E-04	5.56(21)

Table H.8: Simulation data for a 8x8x8x9 lattice.

12x12x12x13 $N = 50\epsilon = 0.01$

Time	$\boldsymbol{\beta}$	**Prcs**	**Machine**	**Stats**	**Term**	$\mathbf{P^1_{Ac}}$	$\mathbf{P^2_{Ac}}$	$\bar{\mathbf{g}}^2$	$\mathbf{dd\bar{g}^2}$	τ_{int}	$\bar{\mathbf{v}}$	$\mathbf{dd\bar{v}}$	$\boldsymbol{\tau}_{\mathbf{int}}$
151.23h	5.8	32	Lonsdale	120000	200/300	0.8641(4)	0.8638	4.49(13)	3.8E-03	13.08(74)	——	—-	—-
136.2h	6.0	32	Lonsdale	120000	200/200	0.9082(4)	0.9086	3.449(53)	1.2E-03	7.20(30)	0.1160(57)	1.4E-04	9.04(42)
145.58h	6.2	32	Lonsdale	120000	200/200	0.9158(4)	0.9153	3.047(41)	9.2E-04	6.82(28)	0.1070(62)	1.6E-04	9.74(47)
135.96h	6.4	32	Lonsdale	120000	300/300	0.9171(4)	0.9177	2.758(32)	6.4E-04	5.82(22)	0.1268(60)	1.5E-04	8.84(41)
123.3h	6.6	32		120000	200/200	0.9183(4)	0.9177	2.415(26)	5.4E-04	6.09(24)	0.1264(64)	1.6E-04	9.07(43)
120.0h	6.8	32		120000	200/200	0.9180(4)	0.9174	2.281(24)	4.9E-04	6.17(24)	0.1195(61)	1.5E-04	8.24(37)
99.46h	7.0	32		120000	200/200	0.9172(4)	0.9157	2.079(19)	3.9E-04	5.63(21)	0.1414(68)	1.7E-04	9.46(45)
106.39h	7.2	32		120000	100/100	0.9034(6)	0.9036	1.890(16)	3.2E-04	5.51(21)	0.1384(67)	1.6E-04	8.85(41)
112.87h	7.4	32		120000	200/200	0.9163(3)	0.9166	1.770(14)	2.7E-04	4.89(18)	0.1563(72)	1.8E-04	9.25(44)
117.41h	7.6	32		120000	200/300	0.9156(3)	0.9149	1.672(13)	2.4E-04	5.22(19)	0.1443(67)	1.6E-04	8.41(38)
87.06h	7.8	32		120000	200/300	0.9148(3)	0.9144	1.595(12)	2.3E-04	4.77(17)	0.1503(79)	2.1E-04	9.82(49)
87.94h	8.0	32		120000	200/300	0.9136(3)	0.9143	1.4994(99)	1.8E-04	4.40(15)	0.1504(70)	1.7E-04	7.98(36)
84.55h	8.2	32		120000	100/100	0.9127(3)	0.9138	1.3976(86)	1.5E-04	4.32(15)	0.1643(76)	1.9E-04	9.12(43)
82.51h	8.4	32		120000	100/100	0.9123(3)	0.9124	1.3508(81)	1.4E-04	4.34(15)	0.1696(75)	1.8E-04	8.75(40)
81.25h	8.6	32		120000	100/100	0.9116(3)	0.9116	1.2901(74)	1.3E-04	4.24(14)	0.1618(74)	1.7E-04	8.09(12)
80.23h	8.8	32		120000	100/100	0.9115(3)	0.9110	1.2368(70)	1.3E-04	4.23(14)	0.1484(73)	1.7E-04	7.57(33)
93.71h	9.0	32		120000	100/100	0.9103(3)	0.9107	1.1924(61)	1.0E-04	3.72(12)	0.1592(77)	1.8E-04	8.34(37)
82.27h	9.3	32		120000	100/100	0.9093(3)	0.9089	1.1090(54)	9.0E-05	3.66(12)	0.1755(78)	1.9E-04	8.23(37)
82.29h	9.6	32		120000	100/100	0.9079(3)	0.9077	1.0582(51)	8.7E-05	3.83(12)	0.1604(80)	1.9E-04	8.06(36)
79.95h	10.0	32		120000	100/100	0.9053(3)	0.9054	0.9758(43)	6.9E-05	3.52(11)	0.1627(75)	1.7E-04	6.98(29)
76.30h	10.3	32		120000	100/100	0.9057(3)	0.9061	0.9267(37)	5.9E-05	3.205(95)	0.1770(79)	1.8E-04	7.24(31)
70.00h	10.6	32		120000	100/100	0.9048(3)	0.9061	0.8889(34)	5.1E-05	2.992(86)	0.1501(78)	1.7E-04	6.83(28)
68.54h	11.0	32		120000	100/100	0.9023(3)	0.9029	0.8400(32)	4.9E-05	3.088(90)	0.1923(81)	1.8E-04	6.88(28)
69.87h	11.3	32	Iitac	120000	100/100	0.9003(3)	0.9001	0.8047(29)	4.3E-05	2.888(81)	0.1669(84)	1.9E-04	7.25(31)
71.04h	11.6	32	Iitac	120000	100/100	0.8987(4)	0.8994	0.7734(27)	4.0E-05	2.880(81)	0.1697(88)	2.0E-04	7.55(32)
65.63h	12.0	32	Iitac	120000	100/100	0.8954(3)	0.8956	0.7287(25)	3.8E-05	2.837(83)	0.1688(80)	1.7E-04	5.73(22)

Table H.9: Simulation data for a 12x12x12x13 lattice.

16x16x16x17 $N = 80\epsilon = 0.00625$

Time	$\boldsymbol{\beta}$	**Prcs**	**Machine**	**Stats**	**Term**	$\mathbf{P^1_{Ac}}$	$\mathbf{P^2_{Ac}}$	$\bar{\mathbf{g}}^2$	$\mathbf{dd\bar{g}^2}$	τ_{int}	$\bar{\mathbf{v}}$	$\mathbf{dd\bar{v}}$	$\boldsymbol{\tau}_{\mathbf{int}}$
113.42h	5.9	256	Stokes/BG	150000	900/900	0.9269	0.9269	4.64(10)	2.1E-0	39.35(36)	0.946(52)	1.1E-04	9.24(50)
105.13h	6.1	2048	BG 36h	160000	900/900	0.8839	0.8834	4.041(83)	1.8E-0	39.14(38)	0.1129(61)	1.4E-04	9.90(42)
160.5h	6.3	128	Iitac	120000	400/400	0.9101	0.9099	3.147(59)	1.5E-0	37.48(35)	0.0931(77)	2.1E-04	9.18(47)
107.72h	6.6	2048	BG 36h	210000	400/400	0.8136	0.8133	2.705(33)	6.3E-0	48.59(31)	0.1222(58)	2.1E-04	9.18(47)
199.28h	7.0	128	Iitac	170000	200/200	0.9378	0.9376	2.198(22)	3.9E-0	46.22(21)	0.1384(63)	1.3E-04	8.69(34)
67.58h	7.6	256	Stokes	150000	200/200	0.9401	0.9407	1.770(15)	2.8E-0	45.72(20)	0.1418(69)	1.5E-04	8.90(34)
64.0h	8.4	256	Stokes	180000	200/200	0.9383	0.9386	1.4135(93)	2.8E-0	45.03(16)	0.1573(74)	1.6E-04	9.11(36)
63.46h	9.0	256	Stokes	180000	200/200	0.9376	0.9384	1.2260(68)	1.0E-0	44.45(13)	0.1749(71)	1.4E-04	7.99(29)
64.21h	10.0	256	Stokes	180000	200/200	0.9366	0.9373	1.0154(47)	6.8E-0	54.08(11)	0.1550(72)	1.4E-04	7.18(25)
57.42h	11.0	256	Stokes	180000	100/100	0.9335	0.9331	0.8635(36)	5.0E-0	53.83(10)	0.1380(79)	1.5E-04	7.42(27)
50.74h	12.0	256	Stokes	172000	100/100	0.9293	0.9296	0.7541(28)	3.7E-0	53.388(87)	0.1692(79)	1.4E-04	6.43(22)

Table H.10: Simulation data for a 16x16x16x17 lattice.

Bibliography

[1] J. S. Schwinger, Phys. Rev. **74** (1948) 1439.

[2] J. S. Schwinger, Phys. Rev. **75** (1948) 651.

[3] J. S. Schwinger, Phys. Rev. **73** (1948) 416.

[4] S. Tomonaga, Prog. Theor. Phys. **1** (1946) 27.

[5] S. I. Tomonaga and J. R. Oppenheimer, Phys. Rev. **74** (1948) 224.

[6] R. P. Feynman, Phys. Rev. **74** (1948) 939.

[7] R. P. Feynman, Phys. Rev. **74** (1948) 1430.

[8] R. P. Feynman, Rev. Mod. Phys. **20** (1948) 367.

[9] F. J. Dyson, Phys. Rev. **75** (1949) 486.

[10] E. Fermi, Nuovo Cim. **11** (1934) 1.

[11] H. Yukawa, Proc. Phys. Math. Soc. Jap. **17** (1935) 48.

[12] R. Haag, Kong. Dan. Vid. Sel. Mat. Fys. Med. **29N12** (1955) 1 [Z. Phys. **141** (1955 PHMAA,46,376-380.1955) 217].

[13] R. F. Streater, A. S. Wightman, PCT, Spin and statistics, and all that. Benjamin, New York, 1964. (Mathematical Physics Monograph Series, Vol. 1) viii+181 pp

[14] K. Osterwalder and R. Schrader, Commun. Math. Phys. **31** (1973) 83.

[15] K. Osterwalder and R. Schrader, Commun. Math. Phys. **42** (1975) 281.

[16] C. N. Yang and R. L. Mills, Phys. Rev. **96** (1954) 191.

[17] S. Weinberg, Phys. Rev. Lett. **19** (1967) 1264.

[18] D. J. Gross and F. Wilczek, Phys. Rev. Lett. **30** (1973) 1343.

[19] H. D. Politzer, Phys. Rev. Lett. **30** (1973) 1346.

[20] D. J. Gross, Nucl. Phys. Proc. Suppl. **74** (1999) 426 [arXiv:hep-th/9809060].

[21] A. M. Jaffe and E. Witten, "Quantum Yang-Mills Theory,"

[22] K. G. Wilson, Phys. Rev. D **10** (1974) 2445.

[23] M. Creutz, Phys. Rev. Lett. **43** (1979) 553 [Erratum-ibid. **43** (1979) 890].

[24] M. Creutz, Phys. Rev. D **21** (1980) 2308.

[25] K. Jansen *et al.*, Phys. Lett. B **372** (1996) 275 [arXiv:hep-lat/9512009].

[26] R. Sommer, arXiv:hep-ph/9711243.

[27] M. Luscher, arXiv:hep-lat/9802029.

[28] S. Sint, Nucl. Phys. Proc. Suppl. **94** (2001) 79 [arXiv:hep-lat/0011081].

[29] M. Luscher, Annales Henri Poincare **4** (2003) S197 [arXiv:hep-ph/0211220].

[30] P. Weisz, arXiv:1004.3462 [hep-lat].

[31] Y. Aoki, PoS **LAT2009** (2009) 012 [arXiv:1005.2339 [hep-lat]].

[32] G. P. Lepage and P. B. Mackenzie, Phys. Rev. D **48** (1993) 2250 [arXiv:hep-lat/9209022].

[33] G. Martinelli, C. Pittori, C. T. Sachrajda, M. Testa and A. Vladikas, Nucl. Phys. B **445** (1995) 81 [arXiv:hep-lat/9411010].

[34] M. Luscher, P. Weisz and U. Wolff, Nucl. Phys. B **359** (1991) 221.

[35] M. Lüscher, R. Narayanan, P. Weisz and U. Wolff, Nucl. Phys. B **384** (1992) 168 [arXiv:hep-lat/9207009].

[36] M. Lüscher, R. Narayanan, R. Sommer, U. Wolff and P. Weisz, Nucl. Phys. Proc. Suppl. **30** (1993) 139.

[37] M. Luscher, R. Sommer, U. Wolff and P. Weisz, Nucl. Phys. B **389** (1993) 247 [arXiv:hep-lat/9207010].

[38] M. Lüscher, R. Sommer, P. Weisz and U. Wolff, Nucl. Phys. B **413** (1994) 481 [arXiv:hep-lat/9309005].

[39] M. Della Morte, R. Frezzotti, J. Heitger, J. Rolf, R. Sommer and U. Wolff [ALPHA Collaboration], Nucl. Phys. B **713** (2005) 378 [arXiv:hep-lat/0411025].

[40] S. Aoki *et al.* [PACS-CS Collaboration], JHEP **0910** (2009) 053 [arXiv:0906.3906 [hep-lat]].

[41] T. Appelquist, G. T. Fleming and E. T. Neil, Phys. Rev. D **79** (2009) 076010 [arXiv:0901.3766 [hep-ph]].

[42] F. Tekin, R. Sommer and U. Wolff, arXiv:1006.0672 [hep-lat].

[43] M. Guagnelli, J. Heitger, C. Pena, S. Sint and A. Vladikas [ALPHA Collaboration], JHEP **0603** (2006) 088 [arXiv:hep-lat/0505002].

[44] K. Symanzik, Nucl. Phys. B **190** (1981) 1.

[45] M. Lüscher, Nucl. Phys. B **254** (1985) 52.

[46] J. C. Collins, Renormalisation. Cambridge University Press. Cambdrige, UK, 1984

[47] S. Sint, Nucl. Phys. B **421** (1994) 135 [arXiv:hep-lat/9312079].

[48] S. Sint, Nucl. Phys. B **451** (1995) 416 [arXiv:hep-lat/9504005].

[49] S. Miyazaki and Y. Kikukawa, arXiv:hep-lat/9409011.

[50] U. M. Heller, Nucl. Phys. B **504** (1997) 435 [arXiv:hep-lat/9705012].

[51] K. Symanzik, "A modified model of Euclidean Quantum Field Theory", New York University Report (1964); J. Math. Physics 7 510 (1966)

[52] K. Symanzik, "Euclidean quantum field theory, in Local quantum theory", (Varena, 1968), ed. R. Jost (Academic Press, New York, 1969)

[53] A. M. Jaffe, Nucl. Phys. B **254** (1985) 31.

[54] M. Creutz, *Quarks, gluons and lattices.* Cambridge University Press, Cambridge, UK, 1983.

[55] I. Montvay and G. Munster, *Quantum fields on a lattice.* Cambridge University Press, Cambridge, UK, 1994.

[56] H. J. Rothe, *Lattice Gauge Theories: An introduction.* World Scientific Lecture Notes in Physics, Vol. 74. (World Scientific, Singapore, 1997).

[57] J. Smit, *Introduction to Quantum Fields on a Lattice.* Cambridge University Press, (Cambridge Lecture Notes in Physics). Cambridge, UK, 2002.

[58] T. DeGrand, C. DeTar, *Lattice methods for Quantum Chromodynamics.* World Scientific. Singapore, 2006.

[59] H. B. Nielsen and M. Ninomiya, Nucl. Phys. B **193** (1981) 173. H. B. Nielsen and M. Ninomiya, Nucl. Phys. B **185** (1981) 20 [Erratum-ibid. B **195** (1982) 541].

[60] L. Susskind, Phys. Rev. D **16** (1977) 3031.

[61] H. S. Sharatchandra, H. J. Thun and P. Weisz, Nucl. Phys. B **192** (1981) 205.

[62] H. Kluberg-Stern, A. Morel, O. Napoly and B. Petersson, Nucl. Phys. B **220** (1983) 447.

[63] K. G. Wilson and J. B. Kogut, Phys. Rept. **12** (1974) 75.

[64] M. Lüscher, Commun. Math. Phys. **54** (1977) 283.

[65] M. Creutz, Phys. Rev. D **15** (1977) 1128.

[66] S. Sint and R. Sommer, Nucl. Phys. B **465** (1996) 71 [arXiv:hep-lat/9508012].

[67] K. Symanzik, "Some Topics In Quantum Field Theory", in: Mathematical problems in theoretical physics, eds. R. Schrader et al., Lecture Notes in physics, Vol 153 (Springer, New York, 1982)

[68] S. Takeda, U. Wolff. One loop results of the SF coupling for pure $SU(3)$ gauge theory on a lattice $T = L \pm a$. May 9, 2007. Unpublished notes.

[69] P. Weisz. A Haan-Fabricius Updating Program for the APE-100 Parallel Computer. Unpublished notes.

[70] P. Weisz. A Cabbibo-Marinari SU(3) Updating Program for the Quadrics Parallel Computer. Unpublished notes.

[71] R. Frezzotti, P. A. Grassi, S. Sint and P. Weisz, Nucl. Phys. Proc. Suppl. **83** (2000) 941 [arXiv:hep-lat/9909003].

[72] R. Frezzotti, P. A. Grassi, S. Sint and P. Weisz [Alpha collaboration], JHEP **0108** (2001) 058 [arXiv:hep-lat/0101001].

[73] S. Sint, PoS **LAT2005** (2006) 235 [arXiv:hep-lat/0511034].

[74] S. Sint, arXiv:hep-lat/0702008.

[75] P. H. Ginsparg and K. G. Wilson, Phys. Rev. D **25** (1982) 2649.

[76] Y. Taniguchi, JHEP **0610** (2006) 027 [arXiv:hep-lat/0604002].

[77] Y. Taniguchi, Mod. Phys. Lett. A **22** (2007) 499.

[78] M. Lüscher, JHEP **0605** (2006) 042 [arXiv:hep-lat/0603029].

[79] M. F. L. Golterman and J. Smit, Nucl. Phys. B **245** (1984) 61.

[80] C. van den Doel and J. Smit, Nucl. Phys. B **228** (1983) 122.

[81] T. Jolicoeur, A. Morel and B. Petersson, Nucl. Phys. B **274** (1986) 225.

[82] S. Sint, Unpublished notes.

[83] P. Pérez-Rubio and S. Sint, PoS **LATTICE2007** (2006) 249 [arXiv:0710.0583 [hep-lat]].

[84] M. Lüscher. Solution of the free Dirac equation on a lattice Unpublished notes

[85] M. Luscher and P. Weisz, Nucl. Phys. B **479** (1996) 429 [arXiv:hep-lat/9606016].

[86] A. Bode, P. Weisz and U. Wolff [ALPHA collaboration], Nucl. Phys. B **576** (2000) 517 [Erratum-ibid. B **600** (2001 ERRAT,B608,481.2001) 453] [arXiv:hep-lat/9911018].

[87] G. Parisi, Nucl. Phys. B **254** (1985) 58.

[88] K. Symanzik, Nucl. Phys. B **226** (1983) 187.

[89] K. Symanzik, Nucl. Phys. B **226** (1983) 205.

[90] M. Luscher and P. Weisz, Commun. Math. Phys. **97** (1985) 59 [Erratum-ibid. **98** (1985) 433].

[91] K. Symanzik, Commun. Math. Phys. **45** (1975) 79.

[92] Y. b. Luo, Phys. Rev. D **55** (1997) 353 [arXiv:hep-lat/9604025].

[93] M. Luscher, S. Sint, R. Sommer and P. Weisz, Nucl. Phys. B **478** (1996) 365 [arXiv:hep-lat/9605038].

[94] G. Keller, Helv. Phys. Acta **66** (1993) 453.

[95] M. Luscher and P. Weisz, Phys. Lett. B **158** (1985) 250.

[96] M. Luscher and P. Weisz, Nucl. Phys. B **240** (1984) 349.

[97] K. Wilson, in New developments in gauge theories, ed. G. 't Hooft et al. (Plenum, New York, 1980)

[98] P. Weisz, Nucl. Phys. B **212** (1983) 1.

[99] P. Weisz and R. Wohlert, Nucl. Phys. B **236** (1984) 397 [Erratum-ibid. B **247** (1984) 544].

[100] B. Sheikholeslami and R. Wohlert, Nucl. Phys. B **259** (1985) 572.

[101] M. Luscher, S. Sint, R. Sommer, P. Weisz and U. Wolff, Nucl. Phys. B **491** (1997) 323 [arXiv:hep-lat/9609035].

[102] K. Jansen and R. Sommer, Nucl. Phys. Proc. Suppl. **63** (1998) 853 [arXiv:hep-lat/9709022].

[103] N. Yamada *et al.* [JLQCD Collaboration and CP-PACS Collaboration], Phys. Rev. D **71** (2005) 054505 [arXiv:hep-lat/0406028].

[104] F. Tekin, R. Sommer and U. Wolff [Alpha Collaboration], Phys. Lett. B **683** (2010) 75 [arXiv:0911.4043 [hep-lat]].

[105] S. R. Sharpe, R. Gupta and G. W. Kilcup, Nucl. Phys. Proc. Suppl. **26** (1992) 197.

[106] S. Takeda, S. Aoki and K. Ide, Phys. Rev. D **68** (2003) 014505 [arXiv:hep-lat/0304013].

[107] R. Frezzotti, S. Sint and P. Weisz [ALPHA collaboration], JHEP **0107** (2001) 048 [arXiv:hep-lat/0104014].

[108] L. D. Faddeev and V. N. Popov, Phys. Lett. B **25** (1967) 29.

[109] M. Lüscher, Selected Topics in Lattice Field Theory, Lectures given at Les Houches (1988), in: Fields, Strings and Critical Phenomena, ed. E. Brézin and J. Zinn-Justin (North Holland, Amsterdam, 1989)

[110] P. Weisz, Computation of the improvement coefficient c_{sw} to 1-loop. 1996 Unpublished notes

[111] P. Weisz, Computation of the effective action of a constant electric field 1-loop order SU(3) gauge theory with dimensional regularization. 1992. Unpublished notes.

[112] P. Perez Rubio, "One loop fermionic contribution to the running coupling," Unpublished notes.

[113] A. D. Kennedy. Montecarlo Methods for Quantum Field theory. Talk given at NTU, Taipei, Taiwan, 10 Sep, 1999.

[114] C. Morningstar, arXiv:hep-lat/0702020.

[115] M. J. Peardon. Algorithms and Numerical Methods. Lectures given at INT Summer School. "Lattice QCD and its applications", Seattle, August 8 - 28, 2007.

[116] M. Lüscher. Computational Strategies in Lattice QCD. Lectures given at Les Houches Summer School in Theoretical Physics, Session XCIII. Modern perspectives in lattice QCD: Quantum field theory and high perfo rmance computing, Les Houches, France, 3 Aug - 28 Aug, 2009.

[117] A. D. Kennedy and P. Rossi, Nucl. Phys. B **327** (1989) 782.

[118] R. Durrett. 1996. "Probability: theory and examples". 2nd ed. Duxbury Press.

[119] G. Grimmett, D. Stirzaker. 2001. "Probability and Random Processes". 3rd ed. Oxford University Press.

[120] U. Wolff [ALPHA collaboration], Comput. Phys. Commun. **156** (2004) 143 [Erratum-ibid. **176** (2007) 383] [arXiv:hep-lat/0306017].

[121] R. Frezzotti, M. Hasenbusch, U. Wolff, J. Heitger and K. Jansen [ALPHA Collaboration], Comput. Phys. Commun. **136** (2001) 1 [arXiv:hep-lat/0009027].

[122] U. Wolff, Monte Carlo error analysis, ALPHA collaboration, internal notes, 2002.

[123] U. Wolff and B. Bunk, Lecture Notes Computational Physics II [in german], `www-com.physik.hu-berlin.de/comphys/comphys.html,` Humboldt University, Berlin, 2002.

[124] M. Gell-Mann and F. E. Low, Phys. Rev. **95** (1954) 1300.

[125] L. P. Kadanoff, Physics **2** (1966) 263.

[126] K. G. Wilson, Rev. Mod. Phys. **47** (1975) 773.

[127] C. G. . Callan, "BROKEN SCALE INVARIANCE AND SCALING LAWS IN ELEMENTARY PARTICLE PHYSICS," Based on talk delivered at Washington Meeting of American Physical Society, Apr 27, 1970"

[128] K. Symanzik, Commun. Math. Phys. **18** (1970) 227.

[129] O. V. Tarasov, A. A. Vladimirov and A. Y. Zharkov, Phys. Lett. B **93** (1980) 429.

[130] M. Luscher and P. Weisz, Nucl. Phys. B **452** (1995) 213 [arXiv:hep-lat/9504006].

[131] M. Luscher and P. Weisz, Nucl. Phys. B **452** (1995) 234 [arXiv:hep-lat/9505011].

[132] B. Alles, A. Feo and H. Panagopoulos, Nucl. Phys. B **491** (1997) 498 [arXiv:hep-lat/9609025].

[133] A. Bode and H. Panagopoulos, Nucl. Phys. B **625** (2002) 198 [arXiv:hep-lat/0110211].

[134] C. Michael and S. Perantonis, Nucl. Phys. Proc. Suppl. **20** (1991) 177.

[135] S. P. Booth, A. Hulsebos, A. C. Irving, A. McKerrell, C. Michael, P. S. Spencer and P. W. Stephenson [UKQCD Collaboration], Nucl. Phys. B **394** (1993) 509 [arXiv:hep-lat/9209007].

[136] R. Sommer, Nucl. Phys. B **411** (1994) 839 [arXiv:hep-lat/9310022].

[137] S. Brandt. Data Analysis. "Statistical and Computational Methods for Scientists and Engineers". Third Edition 1988. Springer

[138] W. H. Press, S. A. Teukolsky, W. T. Vetterling, B. P. Flannery. Numerical Recipes in C. Second Edition 1992. Cambridge University Press.

[139] G. Abbiendi *et al.* [OPAL Collaboration], Eur. Phys. J. C **53** (2008) 21.